Research Report

on

Development of analytical strategies to measure radioisotopes of tin in the environment

Prepared by

Mohammad Majibur Rahman
Graduate Program (PhD)

Supervisor: Dr. Ian Clark
Co-supervisor: Dr. Liam Kieser

Earth and Environmental Sciences: Specialization in Chemical and Environmental Toxicology

Submitted to

The Office of Graduate and Postdoctoral Studies

Submitted in partial fulfillment of the requirements for the degree of Doctor of Philosophy in Earth and Environmental Sciences: Specialization in Chemical and Environmental Toxicology

DECEMBER 13, 2018

This page has intentionally been left blank.

Abstract

Quantification of tin isotopes in environmental samples, particularly the radioactive ^{126}Sn, is important for processes such as the biomonitoring of organotin species, long-term nuclear waste storage and treatment planning. The detection of ^{126}Sn by mass spectrometric methods is, however, hampered by the presence of the stable ^{126}Te isotope. Therefore, separation of tin from tellurium is crucial to minimize isobaric interferences that limit the quantification of ^{126}Sn by Accelerator Mass Spectrometry (AMS) and other instrumental techniques. In the present study, three major accomplishments are discussed: i) development of an analytical strategy to separate tin from tellurium, ii) monitoring of anionic interferences in the separation of tin from tellurium, and iii) suppression of ^{126}Te background to allow the detection of ^{126}Sn by AMS.

Section I (Chapter 2):

In the first phase of the project, an analytical survey was carried out using four Eichrom resins (TRU, TEVA, UTEVA, and DGA) to identify a suitable solid phase chromatographic material to separate tin from tellurium. Standard metal solutions were spiked on batch tests in two acids (HCl and HNO_3) at concentrations ranging from 0.20 to 6.0 mol L^{-1}, and the spiked analytes in solution were measured by ICP-MS. The distribution coefficient, K_D (solid phase/aqueous phase) of tin and tellurium was then calculated for each resin. Results, HCl treatment from 0.20 to 6.0 mol L^{-1}, reveal that the TEVA resin exhibited the highest K_D (27198 mL g^{-1}) for the tin in HCl solution, followed by TRU (24239 mL g^{-1}), DGA (10165 mL g^{-1}), and UTEVA (3232 mL g^{-1}) resins. However, the TRU resin demonstrated the lowest K_D (431 mL g^{-1}) for tellurium in similar acid conditions compared to other substrates (UTEVA 708 mL g^{-1}, DGA 2230 mL g^{-1}, and TEVA 3124 mL g^{-1}). All four resins produced relatively small K_D values (≤ 100 mL g^{-1}) for both tin and tellurium in aqueous HNO_3 medium. A follow up of batch test, in

which the TRU resin was charged on Bio-Rad columns, showed retention of 99.78 ± 0.39% tin and 59.31 ± 1.30% tellurium in the presence of dilute hydrochloric acid (~1.0 mol L^{-1}). Through a study of tin and tellurium desorption from TRU resin with different eluents, it was observed that aqueous hydrofluoric acid (~ 0.50 mol L^{-1}) could wash down up to 92% of loaded tin, while tellurium desorption can be kept as low as 5%. The first phase of our work suggests that the TRU resin offers itself a promising solid phase chromatographic material for the separation of tin from tellurium, while aqueous hydrofluoric acid is shown to be an excellent eluent to selectively wash out of tin from the solid phase.

Section II (Chapter 3):

In the second phase of the project, experimental work was carried out to evaluate the effect of Cl^- and SO_4^{2-} interferences, the two major anions found in natural waters, in the separation of tin from tellurium. Following previous findings, powdered TRU (50–100 μm) resin was used as an adsorbent. Laboratory prepared solutions containing Cl^- and SO_4^{2-} ions were spiked (single Cl^-, single SO_4^{2-}, and Cl^--SO_4^{2-}-mixed spike) with standard solutions of tin and tellurium. Distribution coefficients for adsorbed tin and tellurium were then determined for each solution. An optimization of the reaction time producing the maximum metal-resin interaction was also evaluated.

Results reveal that the average K_D values for tin and tellurium in 3.0 mol L^{-1} hydrochloric acid are 5517 ± 406 and 1310 ± 50 mL g^{-1}, respectively. In the case of tin, the Cl^--spike produced an increase in K_D of 11% from that of the unspiked sample, whereas the mixed-spiked sample faced a reduction of K_D by 7% compared to that of the unspiked sample. The distribution coefficients of tellurium in the presence of tested anion spikes remained unchanged. This observation demonstrates that the distribution coefficients of tin and tellurium onto the solid phase is barely affected by the presence of Cl^- and SO_4^{2-}

contaminants (each present at concentrations of 70.0 mg L^{-1}). Moreover, the adsorption of metal at very low acidic conditions onto the resin in presence of Cl^- and SO_4^{2-} spikes is favored at pH values from 4.0 to 5.0. In alkaline conditions, the resin was found to lose its stability. The TRU resin undergoes denaturation at 2.0 mol L^{-1} of NaOH, while a complete annihilation of resin structure occurred at 3.5 mol L^{-1} of base.

The optimization of the reaction time producing the highest distribution coefficient of metals on the solid phase was carried out by observing batch tests up to 180 minutes of contact time. Results show that the optimum time for the best metal-resin interaction is around 90 minutes. More prolonged interaction time reduce the K_D values for both tin and tellurium.

A thorough adsorption-desorption study for tin and tellurium using TRU chromatographic resin with spiked field samples (surface and groundwaters) show that at least 99% tin is adsorbed in the presence of hydrochloric acid, while the adsorption of tellurium can be maintained at a level as low as 60%. Aqueous hydrofluoric acid can then selectively elute 85% of tin (with a single wash of 100 mg of TRU resin) with tellurium release of less than 10%. Our proposed methodology can be applied successfully for the selective separation of tin from tellurium from surface and groundwater samples containing Cl^- and SO_4^{2-} ions.

Section III (Chapter 4):

In the third phase of our project, a rigorous study was carried out to suppress the ^{126}Te background for the detection of ^{126}Sn by AMS. Laboratory prepared and commercially available SnF_2 along with SnI_2 were used in the preparation of AMS targets (SnF_2 + PbF_2 and SnF_2 + NaI + Ag). Beam-currents for SnF_5^- and SnF_2I^- molecular ions were measured from these targets in the A. E. Lalonde AMS laboratory. Results reveal that:

- tin does not form a stable molecular-beam with iodine, iodine makes the ion-source very unstable, no beam-current was detected with iodide species, even after mixing with silver powder,
- the formation of large SnI_2F^- molecular ion was not confirmed, no detectable signal was observed for this compound,
- no stable beam-current was observed for TeF_3^- and TeF_5^- species,
- the molecule SnF_2 is a good ionic conductor, which produces stable SnF_3^- current,
- the sputtering capacity of SnF_2 is very good and immediate, and SnF_2 + PbF_2 target composition yields a long-lasting SnF_3^- current,
- the ^{126}Sn/^{120}Sn ratio with laboratory prepared SnF_2 was measured as ~4.0×10^{-9}, a suppression of tellurium background to ppb-level,
- the ^{126}Sn/^{118}Sn ratio with the SnF_2 compound was found to be ~7.0×10^{-11}, a drop of background by 2-orders of magnitude,
- the ^{126}Sn/^{118}Sn ratio for the commercial SnF_2 sample was measured as ~3.0×10^{-12}, a drop of background to parts per trillion-level.

The observed ~10^{-12} background is the lowest value ever measured for the AMS quantification of ^{126}Sn, even large AMS techniques have not reported lower ^{126}Sn/^{118}Sn ratios. Therefore, the SnF_2 + PbF_2 target composition is an excellent choice to produce

stable molecular ion beams of tin and reducing interferences caused by the presence of ^{126}Te isotope during the detection of ^{126}Sn by AMS.

Keywords

Tin isotopes, distribution coefficient, solid phase extraction, extraction chromatographic materials, TRU resin, metal adsorption-desorption, ICP-MS, anionic interferences on distribution coefficient, groundwater contamination, AMS detection of ^{126}Sn, ^{126}Te interference, suppression of ^{126}Te background, AMS beam-current.

Statement of originality

This is to certify that the content of this thesis is done by me and has not been submitted elsewhere for any academic degree or diploma.

I also testify that this booklet is independently prepared by me and the assistances received from other sources have been acknowledged or cited as references.

The chapter 4 (AMS detection of ^{126}Sn) has been developed with the generous cooperation of Dr. Xiaolei Zhao, A. E. Lalonde AMS Laboratory, Advanced Research Complex, University of Ottawa. I am indebted to him for his time-consuming help in the analysis of AMS data.

Acknowledgements

I would like to express my deepest sense of gratitude to Prof. Ian Clark and Prof. Liam Kieser, for their kind consent to accept me as a graduate student after the sudden demise of Prof. Robert Jack Cornett. I can recall those critical days when a vibrant research group was facing a serious mentoring problem, fortunately, Ian and Liam came forward and took the burden on their shoulders. The strong moral support, caring guidance, and constant encouragement I have received from them, were amazing. In fact, without their escalating push, I could hardly have finished the time-sensitive project work well before the anticipated deadline. My thankful acknowledgement goes to them.

I am grateful to Dr. Nimal De Silva, Smitarani Mohanty, and Cole MacDonald for their extended cooperation in instrumental troubleshooting during the ICP-MS sample run.

I am particularly indebted to Dr. Xiaolei Zhao for his generous help in AMS data collection and subsequent analysis. In fact, the whole AMS study was accomplished under his active guidance, I owe to him.

Many thanks to Dr. Barbara Francisco for her assistance in placing orders of research materials and other essential lab items. Her curious fashion in maintaining an ordered workplace is truly rewarding.

Special thanks to Monika Wilk for providing groundwater samples.

I would like to thank Timothy Roy and Simon Hayles for their time and effort for the painstaking revision of the early manuscript.

My warm appreciation goes to all my colleagues and friends, especially Uttam Das and Mosammat Khan, for helping me out in different stages of need.

Thanks to all support members, and will wishers, who, directly or indirectly, have helped making my goal a success.

I wish to convey my gratefulness to the Department of Chemistry for offering me the initial graduate placement and providing financial support. It's my pleasure to have had the opportunity to be a member of the NSERC funded CREATE-REACT outreach program, my sincere gratitude goes to them.

Last, but not the least, I am particularly indebted to my family members, especially my parents, wife, and lovely children – Mahi, Marium and Maimuna – for their patience, inspiration, and support over the long-period of my oversea stay.

Dedication

This thesis paper is dedicated to

Prof. Robert Jack Cornett

(1954 – 2017)

Jack, a former Canada Research Chair in Radiochemistry and Environmental Health, University of Ottawa, was my supervisor and research mentor. He will be survived by us for his life-long commitment to science and innovation. Jack died in Ottawa in a tragic bicycle accident at the crossroads of my graduate program.

Table of Contents

Papers and presentations

1. **M. M. Rahman**, C. MacDonald & R. J. Cornett. (**2018**). Separation of tin from tellurium: performance of different extraction chromatographic materials, *Separation Science and Technology*, 53 (13): 2055–2063.
2. **M. M. Rahman**, C. MacDonald & R. J. Cornett. (**2017**). Separation of tin from tellurium: an analytical survey on different absorbing materials for AMS sample preparation, Poster presentation in the 14th International Conference on Accelerator Mass Spectrometry, University of Ottawa, August 14–15.
3. **M. M. Rahman**, C. MacDonald & R. J. Cornett. (**2017**). Separation of tin from tellurium: an analytical survey on different substrates, Abstract in the 14th International Conference on Accelerator Mass Spectrometry: Conference Program Posters, Abstract ID 299, Tract classification Poster: SPT, University of Ottawa, August 14–15.
4. **M. M. Rahman** & R. J. Cornett. (**2017**). Tin and tellurium separation: an analytical survey on adsorbents, 3MT Presentation, NSERC CREATE-REACT Summer School and Research Day, Laval University, Quebec, June 11–14.
5. **M. M. Rahman** & R. J. Cornett. (**2016**). Separation of Sn from Te, 3MT Presentation, NSERC CREATE-REACT Summer School and Research Day, University of Ottawa, August 28–September 1.

Papers in progress

1. **M. M. Rahman**, W. L. Kieser & I. D. Clark. (**2018**). Half-lives and production schemes of tin isotopes (drafting finished).
2. **M. M. Rahman**, W. L. Kieser & I. D. Clark. (**2018**). Separation of tin from tellurium in presence of chloride and sulfate interferences (in progress).
3. **M. M. Rahman**, X. Zhao, W. L. Kieser & I. D. Clark. (**2018**). AMS detection of ^{126}Sn in environmental samples (in progress).
4. **M. M. Rahman**, W. L. Kieser & I. D. Clark. (**2018**). Production, half-life and detection of ^{126}Sn (in progress).

List of Tables

List of Figures

List of Symbol and Abbreviations

Symbol/Abbreviations	Definition
AMS	accelerator mass spectrometry
cm	centimeter
CPS	count per second
d	day
DBT	dibutyltin
FC	faraday cup
fg	femtogram
ft	feet
g	gram
GIC	gas-filled ionization chamber
ICP-MS	inductively coupled plasma mass spectrometry
ISA	isobaric separation of anions
IUPAC	international union of pure and applied chemistry
kV	kilovolt
kg	kilogram
L	liter
m	minute
µg	microgram
MA	magnetic analyzer
mg	milligram
MMT	monomethyltin
MV	megavolt
nA	nano ampere
ng	nanogram
NMR	nuclear magnetic resonance
pA	pico ampere
ppb	parts per billion
ppm	parts per million
ppt	parts per trillion
rms	root mean square
s	second
SPE	solid phase extraction
SSI	slow sequential injection
T	tesla
TBT	tributyltin
TMT	trimethyltin
TDI	tolerable daily intake
V	volt
WHO	world health organization
Y	year

Appendices

Chapter 1:

Introduction

1.1 Tin in the environment

1.1.1 Tin in ancient time

The name 'tin' is coined from the Anglo-Saxon language, with meaning of unknown origin.[1] The chemical symbol of the element, Sn, is derived from the Latin word *stannum* that stands for alloy containing lead.[2] The element was known to human civilization from prehistoric times as a component of the alloy bronze.[3] The 'Bronze Age' can be traced back to *ca.* 3000–1200 BC, especially in Southeastern Europe.[4] In China, during the Shang Dynasty in the late second millennium BC, a highly sophisticated bronze technology was developed which subsequently spread out over Asian countries and other regions of the world.[5] The importance of bronze materials is now accredited in the field of chronological study, trade, warfare, craft production and many more.[6]

1.1.2 Occurrence of tin

Tin is a rare metal which is usually present as cassiterite (SnO_2) commonly associated with granites.[4] Tin can also be concentrated as sulfides, like stannite (Cu_2FeSnS_4), teallite ($PbSnS_2$), canfieldite (Ag_8SnS_6), and cylinderite ($PbSn_4FeSb_2S_{14}$).[7] The natural abundance of tin in the environment is quite low, the concentrations of tin in the earth crust range from 0.1–5.5 ppm.[8–10]

1.1.3 Importance of tin

Tin metal is usually mixed with copper to make hard and tough alloys.[5] Tin-bronze (alloy of ~ 90% copper and ~ 10% tin) was extensively used in weapons, tools, and ornaments.[4] Tin is used to produce a large number of organotin compounds which are extensively used in commercial applications,[11] like wood preservation,[12] industrial catalysts,[13] biocides,[14] heat and light stabilizers for polyvinyl chloride (PVC) materials,[15] and as fluids in electric transformers and capacitors.[16] Tributyltin (TBT) has long been used as antifouling paint in ships and marine vessels.[12,17] However, due to severe ecotoxicological threats, the application of TBT-based antifouling agents on ship paintings was banned in 2008.[13,18]

1.1.4 Tin in food

The geochemical characteristics of tin are unique because of its mobilization and biomethylation to organotin species, such as tributyltin (TBT), dibutyltin (DBT), and monobutyltin (MMT).[15,19] The human body is exposed to tin mainly from the consumption of seafood that contains butyltin species.[15] However, tin can enter into human body from other sources as well. For example, studies reveal that organotin compounds leaching from polyvinyl chloride (PVC) and other household items enter into foodstuffs and cause adverse health effects.[15] It is reported that up to 138 μg/L of Sn, as DBT, was found in wine samples of Canadian super markets.[20] Another study says, 0.05 – 0.15 μg/L of Sn, again as DBT, was detected in Portuguese wines.[15] The present tolerable daily intake (TDI) of DBT is 5 μg of Sn/kg of body weight.[20]

1.2 Properties of tin

1.2.1 Common properties of tin

Some common properties of tin are presented in Table 1.1. One interesting characteristic of tin is that it possesses a magic number. The magic numbers are the result of filling a set of six sub-shells, the known magic numbers are 2, 8, 20, 28, 50, 82 and 126.[21]

Table 1.1: Some common properties of tin.

Parameter	Value	Ref.
Atomic number, Z	50	[2]
Atomic weight, reported in 1811 by Gay-Lussac	117.65	[22]
Atomic weight, reported in 1991 by IUPAC	118.710(7)	[23]
Boiling point	2270 °C	[2]
Density, reported in 1902	7.300	[24]
Electron affinity, eV	1.2	[25]
Electronic configuration	$1s^2 2s^2 2p^6 3s^2 3p^6 3d^{10} 4s^2 4p^6 4d^{10} 5s^2 5p^2$	[2]
Electronegativity	1.96	[26]
First discovery of tin isotope, reported in 1922 by Aston	$^{119–122}$Sn, ^{124}Sn	[27]
Last discovery of tin isotope, reported in 2015 by Lorusso	^{139}Sn	[28]
Ionization potential, eV	7.3	[29]
Melting point	231.9681 °C	[2]
Main oxidation states	+2, +4	[30]
Valence	2, 4	[31]
Specific gravity	5.75 (gray), 7.31 (white)	[2]
Number of isotopes discovered	41	[32]
Number of stable isotopes	10, the greatest number of stable isotopes among all elements in the periodic table	[33, 34]
Self-conjugated nuclide ($N = Z$)	^{100}Sn,$_{N = 50,\ Z = 50}$	[35, 177]
Doubly magic isotopes	^{100}Sn,$_{N = 50}$, ^{132}Sn,$_{N = 82}$	[36, 37]
Isotope with the smallest mass unit	^{99}Sn (98.948530 ± 540)	[32]

Isotope with the largest mass unit	^{139}Sn (138.958730 ± 540)	[32]
Isotope with the shortest half-life	^{138}Sn (210 ± 45 ns)	[38]
Isotope with the longest half-life	^{126}Sn ((2.35 ± 0.2) × 10^6 y))	[39]

1.2.2 Redox properties

In normal environmental conditions, tin compounds are only sparingly soluble in water, and are likely to partition to soils and sediments.[7] Tin can exist in both inorganic and organic forms;[40] the common oxidation states of tin are: –II, 0, +II, and +IV.[41] Although the precise oxidation state of ^{126}Sn in nuclear waste and spent fuel is unknown, the divalent and tetravalent oxidations states are predominant species found in natural waters.[42]

In normal natural conditions, Sn(II) is soluble at concentrations of $<10^{-6}$ M, whereas the solubility of Sn(0) and Sn(IV) is very limited.[43,44]

$$SnO_{2(s)} + 4H^+ = Sn^{4+} + 2H_2O, \quad K_{sp} = 2.1 \times 10^{-8}$$

$$SnO_{(s)} + 2H^+ = Sn^{2+} + H_2O, \quad K_{sp} = 11.8$$

The most important considerations that affect the speciation of tin is pH.[45] At elevated pH, tin (like arsenic) usually stays as anionic forms: SnO_3H^-, SnO_3^{2-}, and at pH 7.0 or below, cationic tin species predominate: $Sn(OH)^+$ and $Sn(OH)_2^{2+}$.[40] At pH greater than 2.0, the solubility of tin compounds is rather low.[45] The pe-pH diagram of tin is presented in Fig. 1.1.

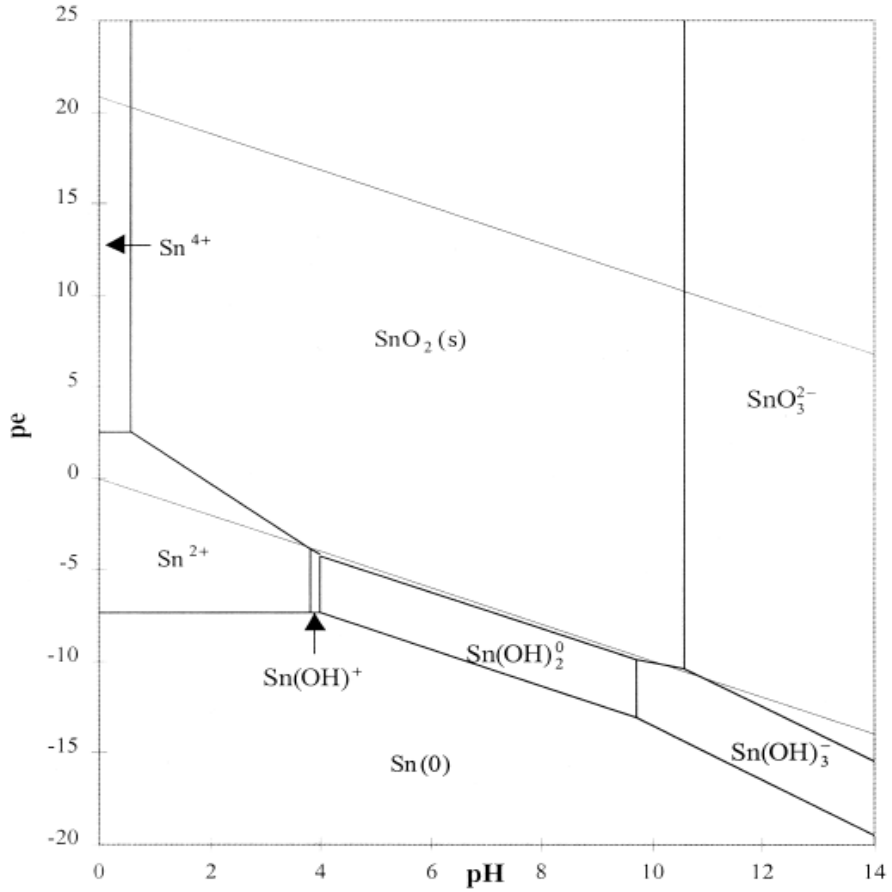

Fig. 1.1 The pe-pH diagram of tin with a dissolved tin activity of 10^{-10} mol L^{-1}.[41]

In natural waters, both Sn(II) and Sn(IV) tend to hydrolyze to form aqueous species.[41] For Sn(IV), the available aqua-complexes are $SnO(OH)_3^-$ at pH ≥ 8.0 and $SnO(OH)_2^0$ at pH < 7.0, whereas for Sn(II), the predominant species in normal pH is mainly $SnO(OH)_2^0$,[41] along with the formation of polymeric forms of Sn(II), like $Sn_2(OH)_2^{2+}$ and $Sn_3(OH)_4^{2+}$.[46]

1.3 Toxicity of tin compounds

1.3.1 Factors affecting toxicity

Tin is an essential element for plant and animal life, inorganic tin is considered as non-toxic.[47,199] Aquatic microorganisms, especially algae and cyanobacteria, can absorb tin compounds and transfer them to higher trophic levels, and undergo biomethylation.[40] The

toxicity of tin compounds usually depends on the state of oxidation states, inorganic or organic forms, and the nature of organic moiety.[19] Though inorganic tin is considered as non-toxic, organotin compounds, particularly butyltin species, are highly toxic.[48] Usually, trialkyltins are more toxic than mono- or disubstituted congeners.[48] Also, the length of alkyl group causes a sharp decrease of biocidal activity.[48]

1.3.2 Toxicity to invertebrates

Inorganic Sn(IV) compounds reportedly show severe toxicity to phytoplankton cyanobaterium, *Synechocystis aquatilis*.[19,40] Living biota are extremely vulnerable to tributyltin toxicity.[49] Many organotin compounds are susceptible to soil microorganisms.[50] Reports reveal, TBT released from boat antifoulants is responsible for poor spatfall and shell thickening in cultivated oysters, *Crassostrea gigas.*[51] Marine mollusc and common mussels are greatly at risk due to TBT induced aqua-toxicity.[52,53] TBT causes "imposex" – a phenomenon in which male sex characteristic develops on female – condition on marine biota, especially on gastropods,[54] it is estimated that more than 260 species of gastropods are affected worldwide.[55]

1.3.3 Toxicity to mammals

Although exposure of butyltin compounds to human body and their toxic effects are not well documented, organotin compounds, as a whole, are considered as endocrine disrupting agents.[20,56] Tributyltin is responsible for the growth inhibition and immunosuppressant effects on marine mammals.[16,57] Trimethyltin causes neuroinflammation,[58] nystagmus imbalance,[59] cognitive impairment,[60] ataxia,[61] and seizures[62] on mammalian bodies. Reports reveal, the administration of monomethyltin to pregnant rats produces impaired offspring with potential apoptotic risk.[63]

1.4 Isotopes of tin

1.4.1 Discovery of tin isotopes

Almost a century ago, F.W. Aston, while working with tin tetramethide on the "Half Tone" photographic plate at the Cavendish Laboratory, Cambridge, UK, surprisingly observed eight spectral lines on the newly installed (in 1919) mass-spectrograph, shown in Fig. 1.2, which correspond atomic weights of 116 (c), 117 (f), 118 (b), 119 (e), 120 (a), 121 (h), 122 (g), and 124 (d). The letter in the bracket indicates intensity, corresponding to chemical weight of tin 118.7. He assumed that these lines might have appeared due to the presence of tin isotopes. However, the assignment of the extremely faint line 121 (h) was uncertain.[27]

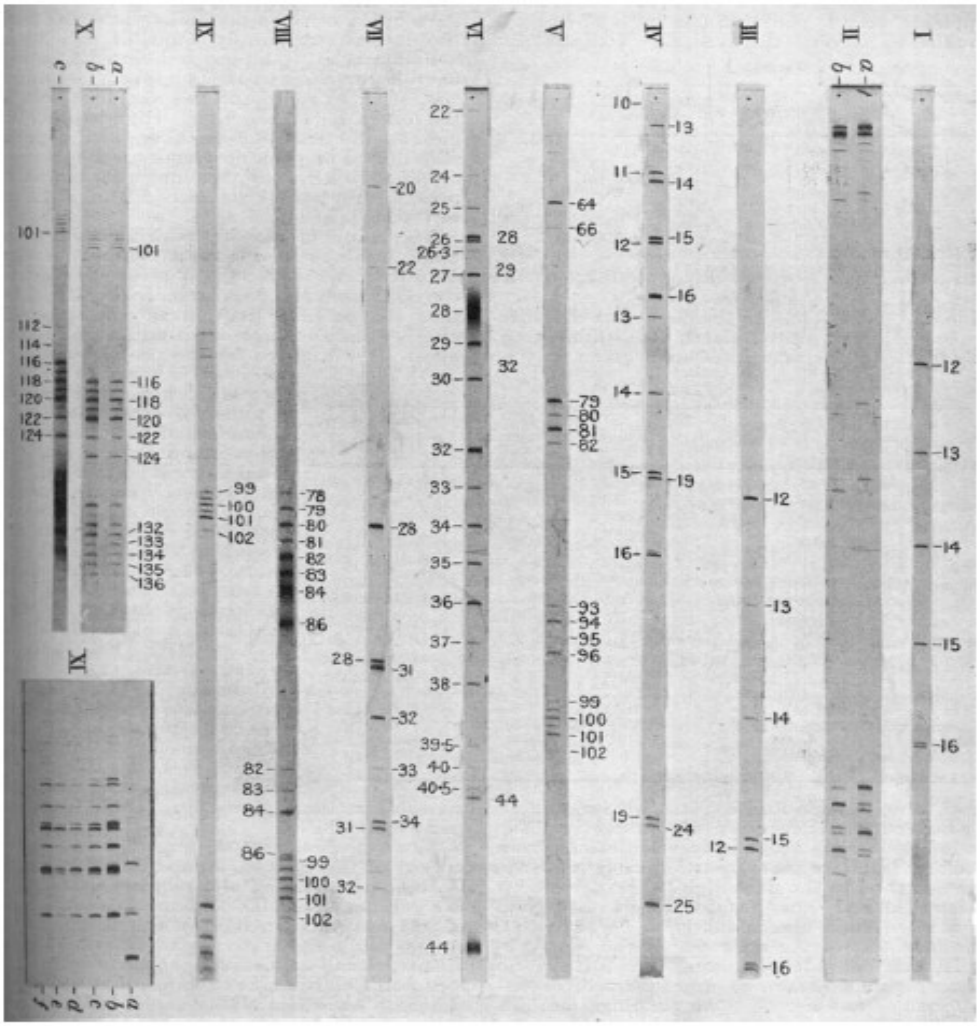

Fig. 1.2 An early mass-spectrograph (1927). The mass analyzer was installed in 1919 at the Cavendish Laboratory, Cambridge, UK. The resolving power of the instrument was sufficient to separate mass lines differing by about 1 in 130, and its accuracy of measurement was about 1 in 1000. X–(*a*) and (*b*) spectra display the even spacing of tin monomethide and xenon lines, while the (*c*) spectrum shows tin isotopes with long exposure time.[63,178]

1.4.2 Stable tin isotopes

Approximately 3,500 stable and radio-nuclides have been identified so far,[65] of which tin possesses 41 isotopes (mass range 99 to 139): 10 stable, 14 neutron-depleted, and 17 neutron-rich isotopes.[32,66] Tin has the greatest number of stable isotopes among all elements in the periodic table.[33,67] Abundances of stable tin isotopes are presented in Table 1.2.

Table 1.2: Abundances of stable tin isotopes.[1]

Isotope $Z = 50$	N	A	***RMS* nuclear charge radii (*fm*)*** [68]	**Produced by** [67]	**Modes of nucleosynthesis** [69,70]	**Abundance (per cent)**	
						Aston (1936) [71]	**IUPAC (1997)** [72]
^{112}Sn	62	112	4.5948	*p*–process	Proton capture	1.1	0.97(1)
^{114}Sn	64	114	4.6099	*p*–process	Proton capture	0.8	0.66(1)
^{115}Sn	65	115	4.6148	*p*–, *r*–, *s*–processes	Proton and neutron captures (rapid and slow)	0.4	0.34(1)
^{116}Sn	66	116	4.6250	*s*–process	Slow neutron capture	15.5	14.54(9)
^{117}Sn	67	117	4.6302	*r*–, *s*–processes	Slow and rapid neutron captures	9.1	7.68(7)
^{118}Sn	68	118	4.6393	*r*–, *s*–processes	Slow and rapid neutron captures	22.5	24.22(9)
^{119}Sn	69	119	4.6438	*r*–, *s*–processes	Slow and rapid neutron captures	9.8	8.59(4)
^{120}Sn	70	120	4.6519	*r*–, *s*–processes	Slow and rapid neutron captures	28.5	32.58(9)
^{122}Sn	72	122	4.6634	*r*–process	Rapid neutron capture	5.5	4.63(3)
^{124}Sn	74	124	4.6735	*r*–process	Rapid neutron capture	6.8	5.79(5)

1.4.3 Radioactive tin isotopes

Short-lived tin isotopes: Among fortyone radioisotopes of tin,[32] the 'doubly magic' ^{100}Sn nucleus ($N = 50$ neutrons and $Z = 50$ protons) possesses completely occupied shells.[73] The ^{113}Sn has a half-life of 115 days, while the half-life of ^{123}Sn is 129 days.[21] The half-life of

^{126}Sn is much longer at ~10^5 y,[74] other isotopes of tin possess half-lives in the order of hours to seconds.[21] Table 1.3 summarizes all known tin isotopes and their decay properties.

Table 1.3: Decay properties of tin isotopes.[32,75,179]

Isotope (Z = 50)	N	**Nuclear *rms* charge radii (fm)** [68]	**Gram atomic weight (g)**	**Half-life**	**Beta-decay energy (MeV)**	**Daughter isotope**
^{99}Sn	49		98.948530#	...	β^+ = 13.430#	
^{100}Sn	50		99.938500	1.16 s	β^+ = 7.030	^{100}In
^{101}Sn	51		100.935260	1.97 s	β^+ = 8.310#	
^{102}Sn	52		101.930290	3.8 s	β^+ = 5.760	^{102}In
^{103}Sn	53		102.928100	7.0 s	β^+ = 7.660	
^{104}Sn	54		103.923105	20.8 s	β^+ = 4.556	^{104}In
^{105}Sn	55		104.921268	34 s	β^+ = 6.303	
^{106}Sn	56		105.916957	1.92 m	β^+ = 3.254	
^{107}Sn	57		106.915714	2.90 m	β^+ = 5.052	
^{108}Sn	58	4.5605	107.911894	10.30 m	β^+ = 2.050	^{108}In
^{109}Sn	59	4.5679	108.911293	18.0 m	β^+ = 3.859	
^{110}Sn	60	4.5785	109.907845	4.154 h	β^+ = 0.628	
^{111}Sn	61	4.5836	110.907741	35.3 m	β^+ = 2.453	
^{112}Sn	62	4.5948	111.904825	STABLE		
^{113}Sn	63	4.6015	112.905176	115.09 d	β^+ = 1.039	^{113}In
^{114}Sn	64	4.6099	113.902780	STABLE		
^{115}Sn	65	4.6148	114.903345	STABLE		
^{116}Sn	66	4.6250	115.901743	STABLE		
^{117}Sn	67	4.6302	116.902954	STABLE		
^{118}Sn	68	4.6393	117.901607	STABLE		
^{119}Sn	69	4.6438	118.903311	STABLE		
^{120}Sn	70	4.6519	119.902202	STABLE		
^{121}Sn	71	4.6566	120.904243	27.03 h	β^- = 0.4031	^{121}Sb
^{122}Sn	72	4.6634	121.903444	STABLE		
^{123}Sn	73	4.6665	122.905725	129.2 d	β^- = 1.4079	^{123}Sb
^{124}Sn	74	4.6735	123.905277	STABLE		

Table 1.3: Decay properties of tin isotopes *(continued)*

Isotope ($Z = 50$)	N	Nuclear *rms* charge radii (fm)	Gram atomic weight (g)	Half-life	Beta-decay energy (MeV)	Daughter isotope
^{125}Sn	75	4.6765	124.907786	9.64 d	β^- = 2.3599	
^{126}Sn	76	4.6833	125.907659	235 ky	β^- = 0.380	^{126}Sb
^{127}Sn	77	4.6867	126.910390	2.10 h	β^- = 3.229	^{127}Sb
^{128}Sn	78	4.6921	127.910507	59.07 m	β^- = 1.268	^{128m}Sb
^{129}Sn	79	4.6934	128.913482	2.23 m	β^- = 4.038	^{129}Sb
^{130}Sn	80	4.7019	129.913975	3.72 m	β^- = 2.153	^{130}Sb
^{131}Sn	81	4.7078	130.917053	56 s	β^- = 4.717	^{131}Sb
^{132}Sn	82	4.7093	131.917824	39.7 s	β^- = 3.089	^{132}Sb
^{133}Sn	83		132.923914	1.46 s	β^- = 8.050	^{133}Sb
^{134}Sn	84		133.928680	890 ms	β^- = 7.587	^{134}Sb
^{135}Sn	85		134.934909	515 ms	β^- = 9.058	
^{136}Sn	86		135.939990	350 ms	β^- = 8.610#	^{137}Sb
^{137}Sn	87		136.946550#	273 ms	β^- = 10.270#	^{137}Sb
^{138}Sn	88		137.951840#	150 ms	β^- = 9.360#	^{137}Sb
^{139}Sn	89		138.958730#	130 ms	β^- = 100	

not purely experimental value

Long-lived tin isotopes: ^{126}Sn is the only long-lived radioisotope of tin, with a half-life of 2.35×10^5 years.[76] ^{126}Sn is a beta (β_{max} 252 keV) and gamma emitting radionuclide,[39] it produces two short-lived daughters, ^{126m}Sb (19 min) and ^{126}Sb (12.4 d), both emit γ-rays at the same energy (87.6 and 86.9 keV).[39] The natural abundance of ^{126}Sn/Sn in the Earth's crust is approximately 10^{-14}.[77] Spontaneous fissions of ^{238}U and ^{239}Pu,[78] nuclear weapon testing fallout,[79] and nuclear fuel reprocessing plants[79] are the main contributers to the anthropogenic input of ^{126}Sn in the environment. Though the fission-yield of ^{126}Sn is very low, only 0.065% by thermal neutron capture of ^{235}U,[80] its long half-life makes it one the most persistent anthropogenic radioisotopes in the environment.[41,77]

1.4.4 Half-lives of tin radioisotopes

The half-life measurement of tin can be traced back to 1936 (April), done by R. Naidu at the Birkbeck College, UK. Geiger-Müller counters filled with air were irradiated with slow neutrons from a radon-beryllium source and the subsequent induced radioactivity of tin was measured. The experiment found two half-lives for the elemental tin (8 ± 2 minutes and 18 ± 2 minutes),[81] apparently having had no understanding of the half-lives of radioactive tin. A few months later (June 1936), J. J. Livingood,[82] while working on the 5-MeV cyclotron in California reported the half-life of the ^{121}Sn isotope, the very first attempt to measure the half-life of any tin isotope. He reported two half-lives for ^{121}Sn: 24 ± 2 hours and 28 ± 2 hours. The present accepted half-life of ^{121}Sn is 27.03 h.[75] The half-lives of all tin isotopes identified so far are presented in Table 1.3.

1.4.5 Decay of tin isotopes

^{126}Sn decays to ^{126}Te (Fig. 1.3) with a half-life of 2.35×10^5 years, *via* the formation of ^{126}Sb intermediate.[76] The transition of ^{126}Sn to ^{126}Sb is followed by the emission of low-energy gamma ray.[77] In the solar system, ^{126}Te is primarily produced by the decay of ^{126}Sn.[83] In order to study the nucleosynthetic processes of ^{126}Te, the elemental fractionation of the parent (Sn) from the daughter (Te) is important.[84]

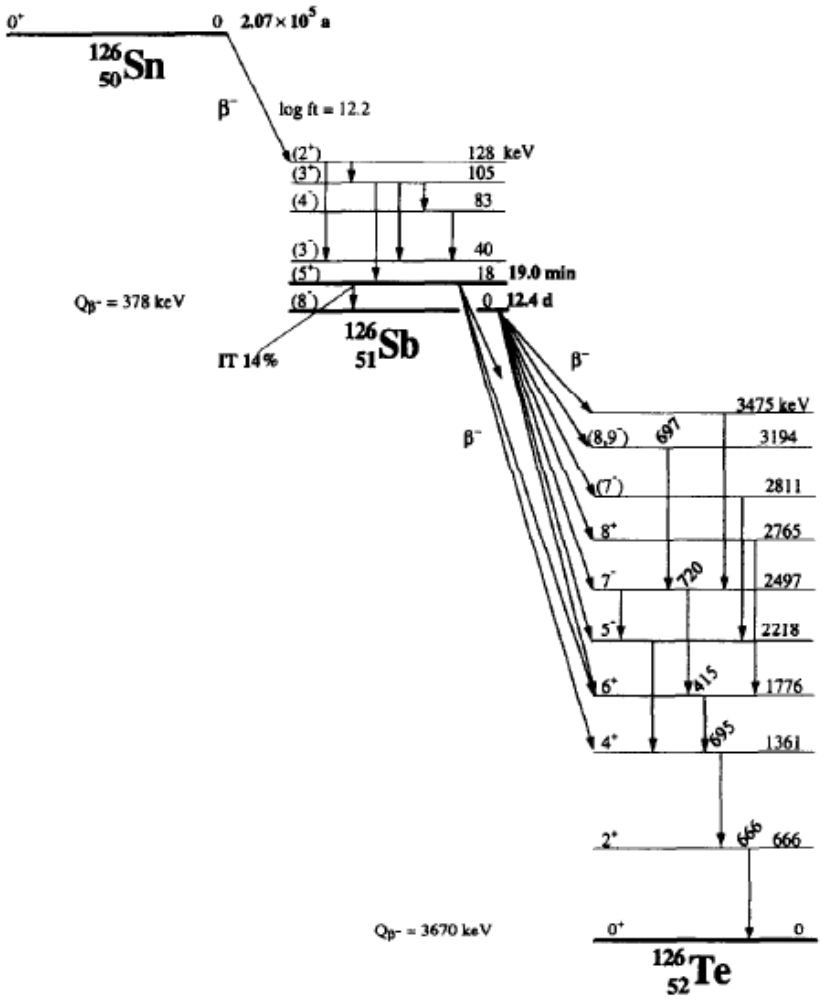

Fig. 1.3 Decay scheme of ^{126}Sn to ^{126}Te.[77]

1.4.6 Applications of tin isotopes

Therapeutic applications: ^{117m}Sn ($T_{½}$ = 13.76 d, γ = 159 keV, 86.4%) is a promising radionuclide with a wide ranges of diagnostic and therapeutic applications,[85,86] especially for single photon emission computed tomography (SPECT).[87] Unlike other therapeutic radioisotopes, e.g., ^{89}Sr and ^{153}Sm, ^{117m}Sn is not a beta-emitter, rather it decays through the emission of low-energy electrons (126.8, 129.4, and 151.6 keV) with very short ranges (0.22 – 0.29 mm) that can destroy body tumors without damaging healthy cells.[88–92] For its long half-life, higher than ^{153}Sm ($T_{½}$ = 46.3 h)[93] and ^{186}Re ($T_{½}$ = 3.78 d),[94] and low myelotoxic effect,[95] ^{117m}Sn isotope is particularly important in the post-therapy

imaging for the palliation of painful bone-metastases,[85,96,97] radiosynovectomy,[94] radioimmunotherapy,[98] atherosclerotic disease,[91] leukemia,[99] as well as bone and breast cancers.[100,101]

Spectroscopic applications: Among ten stable isotopes of tin, three – ^{115}Sn, ^{117}Sn and ^{119}Sn – possess an odd number of neutrons and all of them have a nuclear spin of one-half, I = ½. These isotopes are extensively used in solid state NMR,[102–105] while ^{119}Sn is widely used in Mössbauer spectroscopy.[106–108]

1.5 Tellurium in the environment

1.5.1 Abundances of tellurium

Tellurium (Te) is a metalloid that is extensively used in electronic circuits and devices.[109] The name is derived from the Latin word *Tellus*, after the Roman goddess.[1] Tin, tellurium, and lead are the three most highly enriched metals in atmospheric particulate matter compared against the Earth's crust.[110] However, the natural abundance of tellurium is very low,[111] in the range of 1–5 μg/kg (ppb).[112] Te is commonly found in sulfide and gold ores.[113,114] Tellutium is considered non-esssential and non-beneficial to animals and plants.[201]

1.5.2 General properties of tellurium

Tellurium (like Cd and In) is a good indicator for estimating the role of sulfides in geological systems.[115] The common oxidation states of tellurium are: –II, 0, IV, and VI.[116] Some common properties of Te are presented in Table 1.4.

Table 1.4: Some common properties of tellurium.

Parameter	Value	Ref.
Atomic number, *Z*	52	[2]
Atomic weight	127.60(3)	[23]
Abundance	0.027 ppm (27 ppb)	[117]
Boiling point	989.8 °C	[2]
Electronic configuration	$1s^2 2s^2 2p^6 3s^2 3p^6 3d^{10} 4s^2 4p^6 4d^{10} 5s^2 5p^4$	[2]
Electron affinity, eV	1.971	[25]
Melting point	449.5 °C	[2]
Valence	2, 4, 6	[2]
Specific gravity, 20 °C	6.24	[2]
Number of isotopes	39	[32]
Number of stable isotopes	8	[83]
Isotope with smallest mass unit	^{105}Te (104.943300)	[32]
Isotope with largest mass unit	^{143}Te (142.956760)	[32]

1.5.3 Redox properties of tellurium

In environmental conditions, tellurium is found as telluride (Te^{2-}, H_2Te), tellurite (TeO_3^{2-}, tellurious acid, H_2TeO_3), and tellurate (TeO_4^{2-}, telluric acid, H_2TeO_4).[117–119] Te(VI) is more thermodynamically stable than Te(IV).[117] The Eh–pH diagram of tellurium is presented in Fig. 1.4.[120] In normal pH conditions, the Te(IV) form usually stays at a ratio of $HTeO_3^-$: TeO_3^{2-} of approx. 10^4 : 1.[121]

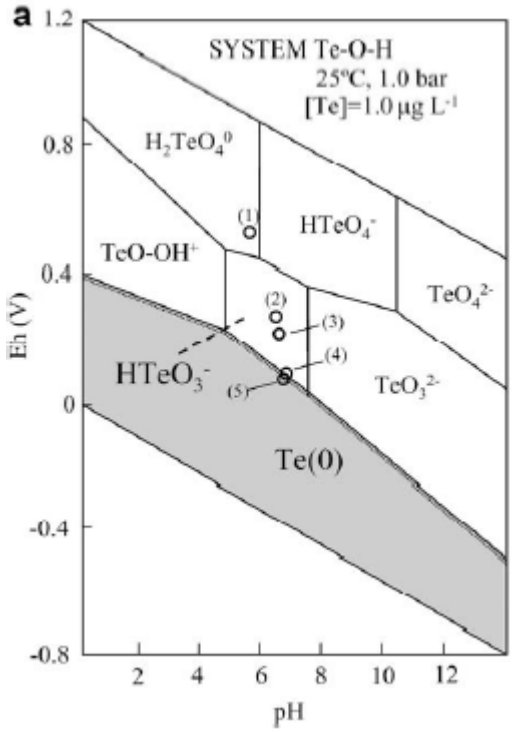

Fig. 1.4. Eh–pH diagram of tellurium.[120]

1.5.4 Isotopes of tellurium

Te has 39 radioisotopes (masses 105 to 143),[32] among these, eight are stable (^{120}Te, ^{122}Te, ^{123}Te, ^{124}Te, ^{125}Te, ^{126}Te, ^{128}Te and ^{130}Te).[75,83] The half-life of ^{128}Te is around $(2.5 \pm 0.3) \times 10^{24}$ y, which is the largest measured half-life of all known radioisotopes.[122] ^{130}Te also possesses a long half-life ($(7.0 \pm 1.0) \times 10^{20}$ y).[122] The longer half-lives of ^{128}Te and ^{130}Te virtually make them stable. The atomic masses and isotopic composition of stable tellurium isotopes are presented in Table 1.5.

Table 1.5: Atomic mases and isotopic compositions of tellurium.[1]

Isotope	Atomic mass/u	Isotopic abundance, % (1998) [72]	Mole fraction (2003 & 2016) [1, 123]
^{120}Te	119.904026(11)	0.09(1)	0.0009(1)
^{122}Te	121.9030558(29)	2.55(12)	0.0255(12)
^{123}Te	122.9042711(20)	0.89(3)	0.0089(3)
^{124}Te	123.9028188(16)	4.74(14)	0.0474(14)
^{125}Te	124.9044241(20)	7.07(15)	0.0707(15)
^{126}Te	125.9033049(20)	18.84(25)	0.1884(25)
^{128}Te	127.9044615(19)	31.74(8)	0.3174(8)
^{130}Te	129.9062229(21)	34.08(62)	0.3408(62)

The major challenge in the determination of ^{126}Sn by mass spectrometry is the isobaric interference of ^{126}Te (18.84% abundance),[72] a decay product of ^{126}Sn. The stable ^{126}Te isotope produces a strong background during the AMS quantification of ^{126}Sn.[124] Fortunately, other short-lived daughter products of ^{126}Sn, e.g., ^{126m}Sb (Z = 51, $T_{½}$ = 19 min) and ^{126}Sb ($T_{½}$ = 12 d), do not significantly interfere in the measurement of ^{126}Sn.[78]

1.6 Research goal and objectives

1.6.1 Rationale of the present study

The identification of tin radioisotopes in environmental samples is crucial for several reasons:

- tin is considered as a potential candidate for the study of isotopic anomalies,[67]
- tin is easily biomethylated by microorganisms.[40] Methylated tin compounds are toxic to aquatic species and mammalian body,[20] therefore, biomonitoring of isotopic organotins is of great importance,

- the long-lived isotope of tin, ^{126}Sn ($T_{½}$ ~10^5 y), draws much attention in nuclear waste disposal considerations.[125] Moreover, the measurement of ^{126}Sn in environmental samples is crucial for long-term nuclear waste storage strategies[126,127] and nuclear waste treatment practices.[39]
- the measurement of ^{126}Te in the solar system requires a better understanding about the abundance of its parent isotope, ^{126}Sn.[84]

1.6.2 Specific research objectives

Our present study will focus on two mains aspects:

i) Separation of tin from tellurium to suppress isobaric interferences of Te during analysis by mass spectrometry, and

ii) The AMS measurement of ^{126}Sn in environmental samples.

Chapter 2:

Separation of tin from tellurium

2.1 Research background

2.1.1 Importance of isobaric separation

The measurement of the concentration of long-lived radionuclides in environmental samples is critical to assess their biological and ecological effects,[128] and nuclear waste disposal management plan.[129] Long-lived radionuclides are typically measured using mass spectrometry, like accelerator mass spectrometry (AMS)[130] and inductively coupled plasma mass spectrometry (ICP-MS).[131] These techniques require the separation of isobaric interferences from the isotope of interest. In this study, our goal is to measure the concentration of ^{126}Sn in environmental samples by AMS. However, the presence of stable ^{126}Te interferes during the AMS measurement of ^{126}Sn.[83,124] Therefore, the first phase of our project aims to separate tin from tellurium by chemical treatment.

2.1.2 Selection of separating method

A separation or preconcentration of metal ions is necessary to avoid background interferences and in fixing the minimum level of detection. The most widely used techniques for separation include solvent extraction,[132] anion exchange,[133] membrane filtration,[134] coprecipitation,[135] cloud point extraction,[136] and solid phase extraction.[137] Among these, solid phase extraction (SPE) is the most favored technique to researchers for its enhanced selectivity and sensitivity.[138] SPE also offers advantages: the elution of

adsorbed analyte with small volume of solvent,[139] high adsorption capacity,[140] stability in severe conditions,[141] cost effective,[142] and ensures less extraction time.[143] In our present study, we have selected solid phase extraction (SPE) technique to quantitatively separate tin from tellurium.

2.1.3 Choice of instrumental technique

In the laboratory, atomic absorption spectrometry,[144] flame atomic absorption spectroscopy (FAAS),[145] electrothermal atomic absorption spectrometry,[146] graphite furnace atomic absorption spectrometry (GF-AAS),[147] atomic fluorescence spectrometry (AFS),[148] and inductively coupled plasma-mass spectrometry (ICP-MS)[149] are the most widely used techniques for the routine analysis of metal ions. ICP-MS is often superior to other traditional techniques for its ultra-low detection capability[150] and multi-elemental analyzing characteristics down to nanogram levels, Fig. 2.1.[58,151]

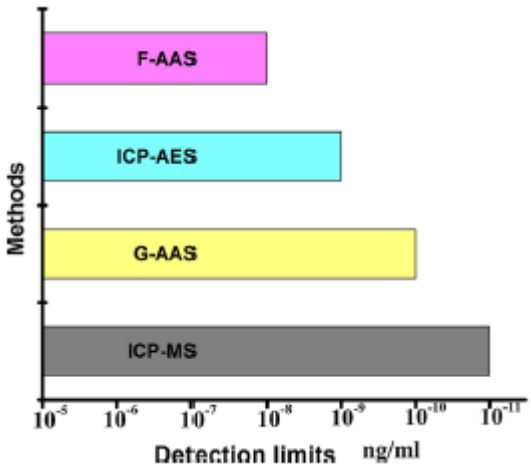

Fig. 2.1 Detection limits by different techniques.[58]

2.2 Previous works on tin separation

2.2.1 Separation of Sn element

The analysis of bronze samples that contained a mixture of elements (Cu, Zn, Cd, In, Sn, Sb, Te, Pb) was carried out by Balliana et al.[152] in dilute HCl medium. The elements were first separated on TRU-Spec anion exchange column in 1 M HCl, and then eluted by 1 M HNO_3. The recovery of Sn was around 100%.

Mason et al.[4] have determined the composition of Sn isotope in 52 Balkan artifacts using MC-ICP-MS technique and found that tin content in artifacts was in the range of 2.1 to 17.8 wt%.

Ahn and Lee[153] have extracted a mixture of Sn, Sb, Bi, As, Cu, Pb, and Zn on tri-n-butylphosphate (TBP) and observed that the extraction of tin is 91% in 9.0 mol L^{-1} HCl, whereas the stripping of tin is 99% at 2.0 mol L^{-1} of NaOH.

A preconcentration of tin from natural water samples was carried out by Costa et al.[154] on oxidized multiwall carbon nanotubes and the characterization of the eluent was done by electrothermal atomic absorption spectrometry. The adsorbed tin was eluted by 2.7 mol L^{-1} of HNO_3 and the elution was 91.5%.

2.2.2 Separation of ^{126}Sn

Zhang et al.[39] have developed a method for the separation of ^{126}Sn isotope. Tin was precipitated as $Sn(OH)_4$ in concentrated NH_4OH, dissolved in HCl, and then transferred to a separatory funnel. The extraction of tin was done with methyl isobutyl ketone.

Dulanská et al.[125] have separated ^{126}Sn isotope from radioactive waste samples using TEVA resin. Tin was first precipitated in ammonium sulfide in 0.5 mol L^{-1} HCl, passed through TEVA column, and then eluted with 2 mol L^{-1} HNO_3. The tin fraction was

measured by gamma spectroscopy. The average activity of ^{126}Sn was observed around 5 Bq L^{-1}.

Andris and Beňa[155] have separated ^{126}Sn isotope using TBP chromatographic resin in hydrochloric acid medium at concentration of 6 mol L^{-1}. Tin was quantitatively stripped off from the resin by 0.1 mol L^{-1} HCl. The characterization of ^{126}Sn was done by gamma spectrometry.

2.3 Experimental

2.3.1 Solid phase extraction by resins

The distribution coefficient of substrates (K_D) into two phases can be exploited to separate a desired analyte from its interfering ions.[128] The distribution coefficient was calculated as follows:

K_D = (metal retained per gram of resin)/(metal retained per mL of liquid)

= mg/g ÷ mg/mL

Therefore, the units of K_D is mL g^{-1}.

In our present study, the distributions of tin and tellurium in solid (resin) phase and aqueous phase were studied on four chromatographic resins. Patented by the Eichrom Technologies Inc.[156] the extraction resins are TRU (octylphenyl-*N,N*-di-isobutyl carbamoylphosphine oxide (CMPO) dissolved in tri-n-butylphosphate, TEVA (trialkyl, methylammonium nitrate or chloride), UTEVA (diphenyl, pentylphosphate or diamyl, amylphosphate), and DGA (*N,N,N',N'*-tetra-n-octyldiglycolamide, or normal DGA resin). The structure of the resins studied is presented in Fig. 2.2. Specific aims of the study were to evaluate: i) the distribution coefficient, K_D, of tin and tellurium on Eichrom resins, ii) appropriate substrates to separate tin from tellurium, and iii) the selective elution of tin

from the solid phase. The systematic assessment provides a solid foundation for the separation of ^{126}Sn from ^{126}Te and a subsequent measurement of ^{126}Sn isotope by AMS.

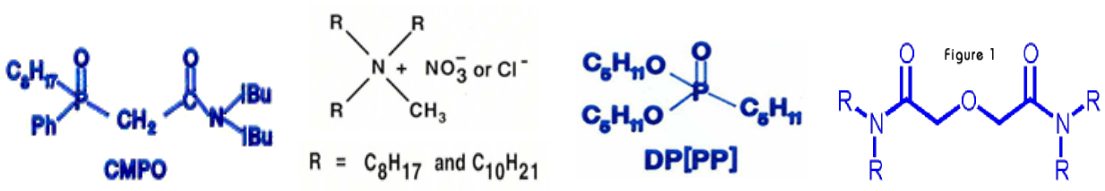

Fig. 2.2 Structures of Eichron resins.[156]

2.3.2 Reagents and materials

Analytical grade hydrochloric acid (37%, 12.03 mol L^{-1}) and nitric acid (68–70%, 15.61 mol L^{-1}) were purchased from Fisher Scientific, Ottawa, ON, Canada. Hydrofluoric acid (48%, 27.19 mol L^{-1}) was supplied by Sigma-Aldrich. Ultrapure water (18.0 MΩ) used for the preparation of eluents and dilution of samples was obtained from a Milli-Q purification system (Millipore, Bedford, MA, USA). Whatman filter papers (1.2 µm pore size, 25 mm diameter) were used to separate the resins from solutions in batch tests. Extraction resins were obtained in the form of 2.0 mL cartridges (50–100 µm) from Eichrom Technologies Inc. (Lisle, IL, USA). Tin (99.9995% pure Sn shot dissolved in tr. HNO_3 and tr. HF, density = 1.00 g/mL) and tellurium (99.9928% pure Te powder dissolved in 10% (v/v) HNO_3, density = 1.085 g/mL) standard solutions (1000 µg mL^{-1}) were purchased from BDH Chemicals (Toronto, ON, Canada), internal stock solutions were prepared daily by serial dilution in 2% (v/v) nitric acid, dissolved in Milli-Q water (18.0 MΩ.cm at 25 ºC). The principal instrument used in this experiment is the Agilent

8800 ICP-MS/MS. The centrifugation was done by an Eppendorf Centrifuge 5804 and a VWR standard analog shaker was used to mix the solutions during batch tests.

2.3.3 Preparation of pH calibration solutions

Seven pH solutions were prepared with pH ranging from 1.0–7.0. The pH of the solutions was measured using a Mettler Toledo multiparameter pH meter. The calibration of the pH meter was done against Mettler Toledo buffers at pH 4.00, 7.00, and 10.00. The pH adjustment was performed using 2% HNO_3 (v/v) solution, also prepared in Milli-Q water. Table 2.1 presents the pH values of the prepared solutions. The observed potential was displayed by the instrument during the measurement of solution pH.

Table 2.1: Observed pH values of prepared solution.

Expected pH	Observed pH	Observed potential (mV)	Temperature (°C)
1.00	1.04	333.9	25
2.00	2.03	281.0	25
3.00	3.03	224.4	25
4.00	4.01	175.9	25
5.00	5.03	121.5	25
6.00	6.04	67.7	25
7.00	7.04	13.4	25

2.3.4 Determination of K_D values by batch test

The K_D (metal adsorbed per gram of solid resin over metal retained per milliliter of water) values for tin and tellurium were determined as follows: 20 mL disposable plastic liquid scintillation vials were charged with 100 mg of resin – TRU, TEVA, UTEVA, or DGA – followed by the addition of 200 µL of standard tin and tellurium solutions (equivalent to 5.0 µg tin and 5.0 µg tellurium, the internal standard solutions were prepared in 2% HNO_3

(v/v), diluted by Milli-Q water, 18.0 MΩ.cm at 25 ºC). Sample vials were treated with either hydrochloric or nitric acid at concentrations ranging from 0.20 to 6.0 mol L^{-1}, total volume was adjusted to 10 mL. These vials were placed in a shaking bath for 2 hours, the contents were then transferred to 15-mL centrifugate tubes (Fisher Brand) and centrifugated for 15 min at 3600 rounds per minute. After filtration of the supernatant and appropriate dilution, the subsequent analysis was carried out by ICP-MS. Calibration curves (for tin and tellurium) were prepared daily for each batch of sample with concentrations of 20, 40, 60, 80, and 100 ppb of either tin or tellurium. The calibration blank, analyte free, was also prepared in 2% HNO_3 (v/v), again diluted by Milli-Q water. The blank was subtracted from the sample reading. A typical calibration curve is shown in Fig. 2.3. Also, the ICP-MS/MS detection conditions are presented in Table 2.2.

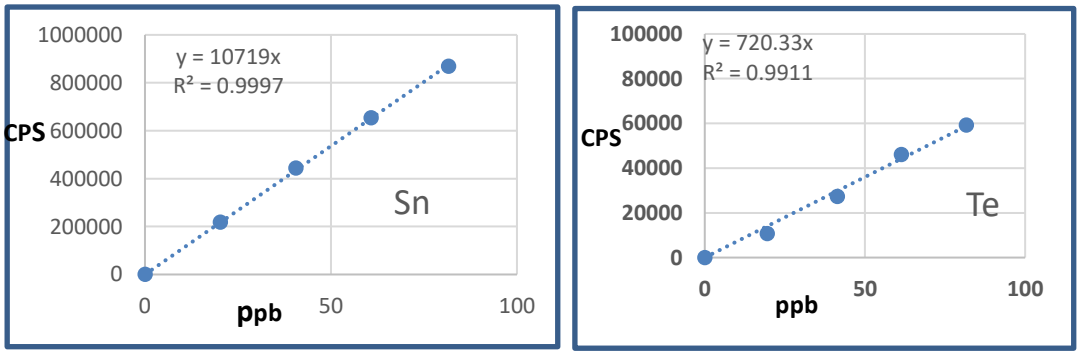

A typical calibration curve for tin, slope = 10719, R^2 = 0.9997

A typical calibration curve for tellurium, slope = 720.33, R^2 = 0.9911

Fig. 2.3 Calibration curves for tin and tellurium.

Table 2.2: ICP-MS/MS detection conditions.

Parameter	Value
RF power	1550 W
Plasma gas flow	15 L min^{-1}
Nebulizer gas flow	1.05 L min^{-1}
Auxiliary gas flow	1.0 L min^{-1}
Nebulizer pumping	0.27 mL min^{-1}
Acquisition time	60 s
Dwell time	0.1 s
Number of replicates	3

2.3.5 Preparation of column test

After the measurement of K_D values from batch test, the TRU resin was chosen as the bed material and aqueous hydrochloric acid as the loading acid. 10-mL polypropylene Bio-Rad columns (9 cm high, conical 0.8 × 4 cm with 30 μm porous bed support) were rinsed thoroughly with 2% (v/v) nitric acid to remove any fine particle adhered on the resin bed, and then washed with Milli-Q water. After air drying, the test columns were packed with TRU resin (50 to 300 mg) and rinsed with 20 mL Milli-Q water to remove any very fine-grained particles adhered on the resin. Packed columns were loaded with 10 mL of 1.0 mol L^{-1} hydrochloric acid, containing 5.0 μg tin and 5.0 μg tellurium. Elutions were accomplished under gravity, at normal laboratory temperature (22 °C), with a typical flow rate of 1.8 mL per min. The optimal packing volume was determined to be 200 mg of TRU resin (1.1 cm high). The loaded metal was eluted with hydrofluoric acid at concentrations ranging from 0.20 to 6.0 mol L^{-1}. Each washing of the resin was accomplished with 10 mL of acid solution, and consecutive washings were performed up to four times. The eluent washes were stored in separate tubes and processed for ICP-MS measurement. To minimize trace interferences of Sn and Te from the matrix, a blank run

was carried out, which was subtracted from the sample reading. The blank was prepared following the same experimental protocol adopted for the sample, except the addition of analytes.

2.4 Results and discussion

2.4.1 Batch test and distribution coefficients

K_D values of Sn in HCl solution: The distribution coefficient, K_D (metal adsorbed per gram of solid resin over the amount retained per mL of liquid) of TRU, TEVA, UTEVA, and DGA resins were calculated for each experiment. All four resins exhibited small K_D values at low concentrations of HCl, with the lowest observed being 151 ± 21 mL g^{-1} for DGA at 0.20 mol L^{-1}, shown in Fig. 2.4 (Appendix 7.5). Two resins–TEVA and UTEVA–showed an increase of K_D while increasing the concentrations of HCl, but exhibited a drop at 6.0 mol L^{-1} HCl. The highest peak in K_D of TEVA (41996 ± 204 mL g^{-1}) and UTEVA (6014 ± 276 mL g^{-1}) were found at HCl concentrations of 2.0 and 5.0 mol L^{-1}, respectively. TRU and DGA resins had higher K_D values at elevated concentrations of acid (6.0 mol L^{-1}). The highest K_D of TRU is 47662 ± 259 mL g^{-1} while that of DGA is 24121 ± 84 mL g^{-1}. Tin in hydrochloric acid solution produced much larger K_D values for all four resins studied. The high K_D value of TRU (47662 ± 259 mL g^{-1}) demonstrates that the adsorption capacity of tin onto this resin in hydrochloric acid solution is approximately 15 times higher than that of the UTEVA resin (3232 mL g^{-1}). The optimal adsorption of metal onto TEVA resin is expected at low concentrations of acid. To determine ^{126}Sn isotope using TEVA resin, Dulanská et al.[127] loaded tin on the resin in 1.0 mol L^{-1} hydrochloric acid.

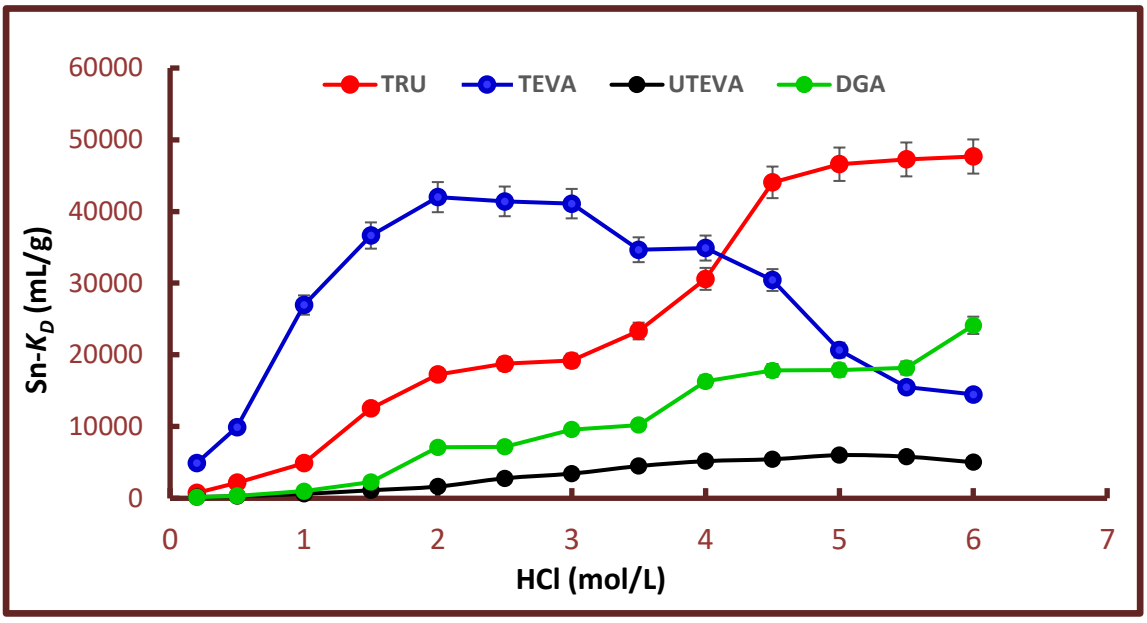

Fig. 2.4 K_D values of tin onto different resins in presence of hydrochloric acid (0.20 to 6.0 mol L^{-1}).

K_D values of Te in HCl solution: The K_D values of tellurium in hydrochloric acid solution are much lower than that of tin on all resins except for TEVA. The distribution of tellurium on TEVA (K_D, 3124 mL g^{-1}) is comparable to that of tin on the UTEVA resin (K_D, 3232 mL g^{-1}). In general, the K_D value for the substrates increase with increasing acid concentration up to a maximum of 6.0 mol L^{-1} HCl, as shown in Fig. 2.5 (Appendix 7.10). The largest value is 9724 ± 248 mL g^{-1} for TEVA, followed by DGA (5774 ± 144 mL g^{-1}), UTEVA (1571 ± 180 mL g^{-1}), and TRU (1197 ± 88 mL g^{-1}) resins. TRU resin shows the lowest K_D for tellurium. The ratio of individual K_D at the highest acid concentration (6.0 mol L^{-1}) over the lowest acid (0.20 mol L^{-1}) for TRU, TEVA, UTEVA, and DGA resins were 5.7, 66.7, 5.8, and 30.2, respectively. This information tells us that the adsorption of tellurium onto TEVA resin is highly affected by the concentration of loading acid. Similar effects were observed in cases of TRU and UTEVA resins. A close inspection on the K_D value of TRU resin reveals that tellurium

adsorption experiences a drop at lower concentrations of hydrochloric acid, but exhibits higher values at elevated acid concentrations. A comparison of the overall K_D values suggests that the adsorption of tellurium on the TRU resin is the lowest and is also less affected by variations in acid concentrations up to 2.0 mol L^{-1} of HCl.

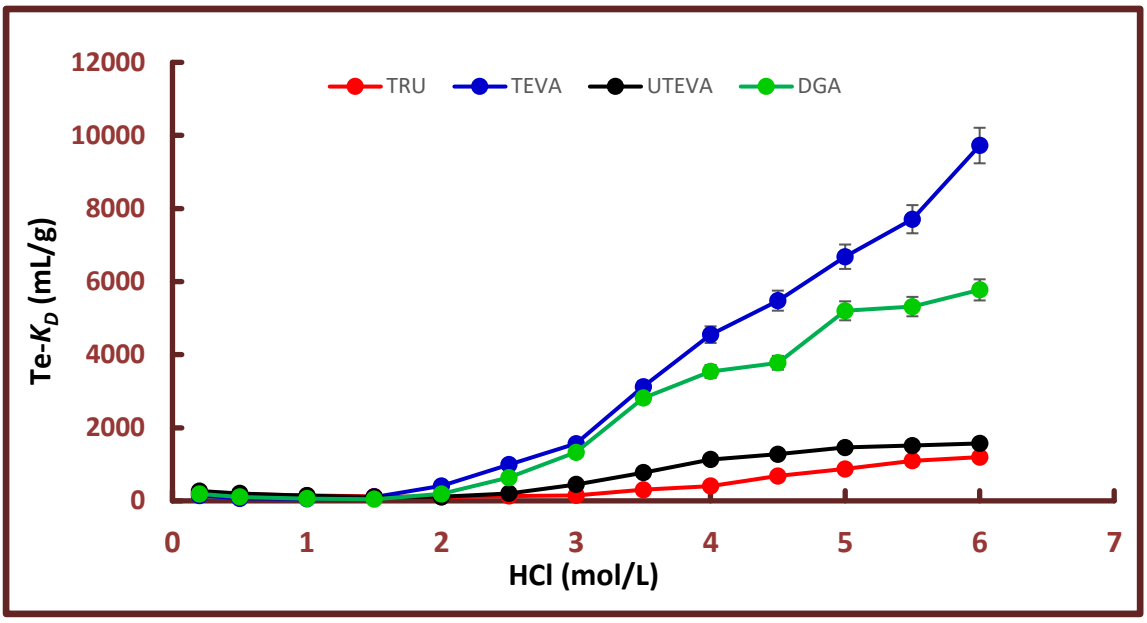

Fig. 2.5 K_D values of tellurium onto different resins in presence of hydrochloric acid (0.20 to 6.0 mol L^{-1}).

***K_D values of Sn in HNO_3 solution*:** Unlike the adsorption of tin in hydrochloric acid, which usually increases with increasing acid concentration, the adsorption of tin in aqueous nitric acid decreases with increasing concentrations of nitric acid, as demonstrated in Fig. 2.6 (Appendix 7.15). All four substrates have produced a similar K_D at 6.0 mol L^{-1} nitric acid (44–49 mL g^{-1}). At 0.20 mol L^{-1} nitric acid, the UTEVA resin has exhibited the highest K_D (487 ± 33 mL g^{-1}), followed by DGA (164 ± 8 mL g^{-1}), TRU (111 ± 4 mL g^{-1}), and TEVA (107 ± 3 mL g^{-1}) resins. On increasing the concentration of loading acid, a sharp decrease of K_D is observed for the UTEVA resin. The ratio of K_D at 0.20 mol L^{-1} acid to that at 6.0 mol L^{-1} for UTEVA resin is 10.9, and this ratio is 3.3 for

DGA, 2.5 for TRU, and 2.2 for TEVA resin. TEVA resin possesses the lowest ratio among all other substrates studied. The overall K_D values suggest that the adsorption of tin onto UTEVA resin in the presence of aqueous nitric acid is more favored at low concentrations of HNO_3 (less than 1.5 mol L^{-1}). The adsorption behaviors of tin on both TRU and TEVA resins are alike and are less affected by the acid concentration. A comparative study on the K_D value of tin in these two acid media (HCl and HNO_3) reveal that tin is preferably adsorbed in aqueous hydrochloric acid. The observation also shows a poor tin retention capacity on the solid phase loaded with nitric acid.

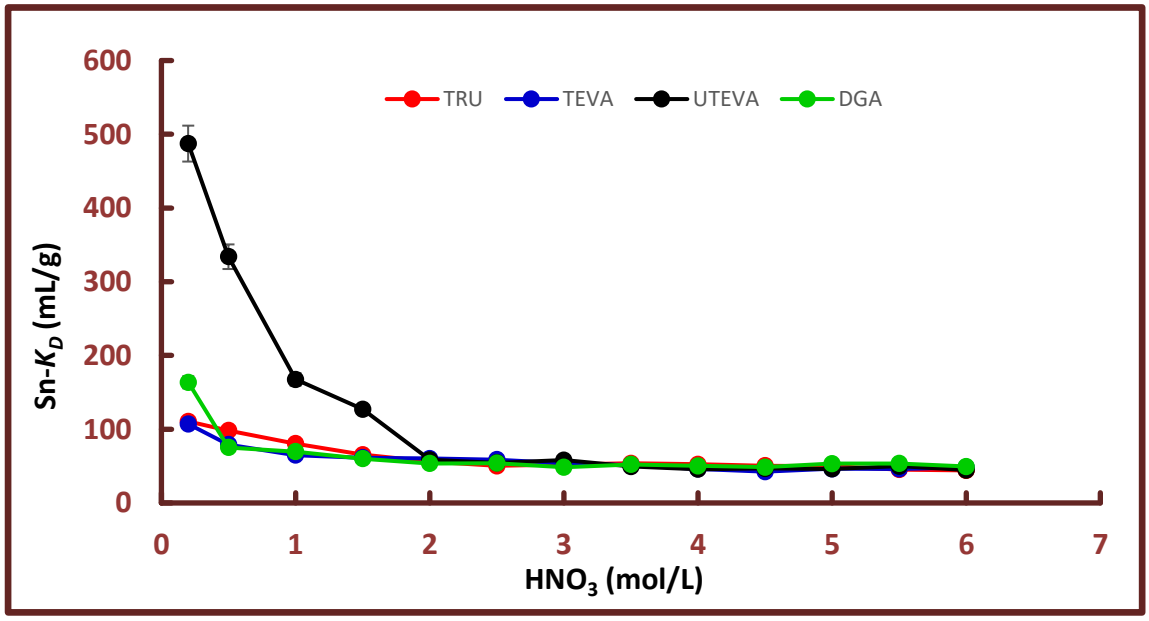

Fig. 2.6 K_D values of tin onto different resins in presence of nitric acid (0.20 to 6.0 mol L^{-1}).

***K_D values of Te in HNO_3 solution*:** Like the adsorption of tin in hydrochloric acid medium, K_D values of all four substrates decrease when the acid concentration increases as indicated in Fig. 2.7 (Appendix 7.20). At 0.20 mol L^{-1} acid, the UTEVA resin exhibits the highest K_D (323 ± 9 mL g^{-1}), followed by DGA (262 ± 6 mL g^{-1}), TRU (251 ± 8 mL g^{-1}), and TEVA (235 ± 7 mL g^{-1}) resins. Both TRU and DGA resins possess similar

adsorption properties at low acid concentration. The TEVA resin, however, shows the lowest average K_D (54 mL g^{-1}) among all four substrates studied, it also has the smallest K_D (26 ± 5 mL g^{-1}) at 6.0 mol L^{-1} nitric acid. Although the adsorption of tellurium onto UTEVA resin at 0.20 mol L^{-1} acid is slightly higher compared to other substrates, the average K_D values demonstrate two distinct resin pairs: TRU–UTEVA and TEVA–DGA. The TRU–UTEVA group possess almost double adsorption capacity (average K_D, 107.5 ± 0.50 mL g^{-1}) than the TEVA–DGA pair (average K_D, 59 ± 5 mL g^{-1}). The UTEVA resin experiences a sharp decline of K_D on bumping the acid concentration. At lower concentrations of acid, below 2.0 mol L^{-1}, the overall adsorption is highly affected by a small increase of acid concentration, however, this scenario becomes steady (K_D values remain stable) from 3.0 to 6.0 mol L^{-1} acid treatment. In fact, the UTEVA resin has the largest adsorption coefficient for both tin (K_D, 487 ± 33 mL g^{-1}) and tellurium (K_D, 323 ± 9 mL g^{-1}) in aqueous nitric acid solution. For TEVA and DGA resins, no sharp change of tellurium adsorption is observed by increasing the acid concentration.

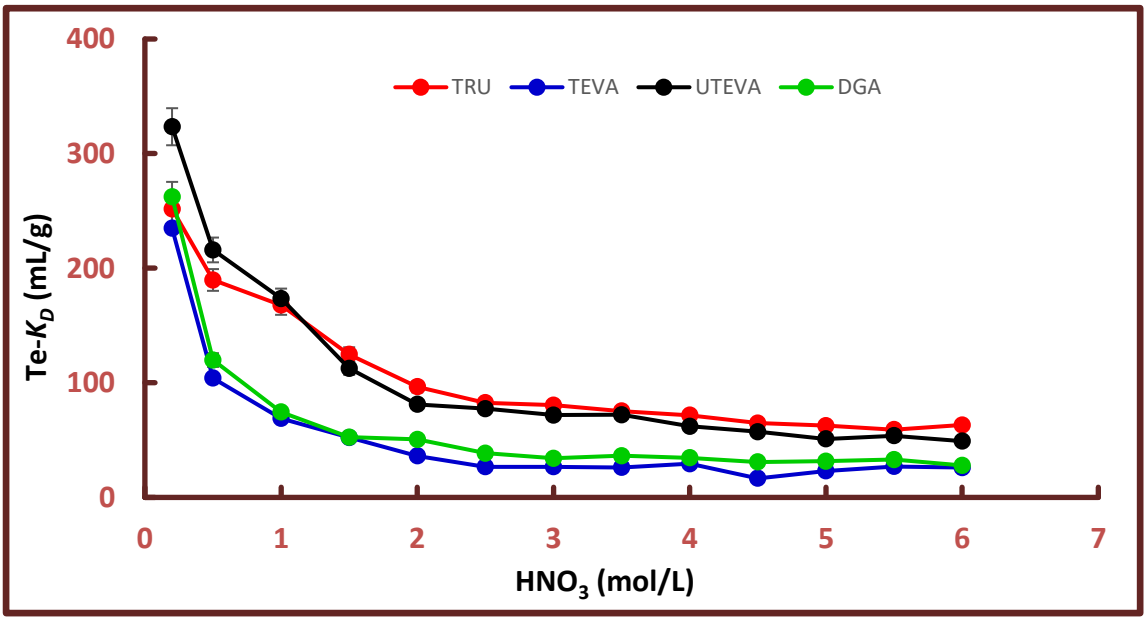

Fig. 2.7 K_D values of tellurium onto different resins in presence of nitic acid (0.20 to 6.0 mol L^{-1}).

***K_D values of Sn in different pH solutions*:** The K_D values of tin for TRU, TEVA, UTEVA, and DGA resins over the entire acidic pH ranges (1.0–7.0, prepared in 2% HNO_3 (v/v)) were calculated for each experiment in a batch test, presented in Fig. 2.8 (Appendix 7.25). In general, the distribution coefficient of Sn increases with increasing pH, which implies that the adsorption of Sn on the solid phase gets increased at elevated pH. However, at pH 6.0, the UTEVA and DGA resins show a drop of K_D before they increased once more at pH 7.0. The TRU resin shows a steady rise of K_D from pH 1.0 to 6.0, then a drop at pH 7.0 (512 ± 101 mL g^{-1}). For the TEVA resin, a sharp increase of K_D was also observed from pH 1.0 (92 ± 13 mL g^{-1}) to pH 2.0 (592 ± 90 mL g^{-1}), and again from pH 3.0 (494 ± 26 mL g^{-1}) to pH 5.0 (1188 ± 388 mL g^{-1}); demonstrating the highest K_D value observed among all four resins. At pH 6.0, the TEVA resin has exhibited a further drop of K_D (1150 ± 453 mL g^{-1}), which was continued till the attainment of the neutral condition of pH 7.0 (901 ± 75 mL g^{-1}). At pH 4.0, the TEVA, UTEVA, and DGA resins all produced similar K_D values (average 670 ± 23 mL g^{-1}), which are almost double that of the TRU resin (322 ± 68 mL g^{-1}). The UTEVA and DGA resins have experienced a similar bump of K_D from pH 1.0 to 4.0, after this point, they have shown a reverse adsoptive nature of Sn–the former got a sharp rise of K_D whereas the latter has displayed a gradual drop. It is worth mention that at the neutral pH of 7.0, two resins–UTEVA and DGA–have demonstrated a rise of K_D, whereas the other two–TRU and TEVA–have suffered a sharp drop.

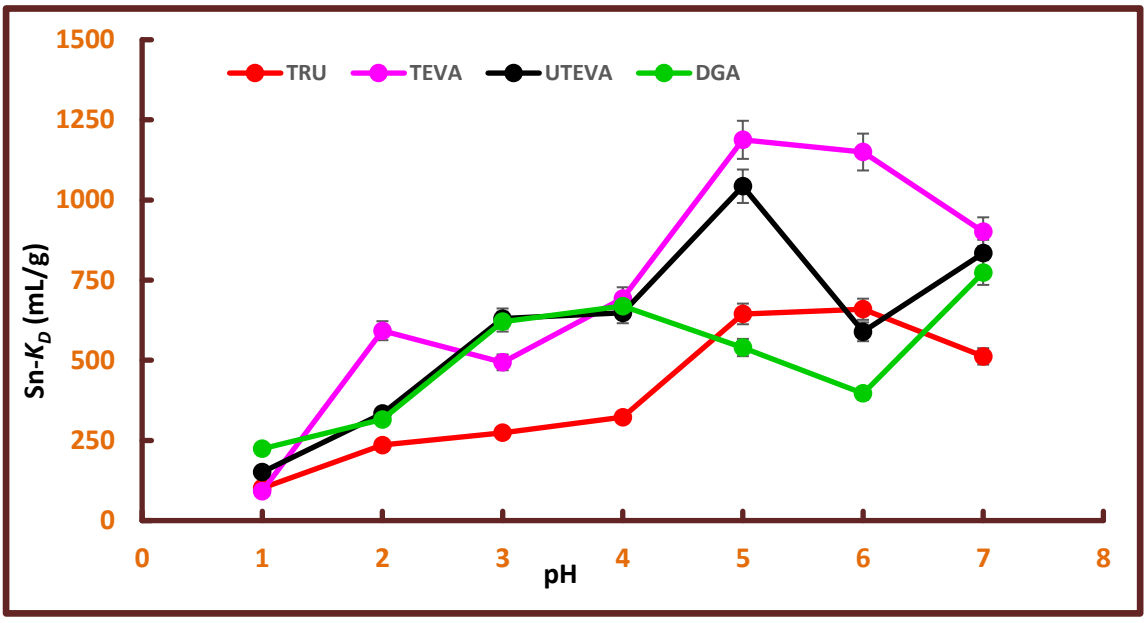

Fig. 2.8 K_D values of tin in different pH solutions (pH 1.0–7.0).

***K_D values of Te in different pH solutions*:** The K_D values of tellurium for TRU, TEVA, UTEVA, and DGA resins over the entire acidic pH ranges (1.0–7.0, again prepared in 2% HNO_3 (v/v)) were calculated for each experiment in a batch test, presented in Fig. 2.9 (Appendix 7.30). All study materials have demonstrated an increase of K_D with increasing pH, the highest K_D value was observed at pH 7.0 for UTEVA (129.9 ± 18 mL g^{-1}). At pH 3.0, the TEVA and UTEVA resins have felt a drop of K_D, whereas the TRU resin has experienced a similar drop at pH 4.0 (322 ± 68 mL g^{-1}). At pH 3.0, the TRU, UTEVA, and DGA resins have produced similar K_D values (average 104 ± 2 mL g^{-1}), while the TEVA resin has exhibited a much lower K_D (93 ± 5 mL g^{-1}). At pH 2.0 and 4.0, two K_D maxima were observed for UTEVA (114 ± 33 mL g^{-1}) and DGA (123 ± 12 mL g^{-1}) resins, respectively. Interestingly, the distribution curve for the TRU and the DGA resins become linear from pH 5.0 to 7.0, the average K_D in this pH range was found as 108.65 ± 0.55 mL g^{-1} for TRU it was 112.62 ± 0.83 mL g^{-1}. This result implies that the TRU and the DGA resins possess pH independent adsorptive characteristics of Te from pH 5.0 to

7.0. On the other hand, in this pH range, UTEVA shows an upward tendency of K_D with increasing pH, whereas TEVA exhibits a downward trend. The overall results show that, tellurium produces a relatively smaller K_D values (101 ± 5 mL g^{-1}) compared to tin (558 ± 143 mL g^{-1}); just as with higher concentration HCl and HNO_3 treatments. It is also clear that the distribution of tellurium onto different study materials is the highest at pH around 4.0.

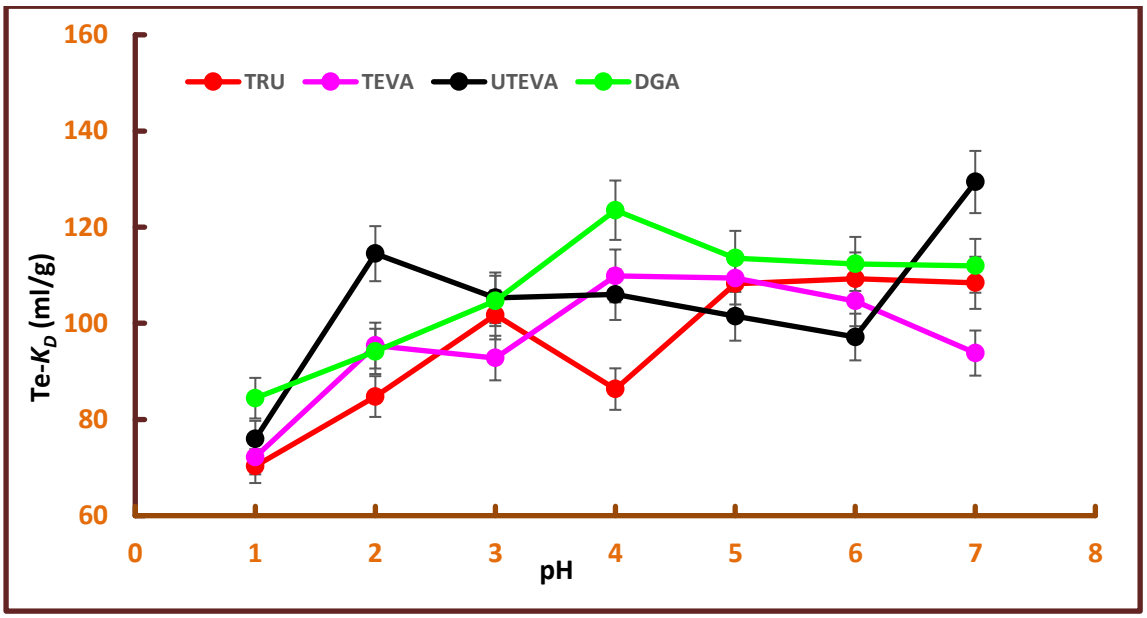

Fig. 2.9 K_D values of tellurium in different pH solutions (pH 1.0–7.0).

2.4.2 Choice of adsorbing material

The K_D values of four Eichrom resins – TRU, TEVA, UTEVA, and DGA – were studied in batch test in HCl and HNO_3 media, presented in Figs. 2.4, 2.5, 2.6, 2.7, 2.8, and 2.9. The results of K_D studies of different substrates reveal that a higher adsorption capacity of tin is achieved in aqueous hydrochloric acid (Fig. 2.5) than that of aqueous nitric acid medium (Fig. 2.5). In contrast, the retention capacities of both tin and tellurium on the substrates are very low in aqueous nitric acid, even the adsorption of tellurium is higher in the case of UTEVA, which essentially became equal to that of DGA resin, as shown in

Fig. 2.10 (Appendix 7.31). Therefore, the adsorption study of either tin or tellurium on the column bed in presence of aqueous nitric acid was abandoned. The TEVA resin possesses the highest adsorption capacity of tin in HCl (K_D, 27232 mL g^{-1}), however, its tellurium retention capacity is also high (K_D, 3124 mL g^{-1}). On the other hand, the TRU resin produced the lowest tellurium adsorption capacity (K_D, 431 mL g^{-1}) in similar concentrations of HCl treatment, shown is Fig. 2.11 (Appendix 7.32), though its tin adsorption coefficient is slightly lower than that of TEVA resin (24239 mL g^{-1} for TRU compared to 27232 mL g^{-1} for TEVA). The ratio of the distribution coefficient of tin over that of tellurium in hydrochloric acid medium are, respectively, 56.2, 4.6, 8.7, and 4.6 for the TRU, TEVA, UTEVA, and DGA resins. Interestingly, both UTEVA and DGA resins yield the same ratio, shown in Fig. 2.12 (Appendix 7.33). The much higher K_D ratio observed in TRU resin indicates a superior selectivity for tin over tellurium. For this reason, TRU resin, conditioned with high concentration HCl, is chosen as the optimal column substrate for separation of tin from tellurium in this study.

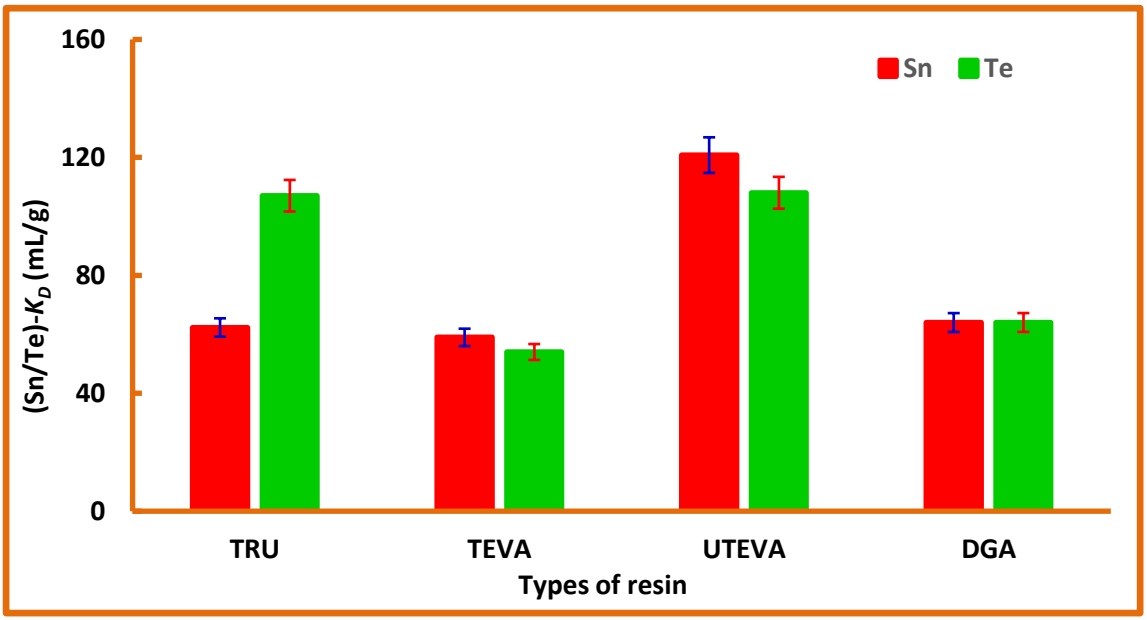

Fig. 2.10 K_D values of tin and tellurium onto different resins in presence of nitric acid (0.20 to 6.0 mol L^{-1}) solution.

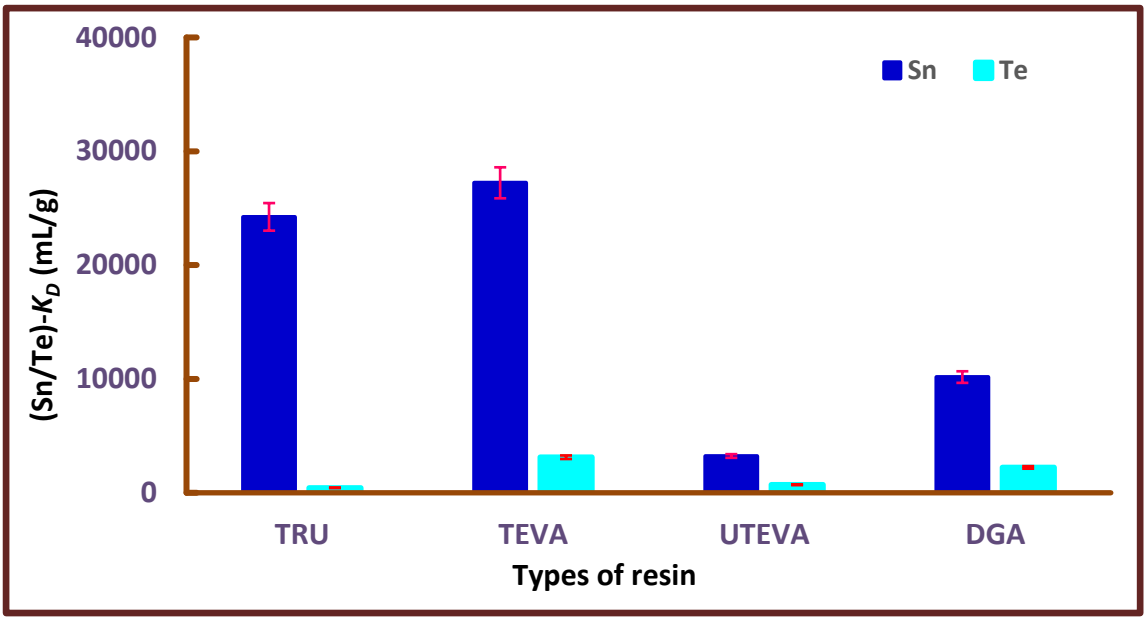

Fig. 2.11 A comparison of K_D values of tin and tellurium onto different resins in presence of hydrochloric acid (0.20 to 6.0 mol L^{-1}) solution.

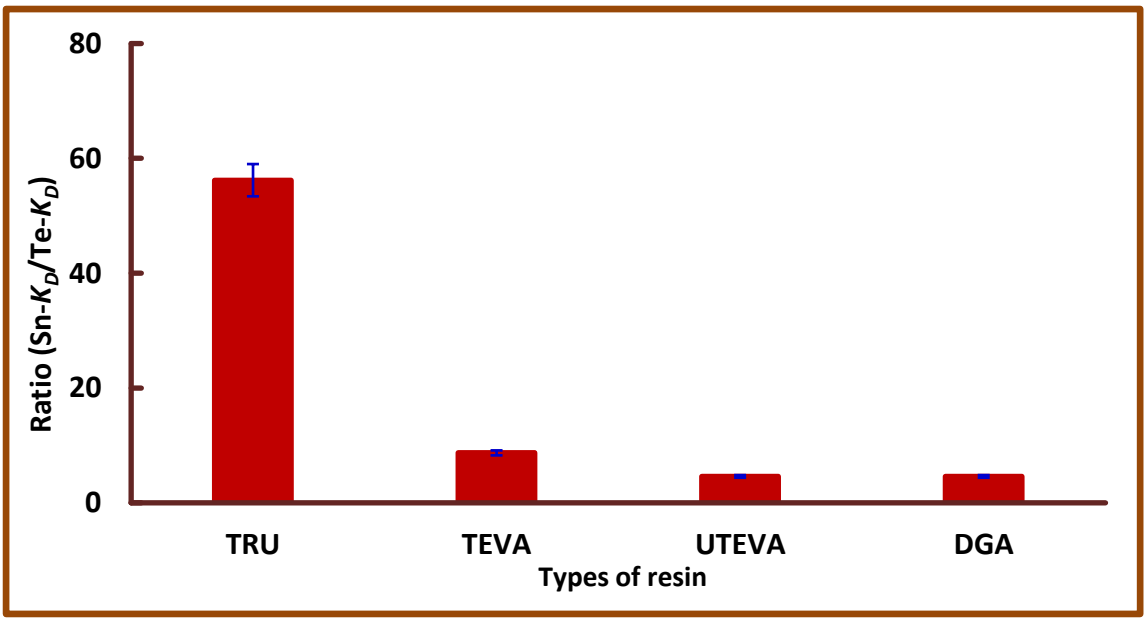

Fig. 2.12 Ratio of Sn and Te K_D values onto different resins in presence of hydrochloric acid (0.20 to 6.0 mol L^{-1}) solution.

2.4.3 Mechanism of adsorption

Unlike liquid-liquid extraction, where partitioning of solutes takes place in two immiscible liquids, the solid-phase extraction encounters the partitioning of solutes between a solid (sorbent) and a liquid phase.[142] The most common interactions in SPE involve the van der Waals or dispersive force, hydrogen bonding, dipole-dipole interactions, and cation-anion interactions.[208,209] In our present study, the TEVA resin has showed the highest adsorption of tin in 1.0 mol L^{-1} of HCl, which can be attributed to the strong dispersive forces acting between the Sn^{2+} ion and the non-polar alkyl groups of the sorbent. On the other hand, the relatively higher adsorption of tin onto the TRU resin can be attributed by the strong dipole-ion interactions operating between the resin and the tin metal. In addition, the conformational disposition of TRU resin (Fig. 2.2) favours in the formation of six-membered stable tin-sorbent adduct.

2.4.4 Column loading

Optimization of packing quantity: The previous batch experiments were done with 100 mg of resin and a mixture of 10 µg tin and tellurium (5.0 µg each). In the column test, an optimization of the packing material is important to ensure better adsorption and elution efficiency. Bio-Rad polypropylene columns were charged with TRU resin at amounts ranging from 25 to 300 mg. Packed columns were loaded with solution containing 5.0 µg of tin and 5.0 µg of tellurium along with an appropriate amount of 1.0 mol L^{-1} of HCl, the total volume was adjusted to 10 mL. The adsorption characteristic of the column bed reveals that it is capable of retaining up to 99.78 ± 0.39 % of tin with 100 mg of resin, shown in Fig. 2.13 (Appendix 7.34). However, with 200 mg material, the adsorption of tin can be as high as 99.95 ± 0.17 %, whereas the adsorption of tellurium in similar

experimental condition is about 60.98 ± 1.26 %. For this reason, the column test was performed with 200 mg of TRU resin.

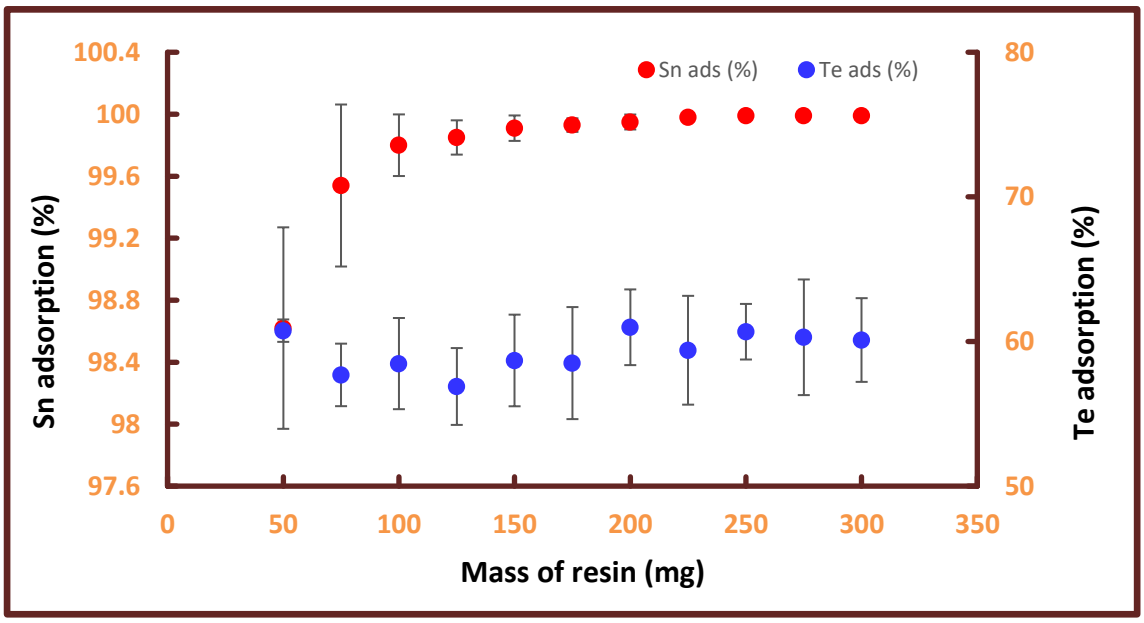

Fig. 2.13 Column packing with TRU resin and adsorptions of tin and tellurium.

Optimization of column loading solution: The distribution coefficient of tin on TRU resin was found to increase with increasing the concentration of hydrochloric acid, up to 5.0 mol L^{-1} (Fig. 2.4). However, at elevated concentrations of acid (≥ 3.0 mol L^{-1}), the adsorption of tellurium also increases. The K_D value of tellurium up to 3.0 mol L^{-1} HCl is relatively low (average 149 mL g^{-1}), whereas at 3.5 mol L^{-1} it almost doubles (302 mL g^{-1}). At low concentration of HCl (≤ 3.0 mol L^{-1}), we expect a high adsorption of tin and a low retention of tellurium. The loading of tin and tellurium on the column bed was performed at 1.0 mol L^{-1} of HCl.

2.4.5 Metal elution from the column bed

Column wash by HCl solution: The packed column loaded with tin and tellurium was first washed with 20 mL Milli-Q water to wash down fine dust particles adhered on the column bed, followed by the hydrochloric acid treatment with concentrations ranging from 1.0 to 12.0 mol L^{-1}, the average leaching of tin was 1.79 ± 1.31% whereas the average leaching of tellurium was 2.07 ± 0.76%, shown in Fig. 2.14 (Appendix 7.35). Unlike other two washing media (HNO_3 and HF), the elution of tellurium is higher than that of tin in HCl solution.

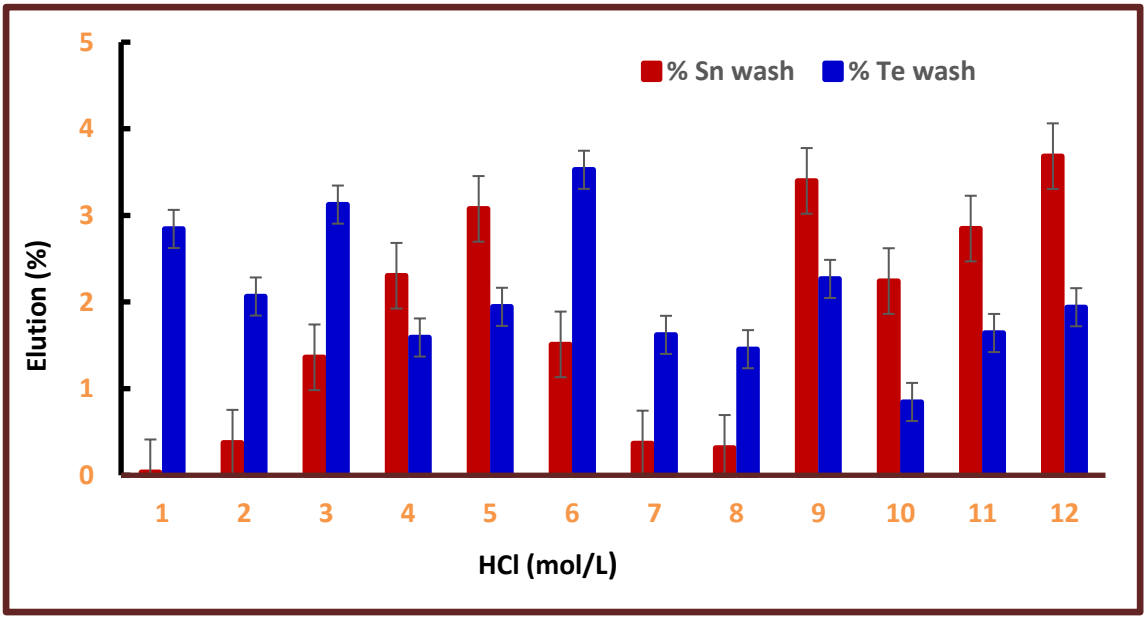

Fig. 2.14 Elution of tin and tellurium with hydrochloric acid (1.0 to 12.0 mol L^{-1}).

Column wash by HNO_3 solution: Again, the loaded columns were washed off with nitric acid (10.0 mL) at concentrations of 0.50 to 6.0 mol L^{-1}. The average leaching of tin was 32.45 ± 13.99% whereas the average leaching of tellurium was 30.68 ± 6.30%, shown in Fig. 2.15 (Appendix 7.36). At 0.50 and 1.0 mol L^{-1} of HNO_3, the leaching of tellurium is higher than that of tin, whereas at elevated concentrations of HNO_3 (2.0 – 6.0 mol L^{-1}),

the leaching of tin outweighs the leaching of tellurium, giving almost the same average value. The leaching of tin at 0.50 mol L^{-1} HNO_3 was 17.00%, and at 6.0 mol L^{-1}, it was 48.50%, a threefold increase. The leaching of tellurium at similar acidic conditions was changed by 58%, which indicate that the washing of tellurium by HNO_3 is much less affected than tin by increasing the concentrations of nitric acid.

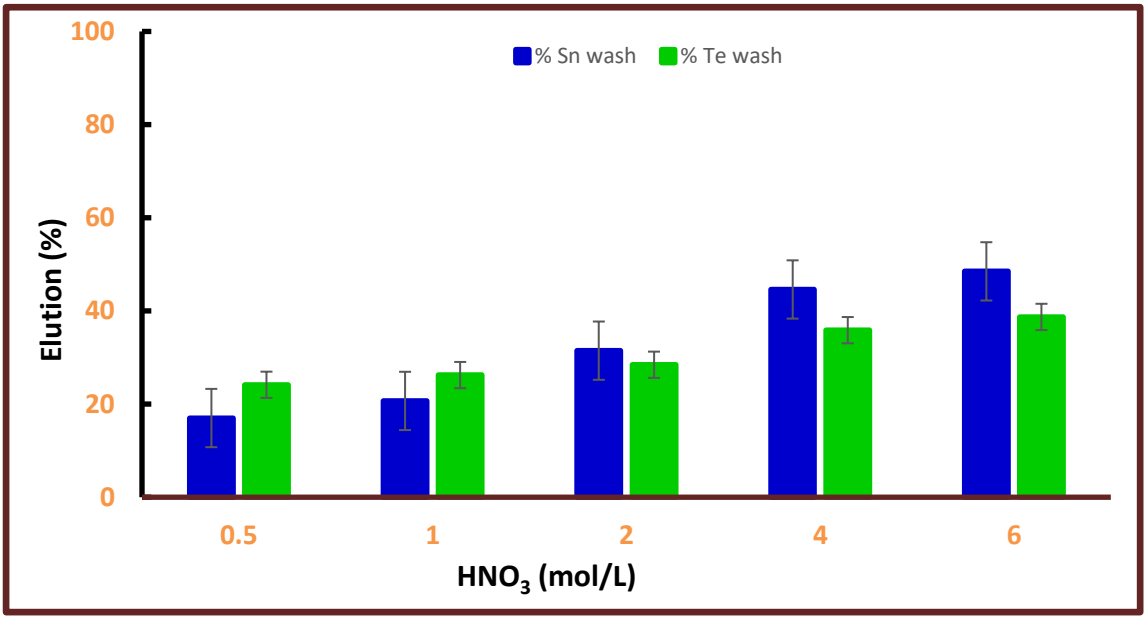

Fig. 2.15 Elution of tin and tellurium with nitric acid solution (0.50 to 6.0 mol L^{-1}).

Column wash by HF solution: Finally, the elution experiment was performed using hydrofluoric acid (HF) at concentrations ranging from 0.20 to 6.0 mol L^{-1}. Results reveal that the percentage of both tin and tellurium elution increase with increasing concentrations of hydrofluoric acid and *vice versa*. The average fraction of tin wash, for the entire range of acid concentrations, from the resin was 95.09 ± 2.19%, while that of tellurium was 13.02 ± 4.71%. At 0.20 mol L^{-1} of HF, tin elution was 88.91% while tellurium elution was 4.54%. At 6.0 mol L^{-1} of acid, tin and tellurium elution were 97.21% and 19.46%, respectively, as shown in Fig. 2.16 (Appendix 7.37).

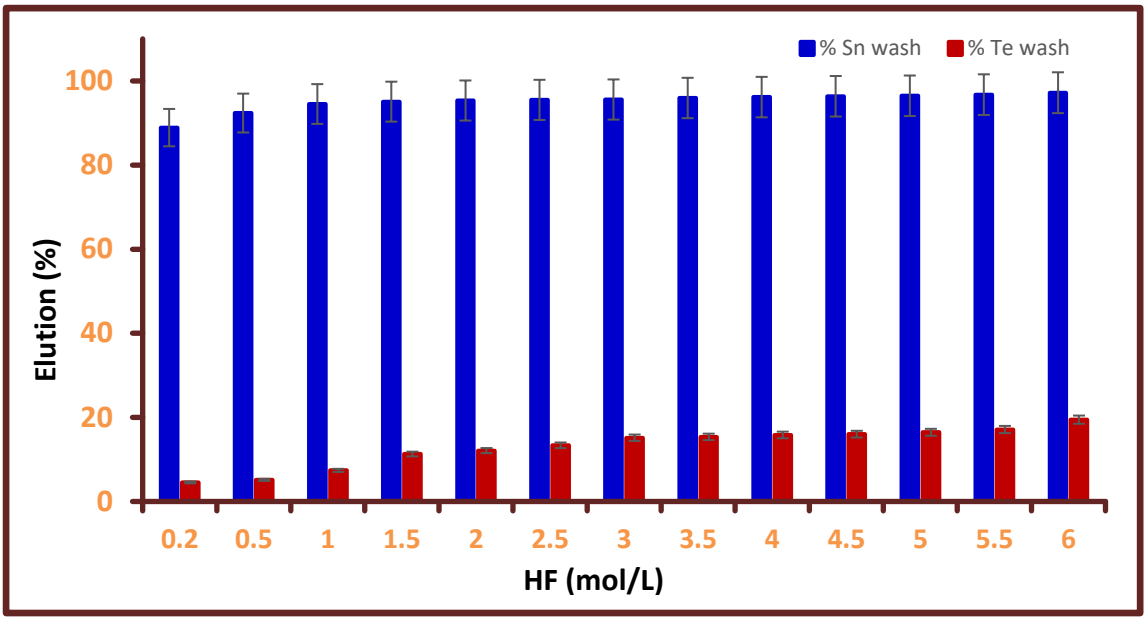

Fig. 2.16 Elution of tin and tellurium from TRU column by hydrofluoric acid (0.20 to 6.0 mol L^{-1}).

A comparison of metal elution: The average eluted fraction of tin in HCl (12.03 mol L^{-1}), HNO_3 (15.61 mol L^{-1}) and HF (27.19 mol L^{-1}) media were 1.79 ± 1.39, 32.45 ± 13.99, and 95.09 ± 2.22%, respectively, whereas the corresponding values for tellurium were 2.07 ± 0.76, 30.68 ± 6.30, and 13.02 ± 4.71%. Although, the leaching of tellurium in HCl solution is the lowest (2.07%), it exhibits a very low elution of (only 1.79%) tin in the wash. In aqueous HNO_3, the leaching of tin and tellurium is well below 50%, Fig. 2.17 (Appendix 7.38). In aqueous HF medium, the leaching of tin is around 95% while the leaching of tellurium is 13%. A comparison on elution profile demonstrates that the aqueous HF offers a bright promise in the selective desorption of tin from the column bed maintaining a low level of tellurium release.

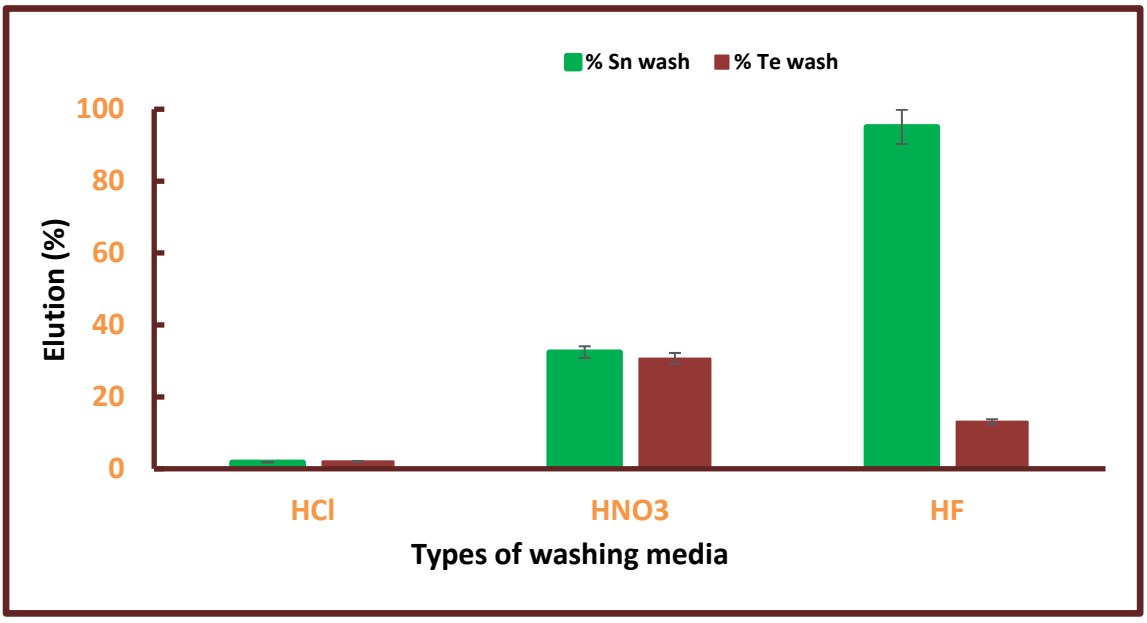

Fig. 2.17 A comparison on the average percentage of tin and tellurium wash by HCl, HNO_3, and HF across all concentrations.

2.4.6 Optimization of eluent volume

Loaded metals were washed off with aqueous HF (0.20–6.0 mol L^{-1}), using 10.0 mL on each washing treatment. After the first wash with 10.0 mL hydrofluoric acid, the average elution of tin was 85.5%, whereas tellurium elution was 6%. At the end of fourth wash, with the same volume of HF, the corresponding elution were 95% and 13%, respectively. As the number of washings increases, the percentage of metal elution (both tin and tellurium) also goes up, as shown in Fig. 2.18 (Appendix 7.39). However, with additional washing treatments, there is a greater chance of significant tellurium contamination in the effluent. Therefore, an optimization of washing volume is necessary to ensure a selective separation of tin. Our desire is to keep the tellurium content as low as possible in the wash effluent, while maintaining a high recovery of tin.

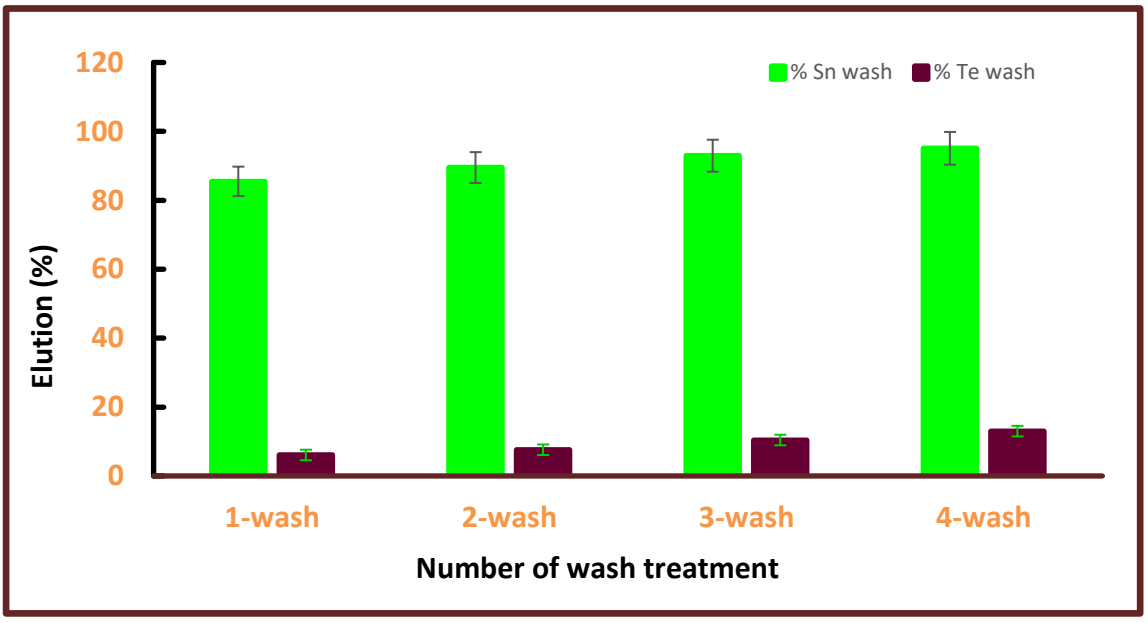

Fig. 2.18 Percent of tin and tellurium elution with the number of wash treatment.

2.4.7 Optimization of eluent condition

Keeping four washes of 10 mL, increasing the concentration of hydrofluoric acid leads to an increase of tin elution from the column bed, but at the same time, it also increases the elution of tellurium. A similar observation, increasing the percent of extraction with increasing acid concentration, was also observed by Ahn and Lee,[153] while doing solvent extraction of tin from a mixture of metals using TBP. They found 68% Sn(IV) extraction at HCl concentration of 1.0 mol L^{-1} and the recovery was raised to 93.6% at 8.0 mol L^{-1} HCl. Zhu et al.[157] have reported that in speciation of Sn(II) and Sn(IV) adsorbed on anion exchange resin (as Cl^{-}–type), the recovery of total tin was 98.7–101.7%. Another report says that the cloud point extraction of tin using 8-hydroxyquinoline and Triton X-114 gave 85.0–112.0% recovery of tin for water samples.[158]

In our present study when the hydrofluoric acid concentration is increased from 0.20 to 1.5 mol L^{-1}, the percent of tin elution goes up from 89% to 95%, and the corresponding percentage of tellurium release shifts from 4.5% to 11%. The ratio of the percent tin

elution to that of tellurium from 0.20 to 1.5 mol L^{-1} acid treatment declines from 19.6 to 8.4, which means that the selectivity of tin separation drops by 57%. At still higher concentrations of acid treatment, the selectivity diminishes rapidly, Fig. 2.19 (Appendix 7.40). In 1.0 mol L^{-1} hydrofluoric acid, tellurium elution is 7.4%, while the eluent has 12% of tellurium at 2.0 mol L^{-1} HF, although the tin elution remains almost the same, 94.5% and 95%, respectively. Columns eluted with hydrofluoric acid having concentrations of 2.5 and 3.5 mol L^{-1} show a small change in the ratio of tin-tellurium in the eluent. At 4.0 mol L^{-1} of HF, the tellurium release is more than 15%, resulting a decrease in separation efficiency. Good separation is, therefore, favoured at low concentrations of hydrofluoric acid.

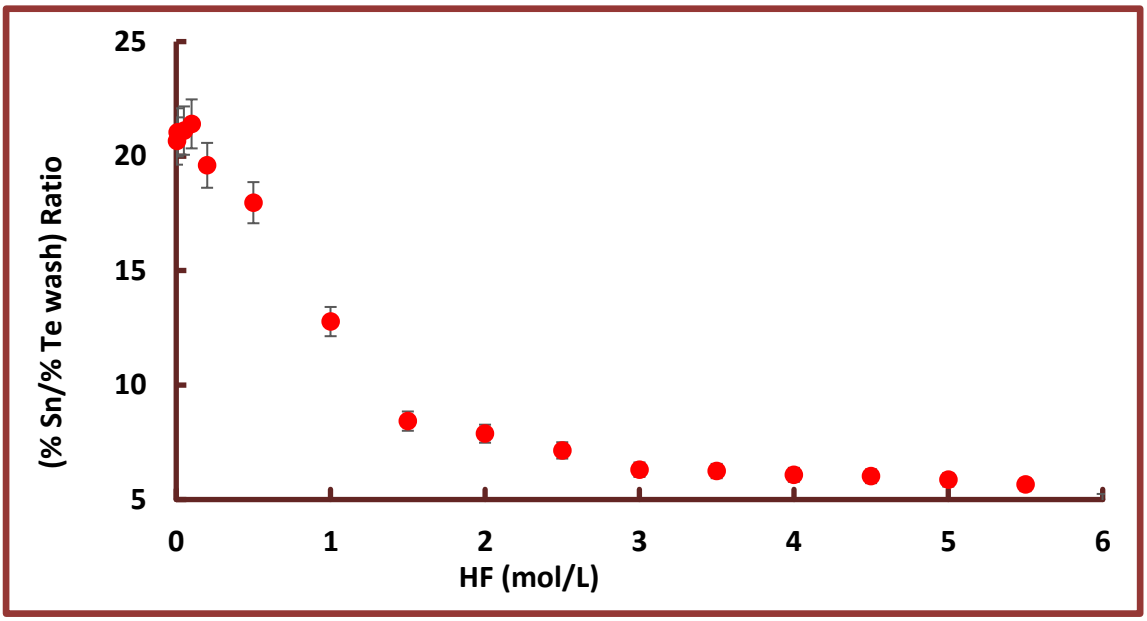

Fig. 2.19 Selectivity of tin and tellurium separation with increasing eluent concentration (0.005 to 6.0 mol L^{-1}).

The ratio of the percent of tin elution over that of tellurium at hydrofluoric acid concentrations down to 0.005 mol L^{-1} reveals that the ratio is maximum (21.4) at 0.10 mol L^{-1} HF. At still lower concentrations, the ratio is relatively small, as demonstrated in

Fig. 2.19. In addition, washing treatments of more than four times release higher amounts of tellurium from the column bed causing a decline of the ratio of tin wash over tellurium wash, shown in Fig. 2.20 (Appendix 7.41). At 0.10 mol L^{-1} of HF, the percent of tin elution is 77% and that of tellurium is 3.6%. On the other hand, at 0.50 mol L^{-1} of HF, the percent of tin and tellurium elution, respectively, 92% and 5%. We can conclude here that a good recovery of tin can be ensured at 0.50 mol L^{-1} of HF (92% Sn and 5% Te) and the best selectivity of tin and tellurium separation is achieved at 0.10 mol L^{-1} of HF (77% Sn and 3.6% Te). Sun and Li[151] have separated seven elements from seawater by *N*-benzoyl-*N*-phenylhydroxylamine (BPHA) supported on microporous acrylic ester polymeric resin and then eluted by HF, the recovery of tin was 99% with 6 mol L^{-1} HF/1 mol L^{-1} HCl. In our present study, the elution of tin from the column bed with 6 mol L^{-1} HF is 97%, similar to that found by Sun and Li.[151] Our report, however, demonstrates an optimum condition of eluent concentration to suppress the elution of tellurium, maximizing the relative release of tin from the column bed.

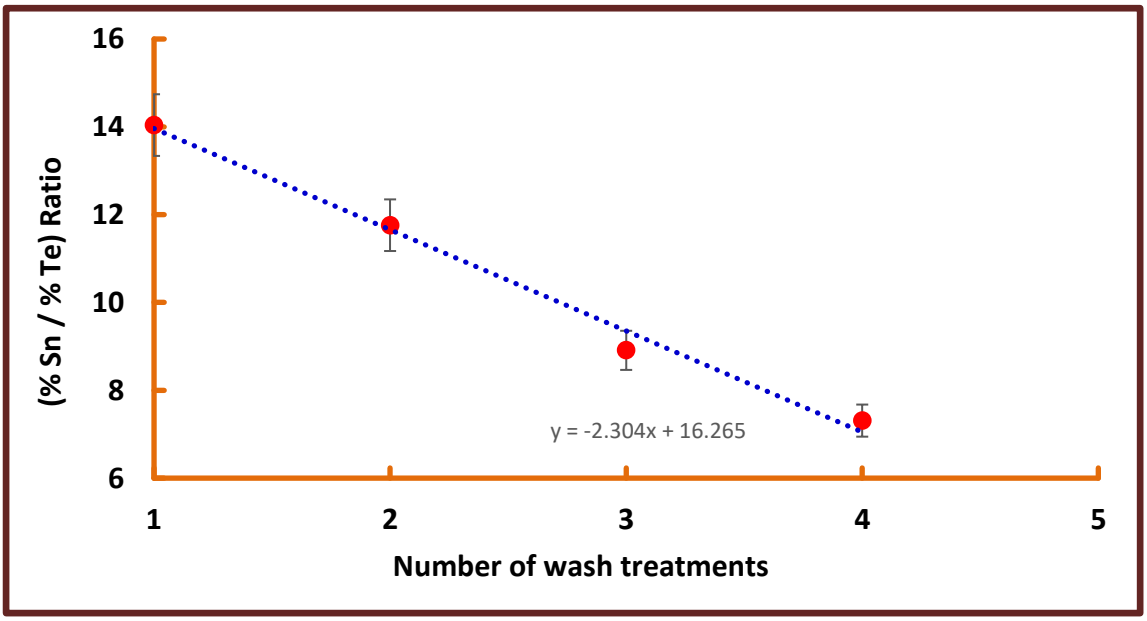

Fig. 2.20 The drop of separation efficiency with the number of washing treatments.

2.5 Conclusions

Our present study has developed a strategy to separate tin and tellurium using a solid phase extraction technique. The overall results are promising and can be applied for the separation of ^{126}Sn from ^{126}Te. Therefore, rare ^{126}Sn isotope can be analyzed by high resolution mass spectrometry, including accelerator mass spectrometry, by minimizing interference from the abundant isobar ^{126}Te. Among the four Eichrom resins studied, the TRU resin is the most effective extraction material to be used for the separation of tin from tellurium. In solutions of aqueous nitric acid, the extraction of both tin and tellurium by different resins (TRU, TEVA, UTEVA, and DGA) are rather poor (K_D < 100 mL g^{-1}). On the other hand, when loaded in hydrochloric acid both tin and tellurium have much higher distribution coefficients (K_D > 16,000 mL g^{-1} for Sn and K_D > 400 mL g^{-1} for Te) on all resins. The distribution coefficient of tin onto the TRU resin column is favored in presence of aqueous hydrochloric acid (1.0 mol L^{-1}), whereas the elution of tin is ensured by washing with dilute hydrofluoric acid. Elevated concentrations of HF increase the elution of tin as well as the elution of tellurium. Therefore, the optimization of the concentration of eluting solution and the number of washing attempts are essential. Our present study reveals that 99.78 ± 0.39% tin adsorption and 59.31 ± 1.32% Te adsorption can be achieved with 200 mg of TRU resin in a solution of 1.0 mol L^{-1} hydrochloric acid. Using 0.50 mol L^{-1} HF, approximately 92% of tin can be eluted with 4 × 10 mL of washings (HF having a concentration of 0.5 mol L^{-1}), keeping the tellurium leaching around 5%.

……

A part of this chapter has been published as "M. M. Rahman, C. MacDonald & R. J. Cornett. (**2018**). Separation of tin from tellurium: performance of different extraction chromatographic materials, *Separation Science and Technology*, 53(13): 2055–2063.

Chapter 3:

Interferences of chloride and sulfate ions in the separation of tin from tellurium

3.1 Research background

3.1.1 Principal ions in water

Natural waters contain a large number of solutes, however, seven major ions contribute at least 90% of the dissolved solids in groundwater: four cations – Na^+, Ca^{2+}, K^+, Mg^{2+}, and three anions – $Cl^–$, $SO_4^{2–}$, and $HCO_3^–$.[159,160] These ions are present at concentrations ranging from 1.0 to 1000 mg $L^{–1}$.[161] Other naturally occurring ions, which are usually present at concentrations less than 0.10 to 10.0 mg $L^{–1}$, include Fe^{2+}, $NO_3^–$, $F^–$, and Sr^{2+}, as well as neutral or uncharged compounds like dissolved silica (H_4SiO_4).[159,160]

3.1.2 Chloride and sulfates in water

Worldwide marine salt deposits (especially chlorides and sulfates) are mainly derived from the climate-mediated solar evaporation of saturated seawater.[162] In fact, chloride and sulfate are the most abundant anionic species, even the first and the third most abundant ions, respectively, in seawater ($Cl^–$ = 55%, Na^+ = 30.62%, and $SO_4^{2–}$ = 7.72% by wt).[162,163] Chloride and sulfate possess many environmental implications, both of them, for example, increase the rate of iron corrosion by destabilizing the anti-corrosion film formed onto the iron surface.[161] Also, high levels of $Cl^–$, $SO_4^{2–}$, $HCO_3^–$, and $NO_3^–$ reduces the reactivity and longevity of zero-valence iron metal in the treatment of contaminated groundwater.[164,165]

3.1.3 Origin of groundwater salinity

Geochemical processes are mainly responsible for the high concentrations of SO_4^{2-} and Cl^- in groundwater interfaces. The most important such processes include gypsum ($CaSO_4.2H_2O$) dissolution and pyrite (e.g., arsenopyrite, FeAsS) oxidation.[166,167] As groundwater salinity is geogenic, occurrences of mineral deposits make up a salinity threat to groundwater reservoirs. In coastal regions, aquifers, with hydraulic connections to saline seawater, are mostly vulnerable to saline water intrusion. Salinity contamination of well groundwater further back from the sea (i.e., upper catchment) may also take place due to density-driven flow. Groundwater pumping, along with other anthropogenic activities, including industrial input like tannery and dye industries, introduces huge amounts of saline water into fresh water ecosystem.[168,169]

3.1.4 Health impacts of chloride and sulfate

Low concentrations of chloride are not considered harmful to the human body, however, elevated concentrations of Cl^- gives water a bitter taste.[167] The WHO recommended drinking water standard for Cl^- is 250 mg L^{-1}, while that for SO_4^{2-} is 400 mg L^{-1}.[170] High-levels of chloride consumption may cause adverse health complications like hypertension, blood pressure, osteoporosis, ventricular hypertrophy, renal stone and asthma.[167,171] High concentrations of sulfate may disrupt water balance and ion-exchange processes.[172] Sulfate concentrations above the maximum threshold imposes health risk, like diarrhea. The most important consequence of SO_4^{2-} reduction is that it produces corrosive and toxic hydrogen sulfide (H_2S).[173,174]

3.1.5 Impacts of Cl^- and SO_4^{2-} on the measurement of Te and Sn in water

The quantifiation of metals in water with salinity contamination is difficult mainly for the presence of chloride and sulfate species. Chloride and sulfate are the two major anions

present almost in all natural waters.[162,163] Therefore, the effect of these two ions on the separation of tin from tellurium poses a great implication. Also, the analysis of Sn, and in particular ^{126}Sn in environmental waters, is also complicated with elevated concentrations of Cl^- and SO_4^{2-} anions, which affects the column separation of the ^{126}Te isobar.[204–207]

3.2 Experimental

3.2.1 Reagents and materials

Preparation of NaCl solution: NaCl (mol wt 58.44, Sigma Aldrich) was kept overnight at 60 °C and 1,000 ppm stock solution (100.0 mL) was prepared by dissolving 0.1634 g of salt into an appropriate amount of deionized water.

Preparation of Na_2SO_4 solution: Anhydrous Na_2SO_4 (mol wt 142.04, J. T. Baker Inc.) was placed in the oven (60 °C) for overnight and 1,000 ppm stock solution (100.0 mL) was prepared by dissolving 0.1463 g of the salt into an appropriate amount of deionized water.

Other common reagents and ancillary lab stuffs are essentially the same as described in chapter 2.

3.2.2 Metal adsorption and desorption

Preparation of batch test: The distribution coefficient, K_D, for tin and tellurium was determined as follows: 15 mL disposable plastic centrifuge tubes (Fisher Brand) were charged with 50 mg of TRU resin, followed by the addition of 200 µL standard tin (matrix: tr. HNO_3 and tr. HF, density = 1.00 g/mL) and tellurium (matrix: 10% (v/v) HNO_3, density = 1.085 g/mL) solutions (equivalent to 5.0 µg tin and 5.0 µg tellurium). The internal standard solutions of tin and tellurium were prepared in 2% HNO_3 (v/v), diluted by Milli-Q water (18.0 MΩ). Sample tubes were treated with hydrochloric acid at

concentrations ranging from 0.20 to 6.0 mol L^{-1}, the final volume was adjusted to 10.0 mL. Additionally, chloride and sulfate (70.0 mg L^{-1} each) solutions were added in separate tubes (for single anion test), along with a mixed charge (70.0 mg L^{-1} each of Cl^- and SO_4^{2-} solution). Again, a blank run was carried out to minimize traces of matrix interferences. The blank was prepared following the same experimental protocol adopted for sample preparation, except the addition of analytes. The blank run was substracted from the sample reading. Calibration curves for tin and tellurium were prepared daily for each batch of sample with concentrations of 20, 40, 60, 80, and 100 ppb of either tin or tellurium. The tubes were placed in a shaking bath for 90 minutes, and then centrifugated for 15 minutes at 3600 rounds per minute. After filtration of the supernatant and appropriate dilution, the subsequent analysis of tin and tellurium was carried out by ICP-MS.

Preparation of column test: 15 mL polypropylene Bio-Rad columns were packed with 100 mg of TRU resin, the column materials were washed with 10 mL of distilled water to remove fine dusts adhered on them. In 15 mL disposable centrifuge tubes, the column solutions were prepared by mixing standard solutions of tin (5.0 μg) and tellurium (5.0 μg), followed by the addition of appropriate amounts of Cl^- and SO_4^{2-}-spikes. Again, the solutions were charged with 3.0 mol L^{-1} of hydrochloric acid, i.e., the loading acid, the final volume was adjusted to 10 mL.

Arrangement for column wash: The loaded columns were washed with hydrofluoric acid at concentrations of 0.50 to 6.0 mol L^{-1}. The washing treatment in chapter 2 was accomplished with 10 mL of HF, and up to four such washings were performed to ensure the maximum amount of tin release, this time, however, the washing treatment was confined to once only, with the same volume of acid solution (10.0 mL). Both aliquots, from adsorption and desorption studies, were collected in separate tubes, and were

submitted, after sufficient dilution, for ICP-MS analysis of tin and tellurium. Three replicates were measured against an experimental blank. The blank was prepared following the same procedure adopted for the sample with an exclusion of tin and tellurium addition.

Addition of field water: For the determination of distribution coefficients (K_D) of tin and tellurium, field water (surface and groundwater) samples were spiked in volumes of 2-, 3-, 4-, and 5-mL, followed by the addition of standard solutions of tin and tellurium metals. In cases of desorption studies, field waters were added to lab solutions at amounts of 2-, 4-, and 6-mL.

3.2.3 Collection of environmental samples

Polypropylene sample bottles were washed with 2% HNO_3 (v/v), followed by a thorough rinse with the sample water (three times). The surface water (500.0 mL) was collected from the Ottawa River (Canada), from an arms-length depth beneath the top water level. The groundwater (1.0 L) sample was taken from an Ottawa (Canada) private tube-well (the 420-ft deep tube-well, installed in a roacky place, has been in operation for 13-years). The sample was collected from the wellhead, prior to any filtration or treatment system. Water samples were acidified with 2% HNO_3 (v/v, 1.50 mL/100 mL), however, an unacidified sample was kept for the chromatographic test of anions.

3.2.4 Chromatographic test of anions

The detection of Cl^- and SO_4^{2-} ions was carried out by ionic liquid chromatographic column (Dionex DX120 Ion Chromatograph). Unacidified surface and groundwater samples were filtered (Whatman mixed cellulose ester membrane filter, 1.2 μm, 25 mm) to remove suspended particles, and then the waters were diluted to two-times and five-times, respectively, with deionized water. Deionized water was used as the sample blank.

A triplicate run was done to ensure reproducibility. Calibration curves for the chromatographic test of anions are presented in Fig. 3.1.

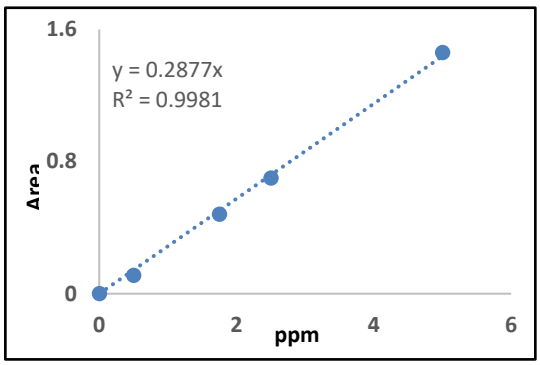

The calibration curve for chloride

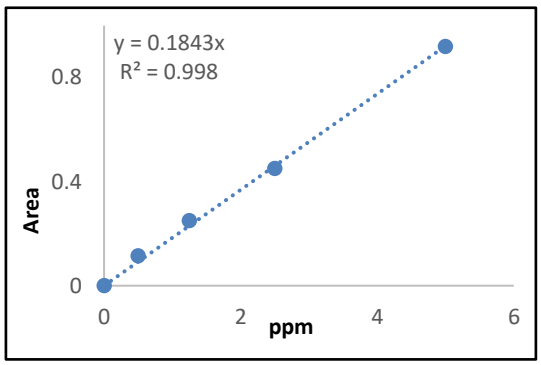

The calibration curve for sulfate

Fig. 3.1 Calibration curves for the measurement of chloride and sulfate anions.

3.3 Results and discussion

3.3.1 Concentrations of chloride and sulfate in tested water

The concentrations of anionic species in waterbodies can vary widely from region to region; for example, the typical concentrations of Cl^- and SO_4^{2-} in river water have been reported as 2.40 and 8.47 mg L^{-1}, respectively, whereas the corresponding values in groundwater were presented as 58.60 and 53.70 mg L^{-1}.[159] Another observations says that surface water Cl^- and SO_4^{2-} concentrations have been measured as 1989 and 290 mg L^{-1}, respectively, while that for groundwater were found as 95.30 and 48.00 mg L^{-1}.[175] In southeast Asia, the average pre-monsoon Cl^- and SO_4^{2-} concentrations in groundwater were detected as 288 and 272 mg L^{-1}, respectively.[167] Generally, the groundwater Cl^- concentration near the Indian Ocean is well above the 300 mg L^{-1} level, but in East African regions, it can fluctuate from as low as 19.00 mg L^{-1} to as high as 3603 mg L^{-1}.[169] Also, river water polluted by acid mine drainage in southwest Spain had shown a

concentration of SO_4^{2-} up to 8460 mg L^{-1}.[200] In our present study, the river water had a concentration of Cl^- as 29.97 mg L^{-1} and that for SO_4^{2-} as 9.78 mg L^{-1}, the corresponding values in groundwater were measured as 71.42 and 69.95 mg L^{-1} (Appendix 7.42).

3.3.2 Effects of chloride and sulfate ions on K_D

The K_D values of tin: The distribution coefficient, K_D, of tin onto TRU surface was evaluated in presence of chloride and sulfate solutions in hydrochloric acid medium at concentrations from 0.20 to 6.0 mol L^{-1}. Disposable centrifuge tubes (15 mL, Fisher Brand) were charged with standard tin and tellurium solutions (5.0 µg each) and the tubes were placed in the shaking bath for 90 minutes. In addition, laboratory prepared Cl^- and SO_4^{2-} solutions were spiked in a set of three different tubes: the first one with 70.0 mg L^{-1} of Cl^-, the second one with 70.0 mg L^{-1} of SO_4^{2-} and the third one with a mixture of 70.0 mg L^{-1} of Cl^- and 70.0 mg L^{-1} of SO_4^{2-} solutions. The final volume was adjusted to 10.0 mL. The spiked solutions were also allowed to keep under the same shaking treatment as did for the unspiked standard solutions.

The K_D values of tin for the unspiked, Cl^--, SO_4^{2-}-, and Cl^--SO_4^{2-}-mixed spikes were calculated in batch tests, presented in Fig. 3.2 (Appendix 7.47). It is worth mention that the measurement of K_D values in chapter 2, Fig. 2.3, for example, was determined with 100 mg of TRU resin and the samples were placed in the shaking bath for 120 minutes. However, the present observation was carried out with 50 mg of resin, to keep wastes as low as possible, and the shaking treatment was optimized to 90 minutes. Results reveal that the Cl^--spike has produced the highest K_D, followed by the SO_4^{2-}, Cl^--SO_4^{2-}-mixed, and the unspiked sample. At the initial point of acid treatment (0.20 mol L^{-1}), the samples have exhibited relatively smaller K_D values (average 159 ± 69 mL g^{-1}), after that all of them undergo a sharp inflation. The peak point was achieved at 3.0 mol L^{-1} of HCl

(average K_D 5517 ± 406 mL g^{-1}), and then they have experienced a slow recess till the very end of acid treatment (6.0 mol L^{-1}). The highest K_D was produced by the Cl^--spike (9623 ± 996 mL g^{-1}), observed at 3.0 mol L^{-1} of HCl. Also, at 3.0 mol L^{-1} of acid, the Cl^-- and the SO_4^{2-}-spikes possess almost the same K_D values, 8815 ± 387 and 8836 ± 950 mL g^{-1}, respectively.

In general, the adsorptive nature of tin on the solid phase in presence of Cl^- and SO_4^{2-} spikes follow an identical behavior with that of the unspiked sample. Having a close look on the distribution curve, it is evident that there are two distinct sets of curves: Cl^- and SO_4^{2-} spikes and the unspiked and mixed spiked samples. The former set possesses relatively higher K_D values (5827 ± 216 mL g^{-1}) compared to the latter group (5207 ± 253 mL g^{-1}). It is interesting that at 4.0 mol L^{-1} of hydrochloric acid, all four samples have produced almost similar K_D values (7750 ± 153 mL g^{-1}). However, at 6.0 mol L^{-1} of acid, the Cl^--spike has led to an enhancement of K_D by 19% than that of the mixed spike. Again, at 5.0 mol L^{-1} of HCl, the unspiked, Cl^--, and the mixed-spiked samples gave comparable adsorptions of tin (K_D 5143 ± 51 mL g^{-1}).

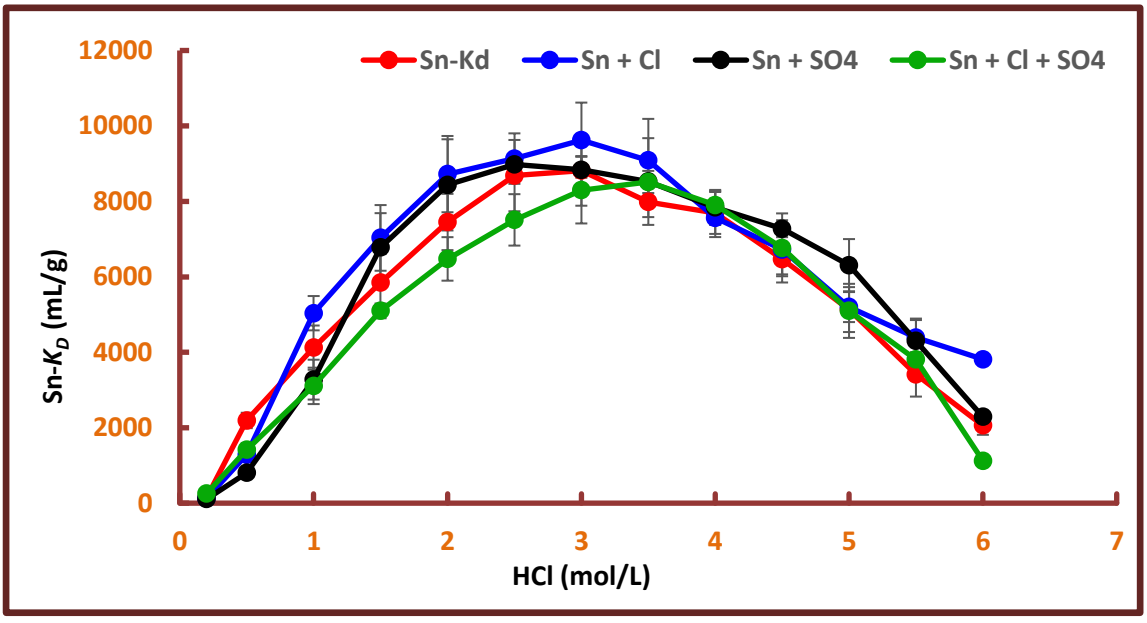

Fig. 3.2 K_D values of tin in presence of chloride and sulfate spikes in HCl medium.

The K_D values of tellurium: The adsorptive nature of tellurium on the resin bed is a little bit different from that of the tin retention. At low concentrations of HCl (0.20 to 2.5 mol L^{-1}), the K_D values of all samples first declined, giving the lowest adsorption at 1.5 mol L^{-1} of HCl, and then increases up to 5.0 mol L^{-1}, shown in Fig. 3.3 (Appendix 7.52). After that, the K_D values have dropped at 6.0 mol L^{-1} of HCl. The K_D values of tellurium for the unspiked, Cl^--, SO_4^{2-}-, and the Cl^--SO_4^{2-}-mixed spiked samples were measured in different concentrations of HCl (0.20 to 6.0 mol L^{-1}). Although the first three samples have produced a similar K_D, but the unspiked sample has shown a different adsorptive behavior after 2.0 mol L^{-1} of HCl. While the Te-K_D values of spiked samples have shown a sharp increase at 2.5 mol L^{-1} of acid, the unspiked sample exhibited a slow rise at 3.0 mol L^{-1} of HCl.

The overall distribution of tellurium in TRU resin shows an *S*-shaped (sigmoid) curve which has three distinct regions, caused by the treatment of 0.20 to 2.0, 2.0 to 4.5, and 4.5 to 6.0 mol L^{-1} of HCl. The first portion of the curve possesses a poor dependency of K_D on the concentrations of loading acid, whereas the other two segments have a strong correlation with the concentration of loading acid. However, the unspiked sample manifests a little variation of K_D on the concentration of acid up to 2.5 mol L^{-1}. Unlike other spiked samples, having displayed the maximum K_D value at around 4.5 mol L^{-1} of acid, the unspiked sample has demonstrated a maximum K_D value at 5.5 mol L^{-1} of HCl (average 3609 ± 84 mL g^{-1}).

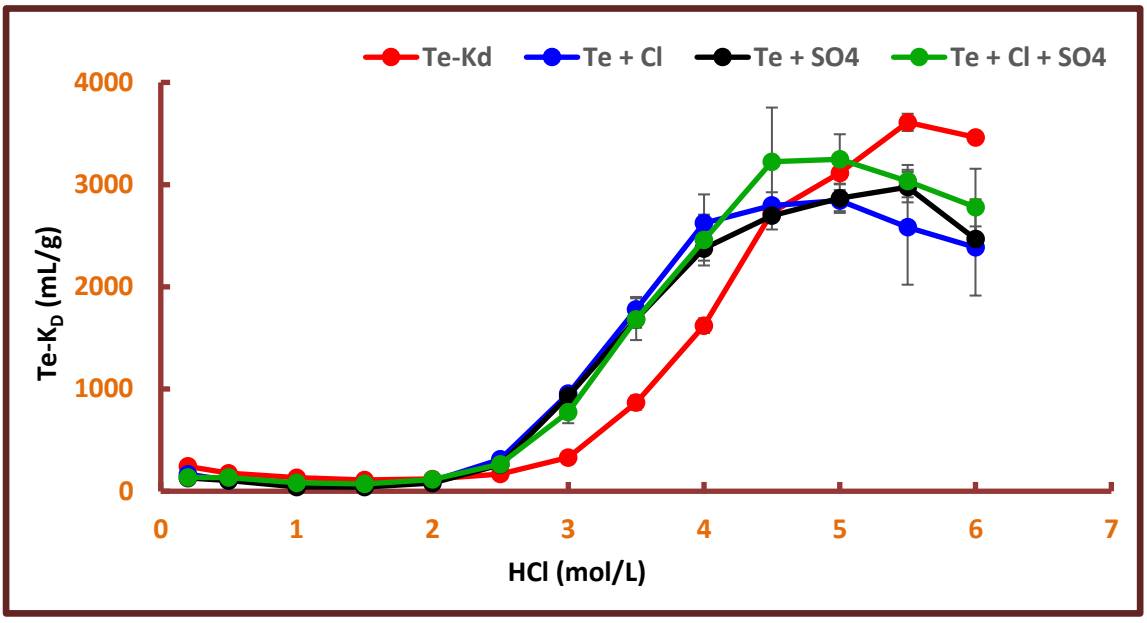

Fig. 3.3 K_D values of tellurium in presence of chloride and sulfate spikes in HCl medium.

A comparison of tin and tellurium K_D: The K_D values for tin and tellurium in aqueous hydrochloric acid were measured for each experiment at HCl concentrations of 0.20 to 6.0 mol L^{-1}, presented in Fig. 3.4 (Appendix 7.53). In the case of tin, the Cl^--spike has experienced an inflation of K_D by 11% from that of the unspiked sample, whereas the mixed-spiked sample has suffered a decrease in K_D of 7% compared to the unspiked one. A preliminary look on the overall distribution coefficients of tin and tellurium states that the adsorption of tin onto the solid phase is not significantly affected by the addition of Cl^- and SO_4^{2-} contaminants (each present at concentrations of 70.0 mg L^{-1}). On the other hand, the percent adsorption of tellurium on the solid phase has remained essentially the same. The average K_D value of tellurium for the unspiked, Cl^--, and SO_4^{2-}-spiked samples was measured as 1285 ± 6 mL g^{-1}, only a small difference from each other. However, the Te-K_D for the mixed spiked sample has exhibited a little higher K_D (1385 mL g^{-1}) compared to that of the unspiked sample. The overall result shows that our present

methodology can be applied successfully to measure the degree of tin adsorption onto the TRU resin in presence of chloride and sulfate anions with very little interfering effects.

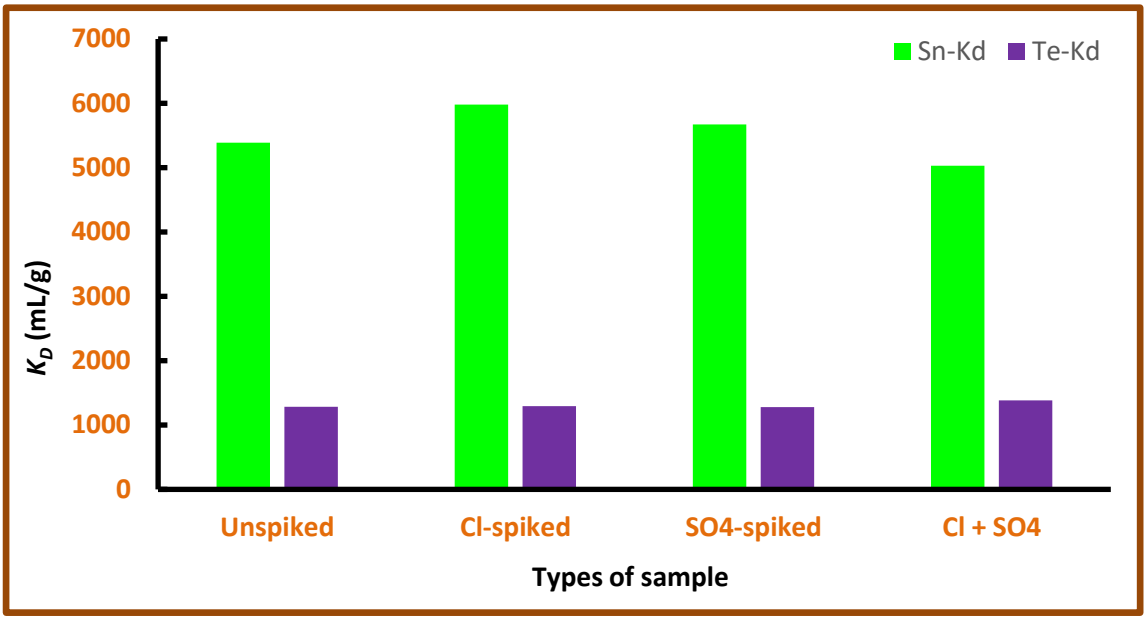

Fig. 3.4 A comparison of K_D values between tin and tellurium produced in HCl medium.

3.3.3 Optimization of contact time

The K_D values of tin: In the earlier batch tests (chapter 2), the distribution coefficients, K_D, of tin and tellurium have been determined by placing the reaction mixture into the scintillation vials, then the contents were kept in the shaking bath for 2-hours. In the present study, disposable centrifuge tubes were charged with appropriate amounts of reactants and the shaking treatment was performed for 180 minutes (20-minute interval) at HCl concentration of 3.0 mol L^{-1}. Results reveal that the tin-metal has produced the maximum K_D value (526 ± 18 mL g^{-1}) in 75 minutes of contact time, whereas the minimum K_D (148 ± 13 mL g^{-1}) was observed after 180 minutes of shaking treatment, Fig. 3.5 (Appendix 7.58). On the other hand, the chloride-, sulfate-, and the chloride-sulfate mixed spikes have produced, respectively, the maximum K_D in 105 (320 ± 32 mL

g^{-1}), 90 (357 ± 57 mL g^{-1}), and 75 (452 ± 40 mL g^{-1}) minutes of shaking treatment. The graph also shows that all three spiked solutions gave much lower K_D values (235, 286, and 289 mL g^{-1}, respectively) than that of the unspiked tin (363 mL g^{-1}). After 90 minutes of shaking, the K_D values of spiked solutions (except the chloride one) decline rapidly. In fact, the chloride-solution has produced the lowest average K_D (235 ± 65 mL g^{-1}) among all four samples. This result represents an understanding on the evaluation of maximum K_D of tin, which can be visualized by optimizing the contact time between 75 to 105 minutes or at around 90 minutes. After the saturation point, the degree of tin adsorption onto the resin surface decreases with increasing the analyte-substrate interaction time. A recent observation says that the maximum sorption (98%) of Sn(II) onto Amberlite XAD-2 resin in presence of alkaline solution (pH 9.5) took place at 120 minutes of contact time.[140]

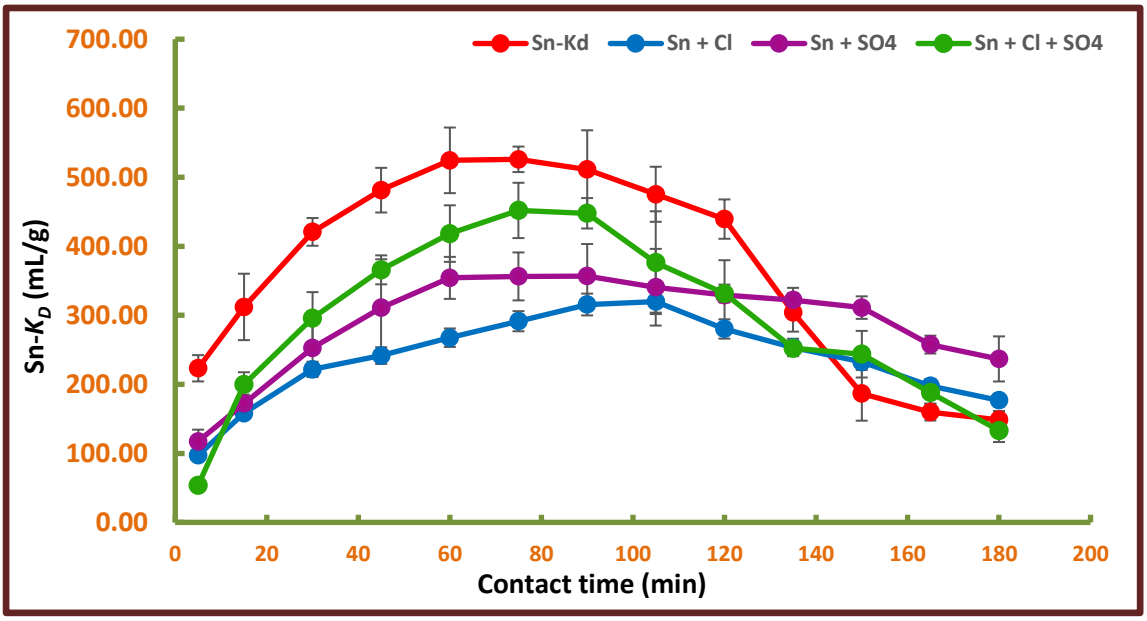

Fig. 3.5 K_D values of tin with respect to different contact times.

The K_D values of tellurium: In this case, the maximum K_D values for the unspiked, chloride-, sulfate-, chloride-sulfate mixed spikes were observed, respectively, after 75 (32 ± 7 mL g^{-1}), 60 (40 ± 6 mL g^{-1}), 105 (30 ± 1 mL g^{-1}), and 90 (35 ± 3 mL g^{-1}) minutes of shaking time, Fig. 3.6 (Appendix 7.63). The K_D values for these solutions follow the order: Cl^-- (27.64 mL g^{-1}) > Cl^--SO_4^{2-}-mixed (26.29 mL g^{-1}) > unspiked- (24.56 mL g^{-1}) > SO_4^{2-}- (18.70 mL g^{-1}) spikes. Like the adsorption of tin, the solutions have also demonstrated the highest distribution of tellurium in the solid phase between 75 to 105 minutes of shaking period. However, the chloride-spike has exhibited the maximum adsorption within 60 minutes of contact time. This is, in fact, the minimum contact time that gave the highest K_D among all four observations. In addition, the chloride-spike has produced the lowest K_D observed (8 ± 3 mL g^{-1}) at the end of a batch test (180 minutes). As with Sn-K_D, the Te-K_D values of all treatments decline gradually after 100-minutes of execution. In practice, a 90-minute shaking period is enough for both tin and tellurium to produce the highest retention of metals onto the resin surface. Again, like the adsorption of tin, a prolonged analyte-substrate interaction may cause a breakage of dipole-ion force operating between the resin and the metal ion. Therefore, the subsequent studies have been carried out by placing the batch materials into the shaking bath for an optimum contact time of 90 minutes.

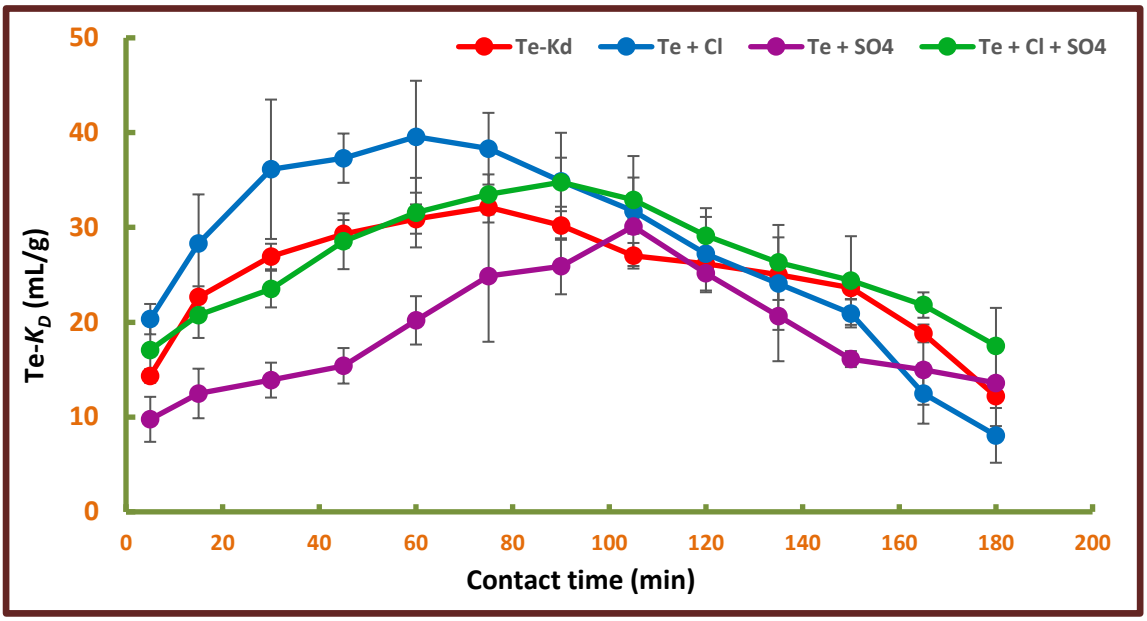

Fig. 3.6 K_D values of tellurium with respect to different contact times.

3.3.4 Effects of pH on K_D values in presence of Cl^- and SO_4^{2-} ions

***The K_D* values of tin:** The K_D values of tin for the unspiked, Cl^--, SO_4^{2-}-, and mixed-spiked samples in TRU resin for the entire pH ranges (1.0 to 7.0) were measured for each experiment in batch tests, presented in Fig. 3.7 (Appendix 7.68). Although the batch experiment was performed in presence of 3.0 mol L^{-1} of HCl, the effect of pH was studied to have a closer look on the behavior of K_D's at very low acidic conditions. It was also observed that the resin had lost stability in basic conditions. The TRU resin undergoes denaturation at 2.0 mol L^{-1} of NaOH, while a complete annihilation of resin structure occurred at 3.5 mol L^{-1} of NaOH.

In general, the K_D value increases with increasing pH of solution. However, at pH 3.0, the Cl^--spike experiences a drop of K_D (408 ± 71 mL g^{-1}) and at pH 4.0, it undergoes a further drop (278 ± 71 mL g^{-1}). In fact, at pH 4.0, all four samples have experienced a drop of K_D, producing an average of 348 ± 89 mL g^{-1}. In addition, at pH 4.0, the unspiked and the mixed-spiked samples have produced almost the same K_D (471 ± 5 mL g^{-1}), a

similar pattern has also been shown by the Cl^-- and the SO_4^{2-}-spikes (K_D is 271 ± 10 mL g^{-1}). At pH 6.0, the SO_4^{2-}- and the mixed-spikes have also experienced a drop of K_D, and then have displayed a sharp rise. While the K_D values of SO_4^{2-}- and the mixed-spikes have increased at pH 7.0 (360 ± 96 and 623 ± 217 mL g^{-1}, respectively), the other two solutions have demonstrated a drop in K_D. Over the entire pH ranges observed, only the unspiked sample has experienced a single drop at pH 4.0, but other three samples have exhibited a double-drop of K_D at pH values from 4.0 to 7.0. Fig. 3.8 (Appendix 7.69) also shows that the average highest K_D (511 ± 52 mL g^{-1}) for all spiked and the unspiked samples was found at pH level of around 5.0. Cigala et al.[176] have observed that tin forms two major species with SO_4^{2-} ions: $SnSO_{4(aq)}$ and $Sn(SO_4)_2^{2-}$. The $SnSO_{4(aq)}$ form predominates in the very acidic conditions, pH < 3.5. On the other hand, tin forms $SnCl_4^{2-}$, $SnCl^+$, and $SnCl_2$ species at highly acidic environments, at pH < 1.[44,46]

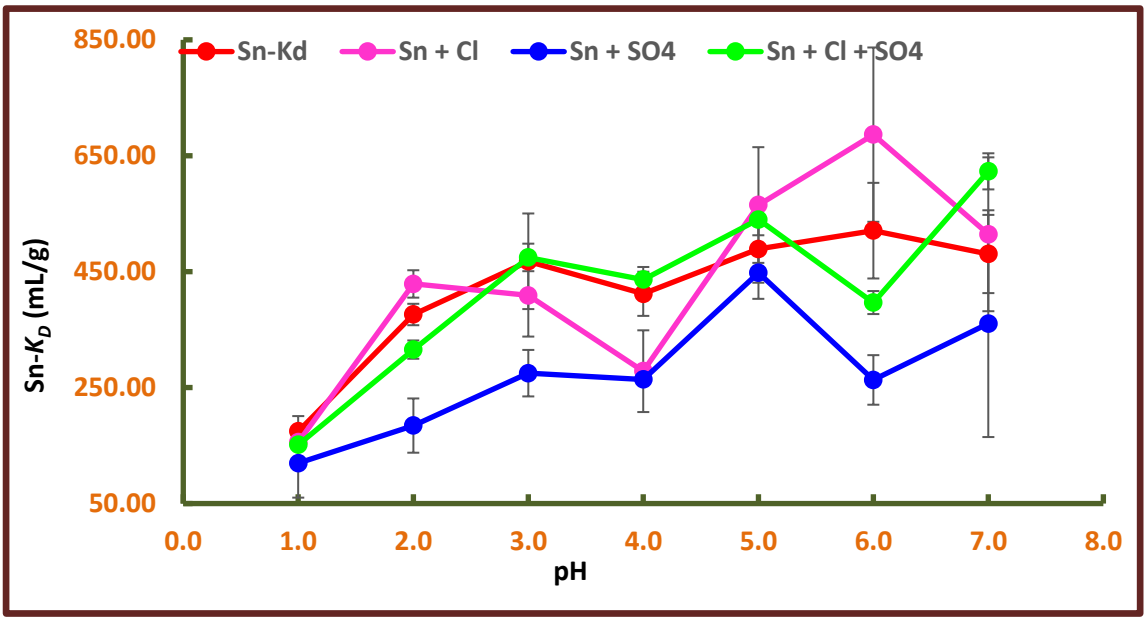

Fig. 3.7 Effects of pH on the K_D values of tin in presence of chloride and sulfate ions.

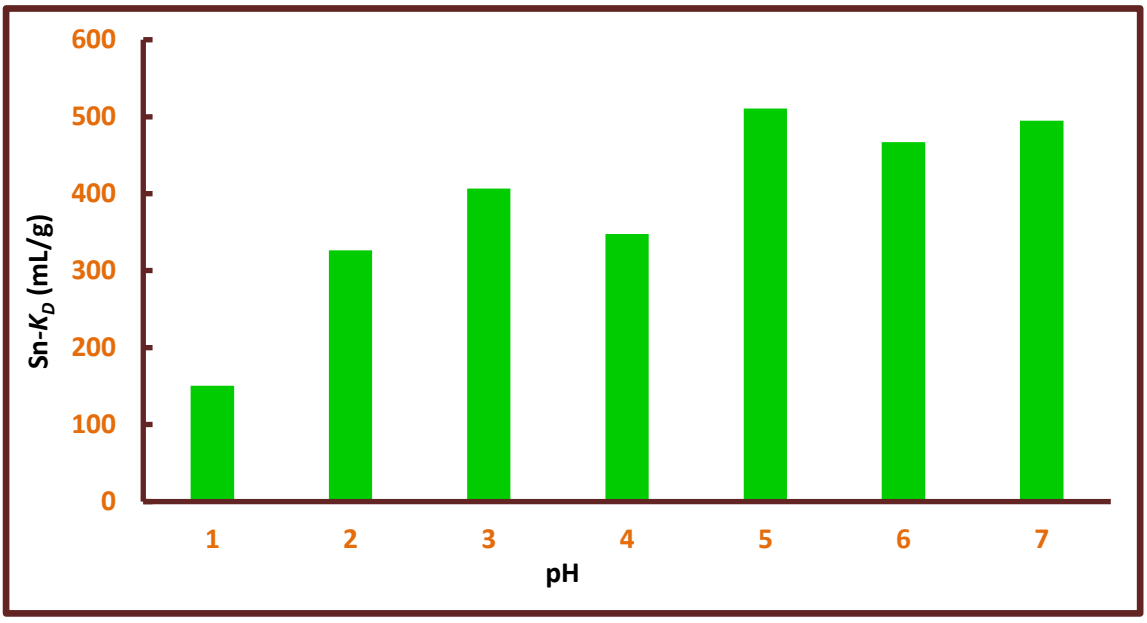

Fig. 3.8 Variation of the average K_D values of tin for all spiked and unspiked samples.

The K_D values of tellurium: The K_D values of tellurium for the unspiked, Cl^--, SO_4^{2-}-, and the Cl^--SO_4^{2-}-mixed-spiked samples in TRU resin for the entire pH ranges (1.0 to 7.0) were measured for each experiment following the same protocol adopted for tin, presented in Fig. 3.9 (Appendix 7.74). Like the distribution of tin, the adsorption of tellurium onto the solid phase gets increased with increasing pH of solution. From pH 1.0 to 6.0, the unspiked and the Cl^--spiked samples display similar behavior, but at pH 7.0, the former gets a sharp increase of K_D, whereas the latter experiences a quick drop. The average K_D of these two samples from pH 2.0 to 6.0 were found as 162 ± 6 and 163 ± 18 mL g^{-1}, respectively. The SO_4^{2-}-spiked sample has shown an inflation of K_D from pH 1.0 to 2.0 (152 ± 8 mL g^{-1} to 229 ± 66 mL g^{-1}), but on increasing the pH of solution from 2.0 to 6.0, it undergoes a steady slash of K_D to produce the minimum value (194 ± 23 mL g^{-1}). Again, at pH 6.0, the K_D value of the SO_4^{2-}-spiked sample has received a sharp inflation and has attained a value of 257 ± 32 mL g^{-1} (at pH 7.0). The Cl^--SO_4^{2-} mixed-

spiked sample has exhibited an increase of K_D while increasing the pH of solution from 1.0 to 5.0, after that point, it shows a drop of K_D until the neutral pH of 7.0 (216 ± 5 mL g^{-1}). The overall distribution curve shows that the adsorption of tellurium in presence of Cl^- and SO_4^{2-} contaminants onto the resin surface is favored at pH 4.0 to 5.0.

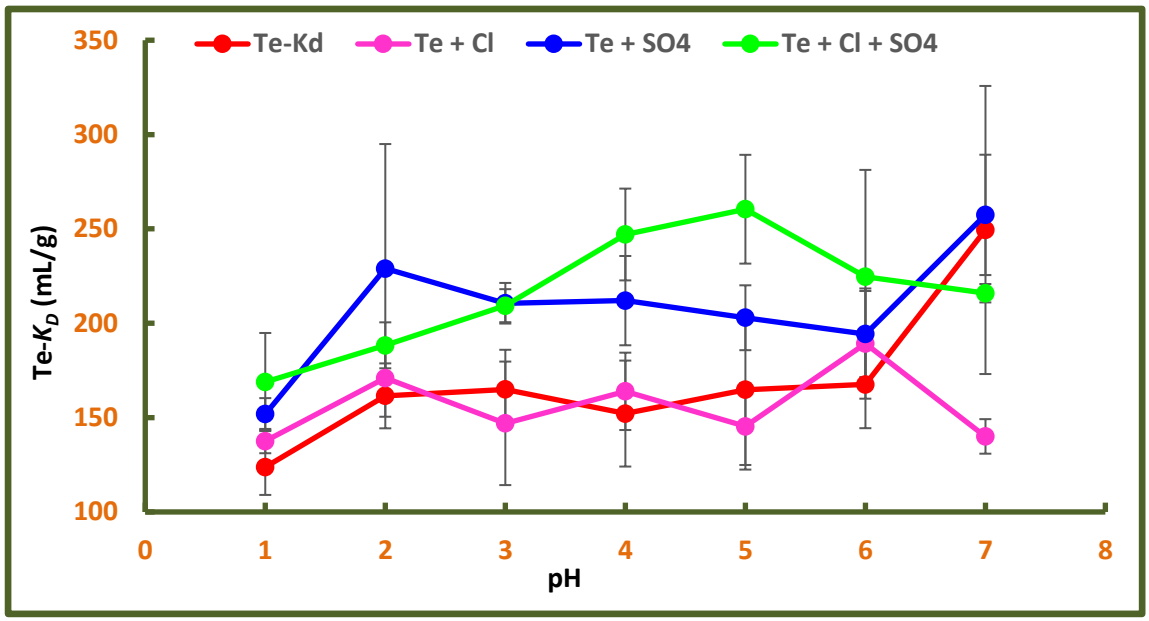

Fig. 3.9 Effects of pH on the K_D values of tellurium in presence of chloride and sulfate ions.

3.3.5 Effects of shaking orientation

The K_D values of tin: The initial experiment to determine the distribution coefficients of tin and tellurium was performed by charging the appropriate amounts of reactants in the disposable scintillation vials, and the vessels were kept on the shaking bath for 2 hours. This time, 15-mL disposable centrifuge tubes were used to study the adsorptive nature of tin and tellurium on the resin. It is worth mention that the tubes were placed horizontally along the direction of shaking, whereas the vials were positioned vertically.

Results reveal that the batch test carried out in the tube has produced relatively higher K_D values compared to the values obtained in the vials. The unspiked, Cl^--, SO_4^{2-}-, and mixed-spiked samples treated in the tube (horizontal alignment) have yielded an average

K_D values of 5386, 6049, 5674, and 5029 mL g^{-1}, respectively, and the corresponding values found in the vial (vertical alignment) follows as 1761, 3116, 2421, and 1901 mL g^{-1}, Fig. 3.10 (Appendix 7.79). The unspiked sample shaken in the tube shows an inflation of K_D by 206%. The Cl^--, SO_4^{2-}-, and the mixed-spiked samples have also garnered inflations in K_D by 94, 134, and 165%, receptively. The unspiked, SO_4^{2-}-, and the mixed-spiked samples treated in the vial at hydrochloric acid concentrations of 0.50 to 3.0 mol L^{-1} have exhibited similar adsorptive nature, but the SO_4^{2-}-spike has shown an inflation of K_D after the treatment of 3.0 mol L^{-1} of HCl. The Cl^--spiked sample shaken in the vial has produced the highest average K_D (3116 mL g^{-1}) among all other vial-samples.

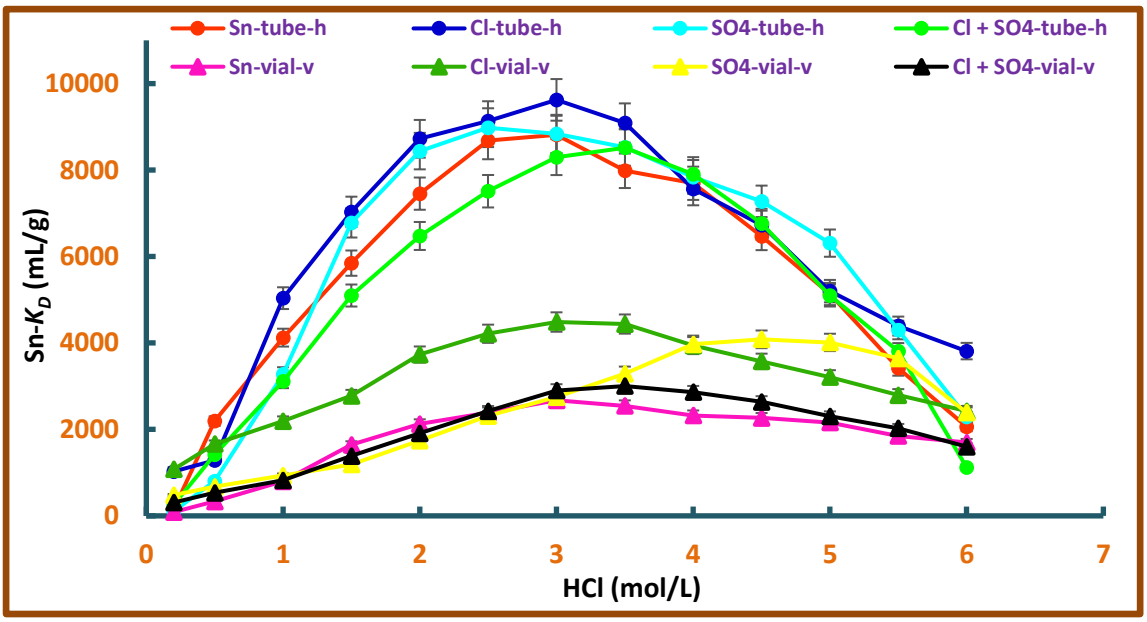

Fig. 3.10 K_D values of tin in different shaking orientations in presence of chloride and sulfate ions, 'h' stands for horizontal and 'v' for vertical alignments. Note that unlike the batch experiment of Chapter 2, where the packing material was 100 mg with shaking time of 120 minutes, in this case, 50 mg of TRU resin was charged in a shaking period of 90 minutes.

The K_D values of tellurium: Like the K_D values of tin, noticeable changes in the K_D values of tellurium have also been observed when the shaking orientations were changed. The general trend of Te-K_D values in the tube (horizontal alignment) stays nearly constant: Cl^--SO_4^{2-}-mixed spike (1385 ± 1370 mL g^{-1}) > Cl^--spike (1292 ± 1214 mL g^{-1}) > unspiked (1283 ± 1426 mL g^{-1}) > SO_4^{2-}-spike (1281 ± 1243 mL g^{-1}), whereas the corresponding values for the vial (vertical alignmnet) decreases as: unspiked (965 ± 1051 mL g^{-1}) > Cl^--SO_4^{2-}-mixed spike (679 ± 654 mL g^{-1}) > Cl^--spike (457 ± 497 mL g^{-1}) > SO_4^{2-}-spike (397 ± 385 mL g^{-1}), Fig. 3.11 (Appendix 7.84). The most important change was observed in the case of SO_4^{2-}-spike, where the tube has produced 3.22-times more K_D than that of vial, an inflation by 222%. The Cl^--spike shaken in the tube has also experienced a similar inflation of K_D (184%). The Cl^--SO_4^{2-}-mixed spike and the unspiked samples, treated in the tube, have produced 104 and 33%, respectively, more K_D than that of vial. The overall result of K_D for Te demonstrates that the unspiked sample receives the minimum impact on the change of shaking position, whereas the effect caused, due the change of orientation, for the spiked-samples is very high.

After a thorough study on the present results, it is apparent that the horizontal shaking, placing the materials in the tube and positioned along the direction of movement (0° position) ensures a well mixing and the spiked elements get maximum interaction with the surface of the adsorbent. Therefore, this position has produced a higher K_D. On the other hand, the content in the vial, positioned vertically along the direction of shaking movement (90° position), is insufficient to thoroughly mix the contents, meaning getting less metal-resin interaction and produces smaller K_D values. For this reason, the subsequent sample treatment has been carried out placing the reaction mixture in the disposable centrifuge tubes (horizontal shaking).

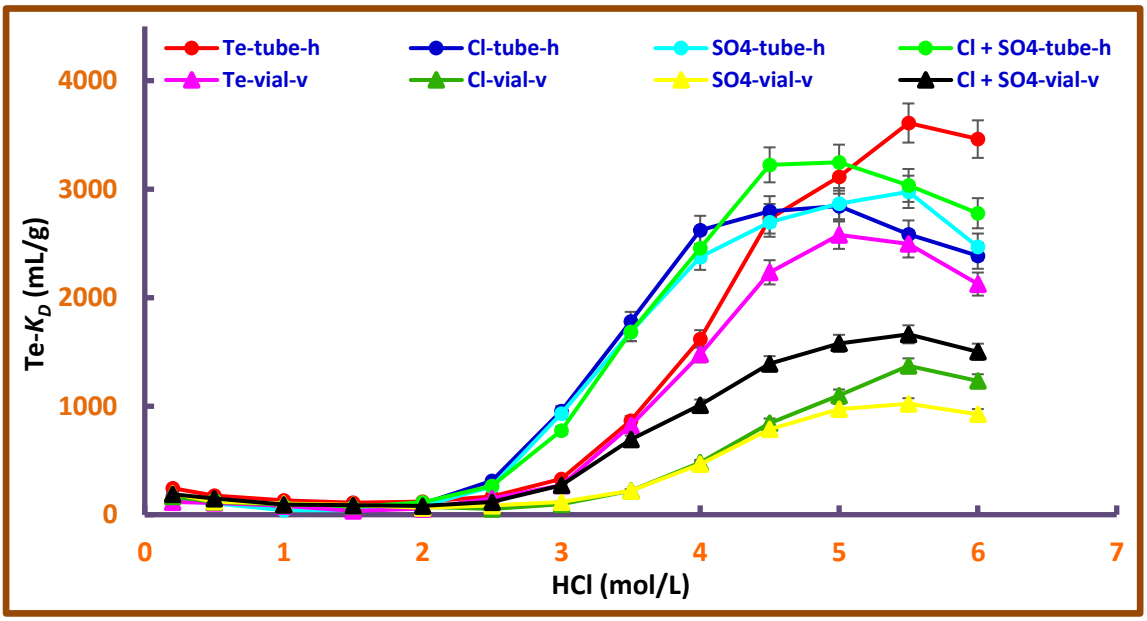

Fig. 3.11 K_D values of tellurium in different shaking orientations in presence of chloride and sulfate ions, 'h' stands for horizontal and 'v' for vertical alignments.

3.3.6 Distribution coefficients with surface water addition

The K_D values of tin: Surface water (collected from Ottawa River) was spiked with standard solutions of tin and tellurium at amounts of 2-, 3-, 4-, and 5-mL of surface water and then the distribution coefficient of individual element has been determined under normal experimental conditions (addition of 5.0 µg of tin and 5.0 µg of tellurium treated at HCl concentrations of 0.20 to 6.0 mol L^{-1}, the final volume was adjusted to 10.0 mL with deionized water).

Results of K_D values for the entire ranges of acid concentrations (0.20 – 6.0 mol L^{-1} of HCl) for the unspiked, 2-, 3-, 4-, and 5-mL-surface water spikes were presented in Fig. 3.12 (Appendix 7.90). In general, the K_D value increases with increasing the concentration of acid up to 4.0 mol L^{-1} of HCl (for the 0-spiked sample, it is 4.5 mol L^{-1}), and then goes down up to the very end of acid treatment (6.0 mol L^{-1}). The 2-mL spiked sample has produced the highest average K_D, whereas the 5-mL spike gave the lowest

value. In fact, the 5-mL spike has demonstrated the lowest K_D throughout the whole ranges of acid treatment. Although the 3-mL spike has exhibited a relatively slow inflation up to 4.0 mol L^{-1} of acid, but it has shown a change after this point, giving the highest average K_D from 4.5 to 6.0 mol L^{-1} (38191 ± 5072 mL g^{-1}). From 5.5 to 6.0 mol L^{-1}, the 0-spiked and the 4-mL spike have shown almost identical drops of K_D, 26682 ± 3503 and 27025 ± 2880 mL g^{-1}, respectively, and a similar observation was also noticed for the cases of 2-, and 3-mL spiked samples, 31921 ± 3403 and 33176 ± 3608 mL g^{-1}, respectively. The overall result demonstrates that the spiked-samples show a decreasing trend in K_D with increasing volume of surface water addition: Sn-K_D for 2 mL > 3 mL > 4 mL > 5 mL. In fact, the 5-mL spike has yielded the lowest observed K_D among all spiked and unspiked samples. Fig. 3.13 (Appendix 7.91) shows the effect of surface water addition on the K_D values of tin.

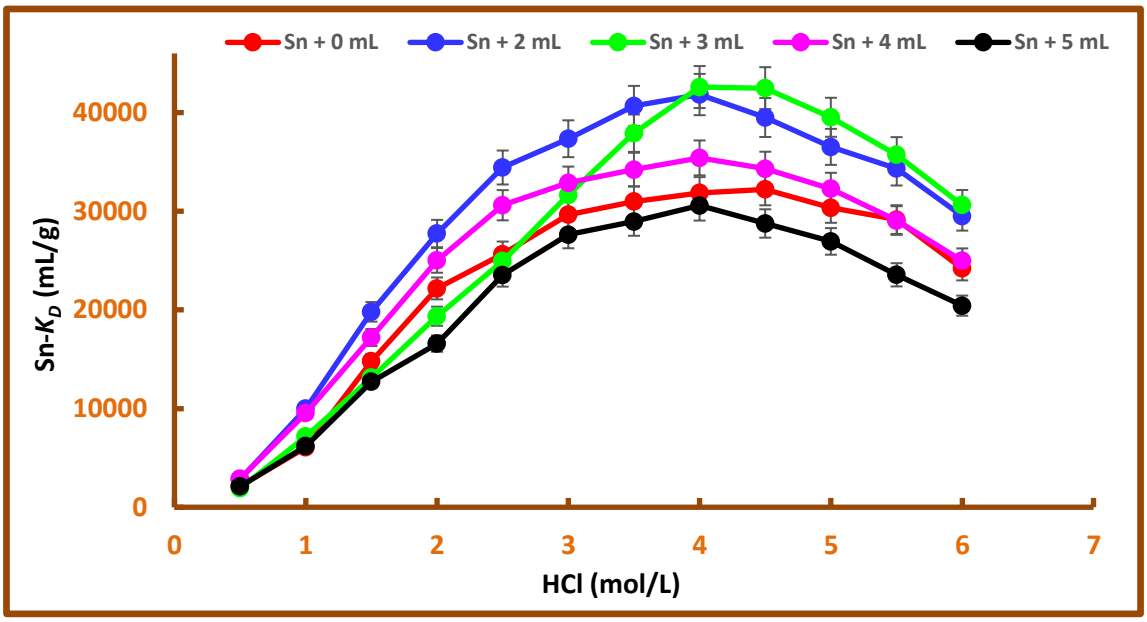

Fig. 3.12 K_D values of tin in presence of surface water. Again, the amount of batch materials and shaking times are different from those presented in Chapter 2.

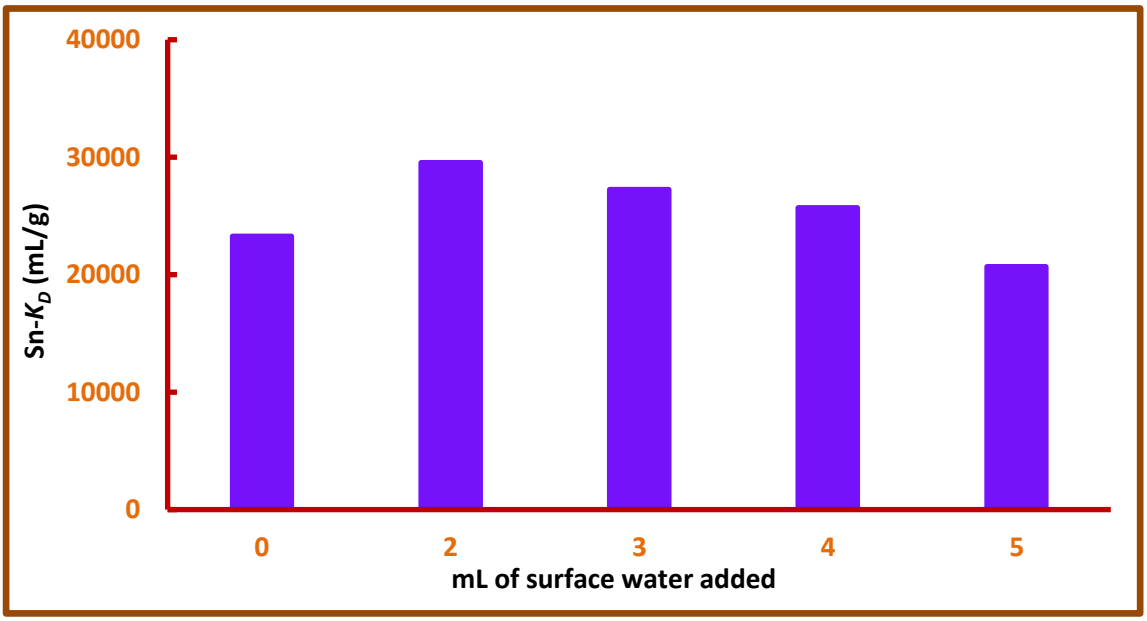

Fig. 3.13 The effect of surface water addition on the K_D values of tin.

The K_D values of tellurium: The K_D values of tellurium in presence of unspiked and spiked samples follow the order: 3-mL (1164 ± 1031 mL g^{-1}) > 5-mL (1140 ± 974 mL g^{-1}) > 2-mL (1089 ± 905 mL g^{-1}) > 4-mL (1087 ± 896 mL g^{-1}) > 0-spike (1032 ± 872 mL g^{-1}), Fig. 3.14 (Appendix 7.97). It is interesting that the 2-mL- and the 4-mL-spiked samples have produced almost the same K_D (1088 ±1.56 mL g^{-1}). Identical behaviors were also noticed in cases of 3-mL- and 5-mL-spiked samples (K_D 1152 ±17 mL g^{-1}). The 0-spike sample has produced the lowest K_D among all samples studied.

The graph manifests that the adsorptive nature of tellurium on the TRU resin is independent of the concentration of HCl from 0.2 to 2.0 mol L^{-1}. After 2.0 mol L^{-1} of HCl, the K_D value increases as per the *S*-shaped sigmoid-curve up to 5.0 mol L^{-1}, and then goes down. At the highest point of K_D (5.0 mol L^{-1} of HCl), the 3-mL-spiked sample shows the maximum value (2568 ±100 mL g^{-1}). In summary, the overall distribution of tellurium on the solid phase increases in presence of surface water, but unlike the

adsorption of tin, where the distribution goes down with increasing amounts of surface water, the distribution of tellurium is rather sporadic.

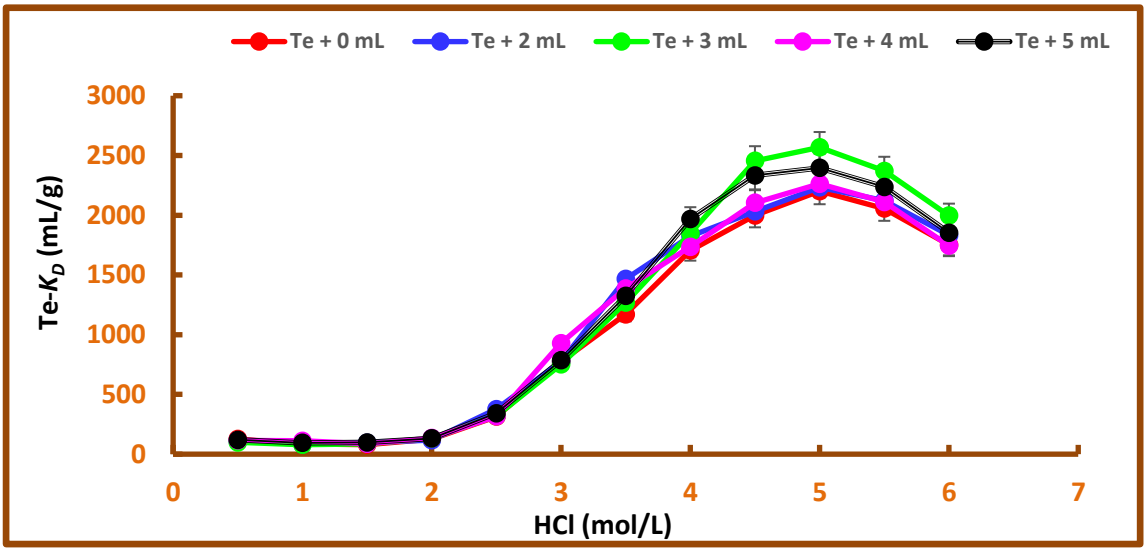

Fig. 3.14 K_D values of tellurium in presence of surface water.

3.3.7 Distribution coefficients with groundwater addition

The K_D values for tin: Like the surface water treatment, groundwater (collected from an Ottawa private house installed in a rocky place) was spiked with standard solutions of tin at amounts of 2-, 3-, 4-, and 5-mL (the very similar experimental conditions adopted for surface water, in order to comply with the overall experimental sequence, groundwater spikes were taken in terms of volume instead of sample mass). The K_D values for the 0-, 2-, 3-, 4-, and 5-mL-spikes were measured for each spike, presented in Fig. 3.15 (Appendix 7.103). This observation dictates that the 3-mL-spike has produced the highest K_D, whereas the 0-spike has the lowest. From 0.20 to 1.5 mol L^{-1} of HCl, all study samples have exhibited similar inflations of K_D, though the 0-spike has kept maintaining the lowest value. At 4.0 mol L^{-1} of HCl, the samples invariably show the highest value of K_D, and then a recession is observed. From 3.0 to 5.0 mol L^{-1} of HCl treatments, the samples exhibit a symmetric inflation or deflation of K_D on either side of the peak point

observed at 4.0 mol L^{-1}. At 4.5 mol L^{-1} of HCl, the 2- and 4-mL spikes have produced almost the same K_D (average 25053 ± 776 mL g^{-1}). Again, from 5.0 to 6.0 mol L^{-1} of HCl, both 2- and 5-mL spikes have demonstrated similar rates of deflation on K_D, their averages were: 24429 ± 422 mL g^{-1} (at 5.0), 20978 ± 401 mL g^{-1} (at 5.5) and 19789 ± 200 mL g^{-1} (at 6.0 mol L^{-1} of HCl). In addition, at 3.0 mol L^{-1} of HCl, 2-, 4-, and 5-mL spikes have almost similar values of K_D (23344 ± 833 mL g^{-1}). The overall scenario of K_D values for tin in presence of groundwater spike indicates that the distribution of tin onto the solid phase increases slightly, and the 3-mL spikes produces the highest K_D, followed by the 5-, 4-, and 2-mL spikes.

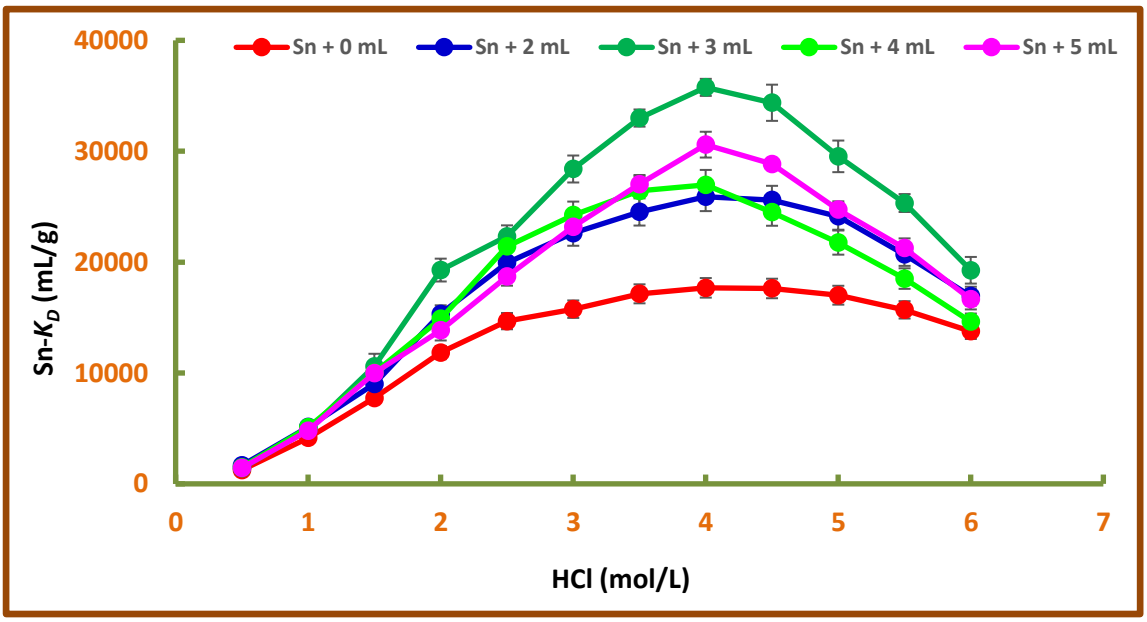

Fig. 3.15 K_D values of tin in presence of groundwater.

The K_D values of tellurium: The K_D values of tellurium in presence of 0-, 2-, 3-, 4-, and 5-mL of groundwater addition were measured in batch tests at HCl concnetrations of 0.50 to 6.0 mol L^{-1}, presented in Fig. 3.16 (Appendix 7.109). Again, like the distribution coefficient of tin, the distribution of tellurium with 0-spike sample is the lowest. The

spiked samples have exhibited the maximum K_D at 4.5 mol L^{-1} of HCl, except the 0-spike, which shows the maximum adsorption of tellurium at 5 mol L^{-1} (1009 ± 25 mL g^{-1}). A close inspection on the overall distribution curve reveals that the samples have experienced a drop of K_D at 1.5 mol L^{-1} of acid treatment. At the peak point of K_D graphs, 2-, 3-, and 4-mL spikes gave similar results (1433 ± 34 mL g^{-1}), and an analogous behavior was also observed from 3.0 to 4.0 mol L^{-1} of HCl. At 3.5 mol L^{-1}, they have produced comparable results (871 ± 34 mL g^{-1}). A similar adsorptive nature of tellurium was also displayed by these samples at 6.0 mol L^{-1} (1051± 25 mL g^{-1}). The overall distribution curve shows three distinct regions: the relatively flat region (0.2 to 2.0), the growth region (2.5 to 4.0), and the depletion region (4.5 to 6.0 mol L^{-1} of HCl treatment). The combined average value of K_D for the 0- and 5-mL spikes (729 ± 49 mL g^{-1}), observed at 6.0 mol L^{-1} of HCl, is almost one-half of the average K_D of 2-, 3-, and 4-mL spikes (1483 ± 24 mL g^{-1}) appeared at 5.5 mol L^{-1} of HCl.

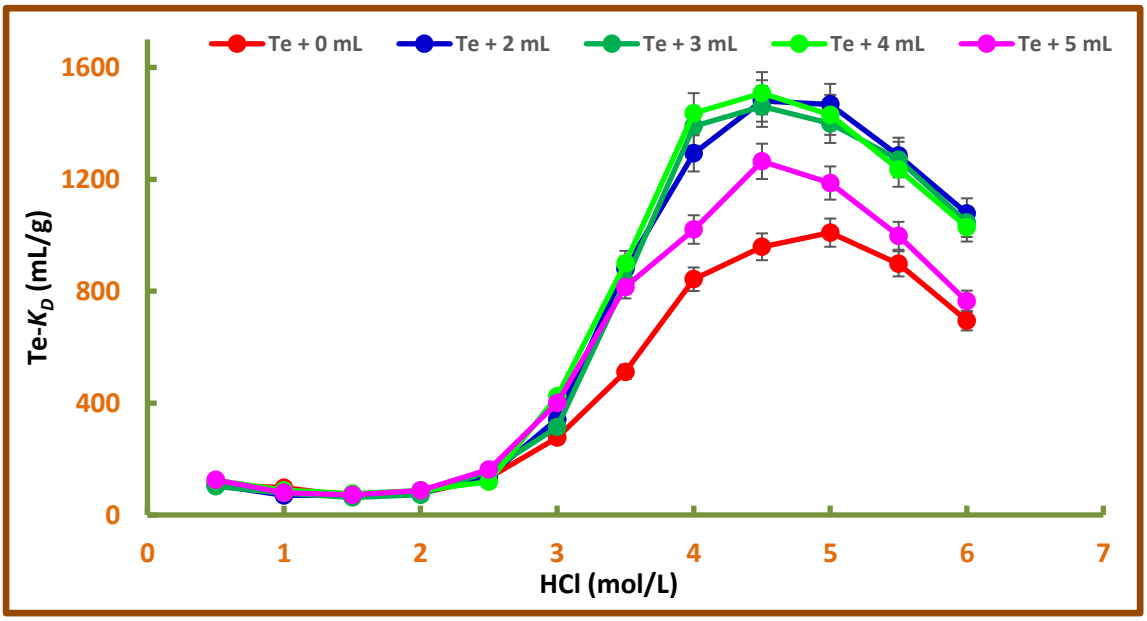

Fig. 3.16 K_D values of tellurium in presence of groundwater.

Comparison between tin and tellurium adsorption: A comparison on the adsorptive behaviors of tin and tellurium on TRU resin in presence of groundwater spike reveals that the adsorption of tin increases with increasing the amount of water added, Fig. 3.17 (Appendix 7.110). Among the four groundwater spikes studied so far, the 3-mL volume shows the highest retention of tin in the solid phase, followed by the 5-mL and 3-mL volumes. On the other hand, the highest adsorption of tellurium is exhibited in presence of 4-mL spike. Both tin and tellurium have demonstrated the lowest adsorptive capacity on the column bed with the zero-addition of groundwater. Similar adsorptive natures of tin are viewed in presence of 2- and 4-mL spikes (17559 ± 88 mL g^{-1}). Also, an analogous attitude is also discerned for the tellurium adsorption in presence of 2- and 3-mL spikes (18668 ± 171 mL g^{-1}). Tables 3.1 (Appendix 7.111) and 3.2 (Appendix 7.112) summarize the observed K_D values of tin and tellurium for both surface and groundwater.

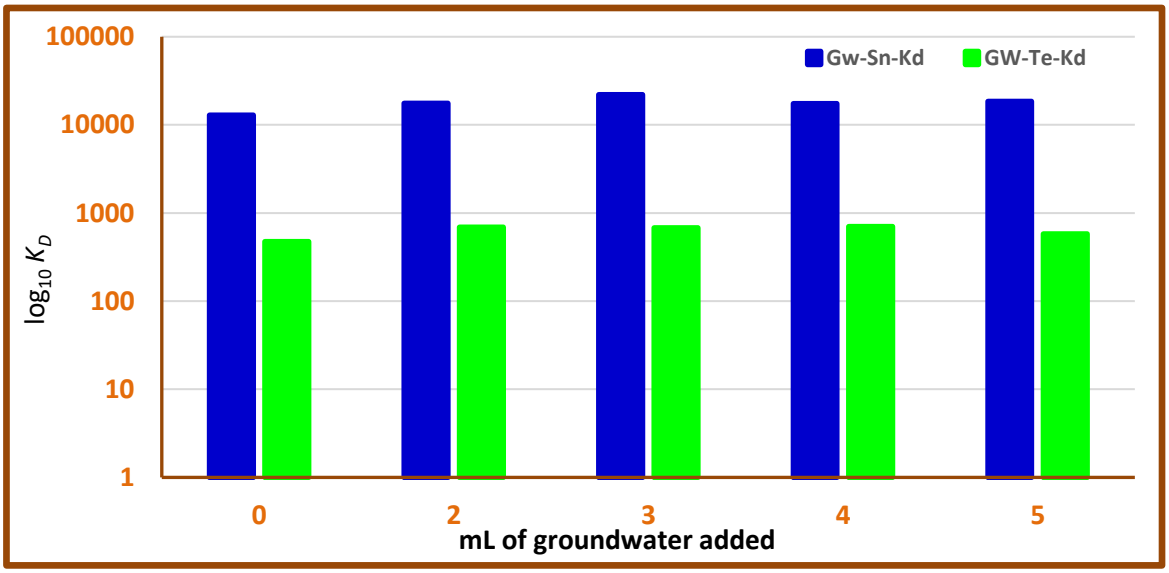

Fig. 3.17 A comparison of on the K_D values of tin and tellurium in presence of groundwater (GW).

Table 3.1: K_D values of tin and tellurium in presence of surface water.

Amount of Sn added (mg L^{-1})	Volume of water added (mL)	Equivalent conc of Cl^- added (mg L^{-1})	Equivalent conc of SO_4^{2-} added (mg L^{-1})	Observed K_D (mL g^{-1})	
				Sn	Te
0.50	0.0	0.00	0.00	23274	1752
0.50	2.0	5.99	1.96	29546	1832
0.50	3.0	8.99	2.93	27256	1997
0.50	4.0	11.99	3.91	25704	1745
0.50	5.0	14.99	4.89	20670	1853

Table 3.2: K_D values of tin and tellurium in presence of groundwater.

Amount of Sn added (mg L^{-1})	Volume of water added (mL)	Equivalent conc of Cl^- added (mg L^{-1})	Equivalent conc of SO_4^{2-} added (mg L^{-1})	Observed K_D (mL g^{-1})	
				Sn	Te
0.50	0.0	0.00	0.00	13756	473
0.50	2.0	14.28	13.99	16931	691
0.50	3.0	21.42	20.99	19264	682
0.50	4.0	28.57	27.98	14631	705
0.50	5.0	35.71	34.98	16648	581

3.3.8 Adsorption-desorption of tin and tellurium with Cl^-- and SO_4^{2-}-spikes

Column loading: The column packing in chapter 2 was optimized with 100 mg of TRU resin, this time, however, the packing load was kept to 50 mg of resin to keep wastes as low as possible. The packed columns were charged with solutions containing: i) 5.0 µg of Sn, 5.0 µg of Te, 70.0 mg L^{-1} of Cl^-, and 3.0 mol L^{-1} of HCl, ii) 5.0 µg of Sn, 5.0 µg of Te, 70.0 mg L^{-1} of SO_4^{2-}, and 3.0 mol L^{-1} of HCl, and iii) a mixed sample with 5.0 µg of Sn, 5.0 µg of Te, 70.0 mg L^{-1} of Cl^-, 70.0 mg L^{-1} of SO_4^{2-}, and 3.0 mol L^{-1} of HCl. Again, the total volume was adjusted to 10.0 mL. Additionally, very similar experimental conditions were maintained as described in chapter 2 for the adsorption-desorption studies of tin and tellurium.

Loading condition: A thorough study on the distribution coefficients of tin and tellurium reveal that the maximum K_D for tin was found at HCl concentrations of around 3.0 mol L^{-1}, while tellurium has shown the highest K_D near the HCl concentration of 5.0 mol L^{-1}. The average adsorption of tin in 3.0 mol L^{-1} of hydrochloric acid is more than 98%, whereas the adsorption of tellurium is close to 60%. Our desire is to keep the amount of tin in the solid phase as high as possible maintaining a lower concentration of tellurium. Therefore, the adsorption of metals on the resin bed was carried out in presence of 3.0 mol L^{-1} of hydrochloric acid.

Washing treatment: In chapter 2, the optimization of washing condition was executed by treating the loaded metal with hydrofluoric acid at concentrations of 0.20 to 6.0 mol L^{-1}. It was also found (chapter 2) that the maximum average desorption of tin (95.09 ± 2.22%) can be ensured after the 4th wash of adsorbed metals, taking 10-mL of HF at a time, maintaining a total volume of 40 mL of washed out solution. Moreover, it was also observed that the 1st wash with 10-mL of HF releases an average of around 86% of tin. Since the optimization of washing volume and a follow up metal desorption was practiced in a greater detail in chapter 2, in the present study, the washing treatment was restricted to once only with 10 mL of hydrofluoric acid at concentrations of 0.50 to 6.0 mol L^{-1}.

Adsorptions of tin and tellurium with Cl^-- and SO_4^{2-}-spikes: The average adsorption of tin and tellurium with Cl^-- and SO_4^{2-}-spikes was found as 99.17 ± 0.35 and 62.48 ± 4.15%, respectively, Fig. 3.18 (Appendix 7.115). Tin with a 0-spike has shown an adsorption of 98.74 ± 0.07%, which is the lowest among all other spiked samples. This was also found true in case of tellurium, the 0-spike gave the lowest adsorption (57.94 ± 1.80%) compared to the spiked samples (average 63.99 ± 3.48%). While the SO_4^{2-}-spike has demonstrated the maximum adsorption of tin (99.59 ± 0.32%), the Cl^--SO_4^{2-}-mixed spike has shown the highest value for tellurium (67.86 ± 2.12%). Interestingly, the Cl^--

spike has exhibited an intermediate adsorption for both tin and tellurium, 99.12 ± 0.09 and 63.04 ± 2.18%, respectively. In addition, the Cl^-- and the mixed-spiked samples have produced a comparable adsorption of tin (average 99.16 ± 0.07%). On the other hand, tellurium has followed increasing trend of adsorption in the order: 0-spike (57.94 ± 1.80) < SO_4^{2-}-spike (61.09 ± 1.45) < Cl^--spike (63.04 ± 2.18) < Cl^--SO_4^{2-}-mixed spike (67.86 ± 2.12%).

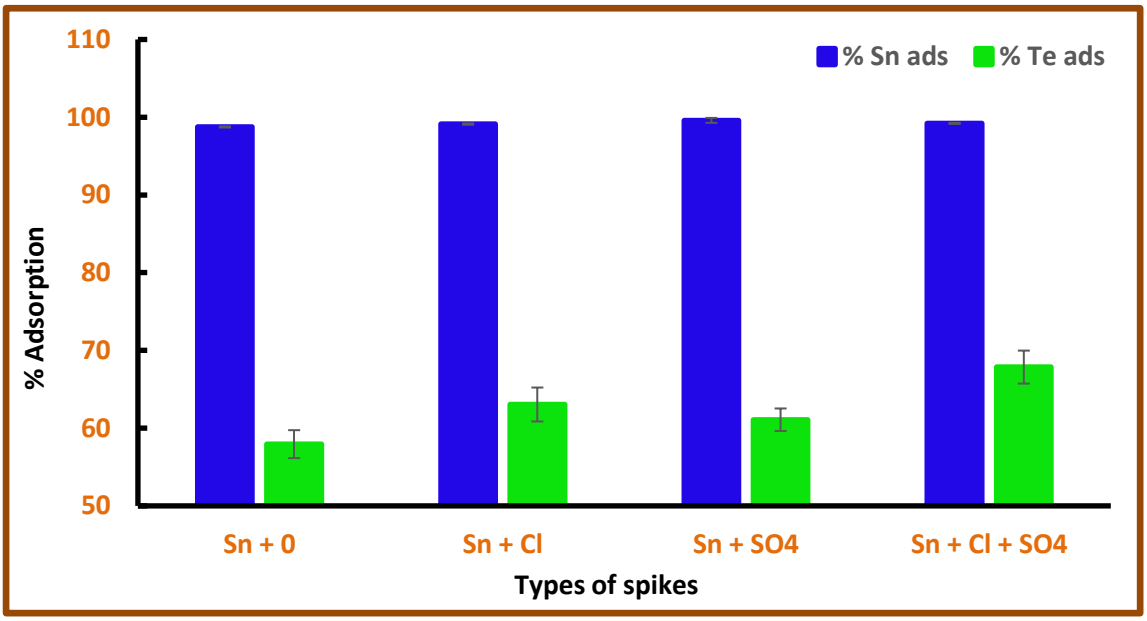

Fig. 3.18 Adsorptions of tin and tellurium in 3.0 mol L^{-1} of HCl solution in presence of chloride and sulfate ions.

***The desorption of tin with Cl^-- and SO_4^{2-}-spikes*:** The average desorption of tin washed by the treatment of hydrofluoric acid at concentrations of 0.50 to 6.0 mol L^{-1} for the 0-, Cl^--, SO_4^{2-}-, and Cl^--SO_4^{2-}-mixed spikes was found as 80.12 ± 2.20, 77.65 ± 5.16, 84.45 ± 5.83, and 85.82 ± 5.51%, respectively, Fig. 3.19 (Appendix 7.120). Note that the percent of metal released out was calculated for a single wash only with 10 mL of HF. Results show that the desorption of tin for the spiked samples are higher than that of the

unspiked sample, except for the Cl^--spike, which exhibited a drop of tin in the wash. At 0.50 mol L^{-1} of HF, the desorption of tin for the Cl^--spike was the lowest (70.28 ± 3.92%), and the SO_4^{2-}-spike has produced the highest (79.33 ± 2.83%) release. The maximum desorption of tin (95.56 ± 2.09%) was noticed for the SO_4^{2-}-spike treated at 6.0 mol L^{-1} of HF, followed by the mixed-spike (94.01 ± 1.02%), again treated with 4.0 mol L^{-1} of HF. On the other hand, at 6.0 mol L^{-1} of HF, the unspiked and the Cl^--spike have demonstrated almost similar desorption of tin, 84.13 ± 2.27 and 84.57 ± 2.89%, respectively. In case of SO_4^{2-}-spiked sample, the desorption of tin has experienced a big effect on the change of HF concentrations. At 0.50 mol L^{-1} of HF, the desorption of tin was 79.33%, whereas at 6.0 mol L^{-1}, it was found as 95.56%, an increase of 20% desorption. A close inspection on the desorption profile of tin reveals that the percent of washing increases with increasing the concentration of HF for the Cl^--spike, whereas the 0-spike shows a steady wash from 1.0 to 4.0 mol L^{-1} of HF. The SO_4^{2-}-spike has also shown an increase of washing efficiency with increasing the concentration of HF, expect for the 3.0 mol L^{-1} of HF treatment, which shows a lower desorption (80.54 ± 11.18%). Again, the Cl^--SO_4^{2-}-mixed spike has demonstrated an increase of tin wash with increasing concentrations of HF from 0.50 to 4.0 mol L^{-1}, beyond this point, a drop of desorption was observed.

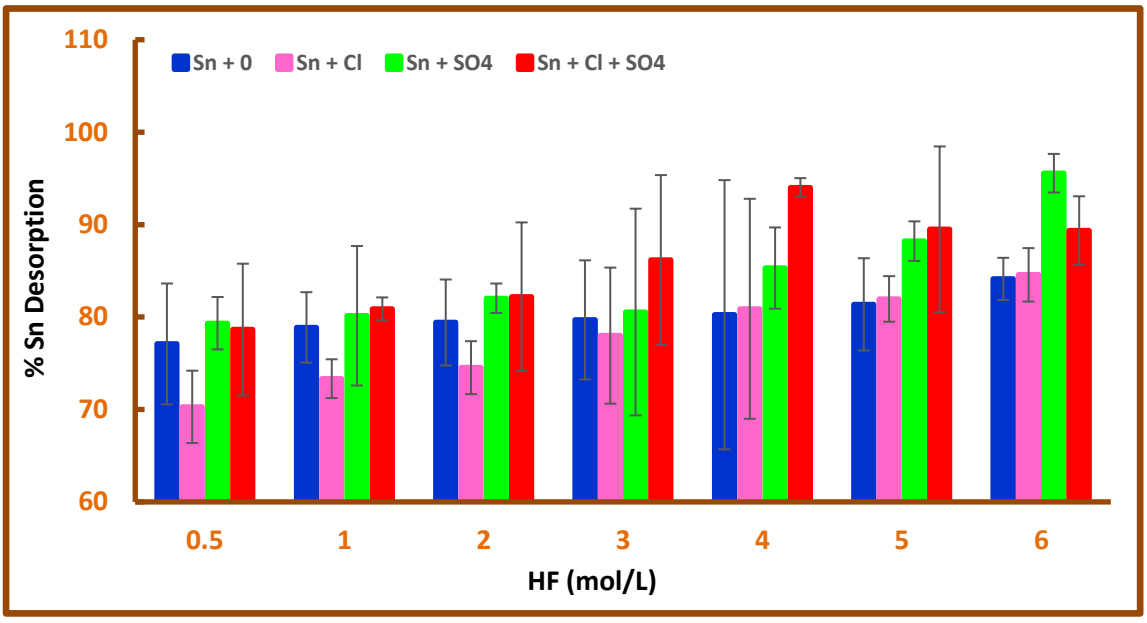

Fig. 3.19 The desorption of tin by hydrofluoric acid treated at concentrations of 0.50 to 6.0 mol L^{-1}.

***The desorption of tellurium with Cl^-- and SO_4^{2-}-spikes*:** The average desorption of tellurium washed by the treatment of hydrofluoric acid at concentrations of 0.50 to 6.0 mol L^{-1} for the 0-, Cl^--, SO_4^{2-}-, and Cl^--SO_4^{2-}-mixed spikes was found as 20.95 ± 3.53, 21.05 ± 3.47, 23.82 ± 4.65, and 16.78 ± 3.67%, respectively, Fig. 3.20 (Appendix 7.125). In general, like the desorption of tin, the percent of tellurium washed out also gets increased with increasing concentrations of hydrofluoric acid. However, the Cl^--spike shows a drop in the percent of tellurium in wash from 5.0 mol L^{-1} (25.94 ± 1.42%) to 6.0 mol L^{-1} (24.24 ± 2.07%) of HF. At 0.50 mol L^{-1} of HF, the desorption of tellurium for the mixed-spike is the lowest (11.91 ± 0.73%), whereas the percent wash for the SO_4^{2-}-spike is the highest (19.17 ± 3.14%). The maximum desorption of tellurium was found for the SO_4^{2-}-spike (30.82 ± 2.70%) treated at HF concentration of 6.0 mol L^{-1}. On increasing the concentration of HF, the SO_4^{2-}- and the mixed-spikes have exhibited an increase of tellurium desorption, but the 0- and the Cl^--spikes have shown a drop of desorption. At

6.0 mol L^{-1} of HF, the desorption of the 0-spike and the mixed-spike have increased 76 and 87%, respectively, against that of the 0.50 mol L^{-1} acid treatment, whereas the desorption of the Cl^--spike has increased by only 52%. Also, at 2.0 mol L^{-1} of acid, a similar desorption of tellurium was observed in cases of 0-, Cl^--, and SO_4^{2-}-spikes (average 20.31 ± 0.11%). Again, at 4.0 mol L^{-1} of acid, the 0- and the Cl^--spike gave almost identical result (average 22.30 ± 0.28%). The overall results of tellurium wash demonstrate that both the Cl^-- and SO_4^{2-}-spikes have shown higher percentage of tellurium release with respect to the 0-spike, whereas the mixed-spike has produced a lower percentage of desorption.

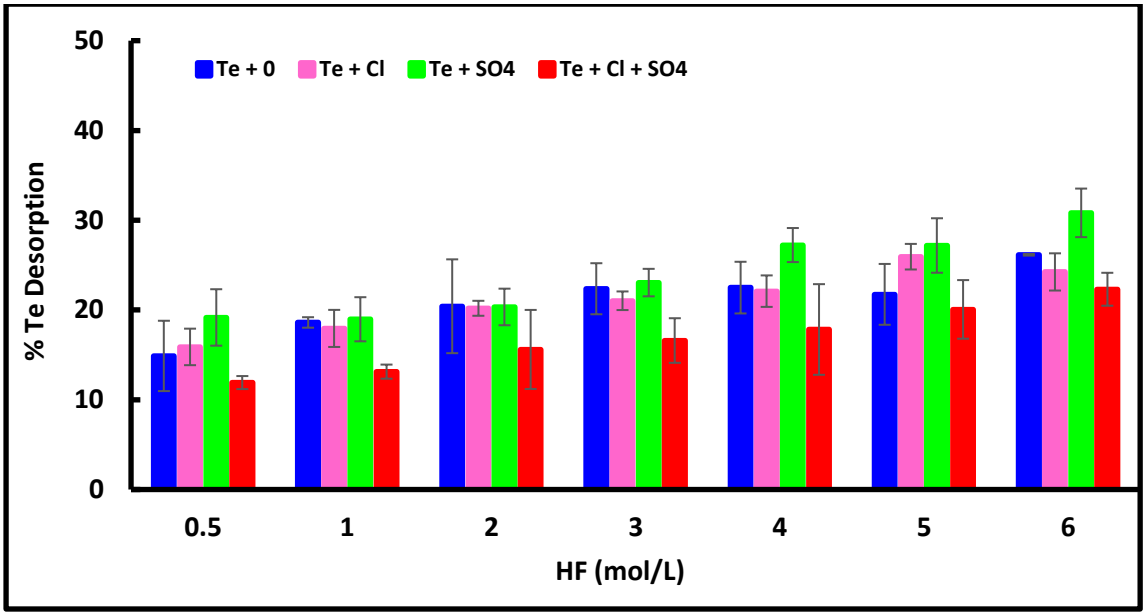

Fig. 3.20 The desorption of tellurium by hydrofluoric acid treated at concentrations of 0.50 to 6.0 mol L^{-1}.

3.3.9 Adsorption-desorption of tin and tellurium with surface water spikes

Adsorptions of tin and tellurium: The average adsorption of tin and tellurium was found as 99.30 ± 0.23 and 63.27 ± 1.62%, respectively, Fig. 3.21 (Appendix 7.128). For both tin and tellurium, the spiked solutions gave a little higher adsorption compared to the

unspiked sample. Interestingly, tellurium has exhibited an elevated percentage of adsorption on increasing the volume of spikes, 62.74 ± 2.88% for 2-mL spike and 65.25 ± 5.15% for 6-mL spike. For tin, on the other hand, the adsorption with 2-mL spike is the highest (99.48 ± 1.02%), followed by the 6-mL (99.38 ± 0.06%) and 4-mL (99.36 ± 0.77%) spikes. Moreover, the average adsorption of tellurium for the spiked samples was observed as 63.90 ± 1.27%.

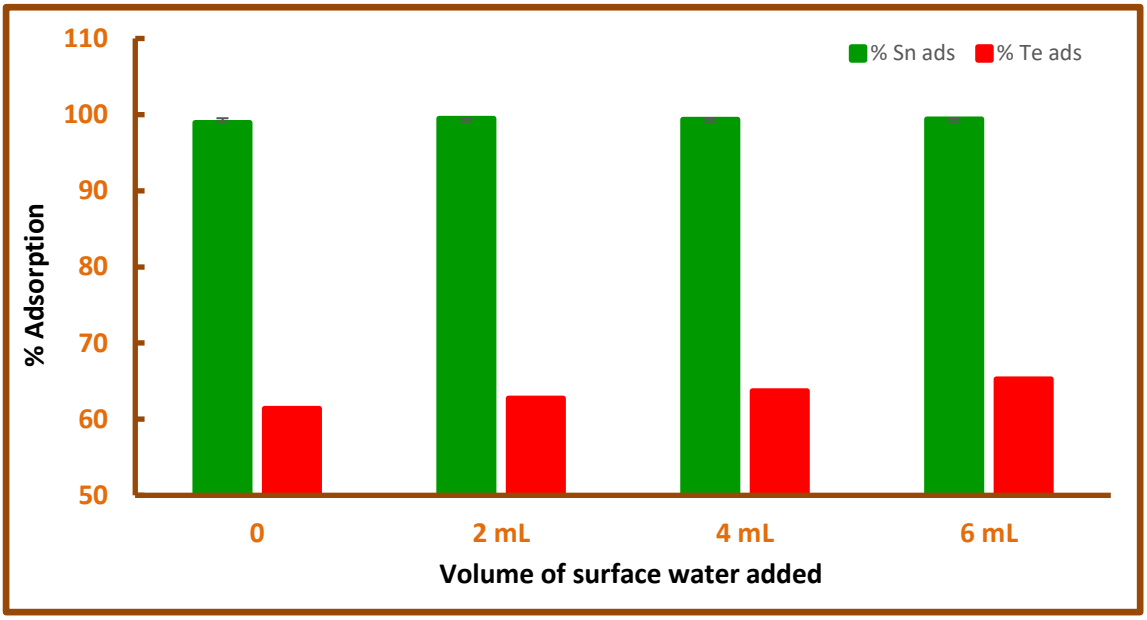

Fig. 3.21 The adsorptions of tin and tellurium in 3.0 mol L^{-1} of HCl solution in presence of surface water.

The desorption of tin with surface water spikes: The average desorption of tin washed by the treatment of hydrofluoric acid at concentrations of 0.50 to 6.0 mol L^{-1} for the 0-, 2-, 4-, and 6-mL spikes was found as 86.89 ± 8.96, 84.29 ± 3.98, 87.22 ± 5.52, and 83.54 ± 4.39%, respectively, Fig. 3.22 (Appendix 7.133). Again, the wash treatment was performed only once with 10 mL of HF. In general, the percentage of tin wash increases with increasing the concentration of hydrofluoric acid. The surface water had a Cl^- concentration of 29.97 mg L^{-1}, while that for SO_4^{2-} was 9.78 mg L^{-1}. The corresponding

values for groundwater were 71.42 and 69.95 mg L^{-1}. As the project aim was to monitor the success of our proposed methodology to separate tin from tellurium in normal environmental conditions, the surface water (with much less analyte content than that of the laboratory standards) was chosen as a test case. A similar testing experiment was also carried out with groundwater spikes. Results show that the 4-mL spike gave the highest desorption than that of the unspiked sample, whereas the 2-mL and the 6-mL spikes have exhibited lower percentages of tin wash. At 0.50 mol L^{-1} of HF, the 4-mL spike gave the maximum desorption (80.79 ± 2.54%), and the 0-spike has produced the lowest (72.76 ± 5.85%) in wash. At 1.0 mol L^{-1} of HF, the spiked samples have exhibited rather an identical washing behavior, the average tin release was 81.16 ± 0.49%. A similar observation was also noticed at 3.0 mol L^{-1} of acid, all three spiked samples have demonstrated comparable desorption of tin (average 84.83 ± 0.81%). At 6.0 mol L^{-1} of HF, the percentage of tin release increases by 31, 15, 18, and 16% for the 0-, 2-, 4-, and 6-mL spikes, respectively, against the values observed at 0.50 mol L^{-1}. It is also clear that the 0-spiked sample has produced almost double wash of tin than that of the 2-mL spike when the concentration of HF increases from 0.50 to 6.0 mol L^{-1}. The 4-mL spike, though gave a relatively poor wash (average 86.95 ± 5.98%) at low concentrations of acid, up to 4.0 mol L^{-1}. A big jump in the percentage of tin release (93.65 ± 3.33%) is seen after the concentration of acid has been raised to 5.0 mol L^{-1}. Again, the onward trend of tin release for the 4.mL spike was continued (95.24 ± 2.72%) up to the highest tested concentration of HF (6.0 mol L^{-1}). On the other hand, a bump of acid concentration by only a single unit, from 1.0 to 2.0 mol L^{-1}, the washing of tin for the 0-spiked sample has increased by 20%, the highest inflation observed between two adjacent points.

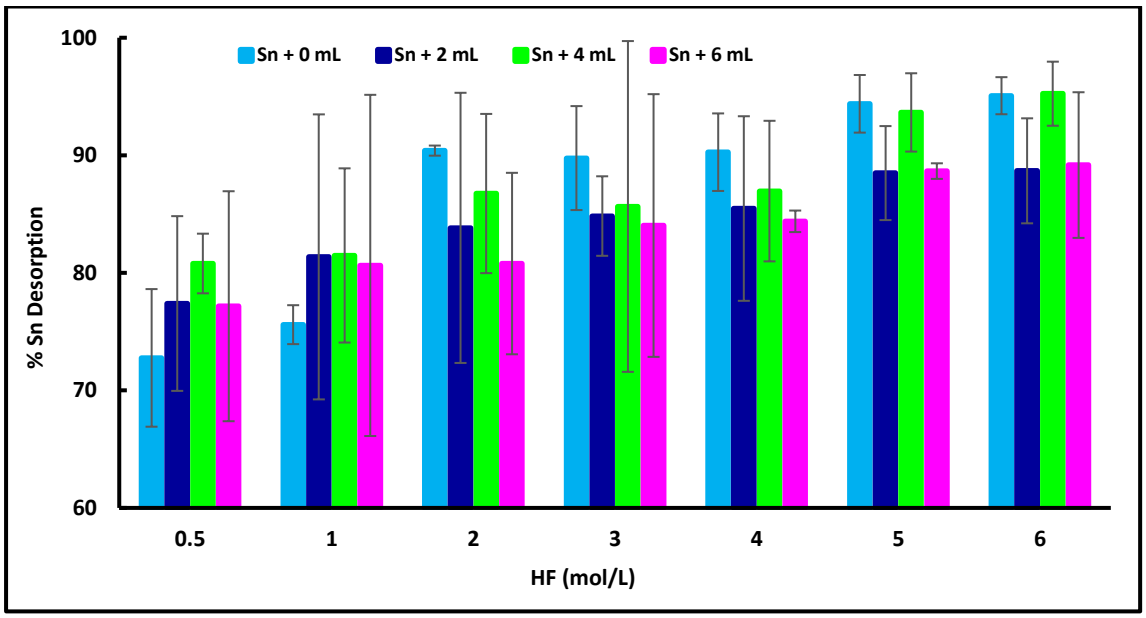

Fig. 3.22 The desorption of tin by hydrofluoric acid (0.50 to 6.0 mol L^{-1}) in presence of surface water.

The desorption of tellurium with surface water spikes: The average desorption of tellurium washed by the treatment of hydrofluoric acid at concentrations of 0.50 to 6.0 mol L^{-1} for the 0-, 2-, 4-, and 6-mL spikes was found as 18.06 ± 7.06, 11.49 ± 4.46, 13.54 ± 4.53, and 17.45 ± 3.95%, respectively, Fig. 3.23 (Appendix 7.138). At 0.50 mol L^{-1} of HF, the 0-spiked sample gave the lowest tellurium wash (6.46 ± 2.61%), whereas the 6-mL spike has shown the highest (12.46 ± 0.76%) desorption. With an increase of HF concentration from 0.50 to 1.0 mol L^{-1}, the desorption of tellurium for the 0-spiked sample has increased by 98%, but the 6-mL spike gave an inflation of only 10%. In general, the percentage of tellurium wash increases with increasing concentrations of HF. However, the 0-spike sample has experienced a small drop of tellurium wash from 4.0 to 5.0 mol L^{-1} of HF (22.35 ± 2.86 to 21.60 ± 3.37%). A similar small drop of elution was also observed in case of 6-mL spike, the percent desorption was dropped from 17.36 ± 2.60 to 15.16 ± 0.76% when the concentration of acid has been changed from 3.0 to 4.0

mol L^{-1}. A change in HF concentration from 0.50 to 6.0 mol L^{-1} causes a bump of tellurium desorption by 302% for the 0-spiked sample, whereas the 2-, 4, and 6-mL spike undergo an increase of desorption by 210, 126, and 87%, respectively. Additionally, the 2-mL spike has experienced a slash tellurium release by 0.35% when the concentration of acid has increased from 4.0 to 5.0 mol L^{-1}. The 4-mL spike has also suffered a small drop of wash after changing the concentration of acid from 4.0 to 5.0 mol L^{-1}. It is evident from the elution curve that the overall increase of tellurium wash has started after treating the sample with 3.0 mol L^{-1} of hydrofluoric acid.

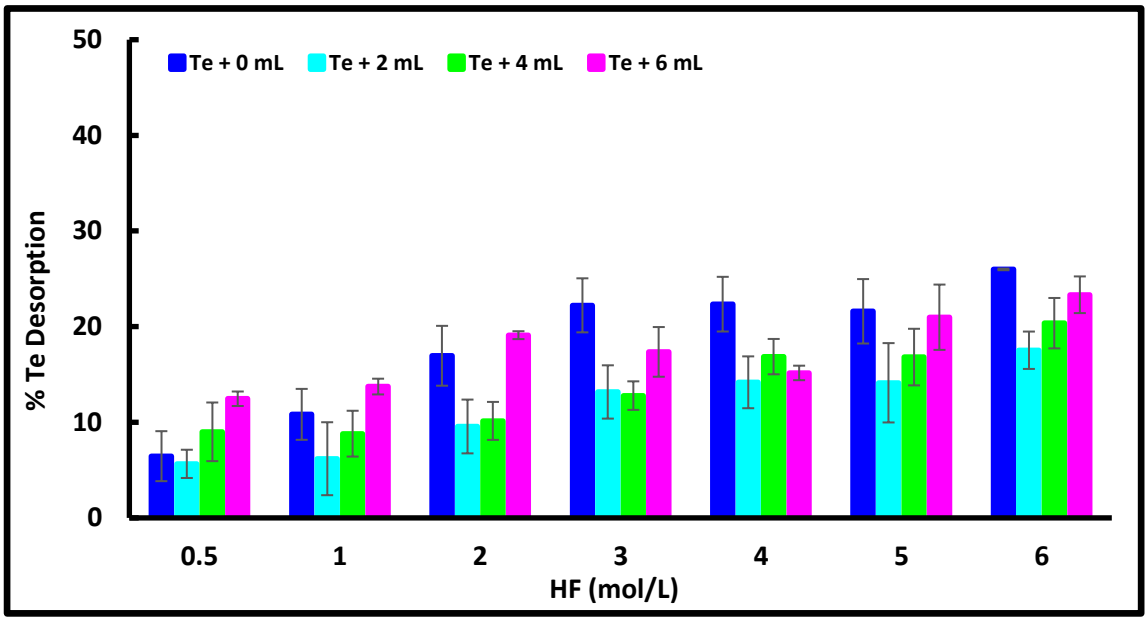

Fig. 3.23 The desorption of tellurium by hydrofluoric acid (0.50 to 6.0 mol L^{-1}) in presence of surface water.

3.3.10 Adsorption-desorption of tin and tellurium with groundwater spikes

Adsorptions of tin and tellurium: The average adsorption of tin and tellurium was found as 99.17 ± 0.35 and 62.48 ± 4.15%, respectively, Fig. 3.24 (Appendix 7.141). Again, the groundwater had a Cl^- and SO_4^{2-} content of 71.42 and 69.95 mg L^{-1}, respectively, quite different from that of surface water (29.97 and 9.78 mg L^{-1}, respectively). The present

observation aims to draw a comparative study on the effectiveness of our methodology to separate tin from tellurium in two different testing conditions. In case of groundwater, the adsorption increases with the addition of groundwater spikes for both the elements. The spiked samples have exhibited an increase of adsorption by 0.58% for tin and 10.46% for tellurium. Tin has shown a drop of adsorption from 99.59 ± 0.32 to 99.21 ± 0.07% when the spike volume has changed from 4- to 6-mL Tellurium also shows a similar change, the 2-mL spike gave more adsorption (63.04 ± 2.18%) than that of the 4-mL spike (61.09 ± 1.45%). In addition, the adsorption of tellurium with the 6-mL spike has increased by 17% compared to the value observed for the unspiked sample.

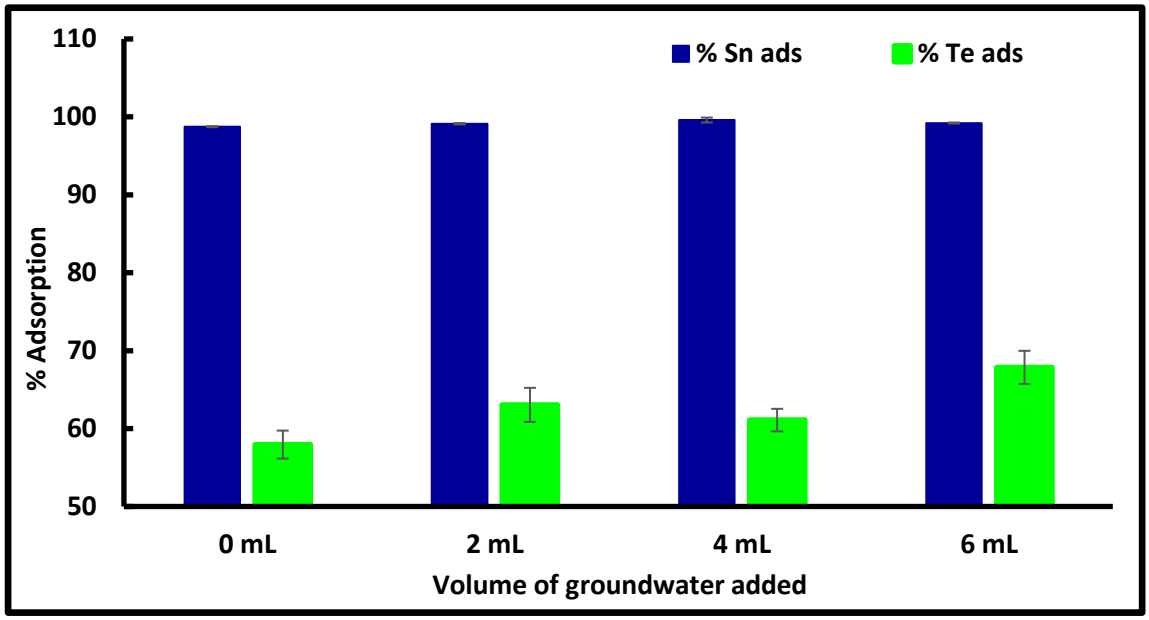

Fig. 3.24 The adsorptions of tin and tellurium in 3.0 mol L^{-1} of HCl solution in presence of groundwater.

The desorption of tin: The average desorption of tin washed by the treatment of hydrofluoric acid at concentrations of 0.50 to 6.0 mol L^{-1} for the 0-, 2-, 4-, and 6-mL spikes was found as 79.38 ± 7.21, 83.65 ± 3.64, 82.03 ± 4.77, and 80.18 ± 7.24%, respectively, Fig. 3.25 (Appendix 7.146). The highest desorption of tin (90.06 ± 6.84%) was viewed with the unspiked sample treated at 6.0 mol L^{-1} of HF, whereas the lowest wash was observed for the 6-mL spike washed by 0.50 mol L^{-1} of acid. In fact, samples washed with 0.50 mol L^{-1} of acid gave the lowest average elution (72.65 ± 4.54%), and samples treated with 6.0 mol L^{-1} of HF gave the highest elution (average 88.37 ± 1.16%). However, for the 2-mL spiked sample, a change in the concentration of HF from 5.0 to 6.0 mol L^{-1} has caused a little increase in the percent desorption of tin (average 87.38 ± 0.14%). Again, although the overall desorption of tin increases with increasing the concentration of HF, the 2-mL spike has experienced a slash of tin wash when the concentration of HF has increased from 1.0 to 2.0 mol L^{-1} (dropped from 82.86 ± 10.41 to 79.31 ± 9.37%). The 4-mL spiked sample also shows a drop of tin wash from 80.70 ± 4.83 to 80.46 ± 4.56% though the concentration of HF has been changed from 1.0 to 2.0 mol L^{-1}. Clearly, the average inflation of tin wash due to an increase of acid concentration was visualized only with low acid treatment, from 1.0 (72.65 ± 4.54%) to 2.0 mol L^{-1} (77.36 ± 5.24%), a change of nearly 6.5%. A close look on the desorption curve reveals that the overall wash of tin is relatively higher at elevated concentrations of hydrofluoric acid. However, the 2- and 4-mL spikes have shown an elevated amount of tin release at 1.0 mol L^{-1} of acid. Moreover, the 4-mL spike gave ≥ 80% elution of tin at HF concentrations of 1.0 mol L^{-1} or more.

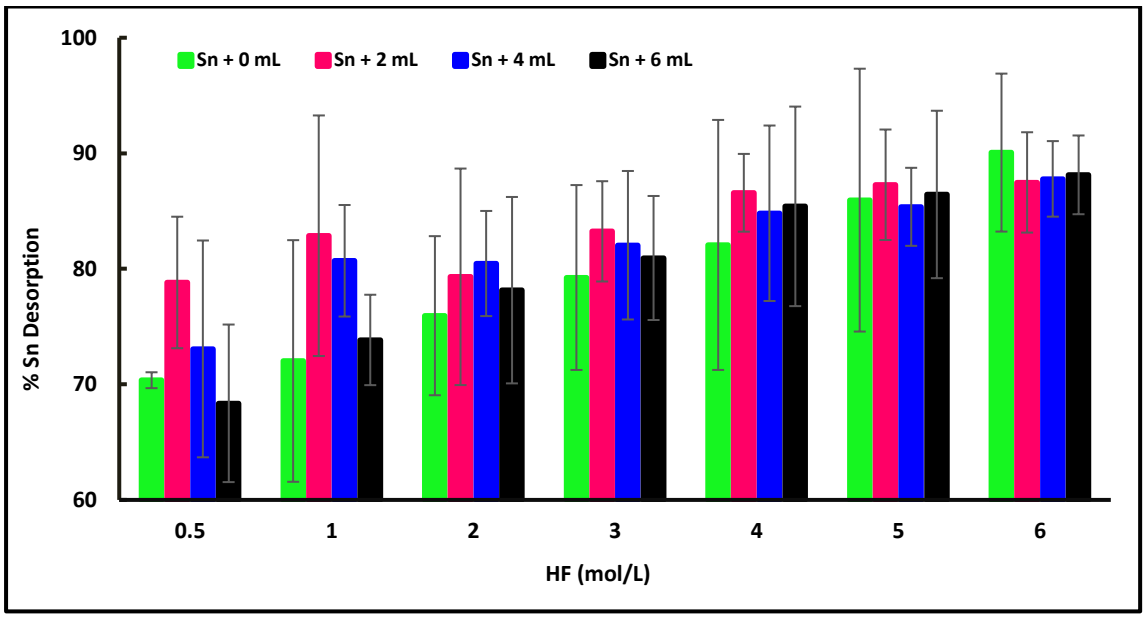

Fig. 3.25 The desorption of tin by hydrofluoric acid (0.50 to 6.0 mol L^{-1}) in presence of groundwater.

The desorption of tellurium: The average desorption of tellurium washed by the treatment of hydrofluoric acid at concentrations of 0.50 to 6.0 mol L^{-1} for the 0-, 2-, 4-, and 6-mL spikes was found as 12.09 ± 6.25, 9.58 ± 3.99, 12.27 ± 7.81, and 8.79 ± 7.53%, respectively, Fig. 3.26 (Appendix 7.151). In general, like the elution of tin, the desorption of tellurium increases with an increase of HF concentration. However, discrepancies were viewed in cases of the unspiked and 2-mL spiked samples. The former has experienced a small drop of wash from 5.0 (18.89 ± 5.05%) to 6.0 mol L^{-1} of HF (17.88 ± 5.80%), whereas the latter has exhibited a little change in elution at 3.0 (10.08 ± 2.44%) to 4.0 (9.52 ± 5.40%) mol L^{-1} of acid wash. The lowest elution of tellurium was observed in case of 6-mL spike (2.72 ± 0.49%) treated at 0.50 mol L^{-1} of HF, and the highest desorption (25.74 ± 2.92%) was achieved with the 4-mL spike treated at 6.0 mol L^{-1} of acid. Also, at 6.0 mol L^{-1} of HF, the unspiked and the 2-mL spiked samples gave a comparable result, average wash is 17.73 ± 0.22%. The 2-mL and the 4-mL spiked samples treated at 2.0 mol L^{-1} of acid also gave similar washes, 7.51 ± 5.71 and 7.20 ±

4.26%, respectively. Moreover, from 0.50 to 2.0 mol L^{-1} of HF, the overall elution of tellurium is relatively low (average 5.42 ± 1.51%). In fact, the 6-mL spike gave a smaller wash from 0.50 to 4.0 mol L^{-1} of acid (average 4.59 ± 1.49%). However, after 4.0 mol L^{-1} of HF, the 6-mL spike has produced an inflation of tellurium wash by 160%. It is promising that at 0.50 mol L^{-1} of HF, all spiked and the unspiked samples have exhibited very low levels of tellurium elution (average 4.05 ± 1.43%). Among the four sets of samples studied, the 6-mL spiked sample presents a small desorption of tellurium, except the 6.0 mol L^{-1} point as well as the previous low trend.

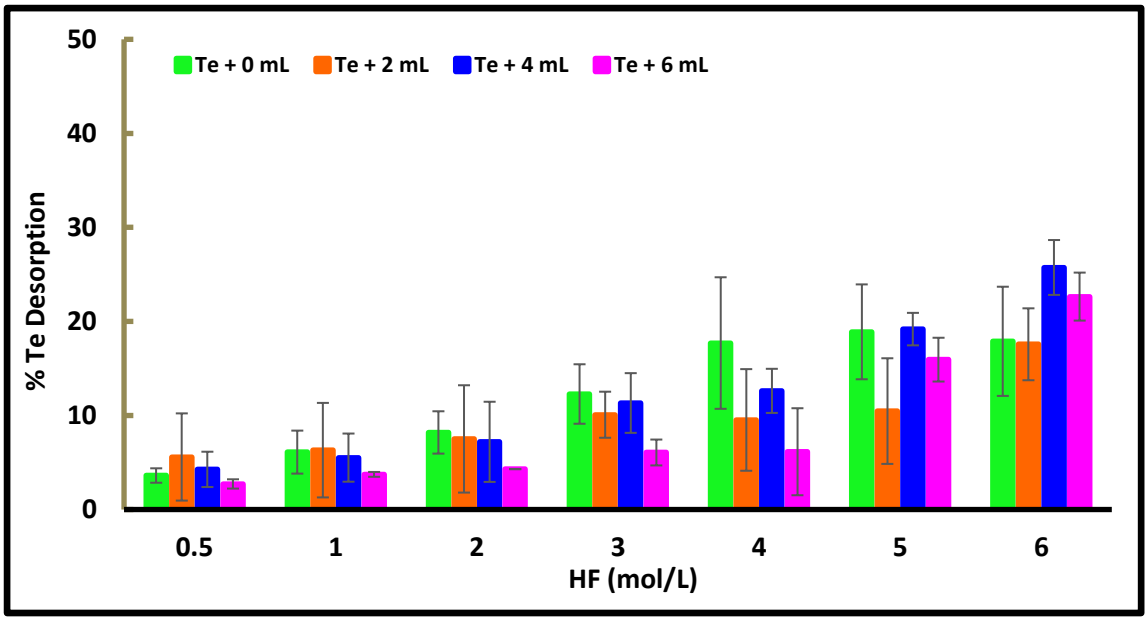

Fig. 3.26 The desorption of tellurium by hydrofluoric acid (0.50 to 6.0 mol L^{-1}) in presence of groundwater.

3.3.11 Desorption experiment with field samples: a comparative study

The desorption of tin with field samples: A comparison on the desorption performance of tin in presence of real field samples reveals that the desorption of tin by treating with aqueous hydrofluoric acid shows a comparable result between the unspiked and the

spiked samples, Fig. 3.27 (Appendix 7.152). In the present study, the surface water had 29.98 ± 0.09 mg L^{-1} of Cl^- and 9.78 ± 0.03 mg L^{-1} of SO_4^{2-} ions, whereas the groundwater contained 71.42 ± 1.57 mg L^{-1} of Cl^- and 69.95 ± 1.69 mg L^{-1} of SO_4^{2-} ions. Although the groundwater contained twice the amount of Cl^- and 7-times more SO_4^{2-} than that of the surface water, the percent of tin elution decreases only by 4.19%. It is worth mention that the adsorption of tin for both surface and groundwater has remained essentially the same.

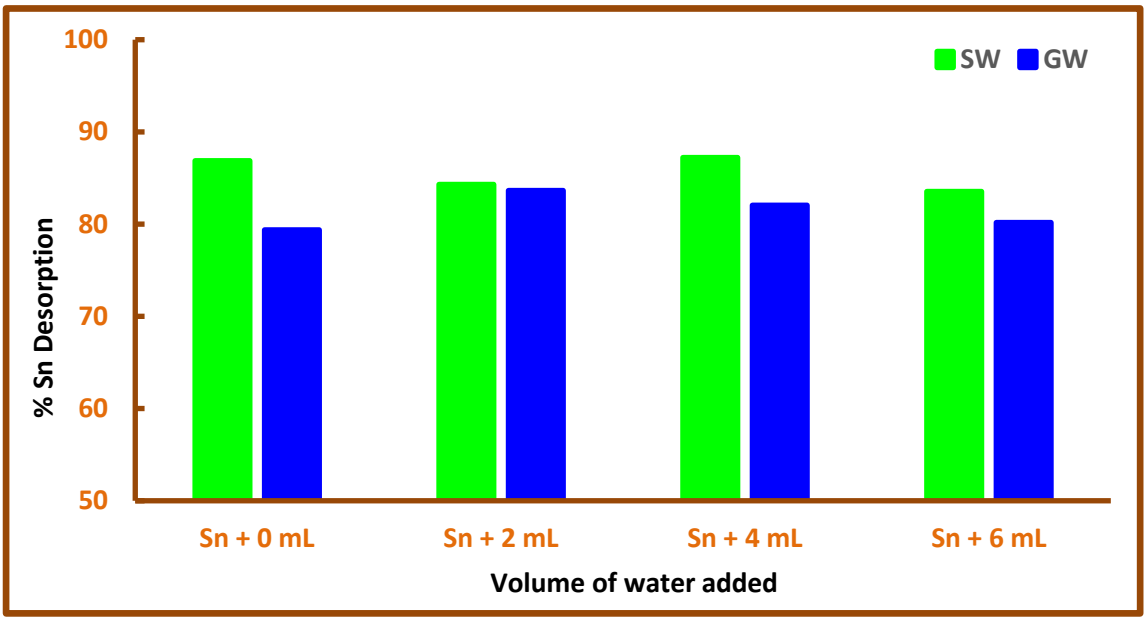

Fig. 3.27 A comparison on the desorption performance of tin in presence of field water, 'SW' stands for surface water, and 'GW' for groundwater.

The desorption of tellurium with field samples: The average desorption of tellurium for surface water is 15.13 ± 3.19%, while that for groundwater is 10.68 ± 1.76%, Fig. 3.28 (Appendix 7.153). Note that the adsorption of tellurium for surface and groundwater was 63.27 ± 1.62 and 62.48 ± 4.15%, respectively. Our goal is to ensure the lowest percentage of tellurium release from the column bed while maintaining a high level of metal in the

solid phase. The elution of tellurium for the 0-spike surface water was found as 18.06 ± 7.06% and that for the spiked samples was observed as 14.16 ± 3.03%. This result implies that the release of tellurium in presence of surface water can be reduced by 27%, which offers a great promise. On the other hand, the corresponding elution of tellurium with the 0-spike and the spiked groundwater samples was found as 12.09 ± 6.25 and 10.21 ± 1.82%, respectively. We can satisfactorily conclude here that our proposed methodology for the separation of tin from tellurium is equally applicable in the treatment of real field water.

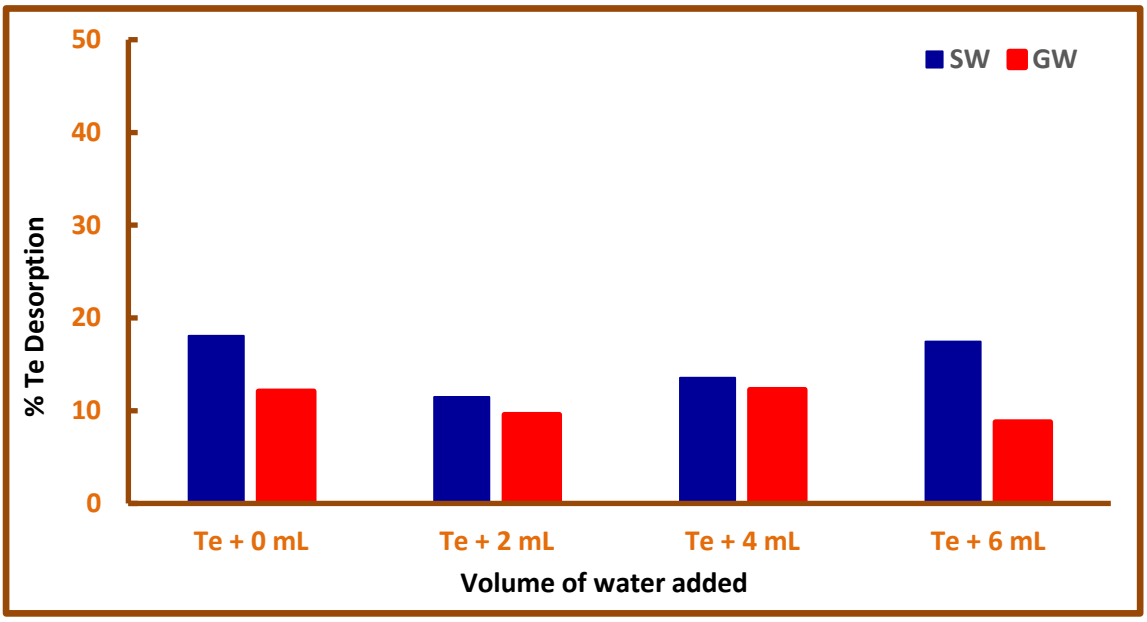

Fig. 3.28 A comparison on the desorption profile of tellurium in presence of field water, 'SW' stands for surface water, and 'GW' for groundwater.

Separation of tin from tellurium from natural water: The performance of our present proposal to separate tin from tellurium in cases of real field water was evaluated from the percent desorption of tin and that of tellurium. The overall result demonstrates that using the TRU resin as the column bed, we can ensure more than 99% of tin adsorption loading with hydrochloric acid, while keeping the tellurium retention as low as 60%. The dilute

hydrofluoric acid can selectively wash off at least 85% of adsorbed tin (single wash), and the tellurium release can be kept to less than 10%. This strategy can be applied successfully in case of real field water samples. Again, the TRU chromatographic resin can be exploited in the separation of tin from tellurium in presence of Cl^- and SO_4^{2-} ions. It is justifiable to say that the current methodology offers a bright promise in the separation of tin from tellurium from contaminated field water, particularly surface and groundwaters contaminated with Cl^- and SO_4^{2-} anions.

3.4 Conclusions

Chloride and sulfate are the two major anions present in almost all waterbodies. In our present study, experimental work has been carried out to evaluate the effect of chloride and sulfate anions on the separation of tin from tellurium. The distribution coefficients of tin and tellurium on the TRU chromatographic resin were determined in presence of laboratory prepared chloride and sulfate solutions along with real field samples (surface and groundwater). In addition, the adsorption-desorption behaviors of tin and tellurium have also been tested with spiked surface and groundwaters.

Results reveal that the distribution of tin and tellurium on the TRU resin loaded with aqueous hydrochloric acid is poorly affected by the presence of chloride and sulfate ions at concentrations of up to 70 mg L^{-1}. The adsorption of the spiked metal on the solid phase remained unchanged.

The optimum contact period for the maximum adsorption of tin in the solid phase is about 90 minutes, a prolonged interaction between the metal and the adsorbate reduces the metal-retention capacity of the solid resin. At pH 4.0 to 5.0, tin shows the highest adsorption on TRU resin.

The shaking orientation does matter on the distribution of spiked metals in solid phase. A horizontal shaking, placing the materials in the centrifuge tube and positioned along the direction of movement, ensures better mixing of materials and hence produces higher distribution coefficients of both tin and tellurium.

The adsorptions of tin in the solid TRU resin in presence of hydrochloric acid and spiked real field samples (surface and groundwater) is greater that 99%, whereas the adsorption of tellurium is around 60%. The adsorption of tin onto TRU resin is favored due to the strong dipole-ion interaction operating between the phospho-ketone group of resin and the Sn(II) ion. In addition, the conformational disposition of TRU resin supports in the formation of six-membered stable tin-sorbent adduct. On the other hand, the more electronegative tellurium does not form effecrive bonding interactions with the polar moiety of the substrate. As a result, the resin possesses relatively limited capacity to adsorp tellurium compared to the retention of tin.

The desorption study reveals that hydrofluoric acid can selectively elute 85% (a single desorption with 100 mg packing material) of tin, while maintaining the tellurium release by 10% or less. The technique is well suited in cases of contaminated surface and groundwaters. The result of our present adsorption-desorption study shows that the TRU chromatographic resin offers a bright promise for the selective separation of tin from tellurium for water samples containing Cl^- and SO_4^{2-} ions.

Chapter 4:

AMS detection of ^{126}Sn

4.1 Background information

4.1.1 Basic principle of AMS

The accelerator mass spectrometry (AMS) is an ultrasensitive technique that can measure certain long-lived radioisotopes (e.g., ^{3}H, ^{10}Be, ^{14}C, ^{26}Al, ^{36}Cl, ^{41}Ca, ^{53}Mn, ^{126}Sn, ^{129}I, ^{236}U, ^{237}Np, and ^{239}Pu) at very low abundances (10^{-12}–10^{-15}) with very high sensitivities (down to 10^{3} – 10^{5} atoms/sample).[180–183] The AMS technique, Fig. 4.1, generally uses a tandem electrostatic, like Van de Graaff or solid state, accelerator to measure the isotopic ratio of radionuclides.[180,183] In the case of ^{14}C/^{12}C, for example, the radioactive isotope (^{14}C) is measured by counting ions, whereas the more abundant stable isotope (^{12}C) is recorded by measuring the electric current from the Faraday detector.[183] A tandem-based AMS system basically follows: i) the production of negative ions from the caesium-sputter ion source, ii) acceleration of molecular negative ions from ground potential to high positive voltage, iii) changing of negative ions to positive ion by stripping off electrons at low gas pressures and then the dissociation of molecular ions, iv) acceleration of positive ions back to the ground potential, v) removal of unwanted background ions by electric and magnetic fields, and vi) identification and counting of individual isotopes with nuclear detectors.[180,183–185]

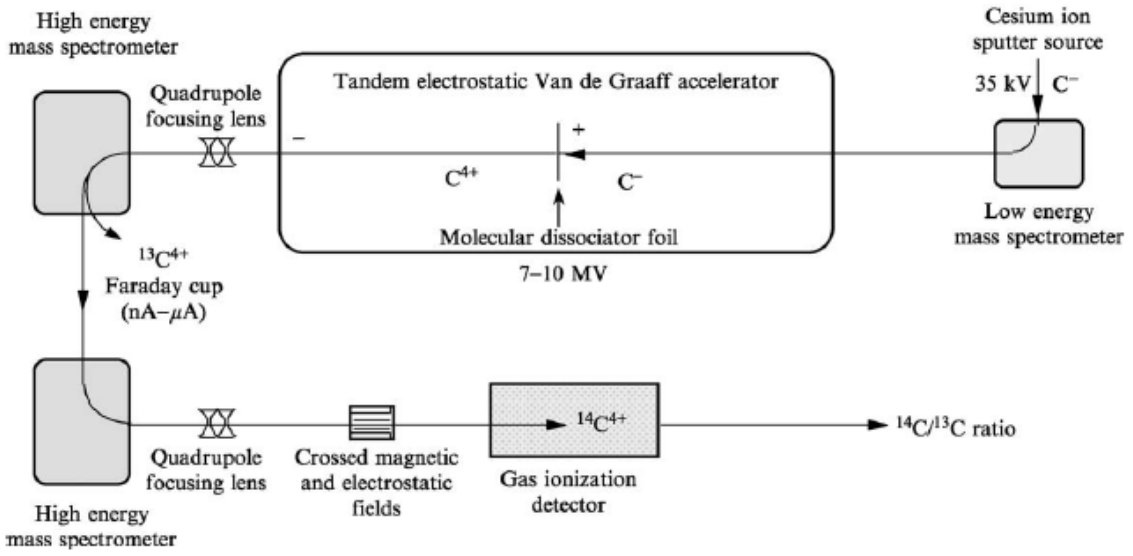

Fig. 4.1 Schematic diagram of the 10 MV accelerator mass spectrometer (AMS) system at the Lawrence Livermore National Laboratory.[186] Note that other systems could use a gas filled canal instead of a foil for molecular dissociation and charge changing.

4.1.2 Facts on ^{126}Sn

Tin possesses 41 radioactive isotopes, and ^{126}Sn is the only long-lived radioisotope of tin having a half-life of ~10^5 y. Most other tin isotopes possess half-lives in the order of hours to seconds, and two with half-lives of days: ^{113}Sn (115 d) and ^{123}Sn (129 d). The long-lived isotope ^{126}Sn is a member of the group of the seven longest-lived abundant products of uranium fission: ^{79}Se ($T_{½}$ = 2.95 × 10^5 y),[187] ^{93}Zr ($T_{½}$ = 1.13 × 10^6 y),[188] ^{99}Tc ($T_{½}$ = 2.1 × 10^5 y),[189] ^{207}Pd ($T_{½}$ = 6.5 × 10^6 y),[190] ^{126}Sn ($T_{½}$ = 2.35 × 10^5 y),[76] ^{129}I ($T_{½}$ = 1.614 × 10^7 y)[191] and ^{135}Cs ($T_{½}$ = 1.6 × 10^6 y).[192] Usually, these long-lived fission products can undergo neutron transmutation, a phenomenon of successive neutron capturing to become a short-lived isotope, which, in turn, transforms to a stable isotope of another element.[193] However, most ^{126}Sn does not undergo transmutation, but rather slowly decays to stable ^{126}Te.[194]

4.1.3 Issues with ^{126}Sn detection

Unlike other long-lived fission products, ^{99}Tc, for example, which has a fission-yield of about 6.13%,[195] ^{126}Sn has a very low fission yield, 0.059 to 0.065%.[80,196] produced from the spontaneous fission of ^{235}U. Moreover, since ^{126}Sn is heavier than all stable and short-lived isotopes of tin, it is highly unlikely to produce ^{126}Sn by photodisintegration reactions on other tin isotopes. This is because the neutron threshold of ^{126}Sn is higher than those of low-mass stable isotopes, like ^{119}Sn or ^{117}Sn. As a result, photodisintegration reaction (γ, n) can produce only stable (the masses of all stable tin isotopes are lower than ^{126}Sn) or short-lived isotopes of tin.[197] ^{126}Sn has two interfering isobars: stable ^{126}Te and ^{126}Xe. Fortunately, ^{126}Xe is not extracted effectively from the ion source, since noble gases do not form stable negative ions.[78] Therefore, the paramount obstacle for the precise determination of ^{126}Sn concentrations in samples is the interference of ^{126}Te.

4.1.4 Present state of ^{126}Sn detection

Kutschera et al.[124] conducted the first AMS measurement of ^{126}Sn at the Argonne ATLAS National Laboratory. They claimed that isobaric ^{126}Te can be separated from ^{126}Sn at high energies (400 MeV) using a magnet filled with nitrogen gas and a gas ionization chamber. However, due to the complexity of the measuring procedure, no absolute concentration of ^{126}Sn was determined.

Gartenmann et al.[78] have measured the ^{126}Sn/Sn ratio in extracted spent fuel rods from nuclear power plants at the ETH Zurich AMS facility. The ratio was measured as (9.23 ± 0.87) × 10^{-6}. It is assumed that crustal rocks contain ^{126}Sn/Sn ratio of approximately 10^{-14}.[77]

Shen et al.[79] have developed an AMS methodology for the determination of ^{126}Sn from the fission product wastes. They claimed that up to 400 nA beam current of ^{126}Sn can be achieved by using a combined target of SnF_2 and extracting SnF_3^-, while reducing the ^{126}Te interference by 2 – 3 orders of magnitude.

Asai et al.[80] have determined the ^{126}Sn content in highly contaminated radioactive waste dumped from a spent nuclear fuel solution using isotope dilution inductively coupled plasma mass spectrometry (ID-ICP-MS). The measured concentration of ^{126}Sn in the spent nuclear fuel solution was found as 0.74 ± 0.14 ng/g.

4.2 Experimental details

4.2.1 Our strategic plan to detect ^{126}Sn

(A) Choosing the AMS target

In the present study, we have planned to conduct three experiments on different AMS targets containing fluoride and iodide molecular ions in various mass compositions. The halogen elements, with high electronegativity, can provide good negative ions and can produce high beam-current. The unique advantage in chosing these two elements from the halogen group of periodic table is that both ^{19}F (100%) and ^{127}I (100% abundance) are monoisotopic elements. On the other hand, chlorine has two stable isotopes: ^{35}Cl (76%) and ^{37}Cl (24%), bromine has two (^{79}Br (51%) and ^{81}Br (49%)) isotopes as well.

In our present study, the molecular ions to be tested for beam current include: i) $^{126}SnF_5^-$, ii) $^{126}Sn^{127}I^{19}F_2^-$ (mass 291) and iii) $^{126}Sn^{127}I_2{}^{19}F^-$.

(i) Experiment #1 on SnF_5^- molecular ion

The compound SnF_2 is prepared in the laboratory *via* wet chemical process; the molecular ion $^{126}SnF_5^-$ is formed from a mixed target matrix of SnF_2 and PbF_2.

Limitations of this study:

Though we are hoping to achieve reasonable beam current from the $^{126}SnF_5^-$ molecular ion, there are a couple sources of uncertainty, like

a) Possible interferences may arise from $^{95}Mo^-$ ions (stable ^{95}Mo 15.87% abundance, may exist in sample matrix): $^{95}MoSn^-$ (95 + 126 = 221) *vs* SnF_5^- (126 + 19 × 5 = 221).

b) Another uncertainty from tellurium contamination from PbF_2 (99.9%).

(ii) Experiment #2 on $^{126}Sn^{127}I^{19}F_2^-$ molecular ion

Powder SnF_2, NaI, and Ag is mixed.

Approximate mol ratio: SnF_2 + NaI + Ag :: 1 : 1 : 1

Approximate mass ratio: 1 : 1 : 1

Molar masses: Sn = 118.710; I = 126.9045; F = 18.9984; Na = 22.98977;

Ag = 107.8682; SnF_2 = 156.707; SnI_2 = 372.519;

NaF = 41.98817; NaI = 149.89424

Mass calculation

$^{126}Sn^{127}I^{19}F_2^-$ = 126 + 127 + 19 × 2 = 291

Limitations of this study:

Again, there are possible uncertainties associated with with the test, like

a) The compound ion $^{126}Te^{127}I^{19}F_2^-$ also possesses the same molecular mass (126 + 127 + 19 × 2 = 291) as the target ($^{126}Sn^{127}I^{19}F_2^-$), and this ion may produce additional beam current causing a potential masking on $^{126}Sn^{127}I^{19}F_2^-$ current.

b) Also, the compound ion $^{126}Te^{165}Ho^-$ (^{165}Ho, 100% natural abundance), with the same molecular mass (126 + 165 = 291), may also contribute to the ion beam.

c) The detection of +5 ions (Sn^{5+} or Te^{5+}) should be clean for all ^{118}Sn, ^{125}Te, ^{126}Sn, and ^{126}Te.

Experiment #3 on $^{126}Sn^{127}I_2{}^{19}F^-$ molecular ion

Powder SnI_2, NaF, and Ag will be mixed.

Approximate mol ratio: SnI_2 + NaF + Ag :: 1 : 1 : 1

Approximate mass ratio: 1 : 1 : 1

Mass calculation:

$^{126}Sn^{127}I_2{}^{19}F^- = 126 + 127 \times 2 + 19 = 399$

Limitations of this test:

This experiment may cause certain setbacks, like

a) The compound ion $^{126}Te^{127}I_2{}^{19}F^-$ also possesses an identical molecular mass (126 + 127 × 2 + 19 = 399), which may exist.

b) The detection of +5 ions should be clean for all ^{118}Sn, ^{125}Te, and ^{126}Sn + ^{126}Te isotopes.

c) In addition, the molecular ion $^{126}Sn^{127}I_2{}^{19}F^-$ may be very low or no sputter yield.

d) Since $^{126}Sn^{127}I_2{}^{19}F^-$ is a heavy molecule compared to the mass of ^{126}Sn, it is likely to produce a poor sputter yield.

(B) Choosing the appropriate ion charge

In the AMS technique, it is crucial to select the right charge of the isotope of interest; in our case, an appropriate selection of $^{126}Sn^{q+}$ is worth consideration. The line of argument for the selection of $q+$ charge follows as:

(i) In case of $q = +1$:

However, the molecular ion $[M]^{+1}$ is common with large number of ions, therefore, $q+1$ charge selection will produce feeble output.

(ii) In case of $q = +2$:

In this case, m/q becomes 63 (= 126/2), there is a strong probability from $^{63}Cu^{1+}$ interferences, therefore, this charge selection carries a poor merit.

(iii) In case of $q = +3$:

A possible interfering effect may arise due to $^{42}Ca^{1+}$, $^{84}Se^{2+}$ or $^{168}Er^{4+}$ ions.

(iv) In case of $q = +4$:

M/q becomes 31.5, an encouraging choice, there is a good chance to overcome possible interferences.

(v) In case of $q = +5$:

M/q becomes 25.5, again, there is a good chance to overcome isobaric interferences.

(C) Efficiency expectation

The efficiency expectation is almost inversely proportional to the state of isotopic charge, a smaller charge selection most likely would produce a high yield. However, depending upon the accelerator configuration, the terminal voltage and the stripper gas pressure, one can obtain higher efficiency for higher charge states. For the A. E. Lalonde-AMS accelerator (University of Ottawa), the highest efficientcy is expected to be at charge state

+3 and that higher and lower charge states are expected to be less efficient. Also, heavier ions are easier to get into higher charge states than lighter ones.

In our present study, we expect that

with q = +1, there is a likelihood of high efficiency,

with q = +2, there is a probability of high efficiency,

with q = +3, still we expect a good yield, at least 10%,

with q = +4, the efficiency may be very poor,

with q = +5, may give a vey low efficiency, the efficiency could drop as low as 1%.

Although a smaller charge selection possibly could yield a good result, there is a burning issue with the low background and high sputter yield. In the case of AMS detection of radioisotopes, in our case ^{126}Sn, it is essential to optimize the experimental condition in such a way that will produce a low tellurium background giving a reasonable tin-beam current. Therefore, a suitable charge selection would be of Sn^{5+}, even though the expected efficiency is very low (may be 1% or below).

(D) Tuning the target condition

In the current project plan, two experiments were performed on the iodide target and one on fluoride, but since the iodine-based molecular ions ($^{126}Sn^{127}I^{19}F_2^-$ and $^{126}Sn^{127}I_2{}^{19}F^-$) are heavier compared to the mass of tin, tuning the target condition is necessary to encourage the production of sufficient heavy-ions.

i) In case of $^{126}Sn^{127}I^{19}F_2^-$ target:

Step 1: $^{118}SnIF_2^- \rightarrow {}^{118}Sn^{5+}$

Step 2: $^{125}TeIF_2^- \rightarrow {}^{125}Te^{5+}$

Step 3: $(^{126}Sn, {}^{126}Te)IF_2^- \rightarrow (^{126}Sn, {}^{126}Te)^{5+}$

Then, we will calculate the ratio of $^{126}Sn/^{118}Sn$.

If $^{126}Sn/^{118}Sn \leq 10^{-11}$, or less, it will work fine, the ^{126}Te has not entered significantly with the ^{126}Sn.

We expect a ratio of:
$(^{126}Sn/^{118}Sn)_{background} \leq 10^{-11}$

ii) In case of $^{126}Sn^{127}I_2{}^{19}F^-$ target:

Step 1: $^{118}SnI_2F^- \rightarrow {}^{118}Sn^{5+}$

Step 2: $^{125}TeI_2F^- \rightarrow {}^{125}Te^{5+}$

Step 3: $(^{126}Sn, {}^{126}Te)I_2F^- \rightarrow (^{126}Sn, {}^{126}Te)^{5+}$

Then, we will calculate the ratio of $^{126}Sn/^{118}Sn$.

Again, if $^{126}Sn/^{118}Sn \leq 10^{-11}$, or less, it will work fine.

We expect a ratio of:
$(^{126}Sn/^{118}Sn)_{background} \leq 10^{-11}$

(E) Our specific goals

(i) Determination of $^{126}Sn/Sn$ detection limit.

(ii) If it works, a comparison on cases with +5 and +3 ion detection will be performed.

(iii) SSI run for 3 beams. As more parameter of the accelerator system than simply the injection magnet need to be adjusted for this measurement, the slow isotope switching is used to allow all parameter to stabilize before the measurement is taken.

a) $^{118}SnX^{-} \rightarrow {}^{118}Sn^{+q}$ in FC,

b) $^{125}TeX^{-} \rightarrow {}^{125}Te^{+q}$,

c) $(^{126}Te, {}^{126}Sn)^{-} \rightarrow (^{126}Te, {}^{126}Sn)^{+q}$

(iv) Choosing the best beam.

4.2.2 Target preparation

(A) AMS run with laboratory samples

(i) Preparation of SnF_2 sample

The first AMS beam current was monitored with the laboratory prepared SnF_2 samples. SnF_2 sample was prepared as follows: 0.6174 g tin ribbon was dissolved in 27.6 mol L^{-1} HF (10.0 mL) in a porcelain crucible, and the solvent was evaporated by an electric heater. The product was dried at 400 °C in a vacuum furnace for 1.0 hour.

(ii) Preparation of SnF_2 target

Five AMS targets were prepared, as follows, with an approximate SnF_2 to PbF_2 (PbF_2 was added as the fluorine source) ratio of 1 : 6, shown in Table 4.1.

Table 4.1: Composition of SnF_2 target.

Sample #	SnF_2 (mg)	PbF_2 (mg)	SnF_2/PbF_2 ratio
MR-1	5.1	30.6	1 : 6.00
MR-2	5.5	38.2	1 : 6.95
MR-3	7.3	49.8	1 : 6.82
MR-4	5.3	43.0	1 : 8.11
MR-5	6.2	43.4	1 : 7.00

(B) AMS run with commercial samples

(i) Preparation of SnF_2 target

Reagent grade SnF_2 (99.5%, mol wt 156.71) was purchased from Sigma-Aldrich. Four AMS targets have been prepared with the following compositions:

SnF_2 + NaI + Ag :: 54.3 mg + 43.2 mg + 241.0 mg Ag

(ii) Preparation of SnI_2 target

Anhydrous SnI_2 (99.9%, mol wt 372.52) was purchased from Sigma-Aldrich. Four AMS targets have been prepared with the follow compositions:

SnI_2 + NaF + Ag :: 66.6 mg + 53.5 mg + 481.0 mg Ag

4.2.3 AMS Settings for ^{126}Sn detection

(i) General setting

- Ion source voltages = 7/28 for $SnIF_2^-$, 7/23 for SnI_2F^-
- Terminal voltage 2.5 MV for all runs
- Detector isobutene pressure = 17.25 mBar for all, Amplifiers ΔE = 20–12.0 for all runs

E_f = 20–12.0 for Sn^{+5} and E_f = 40–12.0 for Sn^{+3} ($^{126}Sn^{+3}$ was not tried, which did not work in earlier tests because of intense $^{42}Ti^{+1}$ ions, so was not considered worth mention)

- Ionizer = 19 A, Cs = 80 °C and Quick Cool = ON (to control Cs flux) for all (iodine run condition)
- All H (horizontal) slits = 1.00/1.00; Stripper = 5×10^{-3} mBar (if needed, 1×10^{-2} for Sn^{+3})

(ii) Experiment with $^{126}Sn^{127}I^{19}F_2^-$

- Ion source and detector setting for this case is the same as in (i)
- AMS tuning for $^{127}I^- \rightarrow {}^{127}I^{+5}$
- If necessary, the use of Cu-clusters to calibrate MA1 (magnetic analyzer)
- AMS tuning for $^{118}Sn^{127}I^{19}F_2^- \rightarrow {}^{118}Sn^{+5}$
- Checking c/s for $^{125}Te^{127}I^{19}F_2^- \rightarrow {}^{125}Te^{+5}$
- Checking c/s for $(^{126}Te + {}^{126}Sn)^{127}I^{19}F_2^- \rightarrow (^{126}Te + {}^{126}Sn)^{+5}$

(iii) Experiment with $^{126}Sn^{127}I_2{}^{19}F^-$

- Ion source and detector setting for this case is the same as in (i)
- AMS tuning for $^{127}I^- \rightarrow {}^{127}I^{+5}$
- If necessary, the use of Cu-clusters to calibrate the first magnetic analyzer (MA1).
- AMS tuning for $^{118}Sn^{127}I_2{}^{19}F^- \rightarrow {}^{118}Sn^{+5}$
- Checking c/s for $^{125}Te^{127}I_2{}^{19}F^- \rightarrow {}^{125}Te^{+5}$
- Checking c/s for $(^{126}Te, {}^{126}Sn)^{127}I_2{}^{19}F^- \rightarrow (^{126}Te, {}^{126}Sn)^{+5}$

(iv) Targets – we have prepared targets with the following combinations:

- 1 (one) Cu-target/Cu-pin for beam-park (Cu/Cu used for all)
- 1 Cu/Al-blank (for LE calibration with Cu-cluster beams, if necessary)
- 1 NaI/Nb-blank (for HE calibration with ^{127}I beams, it was found the best)
- 1 Ag/Cu-Blk (Blank)
- 1 Cu/Cu-Blk
- 1 Al/Cu-Blk
- 4 (four) SnF_2 + NaI + Ag (1 : >0.957 : >0.688 by wt, approximate ratio)
- 4 SnI_2 + NaF + Ag (1 : >0.113 : >0.290 by wt, approximate ratio)
- 1 SnI_2
- 1 SnI_2 + Ag (1 : 1 by volume)
- 1 SnF_2
- 1 SnF_2 + PbF_2 (1 : 5 vol)

(v) Slits = 1.50/1.50, from NaI + Nb (Nb was added as a conducting material) source

For $^{127}I^{-} \rightarrow {}^{127}I^{+5}$

Magnetic field, B_1 = 0.553640 T; bouncer voltage, V_{B1} = 50 V

Terminal voltage, V_T = 2500 kV; magnetic field, B_2 = 0.618240 T

High electric analyzing voltage, V_2 = 71.008 kV,

For $^{125}Te^{-} \rightarrow {}^{125}Te^{+5}$

Bouncer voltage, V_{B1} = 611.20 V

Terminal voltage, V_T = 2540.125 kV

High electric analyzing voltage, V_2 = 72.145 kV

For $^{125}Te^{127}I^{-} \rightarrow {}^{125}Te^{+5}$

Magnetic field, B_1 = 0.786093 T; bouncer voltage, V_{B1} = 611.20 V

Terminal voltage, V_T = 2540.125 kV

Magnetic field, B_2 = 0.591395 T

High electric analyzing voltage, V_2 = 66.016 kV

(vi) Important considerations during the AMS run

- The overall AMS run was carefully monitored to observe the strongest beam-current. The targets were repeatedly screened back and forth to look for a detectable signal, only the target under consideration (SnF_2 + PbF_2) was found good enough to produce a measurable current. Therefore, a thorough study on the remaining targets was not considered essential in the present study.
- To minimize a low ^{126}Te background, the use of special Te-loaded copper target was avoided as it contains up to 100 ppm of Te.
- The use of aluminum target was avoided, since Al has a strong affinity to fluorine, which could make a deliberate shortage of fluoride ions. However, the high background (~10^{-9}) with our prepared SnF_2 sample might have been caused due to the formation of significant amount of AlF_3, most likely originated from the porcelain crucible. Therefore, the preparation of SnF_2 is strongly recommended with the use of teflon vessels.

4.3 Results and discussion

4.3.1 Measurement of beam-current for the prepared samples

(i) SnF_n^--beam current

In the first phase of experiment, the target consists of SnF_2 + PbF_2 in various mixing ratios. The SnF_5^- current was monitored after settling into the steady state and the following beam-currents were observed, Table 4.2:

Table 4.2: Beam-current for SnF_n^- molecular ions (n = 1–5)

Tin isotope	Number of fluorine atoms, *n*	Molecular ion	Observed current (nA) after the injector magnet
^{120}Sn	1	$^{120}SnF^-$	1.3
^{120}Sn	2	$^{120}SnF_2^-$	2.9
^{120}Sn	3	$^{120}SnF_3^-$	44.0
^{120}Sn	4	$^{120}SnF_4^-$	10.0
^{120}Sn	5	$^{120}SnF_5^-$	30.0

The initial study was carried out to monitor the sensitivity for detecting tin metal itself, therefore, the highest abundant (32.58%) ^{120}Sn isotope has been taken as the main consideration. Here, $^{120}SnF_5^-$ and $^{120}SnF_3^-$ molecular ions have produced stronger beam-currents, 30.0 and 44.0 nA, respectively, observed after the injector magnet.

(ii) Beam A for ^{126}Sn detection

The Beam A was originated from $^{120}SnF_5^-$ species. After tuning the beam for $^{120}SnF_5^- \rightarrow {}^{120}Sn^{3+}$ at 2.0×10^{-2} mBar striping pressure (which is high enough to destroy all +3 molecular ions after acceleration), $^{126}SnF_5^- \rightarrow {}^{126}Sn^{3+}$ was counted in the detector. The count rate of $^{126}Sn^{3+}$ ions and the $^{120}Sn^{3+}$ current in front of the detector have produced $^{126}Sn/^{120}Sn = 5.0 \times 10^{-9}$, or a ppb-level background.

(iii) Beam B for ^{126}Sn detection

The Beam B, for $^{126}SnF_3^- \rightarrow {}^{126}Sn^{3+}$ (q = +3), was checked. This time, however, the +1 fragment ions, produced from the SnF_2 + PbF_2 targets, were very strong. Therefore, the beam-current for $^{126}SnF_3^- \rightarrow {}^{126}Sn^{5+}$ (q = +5) was checked. A rather clear spectrum was observed, but the $^{126}Sn/^{120}Sn$ ratio was almost the same, about 3.0×10^{-9}, again, with a ppb-level background.

(iv) Beam C for ^{126}Sn detection

Beam A and B both have about 10% transmission at about 2.5 MV terminal voltage. However, Beam C was $^{120}SnF_5^- \rightarrow {}^{120}SnF_2^{2+}$ at 1.6 MV terminal voltage. This beam can be transmitted by the system, but the efficiency was found to be at 0.1% level with about 1.0×10^{-3} mBar stripping pressure. Although the spectrum of $^{126}SnF_5^- \rightarrow {}^{126}SnF_2^{2+}$ was much clearer for the [126 + 38] mass region, i.e., $^{126}SnF_2^{2+}$ like species, but there were plenty of ions, almost half of these masses, have flooded the [126 + 38] spectrum. The lighter ions interfere in the detector spectrum because the detector measures energy loses, and the AMS is selective for a given mass/charge ratio – an ion with half the mass but double the charge will be detected, but at lower energies. If there are too many counts, the detector is saturated, and cannot measure the higher energy counts with accuracy. The beam was too little to be tuned properly, and the transmission was totally useless. For these reasons, the Beam C has not been considered effective for the quantification of ^{126}Sn isotope.

4.3.2 Mass assignments against beam-current

After fixing all AMS conditions, a long manual scan was performed for the SnF_2 + NaI + Ag target, the variation of beam-current with mass of molecular ions ($^{127}I^-$ anion) is presented in Fig. 4.2. The Table 4.3 shows a detailed assessment on the composition of probable ions.

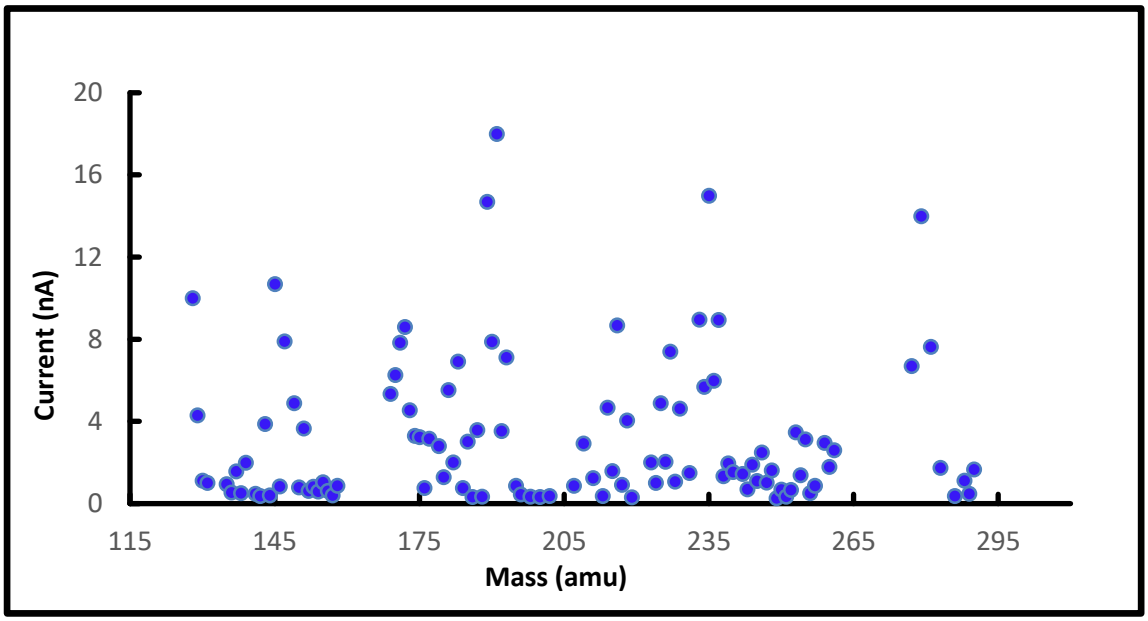

Fig. 4.2 Observed beam-current against mass of molecular ions. Note, the current for mass 127 is 1.96 μA, which is almost 1000 times larger compared to other values.

Table 4.3: Prediction of molecular ions for SnF_2 + NaI + Ag target.

Magnetic field (B, Tesla)	Observed beam-current (nA)	Mass of molecular ion (amu)	Ion prediction	
			More probable molecular ions	Less probable molecular ions
0.55367	1.96 μA	127	$^{127}I^-$ (anion), $^{115}Sn^{12}C^-$, $^{114}Sn^{13}C^-$	$^{114}Sn^{12}CH^-$, $^{112}Sn^{13}CH_2^-$, $^{63}Cu_2H^-$
0.55584	10	128	$^{65}Cu^{63}Cu^-$, $^{109}Ag^{19}F^-$	$^{127}IH^-$, $^{115}Sn^{13}C^-$, $^{116}Sn^{12}C^-$, $^{115}Sn^{12}CH^-$, $^{114}Sn^{12}CH_2^-$, $^{63}Cu_2H_2^-$
0.55800	4.3	129	$^{117}Sn^{12}C^-$, $^{116}Sn^{13}C^-$	$^{127}IH_2^-$, $^{116}Sn^{12}CH^-$, $^{115}Sn^{12}CH_2^-$, $^{65}Cu^{63}CuH^-$
0.56011	1.13	130	$^{65}Cu_2^-$, $^{107}Ag^{23}Na^-$	$^{127}IH_3^-$, $^{118}Sn^{12}C^-$, $^{117}Sn^{13}C^-$
0.56233	1.02	131	$^{119}Sn^{12}C^-$, $^{118}Sn^{13}C^-$	$^{107}Ag^{23}NaH^-$, $^{65}Cu_2H^-$, $^{107}Ag^{12}C_2^-$
0.57095	0.95	135	$^{116}Sn^{19}F^-$, $^{112}Sn^{23}Na^-$	$^{122}Sn^{13}C^-$, $^{122}Sn^{12}CH^-$, $^{109}Ag^{13}C_2^-$
0.57313	0.55	136	$^{117}Sn^{19}F^-$, $^{116}Sn^{19}F^-$	$^{124}Sn^{12}C^-$, $^{122}Sn^{12}CH_2^-$, $^{112}Sn^{12}C_2^-$
0.57511	1.58	137	$^{114}Sn^{23}Na^-$, $^{118}Sn^{19}F^-$	$^{112}Sn^{12}C_2H^-$, $^{124}Sn^{12}CH^-$, $^{124}Sn^{13}C^-$
0.57716	0.51	138	$^{119}Sn^{19}F^-$, $^{115}Sn^{23}Na^-$	$^{63}Cu_2{}^{12}C^-$, $^{124}Sn^{13}CH^-$, $^{107}Ag^{19}F^{12}C^-$, $^{114}Sn^{12}C_2^-$

Table 4.3: Prediction of molecular ions for SnF_2 + NaI + Ag target *(continued)*

Magnetic field (B, Tesla)	Observed beam-current (nA)	Mass of molecular ion (amu)	Ion prediction	
			More probable molecular ions	Less probable molecular ions
0.57932	2.00	139	$^{120}Sn^{19}F^-$, $^{116}Sn^{23}Na^-$	$^{127}I^{12}C^-$, $^{124}Sn^{13}CH_2^-$
0.58350	0.49	141	$^{122}Sn^{19}F^-$, $^{118}Sn^{23}Na^-$	$^{120}Sn^{19}FH_2^-$, $^{63}Cu^{65}Cu^{12}CH^-$, $^{63}Cu^{65}Cu^{13}C^-$
0.58550	0.38	142	$^{119}Sn^{23}Na^-$	$^{65}Cu_2{}^{12}C^-$, $^{65}Cu^{63}Cu^{12}CH_2^-$, $^{65}Cu^{63}Cu^{13}CH^-$
0.58758	3.89	143	$^{120}Sn^{23}Na^-$, $^{124}Sn^{19}F^-$	$^{127}I^{13}CH_3^-$, $^{119}Sn^{12}C_2^-$
0.58955	0.41	144	$^{120}Sn^{12}C_2^-$, $^{109}Ag^{23}Na^{12}C^-$	$^{107}Ag^{23}Na^{12}CH_2^-$, $^{120}Sn^{23}NaH^-$
0.59163	10.7	145	$^{107}Ag^{19}F_2^-$, $^{122}Sn^{23}Na^-$, $^{63}Cu_2{}^{19}F^-$	$^{120}Sn^{13}C^{12}C^-$, $^{120}Sn^{12}C_2H^-$
0.59379	0.84	146	$^{127}I^{19}F^-$	$^{122}Sn^{12}C_2^-$, $^{120}Sn^{23}NaH^-$, $^{122}Sn^{23}NaH^-$
0.59572	7.90	147	$^{124}Sn^{23}Na^-$, $^{109}Ag^{19}F_2^-$, $^{63}Cu^{65}Cu^{19}F^-$	$^{116}Sn^{19}F^{12}C^-$, $^{122}Sn^{13}C^{12}C^-$, $^{127}I^{19}FH^-$
0.59982	4.89	149	$^{107}Ag^{23}Na^{19}F^-$, $^{63}Cu_2{}^{23}Na^-$, $^{65}Cu_2{}^{19}F^-$	$^{124}Sn^{13}C^{12}C^-$, $^{124}Sn^{12}C_2H^-$
0.60187	0.79	150	$^{127}I^{23}Na^-$, $^{112}Sn^{19}F_2^-$	$^{107}Ag^{12}C_2{}^{19}F^-$, $^{124}Sn^{13}C_2^-$, $^{124}Sn^{13}C^{12}CH^-$
0.60385	3.66	151	$^{109}Ag^{23}Na^{19}F^-$	$^{127}I^{12}C_2^-$, $^{120}Sn^{19}F^{12}C^-$, $^{107}Sn^{19}F^{13}C^{12}C^-$
0.60583	0.63	152	$^{114}Sn^{19}F_2^-$	$^{120}Sn^{19}F^{13}C^-$, $^{116}Sn^{12}C_3^-$
0.60786	0.83	153	$^{107}Ag^{23}Na_2^-$, $^{115}Sn^{19}F_2^-$	$^{127}I^{13}C_2^-$, $^{120}Sn^{19}F^{12}CH_2^-$
0.60989	0.60	154	$^{116}Sn^{19}F_2^-$, $^{112}Sn^{23}Na^{19}F^-$	$^{65}Cu_2{}^{12}C_2^-$, $^{118}Sn^{12}C_3^-$, $^{117}Sn^{13}C^{12}C_2^-$
0.61197	1.04	155	$^{109}Ag^{23}Na_2^-$	$^{118}Sn^{13}C^{12}C_2^-$, $^{120}Sn^{23}Na^{12}C^-$
0.61379	0.63	156	$^{114}Sn^{23}Na^{19}F^-$	$^{109}Ag^{23}Na_2H^-$, $^{120}Sn^{23}Na^{12}CH^-$, $^{124}Sn^{19}F^{12}CH^-$, $^{124}Sn^{19}F^{13}C^-$
0.61578	0.40	157	$^{115}Sn^{23}Na^{19}F^-$, $^{119}Sn^{19}F_2^-$	$^{120}Sn^{23}Na^{12}CH_2^-$, $^{122}Sn^{23}Na^{12}C^-$, $^{109}Ag^{23}Na_2H_2^-$
0.61775	0.88	158	$^{116}Sn^{23}Na^{19}F^-$, $^{112}Sn^{23}Na_2^-$	$^{122}Sn^{23}Na^{12}CH^-$, $^{122}Sn^{23}Na^{13}C^-$
0.63897	5.35	169	$^{127}I^{23}Na^{19}F^-$	$^{124}Sn^{19}F^{13}C_2^-$, $^{65}Cu_2{}^{19}F_2H^-$
0.64077	6.26	170	$^{107}Ag^{63}Cu^-$, $^{124}Sn^{23}Na_2^-$, $^{109}Ag^{23}Na^{19}F_2^-$	$^{120}Sn^{19}F_2{}^{12}C^-$, $^{124}Sn^{23}Na_2^-$
0.64272	7.84	171	$^{107}Ag^{63}CuH^-$, $^{114}Sn^{19}F_3^-$	$^{127}I^{19}F^{13}C^{12}C^-$, $^{127}I^{19}I^{12}C_2H^-$
0.64456	8.61	172	$^{107}Ag^{23}Na_2{}^{19}F^-$, $^{109}Ag^{63}Cu^-$, $^{107}Ag^{65}Cu^-$	$^{127}I^{19}F^{13}C_2^-$, $^{127}I^{19}I^{12}C_2H_2^-$, $^{124}Sn^{23}Na^{13}C^{12}C^-$

Table 4.3: Prediction of molecular ions for SnF_2 + NaI + Ag target *(continued)*

Magnetic field (B, Tesla)	Observed beam-current (nA)	Mass of molecular ion (amu)	Ion prediction	
			More probable molecular ions	Less probable molecular ions
0.64635	4.56	173	$^{127}I^{23}Na_2^-$, $^{107}Ag^{65}CuH^-$, $^{122}Sn^{19}F_2{}^{13}C^-$	$^{115}Sn^{23}Na_2{}^{12}C^-$, $^{114}Sn^{23}Na_2{}^{13}C^-$, $^{114}Sn^{23}Na_2{}^{12}CH^-$
0.64827	3.30	174	$^{109}Ag^{65}Cu^-$, $^{124}Sn^{19}F_2{}^{12}C^-$	$^{109}Ag^{63}CuH_2^-$, $^{116}Sn^{23}Na_2{}^{12}C^-$
0.65014	3.25	175	$^{112}Sn^{63}Cu^-$, $^{118}Sn^{19}F_3^-$, $^{109}Ag^{65}CuH^-$	$^{127}I^{23}Na_2H_2^-$, $^{115}Sn^{23}Na_2{}^{12}CH_2^-$, $^{124}Sn^{19}F_2{}^{13}C^-$
0.65204	0.77	176	$^{119}Sn^{19}F_3^-$, $^{115}Sn^{23}Na^{19}F_2^-$	$^{118}Sn^{23}Na_2{}^{12}C^-$, $^{124}Sn^{19}F_2{}^{12}CH_2^-$
0.65384	3.16	177	$^{112}Sn^{65}Cu^-$, $^{120}Sn^{19}F_3^-$, $^{112}Sn^{23}Na_2{}^{19}F^-$, $^{116}Sn^{23}Na^{19}F_2^-$	$^{107}Ag^{23}Na_2{}^{12}C_2^-$, $^{65}Cu_2{}^{23}Na_2H^-$
0.65751	2.81	179	$^{114}Sn^{65}Cu^-$, $^{116}Sn^{63}Cu^-$, $^{122}Sn^{19}F_3^-$, $^{118}Sn^{23}Na^{19}F_2^-$	$^{109}Ag^{23}Na_2{}^{12}C_2^-$, $^{65}Cu_2{}^{23}Na_2H_3^-$, $^{109}Ag^{23}Na_2{}^{12}C_2^-$, $^{107}Ag^{23}Na_2{}^{12}C_2^-$
0.65936	1.30	180	$^{115}Sn^{65}Cu^-$, $^{115}Sn^{63}CuH_2^-$, $^{119}Sn^{23}Na^{19}F_2^-$	$^{109}Ag^{23}Na_2{}^{12}C_2H^-$, $^{118}Sn^{19}F_2{}^{12}C_2^-$
0.66120	5.54	181	$^{116}Sn^{65}Cu^-$, $^{124}Sn^{19}F_3^-$, $^{120}Sn^{23}Na^{19}F_2^-$	$^{109}Ag^{23}Na_2{}^{12}C_2H_2^-$, $^{119}Sn^{19}F_2{}^{12}C_2^-$
0.66300	2.02	182	$^{117}Sn^{65}Cu^-$, $^{119}Sn^{63}Cu^-$	$^{107}Ag^{63}Cu^{12}C^-$, $^{120}Sn^{19}F_2{}^{12}C_2^-$
0.66480	6.92	183	$^{118}Sn^{65}Cu^-$, $^{120}Sn^{63}Cu^-$, $^{122}Sn^{23}Na^{19}F_2^-$	$^{107}Ag^{63}Cu^{12}CH^-$, $^{120}Sn^{19}F_2{}^{12}C_2H^-$
0.66664	0.77	184	$^{127}I^{19}F_3^-$, $^{119}Sn^{65}Cu^-$,	$^{109}Ag^{63}Cu^{12}C^-$, $^{107}Ag^{65}Cu^{12}C^-$
0.66840	3.02	185	$^{120}Sn^{65}Cu^-$, $^{122}Sn^{63}Cu^-$, $^{124}Sn^{23}Na^{19}F_2^-$	$^{127}I^{23}Na_2{}^{12}C^-$, $^{109}Ag^{63}Cu^{12}CH^-$
0.67025	0.33	186	$^{127}I^{23}Na_2{}^{13}C^-$, $^{124}Sn^{23}Na^{19}F_2H^-$	$^{109}Ag^{65}Cu^{12}C^-$, $^{109}Ag^{63}Cu^{13}CH^-$
0.67202	3.58	187	$^{122}Sn^{65}Cu^-$, $^{124}Sn^{63}Cu^-$, $^{107}Ag^{23}Na^{19}F_3^-$	$^{112}Sn^{63}Cu^{12}C^-$, $^{122}Sn^{63}CuH_2^-$, $^{120}Sn^{65}CuH_2^-$, $^{118}Sn^{19}F_3{}^{12}C^-$
0.67385	0.34	188	$^{122}Sn^{65}CuH^-$, $^{124}Sn^{63}CuH^-$	$^{122}Sn^{65}CuH^-$, $^{124}Sn^{63}CuH^-$, $^{119}Sn^{19}F_3{}^{12}C^-$, $^{109}Ag^{65}Cu^{13}CH^-$
0.67554	14.7	189	$^{124}Sn^{65}Cu^-$, $^{63}Cu_3^-$, $^{109}Ag^{23}Na^{19}F_3^-$	$^{114}Sn^{63}Cu^{12}C^-$, $^{122}Sn^{65}CuH_2^-$
0.67737	7.88	190	$^{127}I^{63}Cu^-$, $^{124}Sn^{65}CuH^-$	$^{115}Sn^{63}Cu^{12}C^-$, $^{109}Ag^{19}F_3{}^{12}C_2^-$
0.67912	18.0	191	$^{63}Cu_2{}^{65}Cu^-$, $^{127}I^{63}CuH^-$, $^{107}Ag^{23}Na_2{}^{19}F_2^-$	$^{116}Sn^{63}Cu^{12}C^-$, $^{114}Sn^{65}Cu^{12}C^-$
0.68096	3.54	192	$^{127}I^{65}Cu^-$	$^{117}Sn^{63}Cu^{12}C^-$, $^{115}Sn^{65}Cu^{12}C^-$
0.68262	7.13	193	$^{65}Cu_2{}^{63}Cu^-$, $^{109}Ag^{23}Na_2{}^{19}F_2^-$	$^{118}Sn^{63}Cu^{12}C^-$, $^{116}Sn^{65}Cu^{12}C^-$
0.68617	0.88	195	$^{65}Cu_3^-$, $^{109}Ag^{23}Na_2{}^{19}F_2H_2^-$	$^{120}Sn^{63}Cu^{12}C^-$, $^{118}Sn^{65}Cu^{12}C^-$
0.68802	0.46	196	$^{65}Cu_3H^-$	$^{120}Sn^{63}Cu^{13}C^-$, $^{119}Sn^{65}Cu^{12}C^-$

Table 4.3: Prediction of molecular ions for SnF_2 + NaI + Ag target *(continued)*

Magnetic field (B, Tesla)	Observed beam-current (nA)	Mass of molecular ion (amu)	Ion prediction	
			More probable molecular ions	Less probable molecular ions
0.69150	0.34	198	$^{114}Sn^{23}Na_2{}^{19}F_2^-$	$^{122}Sn^{63}Cu^{13}C^-$, $^{120}Sn^{65}Cu^{13}C^-$
0.69505	0.33	200	$^{116}Sn^{23}Na_2{}^{19}F_2^-$	$^{124}Sn^{63}Cu^{13}C^-$, $^{122}Sn^{65}Cu^{13}C^-$
0.69853	0.38	202	$^{127}I^{63}Cu^{12}C^-$	$^{124}Sn^{65}Cu^{13}C^-$
0.70713	0.87	207	$^{65}Cu_3{}^{12}C^-$	$^{118}Sn^{65}Cu^{12}C_2^-$, $^{120}Sn^{63}Cu^{12}C_2^-$
0.71060	2.93	209	$^{127}I^{63}Cu^{19}F^-$, $^{107}Ag^{63}Cu^{19}F_2H^-$	$^{122}Sn^{63}Cu^{12}C_2^-$, $^{120}Sn^{65}Cu^{12}C_2^-$
0.71403	1.25	211	$^{127}I^{65}Cu^{19}F^-$, $^{127}I^{63}Cu^{19}FH_2^-$, $^{127}I^{23}Na_2{}^{19}F_2^-$	$^{124}Sn^{63}Cu^{12}C_2^-$, $^{107}Ag^{23}Na_2{}^{19}F_3H^-$, $^{122}Sn^{65}Cu^{12}C_2^-$
0.71735	0.38	213	$^{109}Ag^{23}Na_2{}^{19}F_3H^-$	$^{124}Sn^{65}Cu^{12}C_2^-$, $^{122}Sn^{65}Cu^{12}C_2H_2^-$, $^{124}Sn^{63}Cu^{12}C_2H_2^-$
0.71912	4.67	214	$^{107}Ag_2^-$, $^{65}Cu_3{}^{19}F^-$, $^{65}Cu^{63}Cu_2{}^{23}Na^-$	$^{127}I^{63}Cu^{12}C_2^-$, $^{124}Sn^{65}Cu^{13}C^{12}C^-$,
0.72092	1.59	215	$^{127}I^{65}Cu^{23}Na^-$	$^{124}Sn^{65}Cu^{13}C_2^-$, $^{127}I^{63}Cu^{23}NaH_2^-$
0.72253	8.68	216	$^{109}Ag^{107}Ag^-$, $^{65}Cu_2{}^{63}Cu^{23}Na^-$	$^{127}I^{65}Cu^{12}C_2^-$, $^{107}Ag^{107}AgH_2^-$, $^{127}I^{63}Cu^{13}C_2^-$
0.72420	0.92	217	$^{109}Ag^{107}AgH^-$,	$^{127}I^{65}Cu^{13}C^{12}C^-$, $^{127}I^{63}Cu^{13}C_2H^-$
0.72587	4.06	218	$^{109}Ag_2^-$, $^{65}Cu_3{}^{23}Na^-$	$^{127}I^{65}Cu^{13}C_2^-$, $^{124}Sn^{63}Cu^{19}F^{12}C^-$
0.72755	0.31	219	$^{112}Sn^{107}Ag^-$	$^{127}I^{65}Cu^{13}C_2H^-$, $^{124}Sn^{63}Cu^{19}F^{13}C^-$
0.73418	2.02	223	$^{114}Sn^{109}Ag^-$, $^{116}Sn^{107}Ag^-$, $^{120}Sn^{23}Na_2{}^{19}F_3^-$	$^{127}I^{65}Cu^{19}F^{12}C^-$, $^{122}Sn^{65}Cu^{23}Na^{13}C^-$, $^{124}Sn^{63}Cu^{23}Na^{13}C^-$
0.73583	1.02	224	$^{115}Sn^{109}Ag^-$, $^{117}Sn^{107}Ag^-$	$^{124}Sn^{65}Cu^{23}Na^{12}C^-$, $^{114}Sn^{109}AgH^-$, $^{116}Sn^{107}AgH^-$
0.73751	4.90	225	$^{116}Sn^{109}Ag^-$, $^{118}Sn^{107}Ag^-$	$^{124}Sn^{65}Cu^{23}Na^{13}C^-$, $^{115}Sn^{109}AgH^-$, $^{117}Sn^{107}AgH^-$
0.73914	2.05	226	$^{117}Sn^{109}Ag^-$, $^{119}Sn^{107}Ag^-$	$^{107}Ag_2{}^{12}C^-$, $^{116}Sn^{109}AgH^-$, $^{118}Sn^{107}AgH^-$
0.74070	7.41	227	$^{118}Sn^{109}Ag^-$, $^{120}Sn^{107}Ag^-$, $^{124}Sn^{23}Na_2{}^{19}F_3^-$	$^{117}Sn^{109}AgH^-$, $^{119}Sn^{107}AgH^-$
0.74225	1.07	228	$^{119}Sn^{109}Ag^-$, $^{118}Sn^{109}AgH^-$	$^{117}Sn^{109}AgH_2^-$, $^{119}Sn^{107}AgH_2^-$
0.74399	4.63	229	$^{122}Sn^{107}Ag^-$, $^{120}Sn^{109}Ag^-$,	$^{120}Sn^{107}AgH_2^-$, $^{118}Sn^{109}AgH_2^-$
0.74732	1.50	231	$^{124}Sn^{107}Ag^-$, $^{122}Sn^{109}Ag^-$, $^{124}Sn^{107}Ag^-$	$^{109}Ag_2{}^{13}C^-$, $^{122}Sn^{107}AgH_2^-$, $^{120}Sn^{109}AgH_2^-$
0.75047	8.96	233	$^{124}Sn^{109}Ag^-$, $^{107}Ag^{63}Cu_2^-$	$^{122}Sn^{109}AgH_2^-$, $^{114}Sn^{107}Ag^{12}C^-$, $^{112}Sn^{109}Ag^{12}C^-$

Table 4.3: Prediction of molecular ions for SnF_2 + NaI + Ag target *(continued)*

Magnetic field (B, Tesla)	Observed beam-current (nA)	Mass of molecular ion (amu)	Ion prediction	
			More probable molecular ions	Less probable molecular ions
0.75214	5.69	234	$^{127}I^{107}Ag^-$, $^{107}Ag^{63}Cu_2H^-$	$^{115}Sn^{107}Ag^{12}C^-$
0.75368	15.0	235	$^{109}Ag^{63}Cu_2^-$, $^{107}Ag^{65}Cu^{63}Cu^-$	$^{116}Sn^{107}Ag^{12}C^-$, $^{114}Sn^{109}Ag^{12}C^-$
0.75536	5.99	236	$^{127}I^{109}Ag^-$, $^{109}Ag^{63}Cu_2H^-$	$^{117}Sn^{107}Ag^{12}C^-$, $^{115}Sn^{109}Ag^{12}C^-$
0.75691	8.95	237	$^{107}Ag^{65}Cu_2^-$, $^{109}Ag^{65}Cu^{63}Cu^-$	$^{116}Sn^{109}Ag^{12}C^-$, $^{118}Sn^{107}Ag^{12}C^-$
0.75848	1.35	238	$^{107}Ag^{65}Cu_2H^-$, $^{112}Sn^{63}Cu_2^-$, $^{112}Sn^{107}Ag^{19}F^-$	$^{112}Sn^{23}Na_3{}^{19}F_3^-$, $^{116}Sn^{109}Ag^{13}C^-$
0.76010	1.96	239	$^{127}I^{112}Sn^-$, $^{109}Ag^{65}Cu_2^-$	$^{117}Sn^{109}Ag^{13}C^-$, $^{118}Sn^{109}Ag^{12}C^-$
0.76169	1.55	240	$^{112}Sn^{109}Ag^{19}F^-$, $^{112}Sn^{65}Cu^{63}Cu^-$, $^{114}Sn^{63}Cu_2^-$, $^{109}Ag^{65}Cu_2H^-$, $^{114}Sn^{63}Cu_2^-$	$^{114}Sn^{23}Na_3{}^{19}F_3^-$, $^{120}Sn^{107}Ag^{13}C^-$, $^{118}Sn^{109}Ag^{13}C^-$
0.76490	1.45	242	$^{127}I^{115}Sn^-$, $^{112}Sn^{65}Cu_2^-$, $^{112}Sn^{107}Ag^{23}Na^-$, $^{114}Sn^{65}Cu^{63}Cu^-$, $^{116}Sn^{63}Cu_2^-$	$^{116}Sn^{23}Na_3{}^{19}F_3^-$, $^{122}Sn^{107}Ag^{13}C^-$, $^{120}Sn^{109}Ag^{13}C^-$
0.76650	0.70	243	$^{127}I^{116}Sn^-$, $^{115}Sn^{65}Cu^{63}Cu^-$, $^{117}Sn^{63}Cu_2^-$	$^{117}Sn^{23}Na_3{}^{19}F_3^-$, $^{112}Sn^{107}Ag^{12}C_2^-$, $^{122}Sn^{109}Ag^{12}C^-$, $^{124}Sn^{107}Ag^{12}C^-$
0.76807	1.90	244	$^{127}I^{117}Sn^-$, $^{114}Sn^{65}Cu_2^-$, $^{114}Sn^{107}Ag^{23}Na^-$, $^{118}Sn^{63}Cu_2^-$	$^{118}Sn^{23}Na_3{}^{19}F_3^-$, $^{124}Sn^{107}Ag^{13}C^-$, $^{122}Sn^{109}Ag^{13}C^-$
0.76965	1.11	245	$^{127}I^{118}Sn^-$, $^{115}Sn^{65}Cu_2^-$, $^{115}Sn^{107}Ag^{23}Na^-$, $^{118}Sn^{63}Cu_2^-$	$^{119}Sn^{23}Na_3{}^{19}F_3^-$, $^{112}Sn^{109}Ag^{12}C_2^-$, $^{124}Sn^{109}Ag^{12}C^-$
0.77127	2.49	246	$^{114}Sn^{109}Ag^{23}Na^-$, $^{116}Sn^{65}Cu_2^-$, $^{127}I^{119}Sn^-$, $^{63}Cu_3{}^{19}F_3^-$, $^{120}Sn^{63}Cu_2^-$	$^{120}Sn^{23}Na_3{}^{19}F_3^-$, $^{124}Sn^{109}Ag^{13}C^-$, $^{115}Sn^{107}Ag^{12}C_2^-$
0.77287	1.03	247	$^{115}Sn^{109}Ag^{23}Na^-$, $^{127}I^{120}Sn^-$, $^{117}Sn^{65}Cu_2^-$	$^{127}I^{119}SnH^-$, $^{114}Sn^{109}Ag^{12}C_2^-$, $^{116}Sn^{107}Ag^{12}C_2^-$,
0.77440	1.62	248	$^{118}Sn^{65}Cu_2^-$, $^{65}Cu^{63}Cu_2{}^{19}F_3^-$, $^{122}Sn^{63}Cu_2^-$	$^{122}Sn^{23}Na_3{}^{19}F_3^-$, $^{115}Sn^{109}Ag^{12}C_2^-$
0.77602	0.26	249	$^{119}Sn^{65}Cu_2^-$, $^{127}I^{122}Sn^-$	$^{116}Sn^{109}Ag^{12}C_2^-$, $^{118}Sn^{107}Ag^{12}C_2^-$
0.77752	0.69	250	$^{120}Sn^{65}Cu_2^-$, $^{65}Cu_2{}^{63}Cu^{19}F_3^-$, $^{124}Sn^{63}Cu_2^-$	$^{124}Sn^{23}Na_3{}^{19}F_3^-$, $^{119}Sn^{107}Ag^{12}C_2^-$, $^{112}Sn^{107}Ag^{19}F^{12}C^-$
0.77905	0.34	251	$^{127}I^{124}Sn^-$, $^{124}Sn^{63}Cu_2H^-$	$^{120}Sn^{107}Ag^{12}C_2^-$, $^{118}Sn^{109}Ag^{12}C_2^-$
0.78060	0.68	252	$^{122}Sn^{65}Cu_2^-$, $^{65}Cu_3{}^{19}F_3^-$, $^{124}Sn^{65}Cu^{63}Cu^-$	$^{119}Sn^{109}Ag^{12}C_2^-$, $^{114}Sn^{107}Ag^{19}F^{12}C^-$
0.78220	3.48	253	$^{127}I^{107}Ag^{19}F^-$, $^{127}I^{63}Cu_2^-$	$^{127}I^{23}Na_3{}^{19}F_3^-$, $^{120}Sn^{109}Ag^{12}C_2^-$
0.78379	1.39	254	$^{124}Sn^{65}Cu_2^-$, $^{122}Sn^{65}Cu_2H_2^-$	$^{114}Sn^{109}Ag^{19}F^{12}C^-$, $^{116}Sn^{107}Ag^{19}F^{12}C^-$

Table 4.3: Prediction of molecular ions for SnF_2 + NaI + Ag target *(continued)*

Magnetic field (B, Tesla)	Observed beam-current (nA)	Mass of molecular ion (amu)	Ion prediction	
			More probable molecular ions	Less probable molecular ions
0.78520	3.13	255	$^{127}I^{109}Ag^{19}F^-$, $^{127}I^{65}Cu^{63}Cu^-$	$^{122}Sn^{109}Ag^{12}C_2^-$, $^{124}Sn^{107}Ag^{12}C_2^-$, $^{115}Sn^{109}Ag^{19}F^{12}C^-$, $^{117}Sn^{107}Ag^{19}F^{12}C^-$
0.78672	0.51	256	$^{109}Ag^{65}Cu^{63}Cu^{19}F^-$, $^{107}Ag^{65}Cu_2{}^{19}F^-$	$^{116}Sn^{109}Ag^{19}F^{12}C^-$, $^{118}Sn^{107}Ag^{19}F^{12}C^-$
0.78820	0.87	257	$^{127}I^{65}Cu_2^-$, $^{107}Ag^{65}Cu_2{}^{19}FH^-$	$^{124}Sn^{109}Ag^{12}C_2^-$, $^{117}Sn^{109}Ag^{19}F^{12}C^-$
0.79148	2.97	259	$^{109}Ag^{65}Cu_2{}^{19}FH^-$	$^{127}I^{107}Ag^{13}C^{12}C^-$
0.79305	1.79	260	$^{109}Ag^{65}Cu^{63}Cu^{23}Na^-$, $^{107}Ag^{65}Cu_2{}^{23}Na^-$,	$^{127}I^{109}Ag^{12}C_2^-$, $^{109}Ag^{63}Cu_2{}^{13}C^{12}C^-$
0.79459	2.61	261	$^{112}Sn^{107}Ag^{23}Na^{19}F^-$	$^{127}I^{109}Ag^{13}C^{12}C^-$
0.81864	6.70	277	$^{107}Ag_2{}^{63}Cu^-$, $^{127}I^{112}Sn^{19}F_2^-$	$^{118}Sn^{109}Ag^{19}F_2{}^{12}C^-$, $^{120}Sn^{107}Ag^{19}F_2{}^{12}C^-$
0.82159	14.0	279	$^{107}Ag_2{}^{65}Cu^-$, $^{109}Ag^{107}Ag^{63}Cu^-$, $^{127}I^{114}Sn^{19}F_2^-$	$^{120}Sn^{109}Ag^{19}F_2{}^{12}C^-$, $^{122}Sn^{107}Ag^{19}F_2{}^{12}C^-$
0.82452	7.64	281	$^{109}Ag_2{}^{63}Cu^-$, $^{109}Ag^{107}Ag^{65}Cu^-$, $^{127}I^{116}Sn^{19}F_2^-$	$^{122}Sn^{109}Ag^{19}F_2{}^{12}C^-$, $^{124}Sn^{107}Ag^{19}F_2{}^{12}C^-$
0.82747	1.75	283	$^{109}Ag_2{}^{65}Cu^-$, $^{127}I^{118}Sn^{19}F_2^-$	$^{127}I^{112}Sn^{19}F^{13}C^{12}C^-$, $^{124}Sn^{109}Ag^{19}F_2{}^{12}C^-$
0.83184	0.38	286	$^{109}Ag^{65}Cu_2{}^{23}Na_2H^-$	$^{127}I^{116}Sn^{19}F^{12}C_2^-$, $^{127}I^{114}Sn^{19}F^{13}C_2^-$
0.83472	1.12	288	$^{127}I^{115}Sn^{23}Na_2^-$	$^{127}I^{118}Sn^{19}F^{12}C_2^-$, $^{127}I^{116}Sn^{19}F^{13}C_2^-$
0.83617	0.49	289	$^{127}I^{124}Sn^{19}F_2^-$, $^{127}I^{116}Sn^{23}Na_2^-$, $^{127}I^{120}Sn^{23}Na^{19}F^-$	$^{127}I^{119}Sn^{19}F^{12}C_2^-$, $^{127}I^{117}Sn^{19}F^{13}C_2^-$
0.83769	1.67	290	$^{127}I^{120}Sn^{23}Na^{19}FH^-$, $^{127}I^{117}Sn^{23}Na_2^-$, $^{107}Ag^{63}Cu2^{19}F_3^-$	$^{127}I^{119}Sn^{23}Na^{19}FH_2^-$, $^{127}I^{120}Sn^{19}F^{12}C_2^-$, $^{127}I^{120}Sn^{19}F^{12}C_2^-$, $^{127}I^{116}Sn^{23}Na_2H^-$

From the above table, it is clear, in spite of our expectation, that $^{126}SnF_2I^-$ molecular ions could form, but no such ions were observed. The molecular ions were predicted based on

the composition of target materials. The previous sample run may contribute traces of carbon contamination.

4.3.3 Quantification of ^{126}Sn from the beam-current

i) SnI_2 + NaF + Ag target

The targets containing SnI_2 + NaF + Ag composition was scanned at first to see any detectable beam-current, and the results of the AMS run is presented in Table 4.4.

Table 4.4: Observed beam-current for SnI_2^- molecular ion.

Composition	$^{125}TeI_3^- \rightarrow {}^{125}Te^{5+}$	$^{118}SnI_3^- \rightarrow {}^{118}Sn^{5+}$	[^{126}Sn]/[Sn] ratio
SnI_2	No detectable count	No stable current	Not measured
SnI_2 + NaF + Ag	> 10 c/s	No stable current	Not measured
Ag-blank	~ 0.10 c/s	No stable current	Not measured

Table 4.4 shows that the beam-current, due to SnI_2F^- heavy molecular ion (produced from the target containing SnI_2 + NaF + Ag composition), is almost zero. This observation states that the SnF_2I^- or SnI_2F^- species do not exist, or not abundant enough to be detected accurately. In case of NaI + Nb tuning target (Nb powder was added to enhance the conductivity), the $^{125}Te^{+5}$ count rate, after the injection of $^{125}Te^-$, was found as ~3,000 c/s, however, the count rate was dropped to ~0.01 c/s after the injection of $^{125}TeI^-$, a reduction by 5-orders of magnitude.

The drop of beam-current after the addition of either SnI_2 or mixture of SnI_2 + Ag clearly shows that the relatively bulky SnI_2 molecule is not a good ionic conductor, the conductivity does not change even after the addition of Ag powder. The absence of detectable SnI^- current further confirms that any material consisting SnI_2 compound will

make the ion source unstable. Therefore, all considerations involving iodine must be dropped off for the development of ^{126}Sn-AMS detection plan.

ii) SnF_2 + NaI + Ag target

Results from the first AMS run (Table 4.4) reveals that iodine-based target materials are non-conductive, or exhibit no detectable beam-current. Based on this argument, a thorough study on the SnF_2 + NaI + Ag target has not been carried out. Therefore, the detection of ^{126}Sn with targets containing I_2 molecular species was discarded.

iii) SnF_2 + PbF_2 target (laboratory prepared SnF_2)

The laboratory prepared SnF_2 sample has been tested again, and the findings are presented in Table 4.5.

Table 4.5: Observed beam-current for SnF_2^- molecular ion with target composition of SnF_2 + PbF_2 (prepared sample).

Composition	$^{125}TeF_3^- \rightarrow {}^{125}Te^{5+}$	$^{118}SnF_3^- \rightarrow {}^{118}Sn^{5+}$	[^{126}Sn]/[Sn] ratio
SnF_2	~ 1.0 c/s	5.3 nA	~ 1.0×10^{-10}
SnF_2 + PbF_2	~ 0.50 c/s	3.9 nA	~ 7.0×10^{-11}
PbF_2-blank	~ 0.10 c/s	2.2 pA	~ 2.0×10^{-8}

Table 4.5 shows that the PbF_2 blank produces the lowest tellurium count, whereas SnF_2 gives 10-times more tellurium signal than that of lead fluoride. The highest beam-current (5.3 nA) was observed with SnF_2, whereas the PbF_2 blank has produced the lowest count. The laboratory prepared SnF_2 sample gave the ^{126}Sn/^{120}Sn ratio as ~10^{-9} or at the ppb level suppression of background. It is a relatively high ratio. This strong background might have been caused due to the presence of stable ^{120}Te isotope (0.096% natural abundance). However, the prepared SnF_2 sample in the mixed matrix gave the ^{126}Sn/^{118}Sn

ratio as ~10^{-11}, a reduction of background by two-orders of magnitude compared to the value recorded for $^{126}Sn/^{120}Sn$. As the ^{118}Sn isotope is almost free from isobaric interferences of potential stable or long-lived congeners, this low detection limit is very prospective for the development of strategic plans in the dectetion of ^{126}Sn isotope by AMS. Therefore, a change in the target composition of target materials based on SnF_2 compound would produce a strong sputter yield.

iv) $^{126}Sn/^{120}Sn$ *vs* $^{126}Sn/^{118}Sn$ ratios

The initial experiment was performed to monitor the detector signal for the tin metal itself, therefore, the beam-current of the most abundant stable isotope, ^{120}Sn (32.58% natural abundance) was checked. The molecular ions $^{120}SnF^-$, $^{120}SnF_2^-$, $^{120}SnF_3^-$, $^{120}SnF_4^-$, and $^{120}SnF_5^-$ gave sputter-current of 1.3, 2.9, 44.0, 10.0, and 30.0 nA, respectively. The detector count of $^{126}Sn^{3+}$ ions and the $^{120}Sn^{3+}$ beam-current have produced a $^{126}Sn/^{120}Sn$ ratio of ~10^{-9}, which implies a suppression of ^{126}Te background in the ppb-level. Though this ratio was quite high, well above our expected value of 10^{-11}, but the result was very promising. The relatively high background might have been caused due to the presence of stable ^{120}Te.

Again, the beam-current of ^{118}Sn was checked. Although the natural abundance of ^{118}Sn is low (24.22%, compared to 32.58% of ^{120}Sn), but it is almost free from isobaric interferences. The effect of ^{118}Te ($T_{½}$ = 6 d) can be removed easily by sample aging, and other short-lived isotopes, e. g., ^{118}Cd (50.3 m), ^{118}I (13.7 m), and ^{118}Xe (6 m) most likely will not extracted effectively during the AMS detection of long-lived ^{126}Sn. For this reason, the subsequent beam-current was recorded for the stable ^{118}Sn, and the $^{126}Sn/^{118}Sn$ ratio was calculated in the final observation. In our present study, the measurement of

^{118}Sn beam-current has produced a ^{126}Sn/^{118}Sn ratio of ~10^{-11}, which excellently conforms with our expected background of ≤10^{-11}. This surprising result has motivated us to apply the experimental idea to observe the ^{118}Sn-current of commercial SnF_2. Fortunately, the purchased SnF_2 gave the ^{126}Sn/^{118}Sn ratio of ~10^{-12}, a further drop of ^{126}Te background to parts per trillion-level.

v) SnF_2 + PbF_2 target (commercial SnF_2)

The purchased SnF_2 sample has been tested for a better suppression of tellurium background, and the results are presented in Table 4.6.

Table 4.6: Observed beam-current for SnF_2^- molecular ion with target composition of SnF_2 + PbF_2 (commercial ample.

Composition	$^{125}TeF^{3-} \rightarrow {}^{125}Te^{5+}$	$^{118}SnF^{3-} \rightarrow {}^{118}Sn^{5+}$	[^{126}Sn]/[^{118}Sn] ratio
SnF_2	~ 0.05 c/s	500 pA	2.0×10^{-11}
SnF_2 + PbF_2	~ 0.10 c/s	6.0 nA	3.0×10^{-12}
PbF_2-blank	~ 0.10 c/s	1.6 pA	1.0×10^{-8}

After tuning the AMS by $^{127}I^- \rightarrow {}^{127}I^{+5}$ with all H-slits open to 1.50/1.50, the $^{118}SnF_3^- \rightarrow {}^{118}Sn^{+5}$ gave a beam-current of 6.0 nA in the gas ionization chamber-Faraday cup (GIC-FC), and the $^{126}TeF_3^- \rightarrow {}^{126}Te^{+5}$ system gave a count of ~0.1 c/s. The process gave the ^{126}Sn/^{118}Sn ratio of ~3.0×10^{-12}. This is the lowest detected background ever for the quantification of ^{126}Sn by any AMS technique, even larger AMS facilities have not reported ratio lower than this value. In the present study, reagent grade SnF_2 (99.5%) was used to prepare AMS targets, which may contribute significant amount of matrix impurity. The ICP standard solution of tin contains 99.9995% pure Sn shot,

therefore, we can expect that the ^{126}Te background could be reduced even more with ultrapure target materials.

Thanks to A. E. Lalonde AMS technique for its high sensitivity and for offering an elegant route to suppress ^{126}Te background during the measurement of ^{126}Sn. Recently, Shen et al.[198] have used SnF_2 target to prepare SnF_3^- molecular ion in the detection of ^{126}Sn, and have found the ^{126}Sn/Sn ratio as $(1.92 \pm 1.13) \times 10^{-10}$. Our observation suggests that SnF_2-based target produces strong sputter yield and shows the highest beam-current compared to other tested compounds. A comparison on the observed ^{126}Sn/Sn ratio with different target materials is presented in Table 4.7.

Table 4.7: Different target materials and the observed ^{126}Sn/^{120}Sn and ^{126}Sn/^{118}Sn ratios.

Target composition	Types of materials	Types of isotope	Observed ^{126}Sn/Sn ratio
SnI_2 + NaF + Ag	Powdered matrix	^{126}Sn/^{118}Sn	No beam-current
SnF_2 + PbF_2	Prepared SnF_2	^{126}Sn/^{120}Sn	~ 3.0×10^{-9}
SnF_2 + PbF_2	Prepared SnF_2	^{126}Sn/^{118}Sn	~ 7.0×10^{-11}
SnF_2 + PbF_2	Commercial SnF_2	^{126}Sn/^{118}Sn	~ 3.0×10^{-12}

Results on Table 4.7 further confirms that the effective suppression of ^{126}Te background is directly related to the purity of sample matrix, a large impurity potentially masks the tin beam-current. The relatively pure commercial SnF_2 gave the lowest background compared to the prepared one. Again, with the same type of material (prepared SnF_2), the efficiency of ^{126}Sn/^{118}Sn (~10^{-11}) outweighs the efficiency of ^{126}Sn/^{120}Sn (~10^{-9}) by two-orders of magnitude.

Now, a comparison of our present result with that of the previously recorded ^{126}Sn/^{118}Sn ratio is shown in Table 4.7.

Table 4.8: A comparison on the $^{126}Sn/^{118}Sn$ ratios observed by different study groups.

Year	Author	Lab	Method	Target source	Condition	$^{126}Sn/Sn$ ratio	Ref.
1989	Kutschera et al.	ATLAS	AMS	…	Using gas-filled magnet and gas ionization chamber at high energy (> 400 MeV)	$\sim 10^{-7}$	[124]
1996	Gartenmann et al.	Zurich	AMS	…	Gas ionization chamber combined with projectile X-ray detection	9.23×10^{-6}	[78]
2009	Shen et al.	Beijing	AMS	Commercial SnF_2	SnF_3^- molecular ion from SnF_2 target at 13 MV energy	1.92×10^{-10}	[198]
2011	Shen et al.	Beijing	AMS	Prepared SnF_2	SnF_3^- molecular ion from SnF_2 target at 13 MV energy	1.92×10^{-10}	[79]
2018	**Present work**	**Ottawa**	**AMS**	**Prepared SnF_2**	**SnF_3^- molecular ion from SnF_2 target at 3 MV energy**	**7.00×10^{-11}**	**…**
2018	**Present work**	**Ottawa**	**AMS**	**Commercial SnF_2**	**SnF_3^- molecular ion from SnF_2 target at 3 MV energy**	**3.00×10^{-12}**	**…**

4.4 Conclusions

a) Summary of findings

Our present study demonstrates a reduction of tellurium isotope and have found the background level to ppt-level, the specific observations are:

(i) SnF_3^- beam-current can easily be made.

(ii) TeF_3^- is not easily formed, or if it does, its availability is not sufficient to produce detectable current.

(iii) The $^{126}Sn/^{120}Sn$ ratio for the prepared SnF_2 sample was found as ~4.0×10^{-9}, that is a ppb-level background.

(iv) The $^{126}Sn/^{118}Sn$ ratio for the same SnF_2 mixed with PbF_2 (1 : 5 ratio) sample was observed as ~7.0×10^{-11}, a drop of background by 2-orders of magnitude.

(v) The $^{126}Sn/^{118}Sn$ ratio for the commercial SnF_2 sample was found to be ~3.0×10^{-12}, a drop of background to ppt-level.

b) Important observations

(i) Tin does not form molecular-beam with iodine. Iodine species in the target makes the ion source very unstable, no detectable beam-current even after mixing with silver powder.

(ii) The only stable tin-beam was found as SnF_3^-.

(iii) The molecule SnF_2 itself is a good ionic conductor, its sputter capacity is very good and immediate, which produces a large SnF_3^- current, but the current does not stay stable for long.

(iv) The SnF_2 + PbF_2 target yields a long-lasting SnF_3^- current (PbF_2 provides more fluoride to donate to SnF_2 and produce a steady beam of SnF_3^-).

(v) $SnIF_2^-$ molecular ions were not found, either they do not exist or they are not stable enough to be detected.

(vi) Tellurium can produce a beam, but it disappears quickly. In fact, both TeF_3^- and TeF_5^- currents decline rapidly.

(vii) Te^-, TeI^-, I_2^-, I^- species are rare.

(viii) The heavy SnI_2F^- molecular ion was not found.

(ix) Both TeF_3^- and TeF_5^- current decline rapidly,

c) Further considerations

(i) The best low-energy AMS study for the detection of ^{126}Sn isotope would be the SSI run for 3 beams with the following three isotopes:

- $^{120}SnF_3^- \rightarrow {}^{120}Sn^{+5}$ by FC (along with the tuning beam),
- $(^{126}Sn, {}^{126}Te)F_3^- \rightarrow (^{126}Sn, {}^{126}Te)^{+5}$ by GIC, and
- $^{128}TeF_3^- \rightarrow {}^{128}Te^{+5}$ or $^{125}TeF_3^- \rightarrow {}^{125}Te^{+5}$ by GIC using ^{129}I-run AMS conditions, except with the stripper at 5×10^{-3}, detector at 15 mBar, E_f-gain at 20–12.0.

(ii) The targets were prepared by $SnF_2 + PbF_2$ (1 : 5 ratio by weight). Though this weight ratio is ideal to gain a reasonable beam-current, but if the actual sample material is SnX, the targets can be made by $SnX + PbF_2$ (1 : 10 ratio by weight).

(iii) For the preparation of SnF_3^- ion, both SnF_2 + Ag and $SnF_2 + PbF_2$ combinations seem work fine, but the latter will produce more SnF_3^- current.

(iv) $Te[^{57}Fe^-]$ may also exist (which has the same mass with TeF_3^-), so avoiding Fe in SnF_2 is important. But, Fe and Te contaminations are rare in SnF_2, hopefully $Te[^{57}Fe^-]$ can be controlled at low levels.

d) Future goals

(i) Determination of transmission efficiency for $^{120}SnF_3^- \rightarrow {}^{120}Sn^{+5}$.

(ii) Tuning the key AMS conditions, procedures, and spectra.

(iii) Preparation of ^{126}Sn standard materials by the double neutron capture to stable ^{124}Sn (5.79% abundance) isotope in the SLOWPOKE nuclear reactor at the Royal Millitary College (RMC), Kingston, Ontario, Canada. Table 4.9 shows a comparison on the neutron capture cross sections of our target material with those of other stable tin isotopes.

(iv) Making a dilution series and preparing a linearity test with an automated SSI run.

(v) AMS detection of ^{126}Sn in natural samples from nuclear treatment plants, like Chalk River Atomic Energy crude wastes and other nuclear testing sites.

Table 4.9: The target characteristics for the preparation of ^{126}Sn by double neutron capture.

Isotope	Target	Target half-life	Target abundance	Reaction	Neutron capture cross section (barn)[202,203]
^{113}Sn	^{112}Sn	STABLE	0.973%	$^{112}Sn(n, \gamma)^{113}Sn$	$^{112}Sn = 0.860 \pm 0.090$
^{123}Sn	^{122}Sn	STABLE	4.629%	$^{122}Sn(n, \gamma)^{123}Sn$	$^{122}Sn = 0.139 \pm 0.015$
^{125}Sn	^{124}Sn	STABLE	5.789%	$^{124}Sn(n, \gamma)^{125}Sn$	$^{124}Sn = 0.134 \pm 0.005$
^{126}Sn	^{125}Sn	9.4 d	…	$^{125}Sn(n, \gamma)^{126}Sn$	

Chapter 5:

Concerns and future directions

5.1 Separation of tin from tellurium

5.1.1 Concerns

i) The column separation of tin from tellurium was carried out at standard laboratory conditions (25 °C, normal pressure), the effects of temperature and pressure were not tested.

ii) The speciation of tin was not evaluated.

5.1.2 Future directions

i) A thorough separation study with samples collected from different locations.

ii) A comparison on separation efficiency with Sn(II) and Sn(IV) spikes.

5.2 Interferences of chloride and sulfate ions in the separation of tin from tellurium

5.2.1 Concerns

i) The interference from major cations has not been observed.

ii) The adsorptive behavior of tin in the presence of marine water has not been carried out.

5.2.2 Future directions

i) The separation of tin from tellurium in presence of cationic species.

ii) Performance of the separation experiment in presence of artificial sea water.

5.3 AMS detection of ^{126}Sn

5.3.1 Concerns

(i) The overall ^{126}Sn/Sn background for the laboratory prepared sample was at about 1 ppb (10^{-9}), whereas for the commercial sample, the background was in the ppt (10^{-12}) level.

(ii) Much of tellurium background might have originated from the PbF_2 compound itself.

5.3.2 Future directions

(i) Using PbF_2 alternatives as the fluoride source.

(ii) The use of ISA technique, after sufficient development, can offer an effective (hopefully an efficient) solution in reducing the $^{126}TeF_5^-$ [126 + 19 × 5 = 221] and $^{126}Te^{95}Mo^-$ [126 + 95 = 221] interferences in the monitoring of $^{126}SnF_5^-$ [126 + 19 × 5 = 221] beam.

Chapter 6:

References

[1]. J. R. de Laeter, J. K. Böhlke, P. D. Bièvre, H. Hidaka, H. S. Peiser, K. J. R. Rosman & P. D. P. Taylor. (**2003**). Atomic weights of the elements: review 2000 (IUPAC Technical Report). *Pure Appl Chem*, 75: 683–800.

[2]. R. C. Weast, M. J. Astle & W. H. Beyer. (**1988**). CRC Handbook of Chemistry and Physics, 69th edn, CRC Press, Inc., Florida.

[3]. F. Bandama, S. Hall & S. Chirikure. (**2015**). Eiland crucibles and the earliest relative dating for tin and bronze working in southern Africa. *J Archaeol Sci,* 62: 82–91.

[4]. A. H. Mason, W. G. Powell, H. A. Bankoff, R. Mathur, A. Bulatović, V. Filipović & J. Ruiz. (**2016**). Tin isotope characterization of bronze artifacts of the central Balkans. *J Archaeo Sci*, 69: 110–117.

[5]. E. Yamazaki, S. Nakai, Y. Sahoo, T. Yokoyama, H. Hifune, T. Saito, J. Chen, N. Takagi, N. Hokanishi & A. Yasuda. (**2014**). Feasibility studies of Sn isotope composition for provenancing ancient bronzes. *J Archaeol Sci*, 52: 458–467.

[6]. Q. Wang, S. Strekopytov, B. W. Roberts & N. Wilkin. (**2016**). Tin ingots from a probable Bronze Age shipwreck off the coast of Salcombe, Devon: composition and microstructure. *J Archaeol Sci,* 67: 80–92.

[7]. P. Howe. (**2005**). Tin and inorganic tin compounds: concise international chemical assessment document 65, World Health Organization (WHO), Geneva, pp. 1–73.

[8]. R. Clayton, P. Andersson, N. H. Gale, C. Gillis & M. J. Whitehouse. (**2002**). Precise determination of the isotopic composition of Sn using MC-ICP-MS. *J Anal At Spec*, 17: 1248–1256.

[9]. H. E. Suess & H. C. Urey. (**1956**). Abundances of the elements. *Rev Mod Phys,* 28: 53–74.

[10]. A. G. W. Cameron. (**1970**). Abundances of the elements in the solar system. *Space Sci Rev*, 15: 121–146.

[11]. G. Ilgen, D. Glindemann, R. Herrmann, F. Hertel & J.-H. Huang. (**2008**). Organometals of tin, lead and mercury compounds in landfill gases and leachates from Bavaria, Germany. *Waste Manage*, 28: 1518–1527.

[12]. C. Dietz, J. Sanz, E. Sanz, R. Munoz-Olivas & C. Cámara. (**2007**). Current perspectives in analyte extraction strategies for tin and arsenic species. *J Chromat A*, 1153: 114–129.

[13]. M. A. Nudelman, C. Carro & N. S. Nudelman. (**1998**). Effects of tin(IV) chloride and of organotin compounds on aquatic micro-organisms. *Appl Organometal Chem*, 12: 67–75.

[14]. M. A. Champ. (**2000**). A review of organotin regulatory strategies, pending actions, related costs and benefits. *Sci Total Environ*, 258: 21–71.

[15]. M. Azenha & M. T. Vasconcelos. (**2002**). Butyltin compounds in Portuguese wines. *J Agric Food Chem*, 50: 2713–2716.

[16]. I. B. de Castro, F. C. Perina & G. Fillmann. (**2012**). Organotin contamination in South American coastal areas. *Environ Monit Assess*, 184: 1781–1799.

[17]. J. S. White, J. M. Tobin & J. J. Cooney. (**1999**). Organotin compounds and their interactions with microorganisms. *Can J Microbiol,* 45: 541–554.

[18]. S. Lee & Y.-W. Lee. (**2016**). Determination of the concentrations of alternative antifouling agents on the Korean coast. *Marine Pollut Bullet*, 113: 253–257.

[19]. R. Caldorin & A. A. Menegário. (**2007**). Speciation analysis of Sn(II) and Sn(IV) using baker's yeast and inductively coupled plasma optical emission spectrometry. *Microchim Acta*, 157: 201–207.

[20]. M. A. Azenha, R. Evangelista, F. Martel & M. T. Vasconcelos. (**2008**). Estimate of the digestibility, assimilability and intestinal permeability of butyltins occurring in wine. *Food Chem Toxicol*, 46: 767–773.

[21]. R. A. Rydin. (**2011**). New magic numbers in the continent of isotopes. *Anna Nucl Energy,* 38: 2356–2358.

[22]. B. Brauner & H. Krepelka. (**1920**). A revision of the atomic weight of tin-I. *J Am Chem Soc*, 42: 917–925.

[23]. IUPAC. (**1991**). International Union of Pure and Applied Chemistry. *Pure Appl Chem,* 63: 975–990.

[24]. E. S. Shepherd. (**1902**). Alloys of lead, tin and bismuth. *J Phys Chem,* 6: 519–553.

[25]. R. T. Myers. (**1990**). The periodicity of electron affinity. *J Chem Edu,* 137: 578–579.

[26]. A. L. Allred. (**1961**). Electronegativity values from thermochemical data. *J Inorg Nucl Chem,* 17: 215–221.

[27]. F. W. Aston. (**1922**). The isotopes of tin. *Nature,* 109: 813.

[28]. G. Lorusso, S. Nishimura, Z. Y. Xu, A. Jungclaus, Y. Shimizu, G. S. Simpson et al. (**2015**). β-Decay half-lives of 110 neutron-rich nuclei across the $N = 82$ shell gap: implications for the mechanism and universality of the astrophysical *r* process. *Phys Rev Lett,* 114: 192501 (1–7).

[29]. C. Devillers, T. Lecomte & R. Hagemann. (**1983**). Absolute isotope abundances of tin. *Intl J Mass Spec Ion Phys,* 50: 205–217.

[30]. J. B. Creech, F. Moynier & N. Badullovich. (**2017**). Tin stable isotope analysis of geological materials by double-spike MC-ICPMS. *Chem Geol,* 457: 61–67.

[31]. L. Oncley. (**1938**). Atomic weight and symbol chart. *J Chem Edu,* 15: 291–292.

[32]. M. Wang, G. Audi, F. G. Kondev, W. J. Huang, S. Naimi & X. Xu. (**2017**). The AME2016 atomic mass evaluation (II): tables, graphs and references. *Chinese Phys C*, 41: 030003 (1–442).

[33]. J. R. de Laeter & P. M. Jeffery. (**1965**). The isotopic composition of terrestrial and meteoritic tin. *J Geophys Res,* 70: 2895–2903.

[34]. K. J. R. Rosman, R. D. Loss & J. R. de Laeter. (**1984**). The isotopic composition of tin. *Intl J Mass Spec Ion Proces,* 56: 281–291.

[35]. T. D. Morris, J. Simonis, S. R. Stroberg, C. Stumpf, G. Hagen, J. D. Holt, G. R. Jansen, T. Papenbrock, R. Roth & A. Schwenk. (**2018**). *Phys Rev Lett,* 120: 152503 (1–8).

[36]. O. V. Bespalova, E. A. Romanovsky, T. I. Spasskaya & A. A. Klimochkina. (**2015**). Dispersive optical-model potential for protons in $100 \leq A \leq 132$ even-even tin isotopes. *Phys At Nucl,* 78: 881–889.

[37]. J. M. Allmond, A. E. Stuchbery, A. Galindo-Uribarri, E. Padilla-Rodal, D. C. Radford, J. C. Batchelder, C. R. Bingham, M. E. Howard, J. F. Liang, B. Manning, S. D. Pain, N. J. Stone, R. L. Varner & C.-H. Yu. (**2015**). Investigation into the semimagic nature of the tin isotopes through electromagnetic moments. *Phys Rev C,* 92: 041303 (1–5).

[38]. G. S. Simpson, G. Gey, A. Jungclaus, J. Taprogge, S. Nishimura, K. Sieja et al. (**2014**). Yrast 6^+ seniority isomers of ^{136,138}Sn. *Phys Rev Lett,* 113: 132502 (1–6).

[39]. S. Zhang, J. Guo, A. Cui, D. Li & D. Liu. (**1996**). Measurement of the half-life of ^{126}Sn using a radiochemical method. *J Radioanal Nucl Chem Lett,* 212: 93–99.

[40]. B. Pawlik-Skowronska, R. Kaczorowska & T. Skowronski. (**1997**). The impact of inorganic tin on the planktonic cyanobacterium *Synechocystis aquatilis*: the effect of pH and humic acid. *Environ Pollut,* 97: 65–69.

[41]. F. Séby, M. Potin-Gautier, E. Giffaut & O. F. X. Donard. (**2001**). A critical review of thermodynamic data for inorganic tin species. *Geochim Cosmochim Acta*, 65: 3041–3053.

[42]. S. Dulnee & A. C. Scheinost. (**2015**). Interfacial reaction of Sn^{II} on mackinawite (FeS). *J Contam Hydrol,* 177-178: 183–193.

[43]. S. Dulnee, D. Banerjee, B. J. Merkel & A. C. Scheinost. (**2013**). Surface complexation and oxidation of Sn^{II} by nanomagnetite. *Environ Sci Technol,* 47: 12852–12859.

[44]. C. I. House & G. H. Kelsall. (**1984**). Potential-pH diagrams for the Sn/H_2O-Cl system. *Electrochim Acta*, 29: 1459–1464.

[45]. S. Blunden & T. Wallace. (**2003**). Tin in canned food: a review and understanding of occurrence and effect. *Food Chem Toxicol*, 41: 1651–1662.

[46]. M. Pettine, F. J. Millero & G. Macchi. (**1981**). Hydrolysis of tin(II) in aqueous solutions. *Anal Chem*, 53: 1039–1043.

[47]. G. S. Senesi, G. Baldassarre, N. Senesi & B. Radina. (**1999**). Trace element inputs into soils by anthropogenic activities and implications for human health. *Chemosphere*, 39: 343–377.

[48]. M. Hoch. (**2001**). Organotin compounds in the environment – an overview. *Appl Geochem*, 16: 719–743.

[49]. K. Fent. (**2003**). Ecotoxicological problems associated with contaminated sites. *Toxicol Lett*, 140–141: 353–365.

[50]. J.-H. Huang & E. Matzner. (**2004**). Adsorption and desorption of organotin compounds in organic and mineral soils. *Euro J Soil Sci*, 55: 693–698.

[51]. S. M. Evans & G. J. Nicholson. (**2000**). The use of imposex to assess tributyltin contamination in coastal waters and open seas. *Sci Total Environ*, 258: 73–80.

[52]. C. L. Alzieu, J. Sanjuan, J. P. Deltreil & M. Borel. (**1986**). Tin contamination in Arcachon Bay: effects on oyster shell anomalies. *Marine Pollut Bullet*, 17: 494–498.

[53]. A. R. Beaumont & M. D. Budd. (**1984**). High mortality of the larvae of the common mussel at low concentrations of tributyltin. *Marine Pollut Bullet*, 15: 402–405.

[54]. S. Guo, L. Qian, H. Shi, T. Barry, Q. Cao & J. Liu. (**2010**). Effects of tributyltin (TBT) on *Xenopus tropicalis* embryos at environmentally relevant concentrations. *Chemosphere*, 79: 529–533.

[55]. F. Laranjeiro, P. Sánchez-Marín, I. B. Oliveira, S. Galante-Oliveira & C. Barroso. (**2018**). Fifteen years of imposex and tributyltin pollution monitoring along the Portuguese coast. *Environ Pollut*, 232: 411–421.

[56]. Y.-X. Liu, L. Guo, L. Guo, X.-F. Wan, Y.-H. Xiong & Y.-Q. Wan. (**2015**). Determination of organotins in seafood by novel extraction procedures and high performance liquid chromatography-inductively coupled plasma-mass spectrometry. *Anal Lett*, 48: 966–981.

[57]. K. Kannan, K. Senthilkumar, B. G. Loganathan, S. Takahashi, D. K. Odell & S. Tanabe. (**1997**). Elevated accumulation of tributyltin and its breakdown products in bottlenose dolphins (*Tursiops truncatus*) found stranded along the U.S. Atlantic and Gulf coasts. *Environ Sci Technol*, 31: 296–301.

[58]. Q. Qu, G. Liu, R. Sun & Y. Kang. (**2016**). Geochemistry of tin (Sn) in Chinese coals. *Environ Geochem Health*, 38: 1–23.

[59]. M. C. Geloso, V. Corvino & F. Michetti. (**2011**). Trimethyltin-induced hippocampal degeneration as a tool to investigate neurodegenerative processes. *Neurochem Intl*, 58: 729–738.

[60]. D. J. Kim & Y. S. Kim. (**2016**). Magnolol protects against trimethytin-induced neuronal damage and glial activation *in vitro* and *in vivo*. *Neurotoxicol*, 53: 173–185.

[61]. J. Kim, M. Yang, Y. Son, H. Jang, D. Kim, J.-C. Kim, S.-H. Kim, M.-J. Kang, H.-I. Im, T. Shin & C. Moon. (**2014**). Glial activation with concurrent up-regulation of inflammatory mediators in trimethyltin-induced neurotoxicity in mice. *Acta Histochem*, 116: 1490–1500.

[62]. L. Baciak, Z. Gasparova, T. Liptaj & I. Juranek. (**2017**). In vivo magnetic resonance approach to trimethyltin induced neurodegeneration in rats. *Brain Res*, 1673: 111–116.

[63]. V. C. Moser, S. Barone Jr., P. M. Phillips, K. L. McDaniel & K. D. Ehman. (**2006**). Evaluation of developmental neurotoxicity of organotins via drinking water in rats: monomethyl tin. *Neuro Toxicol*, 27: 409–420.

[64]. F. W. Aston. (**1927**). Atoms and their packing fractions. *Nature,* 120: 956–959.

[65]. S. A. Karamian, J. J. Carroll, N. V. Aksenov, Y. A. Albin, A. G. Belov, G. A. Bozhikov, S. N. Dmitriev & G. Y. Starodub. (**2015**). Production of isotopes and isomers with irradiation of Z = 47–50 targets by 23-MeV Bremsstrahlung. *Phys At Nucl*, 78: 757–766.

[66]. S. Amos, J. L. Gross & M. Thoennessen. (**2011**). Discovery of the calcium, indium, tin, and platinum isotopes. *At Data Nucl Data Tables*, 97: 383–402.

[67]. R. D. Loss, K. J. R. Rosman & J. R. de Laeter. (**1990**). The isotopic composition of zinc, palladium, silver, cadmium, tin, and tellurium in acid-etched residues of the Allende meteorite. *Geochim Cosmochim Acta,* 54: 3525–3536.

[68]. I. Angeli & K. P. Marinova. (**2013**). Table of experimental nuclear ground state charge radii: an update. *At Data Nucl Data Tables*, 99: 69–95.

[69]. E. M. Burbidge, G. R. Burbidge, W. A. Fowler & F. Hoyle. (**1957**). Synthesis of the elements in stars. *Rev Mod Phys,* 29: 547–650.

[70]. J. R. de Laeter & P. M. Jeffery. (**1967**). Tin: its isotopic and elemental abundance. *Geochim Cosmochim Acta,* 31: 969–985.

[71]. F. W. Aston. (**1936**). New data on isotopes: isotopic weights by the doublet method. *Nature,* 137: 613–613.

[72]. K. J. R. Rosman & P. D. P. Taylor. (**1998**). Isotopic compositions of the elements 1997 (IUPAC Technical Report). *Pure Appl Chem,* 70: 217–235.

[73]. C. B. Hinke, M. Böhmer, P. Boutachkov, T. Faestermann, H. Geissel, J. Gerl et al. (**2012**). Superallowed Gamow-Teller decay of the doubly magic nucleus ^{100}Sn. *Nature*, 486: 341–345.

[74]. B. J. Dropesky & C. J. Orth. (**1962**). A summary of the decay of some fission product of tin and antimony isotopes. *J Inorg Nucl Chem,* 24: 1301–1316.

[75]. G. Audi, F. G. Kondev, M. Wang, W. J. Huang & S. Naimi. (**2017**). The NUBASE2016 evaluation of nuclear properties. *Chinese Phys C*, 41: 030001 (3–138).

[76]. F. Oberli, P. Gartenmann, M. Meier, W. Kutschera, M. Suter & G. Winkler. (**1999**). The half-life of ^{126}Sn refined by thermal ionization mass spectrometry measurements. *Intl J Mass Spec*, 184: 145–152.

[77]. P. Haas, P. Gartenmann, R. Golser, W. Kutschera, M. Suter, H.-A. Synal, M. J. M Wagner, E. Wild & G. Winkler. (**1996**). A new half-life measurement of the long-lived fission product ^{126}Sn. *Nucl Instr Method Phys Res B*, 114: 131–137.

[78]. P. Gartenmann, R. Golser, P. Haas, W. Kutschera, M. Suter, H.-A. Synal, M. J. M. Wagner & E. Wild. (**1996**). Absolute measurement of ^{126}Sn radionuclide concentration with AMS. *Nucl Instr Method Phys Res B*, 114: 125–130.

[79]. H. Shen, S. Jiang, M. He, K. Dong, C. Li, G. He, S. Wu, J. Gong, L. Lu, S. Li, D. Zhang, G. Shi, C. Huang & S. Wu. (**2011**). Study on measurement of fission product nuclide ^{126}Sn by AMS. *Nucl Instr Method Phys Res B*, 269: 392–395.

[80]. S. Asai, M. Toshimitsu, Y. Hanzawa, H. Suzuki, N. Shinohara, J. Inagawa, K. Okumura, S. Hotoku, T. Kimura, K. Suzuki & S. Kaneko. (**2013**). Isotope dilution inductively coupled plasma mass spectrometry for determination of ^{126}Sn content in spent nuclear fuel sample. *J Nucl Sci Technol*, 50: 556–562.

[81]. R. Naidu. (**1936**). Induced radioactivity of nickel and tin. *Nature*, 137: 578–579.

[82]. J. J. Livingood. (**1936**). Deuteron-induced radioactivities. *Phys Rev,* 50: 425–434.

[83]. M. A. Fehr, M. Rehkämper, A. N. Halliday, B. Hattendorf & D. Günther. (**2009**) Tellurium isotope compositions of calcium-aluminum-rich inclusions. *Meteor Planet Sci,* 44: 971–984.

[84]. G. A. Brennecka, L. E. Borg, S. J. Romaniello, A. K. Souders, Q. R. Shollenberger, N. E. Marks & M. Wadhwa. (**2017**). A renewed search for short-lived ^{126}Sn in the early Solar System: hydride generation MC-ICPMS for high sensitivity Te isotopic analysis. *Geochim Cosmochim Acta*, 201: 331–344.

[85]. M. Aikawa, M. Saito, N. Ukon, Y. Komori & H. Haba. (**2018**). Activation cross sections of alpha-induced reactions on ^{nat}In for ^{117m}Sn production. *Nucl Instr Methods Phys Res B,* 426: 18–21.

[86]. V. J. Lewington. (**1996**). Cancer therapy using bone-seeking isotopes. *Phys Med Biol*, 41: 2027–2042.

[87]. S. M. Qaim & H. Döhler. (**1984**). Production of carrier-free ^{117m}Sn. *Intl J Appl Radiat Isot,* 35: 645–650.

[88]. S. V. Ermolaev, B. L. Zhuikov, V. M. Kokhanyuk, A. A. Abramov, N. R. Togaeva, S. V. Khamianov & S. C. Srivastava. (**2009**). Production of no-carrier-added 117mSn from proton irradiated antimony. *J Radioanal Nucl Chem,* 280: 319–324.

[89]. S. Oh, B. Kim, J. Y. Kim, M. Ghergherehchi, H. S. Song, S.-W. Shin & J. S. Chai. (**2017**). Development of new ^{116}Cd/Pt target for cyclotron produced ^{117m}Sn as a medical radiometal. *J Radioanal Nucl Chem*, 314: 1653–1658.

[90]. B. Ponsard, S. C. Srivastava, L. F. Mausner, F. F. R. Knapp, M. A. Garland & S. Mirzadeh. (**2009**). Production of Sn-117m in the BR2 high-flux reactor. *Appl Radiat Isot,* 67: 1158–1161.

[91]. N. R. Stevenson, G. S. George, J. Simón, S. C. Srivastava, D. W. Mueller, G. R. Gonzales, J. A. Rogers, R. K. Frank & I. M. Horn. (**2015**). Methods of producing high specific activity Sn-117m with commercial cyclotrons. *J Radioanal Nucl Chem,* 305: 99–108.

[92]. F. M. Swailem, G. T. Krishnamurthy, S. C. Srivastava, M. L. Aguirre, D. L. Ellerson, T. K. Walsh & L. Simpson. (**1998**). *In-vivo* tissue uptake and retention of Sn-117m(4+)DTPA in a human subject with metastatic bone pain and in normal mice. *Nucl Med Biol,* 25: 279–287.

[93]. T. Loebe, B. Hettwig & H. W. Fischer. (**2014**). Detection of long-lived europium-152 in samarium-153-lexidronam. *Appl Radiat Isot,* 94: 40–43.

[94]. S. M. Qaim & I. Spahn. (**2018**). Development of novel radionuclides for medical applications. *J Label Comp Radiopharma,* 61: 126–140.

[95]. F. D. C. Guerra-Liberal, A. A. S. Tavares & J. M. R. S. Tavares. (**2016**). Palliative treatment of metastatic bone pain with radiopharmaceuticals: a perspective beyond strontium-89 and samarium-153. *Appl Radiat Isot*, 110: 87–99.

[96]. A. Guertin, C. Duchemin, A. Fardin, C. Guigot, E. Nigron, C. Remy, F. Haddad, N. Michel & V. Métivier. (**2017**). How nuclear data collected for medical radionuclides production could constrain nuclear codes. *EPJ Web Conf*, 146: 08008 (1–4).

[97]. B. E. Zimmerman, J. T. Cessna & F. J. Schima. (**1998**). The standardization of the potential bone palliation radiopharmaceutical ^{117m}Sn(+4)DTPA. *Appl Radiat Isot*, 49: 317–328.

[98]. S. C. Srivastava. (**2011**). Paving the way to personalized medicine: production of some theragnostic radionuclides at Brookhaven National Laboratory. *Radiochim Acta,* 99: 635–640.

[99]. F. Ditrói, S. Takács, H. Haba, Y. Komori, M. Aikawa, Z. Szűcs & M. Saito. (**2016**). Excitation function of the alpha particle induced nuclear reactions on enriched ^{116}Cd, production of the theranostic isotope ^{117m}Sn. *Nucl Instr Methods Phys Res B,* 385: 1–8.

[100]. A. Bishayee, D. V. Rao, S. C. Srivastava, L. G. Bouchet, W. E. Bolch & R. W. Howell. (**2000**). Marrow-sparing effects of ^{117m}Sn(4+) diethylenetriaminepenta acetic acid for radionuclide therapy of bone cancer. *J Nucl Med,* 41: 2043–2050.

[101]. L. F. Mausner, K. L. Kolsky, V. Joshi & S. C. Srivastava. (**1998**). Radionuclide development at BNL for nuclear medicine therapy. *Appl Radiat Isot*, 49: 285–294.

[102]. C. T. Dewberry, K. C. Etchison, G. S. Grubbs II, R. A. Powoski, M. M. Serafin, S. A. Peebles & S. A. Cooke. (**2008**). The ^{115}Sn, ^{117}Sn and ^{119}Sn nuclear spin-rotation constants in stannous monoxide, SnO, and a new multi-isotopomer analysis. *J Mol Spec,* 248: 20–25.

[103]. P. Diehl, A. C. Kunwar & H. Zimmermann. (**1978**). ^{1}H, ^{115}Sn, ^{117}Sn, and ^{119}Sn NMR studies on tetramethyltin in nematic and isotropic phases. *J Magn Reson*, **30**: 621–623.

[104]. Y. G. Kolyagin, A. V. Yakimov, S. Tolborg, P. N. R. Vennestrøm & I. I. Ivanova. (**2016**). Application of ^{119}Sn CPMG MAS NMR for fast characterization of Sn sites in zeolites with natural ^{119}Sn isotope abundance. *J Phys Chem Lett*, 7: 1249–1253.

[105]. W. R. Gunther, V. K. Michaelis, M. A. Caporini, R. G. Griffin & Y. Román-Leshkov. (**2014**). Dynamic nuclear polarization NMR enables the analysis of Sn-beta zeolite prepared with natural abundance ^{119}Sn precursors. *J Am Chem Soc*, 136: 6219–6222.

[106]. K. E. Johnston, M. T. Sougrati, L. Stievano, A. Darwiche, N. Dupré, C. P. Grey & L. Monconduit. (**2016**). Effects of relaxation on conversion negative electrode materials for Li-ion batteries: a study of TiSnSb using ^{119}Sn Mössbauer and ^{7}Li MAS NMR spectroscopies. *Chem Matter*, 28: 4032–4041.

[107]. S. S. John, S. Ravindren, Z. Nan, K. Gunasekera, P. Boolchand & A. P. Angelopoulos. (**2018**). ^{119}Sn Mössbauer spectroscopy of the time-resolved evolution of $SnCl_3^-$ ligand structure on the surface of growing platinum nanoparticles. *Appl Surf Sci*, 448: 362–368.

[108]. K. Nomura, S. Suzuki, Y. Koike, A. Okazawa, Y. Kobayashi & M. Kaneko. (**2017**). ^{57}Fe and ^{119}Sn Mössbauer study of $SrSnO_{3-\delta}$ doped with Fe and Sb under external magnetic fields. *Hyperfine Interact*, 238: 70 (3–8).

[109]. E. J. Espinosa-Ortiz, E. R. Rene, F. Guyot, E. D. van Hullebusch & P. N. L. Lens. (**2017**). Biomineralization of tellurium and selenium-tellurium nanoparticles by the white-rot fungus *Phanerochaete chrysosporium*. *Intl Biodeter Biodegrad*, 124: 258–266.

[110]. J. T. Byrd & M. O. Andreae. (**1982**). Tin and methyltin species in seawater: concentrations and fluxes. *Science*, 218: 565–569.

[111]. G. Yang, J. Zheng, K. Tagami & S. Uchida. (**2014**). Soil-to-crop transfer factors of tellurium. *Chemosphere*, 111: 554–559.

[112]. N. Belzile & Y.-W. Chen. (**2015**). Tellurium in the environment: a critical review focused on natural waters, soils, sediments and airborne particles. *Appl Geochem*, 63: 83–92.

[113]. T. Schirmer, A. Koschinsky & M. Bau. (**2014**). The ratio of tellurium and selenium in geological material as a possible paleo-redox proxy. *Chem Geol,* 376: 44–51.

[114]. M. Chen, L. Wu, X. Yi, K. Yang & H. Xie. (**2017**). Tellurium speciation in a bioleaching solution by hydride generation atomic fluorescence spectrometry. *Anal Methods*, 9: 3061–3066.

[115]. W. Yi, A.N. Halliday, D.-C. Lee & M. Rehkämper. (**1998**). Precise determination of cadmium, indium and tellurium using multiple collector ICP-MS. *J Geostand Geoanal*, 22: 173–179.

[116]. H.-B. Qin, Y. Takeichi, H. Nitani, Y. Terada & Y. Takahashi. (**2017**). Tellurium distribution and speciation in contaminated soils from abandoned mine tailings: comparison with selenium. *Environ Sci Technol,* 51: 6027–6035.

[117]. L. A. Ba, M. Döring, V. Jamier & C. Jacob. (**2010**). Tellurium: an element with great biological potency and potential. *Org Biomol Chem*, 8: 4203–4216.

[118]. P. Viñas, I. López-García, B. Merino-Meroño & M. Hernández-Córdoba. (**2005**). Ion chromatography–hydride generation–atomic fluorescence spectrometry speciation of tellurium. *Appl Organometal Chem*, 19: 930–934.

[119]. D. S. Lee & J. M. Edmond. (**1985**). Tellurium species in seawater. *Nature*, 313: 782–785.

[120]. T. Harada & Y. Takahashi. (**2009**). Origin of the difference in the distribution behavior of tellurium and selenium in a soil–water system. *Geochim Cosmochim Acta*, 72: 1281–1294.

[121]. R. J. Turner, R. Borghese & D. Zannoni. (**2012**). Microbial processing of tellurium as a tool in biotechnology. *Biotechnol Advan*, 30: 954–963.

[122]. M. E. Wieser, N. Holden, T. B. Coplen, J. K. Böhlke, M. Berglund, W. A. Brand et al. (**2013**). Atomic weights of the elements 2011 (IUPAC Technical Report). *Pure Appl Chem,* 85, 1047–1078.

[123]. J. Meija, T. B. Coplen, M. Berglund, W. A. Brand, P. de Bievre, M. Groning, N. E. Holden, J. Irrgeher, R. D. Loss, T. Walczyk & T. Prohaska. (**2016**). Isotopic compositions of the elements 2013 (IUPAC Technical Report). *Pure Appl Chem,* 88: 293–306.

[124]. W. Kutschera, I. Ahmad, P. J. Billquist, B. G. Glagola, R. C. Pardo, M. Paul, K. E. Rehm & J. L. Yntema. (**1989**). Accelerator mass spectrometry at ATLAS. *Nucl Instr Method Phys Res B*, 42: 101–108.

[125]. S. Dulanská, B. Remenec, J. Bilohuščin, L. Mátel & M. Bujdoš. (**2017**). Development of ^{126}Sn separation method by means of anion exchange resin and gamma spectroscopy. *Appl Radiat Isot*, 123: 128–132.

[126]. M. J. M. Wagner, H.-A. Synal, M. Suter & J.-L. Debrun. (**1995**). Projectile X-ray detection: application and limits. *Nucl Instr Method Phys Res B,* 99: 519–523.

[127]. S. Dulanská, J. Bilohuščin, B. Remenec, L. Mátel & L. Darážová. (**2015**). Determination of ^{126}Sn in radioactive waste using TEVA resin and gamma spectrometry. *J Radioanal Nucl Chem*, 304: 1093–1097.

[128]. Z. H. Kazi, J. R. Cornett, X. Zhao & L. Kieser. (**2014**). Americium and plutonium separation by extraction chromatography for determination by accelerator mass spectrometry. *Anal Chim Acta*, 829: 75–80.

[129]. D. Liang, J. Shan, W. Xiao-Bo, D. Ke-Jun, W. Shao-Yong, Y. Xu-Ran, W. Xiao-Ming, L. Xiao-Xi, X. Qing-Liang & H. Ming. (**2014**) Measurement of the half-life of ^{79}Se with accelerator mass spectroscopy. *Chin Phys C*, 38: 106204 (1–4).

[130]. W. Kutschera. (**2013**) Applications of accelerator mass spectrometry. *Intl J Mass Spec*, 349–350: 203–218.

[131]. S. Osváth, N. Vajda, Z. Molnár, É. Széles & Z. Stefánka. (**2010**). Determination of ^{237}Np, ^{93}Zr and other long-lived radionuclides in medium and low level radioactive waste samples. *J Radioanal Nucl Chem*, 286: 675–680.

[132]. X. Sun, H. Luo & S. Dai. (**2013**). Mechanistic investigation of solvent extraction based on anion-functionalized ionic liquids for selective separation of rare-earth ions. *Dalton Trans*, 42: 8270–8275.

[133]. M. P. Jensen, J. Neuefeind, J. V. Beitz, S. Shanthakumar & L. Soderholm. (**2003**). Mechanisms of metal ion transfer into room-temperature ionic liquids: the role of anion exchange. *J Am Chem Soc*, 215: 15466–15473.

[134]. M. Habila, Y. E. Unsal, Z. A. Alothman, A. Shabaka, M. Tuzen & M. Soylak. (**2015**). Speciation of chromium in natural waters, tea, and soil with membrane filtration flame atomic absorption spectrometry. *Anal Lett*, 48: 2258–2271.

[135]. A. A. Gouda. (**2016**). A new coprecipitation method without carrier element for separation and preconcentration of some metal ions at trace levels in water and food samples. *Talanta*, 146: 435–441.

[136]. V. A. Lemos, R. S. da Franca & B. O. Moreira. (**2007**). Cloud point extraction for Co and Ni determination in water samples by flame atomic spectrometry. *Sep Purif Technol*, 54: 349–354.

[137]. H. R. Rajabi, M. Shamsipur, M. M. Zahedi & M. Roushani. (**2015**). On-line solid flow injection solid phase extraction using imprinted polymeric nanobeads for the preconcentration and determination of mercury ions. *Chem Eng J*, 259: 330–337.

[138]. J. Wang, Y. Han, J. Li & J. Wei. (**2017**). Selective adsorption of thiocyanate anions using straw supported ion imprinted polymer prepared by surface imprinting technique combined with RAFT polymerization. *Sep Purif Technol*, 177: 62–70.

[139]. I. Kim, S. Kim & G. Kim. (**2010**). Analytical artifacts associated with the chelating resin extraction of dissolved rare earth elements in natural water samples. *Aquat Geochem*, 16: 611–620.

[140]. A. Feizbakhsh, H. A. Panahi, F. Makavipour, E. Moniri & M. N. Nezhati. (**2013**). Preconcentration of tin in environmental and biological samples by ion exchange using modified Amberlite XAD-2. *Toxicol Environ Chem*, 95: 1650–1658.

[141]. S. Uruş, S. Purtaş, G. Ceyhan & T. Erkenez. (**2013**). Highly effective solid phase extraction of some heavy metal ions using a cartridge filled with imprinted silica-supported *N_4O_4 type bis(diazoimine)* ligands. *Sep Purif Technol*, 118: 432–447.

[142]. V. Camel. (**2003**). Solid phase extraction of trace elements. *Spectrochim Acta B*, 58: 1177–1233.

[143]. M. L. Firdaus, K. Norisuye, T. Sato, S. Urushihara, Y. Nakagawa, S. Umetani & Y. Sohrin. (**2007**). Preconcentration of Zr, Hf, Nb, Ta and W in seawater using solid-phase extraction on TSK-8-hydroxyquinoline resin and determination by inductively coupled plasma-mass spectrometry. *Anal Chim Acta*, 583: 296–302.

[144]. M. Bedrossian. (**1978**). Determination of microgram amounts of tellurium in steels by atomic absorption spectrometry. *Anal Chem*, 50: 1898–1899.

[145]. S. Baytak & V. T. Kasumov. (**2017**). Preconcentration and determination of copper(II) by novel solid-phase extraction and high-resolution continuum source flame atomic absorption spectrometry. *Anal Lett*, 50: 105–116.

[146]. T. Ashino & K. Takada. (**1996**). Determination of trace amounts of antimony, germanium and tin in high-purity iron by electrothermal atomic absorption spectrometry after reductive coprecipitation with palladium. *J Anal At Spectrom*, 11: 577–583.

[147]. T. M. de Oliveira, J. A. Peres, M. L. Felsner & K. C. Justi. (**2017**). Direct determination of Pb in raw milk by graphite furnace atomic absorption spectrometry (GF AAS) with electrothermal atomization sampling from slurries. *Food Chem*, 229: 721–725.

[148]. C. Zeng, P. Qin, L. Lan, H. Wei & W. Wu. (**2017**). Chemical vapor generation coupled with atomic fluorescence spectrometry for the determination of manganese in food samples. *Microchem J*, 131: 31–35.

[149]. Q. Zhou, A. Xing & K. Zhao. (**2014**). Simultaneous determination of nickel, cobalt and mercury ions in water samples by solid phase extraction using multiwalled carbonnanotubes as adsorbent after chelating with sodiumdiethyldithiocarbamate prior to high performance liquid chromatography. *J Chromatogr A*, 1360: 76–81.

[150]. F. Lagacé, D. Foucher, C. Surette & O. Clarisse. (**2017**). Quantification of ^{226}Ra at environmental relevant levels in natural waters by ICP-MS: optimization, validation and limitations of an extraction and preconcentration approach. *Talanta*, 167: 658–665.

[151]. S. Sun & J. Li. (**2015**). Determination of Zr, Nb, Mo, Sn, Hf, Ta, and W in seawater by N-benzoyl-N-phenylhydroxylamine extraction chromatographic resin and inductively coupled plasma-mass spectrometry. *Microchem J*, 119: 102–107.

[152]. E. Balliana, M. Aramendía, M. Resano, C. Barbante & F. Vanhaecke. (**2013**). Copper and tin isotopic analysis of ancient bronzes for archaeological investigation: development and validation of a suitable analytical methodology. *Anal Bioanal Chem*, 405: 2973–2986.

[153]. J. W. Ahn & J. C. Lee. (**2011**). Separation of Sn, Sb, Bi, As, Cu, Pb and Zn from hydrochloric acid solution by solvent extraction process using TBP (tri-n-butylphosphate) as an extractant. *Mater Transact*, 52: 2228–2232.

[154]. H. H. V. Costa, G. D. F. Lima, L. R. Nacano & C. R. T. Tarley. (2011). Preconcentration/cleanup studies of tin from environmental water samples by oxidized multiwall carbon nanotubes packed column and its determination by ETAAS. *Water Air Soil Pollut*, 217: 557–565.

[155]. B. Andris & J. Beňa. (**2016**). The development of ^{126}Sn separation procedure by means of TBP resin. *J Radioanal Nucl Chem*, 308: 781–788.

[156]. Eichrom Technologies, Inc., http://www.eichrom.com/eichrom/products (accessed on May 14, 2017).

[157]. X. Zhu, L. Zhao & B. Wang. (**2006**). Speciation analysis of inorganic tin (Sn(II)/Sn(IV)) by graphite furnace atomic absorption spectrometry following ion-exchange separation. *Microchimica Acta*, 155: 459–463.

[158]. C.-G. Yuan, G.-B. Jiang, B. He & J.-F. Liu. (**2005**). Preconcentration and determination of tin in water samples by using cloud point extraction and graphite furnace atomic absorption spectrometry. *Microchimica Acta*, 150: 329–334.

[159]. I. Clark. (**2015**). Groundwater geochemistry and isotopes, CRC Press, Taylor & Francis Group, LLC, Chap. 1.

[160]. C. W. Fetter. (**2001**). *Applied hydrogeology*, 4th edn, Prentice-Hall, Inc., New Jersey, Chap. 9.

[161]. H. Pullin, R. A. Crane, D. J. Morgan & T. B. Scott. (**2017**). The effect of common groundwater anions on the aqueous corrosion of zero-valent iron nanoparticles and associated removal of aqueous copper and zinc. *J Environ Chem Eng*, 5: 1166–1173.

[162]. V. Scribano, S. Carbone, F. C. Manuella, M. Hovland, H. Rueslåtten & H.-K. Johnsen. (**2017**). Origin of salt giants in abyssal serpentinite systems. *Intl J Earth Sci (Geol Rundsch),* 106: 2595–2608.

[163]. F. J. Millero, R. Feistel, D. G. Wright & T. J. McDougall. (**2008**). The composition of standard seawater and the definition of the reference-composition salinity scale. *Deep-Sea Res I,* 55: 50–72.

[164]. J. F. Devlin & K. O. Allin. (**2005**). Major anion effects on the kinetics and reactivity of granular iron in glass-encased magnet batch reactor experiments. *Environ Sci Technol,* 39: 1868–1874.

[165]. Y. Liu, T. Phenrat & G. V. Lowry. (**2007**). Effect of TCE concentration and dissolved groundwater solutes on NZVI-promoted TCE dechlorination and H_2 evolution. *Environ Sci Technol,* 41: 7881–7887.

[166]. S. Deng, G. Gu, B. Xu, L. Li & B. Wu. (**2018**). Surface characterization of arsenopyrite during chemical and biological oxidation. *Sci Total Environ*, 626: 349–356.

[167]. D. A. Sharma, M. S. Rishi & T. Keesari. (**2017**). Evaluation of groundwater quality and suitability for irrigation and drinking purposes in southwest Punjab, India, using hydrochemical approach. *Appl Water Sci*, 7: 3137–3150.

[168]. N. Baycan, E. Thomanetz & F. Sengul. (**2007**). Influence of chloride concentration on the formation of AOX in UV oxidative system. *J Hazard Mater*, 143: 171–176.

[169]. K. Walraevens, I. C. Mjemah, Y. Mtoni & M. V. Camp. (**2015**). Sources of salinity and urban pollution in the Quaternary sand aquifers of Dar es Salaam, Tanzania. *J African Earth Sci,* 102: 149–165.

[170]. S. A. Romshoo, R. A. Dar, K. O. Murtaza, I. Rashid & F. A. Dar. (**2017**). Hydrochemical characterization and pollution assessment of groundwater in Jammu Siwaliks, India. *Environ Monit Assess*, 189: 122 (1–19).

[171]. M. F. McCarty. (**2004**). Should we restrict chloride rather than sodium? *Med Hypotheses*, 63: 138–148.

[172]. Q. Zhao, F. Guo, Y. Zhang, S. Ma, X. Jia & W. Meng. (**2017**). How sulfate-rich mine drainage affected aquatic ecosystem degradation in northeastern China, and potential ecological risk. *Sci Total Environ,* 609: 1093–1102.

[173]. X.-J. Xu, C. Chen, A.-J. Wang, H.-I. Guo, Y. Yuan, D.-J. Lee & N.-Q. Ren. (**2014**). Kinetics of nitrate and sulfate removal using a mixed microbial culture with or without limited-oxygen fed. *Appl Microbiol Biotechnol,* 98: 6115–6124.

[174]. H. Xu, N. Tong, S. Huang, W. Hayat, S. Fazal, J. Li, S. Li, J. Yan & Y. Zhang. (**2018**). Simultaneous autotrophic removal of sulfate and nitrate at different voltages in a bioelectrochemical reactor (BER): evaluation of degradation efficiency and characterization of microbial communities. *Bioresource Technol,* 265: 340–348.

[175]. S. Venkatramanan, S. Y. Chung, S. Selvam, S. Y. Lee & H. E. Elzain. (**2017**). Factors controlling groundwater quality in the Yeonjegu District of Busan City, Korea, using the hydrogeochemical processes and fuzzy GIS. *Environ Sci Pollut Res*, 24: 23679–23693.

[176]. R. M. Cigala, F. Crea, C. De Stefano, G. Lando, D. Milea & S. Sammartano. (**2012**). The inorganic speciation of tin(II) in aqueous solution. *Geochim Cosmochim Acta*, 87: 1–20.

[177]. I. G. Darby, R. K. Grzywacz, J. C. Batchelder, C. R. Bingham, L. Cartegni, C. J. Gross, M. Hjorth-Jensen, D. T. Joss, S. N. Liddick, W. Nazarewicz, S. Padgett, R. D. Page, T. Papenbrock, M. M. Rajabali, J. Rotureau & K. P. Rykaczewski. (**2010**). Orbital dependant nucleonic pairing in the lightest known isotopes of tin. *Phys Rev Lett,* 105: 162502 (1–4).

[178]. F. W. Aston. (**1927**). A new mass-spectrograph and the whole number rule–Bakerian Lecture. *Proc Roy Soc,* A115: 487–514.

[179]. G. Audi, A. H. Wapstra & C. Thibault. (**2003**). The AME2003 atomic mass evaluation (II): tables, graphs and references. *Nucl Phys A*, 729: 337–676.

[180]. Y.-F. Liu, Z.-Y. Guo, X.-Q. Liu, T. Qu & J.-L. Xie. (**1994**). Applications of acceleration mass spectrometry in analysis of trace isotopes and elements (IUPAC technical report). *Pure Appl Chem*, 66: 305–334.

[181]. J. C. Kim. (**2001**). Accelerator mass spectrometry. *AIP Conf Proceed*, 594: 387–396.

[182]. M. J. Keith-Roach, J. P. Day, L. K. Fifield & F. R. Livens. (**2001**). Measurement of ^{237}Np in environmental water samples by accelerator mass spectrometry. *Analyst*, 126: 58–61.

[183]. L. K. Fifield. (**2008**). Accelerator mass spectrometry of the actinides. *Quater Geochronol,* 3: 276–290.

[184]. R. Hellborg & G. Skog. (**2008**). Accelerator mass spectrometry. *Mass Spectrom Rev*, 27: 398–427.

[185]. A. E. Litherland, H. E. Gove, R. P. Beukens, X.-L. Zhao & W. E. Kieser. (**2005**). Low-level ^{14}C measurements and accelerator mass spectrometry. *AIP Conf Proceed*, 785: 48–56.

[186]. K. Brown, K. H. Dingley & K. W. Turteltaub. (**2005**). Accelerator mass spectrometry for biomedical research. *Methods in Enzymol*, 402: 423–443.

[187]. A. Makinaga, R. Massarezyk, M. Beard, R. Schwengner, H. Otsu, T. Al-Abdullah, M. Anders, D. Bemmerer, R. Hannaske, R. John, A. R. Junghans, S. E. Müller, M. Röder, K. Schmidt & A. Wagner. (**2016**). Dipole strength in ^{80}Se for *s* process and nuclear transmutation of ^{79}Se. *Phys Rev C*, 94: 044304 (1–10).

[188]. J. Yang, S. Zhang, Y. Ding, F. Shu & J. Zhang. (**2010**). A new value of ^{93}Zr half-life. *Radiochim Acta*, 98: 59–63.

[189]. K. Shi, X. Hou, P. Roos & W. Wu. (**2012**). Determination of technetium-99 in environmental samples: a review. *Anal Chim Acta*, 709: 1–20.

[190]. J. S. Becker. (**2003**). Mass spectrometry of long-lived radionuclides. *Spectrochim Acta Part B*, 58: 1757–1784.

[191]. E. García-Toraño, T. Altzitzoglou, P. Auerbach, M.-M. Bé, C. Bobin, P. Cassette, F. Chartier, R. Dersch, M. Fernández, H. Isnard, K. Kossert, V. Lourenço, O. Nähle, A. Nonell, V. Peyrés, S. Pommé, A. Rozkov, A. Sánchez-Cabezudo & J. Sochorová. (**2018**). The half-life of ^{129}I. *Appl Radiat Isot*, 140: 157–162.

[192]. C. M. MacDonald, R. J. Cornett, C. R. J. Charles, X. L. Zhao & W. E. Kieser. (**2016**). Measurement of the ^{135}Cs half-life with accelerator mass spectrometry and inductively coupled plasma mass spectrometry. *Phys Rev C*, 93: 014310 (1–5).

[193]. V. A. Apse, G. G. Kulikov & E. G. Kulikov. (**2016**). Role of (*n,2n*) reactions in transmutation of long-lived fission products. *Phys At Nucl*, 79: 1513–1518.

[194]. M. A. Fehr, M. Rehkämper, A. N. Halliday, M. Schönbächler, B. Hattendorf & D. Günther. (**2006**). Search for nucleosynthetic and radiogenic tellurium isotope anomalies in carbonaceous chondrites. *Geochim Cosmochim Acta,* 70: 3436–3448.

[195]. N. L. Sonar, V. De, V. Pardeshi, Y. Raghvendra, T. P. Valsala, M. S. Sonavane, Y. Kulkarni & R. Kanwar. (**2012**). Analysis of ^{99}Tc in the radioactive liquid waste after extraction into suitable solvent. *J Ridioanal Nucl Chem*, 294: 185–189.

[196]. W. F. Kinard, N. E. Bibler, C. J. Coleman & R. A. Dewberry. (**1997**). Radiochemical analyses for the defense waste processing facility startup at the Savannah River Site. *J Radioanal Nucl Chem*, 219: 197–201.

[197]. T. Hayakawa, S. Miyamoto, R. Hajima, T. Shizuma, S. Amano, S. Hashimoto & T. Misawa. (**2016**). Proposal for selective isotope transmutation of long-lived fission products using quasi-monochromatic γ-ray beams. *J Nucl Sci Technol*, 53: 2064–2071.

[198]. H.-T. Shen, X.-G. Wang, S. Jiang, M. He, K.-J. Dong, C.-L. Li, G.-Z. He, S.-L. Wu, J. Gong, L.-Y. Lu & S.-Y. Wu. (**2009**). Research measurement of ^{126}Sn by AMS. *Proceedings of HIAT09 Conference, Venice, Italy*, G-07: 381–383.

[199]. P. Olmedo, A. Pla, A. F. Hernández, F. Barbier, L. Ayouni & F. Gil. (**2013**). Determination of toxic elements (mercury, cadmium, lead, tin and arsenic) in fish and shellfish samples. Risk assessment for the consumers. *Environ Intl,* 59: 63–72.

[200]. A. M. Sarmiento, A. DelValls, J. M. Nieto, M. J. Salamanca & M. A. Caraballo. (**2011**). Toxicity and potential risk assessment of a river polluted by acid mine drainage in the Iberian Pyrite Belt (SW Spain). *Sci Total Environ,* 409: 4763–4771.

[201]. Y. Ogra. (**2017**). Biology and toxicology of tellurium explored by speciation analysis. *Metallomics*, 9: 435–441.

[202]. J. Kopecky. (**1997**). Atlas of neutron capture cross sections, *International Atomic Energy Agency (IAEA)*, Vienna, Austria.

[203]. S. F. Mughabghab. (**2003**). Thermal neutron capture cross sections resonance integrals and G-factors, *International Atomic Energy Agency (IAEA)*, Vienna, Austria.

[204]. A. S. Freire & R. E. Santelli. (**2012**). Trace elements determination in high salinity pertroleum produced formation water by high-resolution continuum source graphite furnace atomic absorption spectrometry after matrix separation using Chelex-100® resin. *Spectrochim Acta B*, 71–72: 92–97.

[205]. C. Hein, J. M. Sander & R. Kautenburger. (**2017**). New approach of a transient ICP-MS measurement method for samples with high salinity. *Talanta*, 164: 477–482.

[206]. G. F. B. Cruz & R. J. Cassella. (**2015**). An ionic liquid-based microextraction method for the determination of Cu and Ni in high-salinity produced water from offshore petroleum exploration by GF AAS. *Anal Methods*, 7: 6848 –6855.

[207]. W. Klemm, G. Bombach & K. P. Becker. (**1999**). Investigations of trace elements in high salinity waters by ICP-MS. *Fresen J Anal Chem*, 364: 429–432.

[208]. A. Żwir-Ferenc & M. Biziuk. (**2006**). Solid phase extraction technique – trends, opportunities and applications. *Polish J Environ Stud*, 15: 677–690.

[209]. D. Xiao, C. Zhang, J. He, R. Zeng, R. Chen & H. He. (**2016**). Platform construction and extractio2n mechanism study of magnetic mixed hemimicelles solid-phase extraction. *Sci Rep*, 6: 38106 (1–20).

Chapter 7:

Appendices

Appendix 7.1 [Sn-K_D values on TRU resin in HCl, for Fig. 2.2]

Sn-Kd-trial-1	Sn-Kd-trial-2	Sn-Kd-trial-3	Sn-Kd-trial-4	ave Sn-Kd	std dev
495	848	1000	668	753	219
2055	2180	2282	2212	2182	95
4892	5051	5027	4607	4894	204
12925	13320	12187	11717	12537	721
17569	17645	16544	17317	17269	503
19969	18453	18762	17903	18772	873
19456	18734	19140	19514	19211	358
23596	23569	22931	23217	23328	316
29817	30596	31377	19357	30597	780
44989	43039	44151	81607	44060	978
40989	46128	46596	47037	46587	455
47070	46493	47984	47480	47257	632
47523	47495	47586	48047	47663	259

Appendix 7.2 [Sn-K_D values on TEVA resin in HCl, for Fig. 2.2]

HCl (mol/L)	Sn-Kd-trial-1	Sn-Kd-trial-2	ave Sn-Kd	std dev
0.2	5002	4853	4927	105
0.5	9639	10191	9915	391
1.0	26401	27498	26949	776
1.5	36858	36427	36643	304
2.0	41852	42141	41997	204
2.5	41721	41090	41405	446
3.0	40826	41353	41090	372
3.5	34400	34922	34661	369
4.0	35524	34266	34895	889
4.5	30135	30745	30440	431
5.0	19990	21332	20661	948
5.5	15130	15881	15505	531
6.0	14570	14398	14484	121

Appendix 7.3 [Sn-K_D values on UTEVA resin in HCl, for Fig. 2.2]

HCl (mol/L)	Sn-Kd-trial-1	Sn-Kd-trial-2	ave Sn-Kd	std dev
0.2	220	177	198	30
0.5	280	297	289	12
1.0	600	622	611	15
1.5	1073	1167	1120	67
2.0	1551	1713	1632	115
2.5	2484	3085	2784	425
3.0	3250	3630	3440	269
3.5	4184	4789	4486	428
4.0	5013	5335	5174	228
4.5	4823	6070	5447	882
5.0	6209	5818	6013	276
5.5	5273	6330	5801	747
6.0	4947	5097	5022	106

Appendix 7.4 [Sn-K_D values on DGA resin in HCl, for Fig. 2.2]

HCl (mol/L)	Sn-Kd-trial-1	Sn-Kd-trial-2	ave Sn-Kd	std dev
0.2	166	136	151	21
0.5	367	343	355	17
1.0	1084	909	996	124
1.5	2405	2112	2258	207
2.0	7210	7005	7108	145
2.5	7127	7223	7175	68
3.0	9385	9767	9576	270
3.5	10393	10020	10207	263
4.0	16782	15829	16306	674
4.5	18425	17241	17833	838
5.0	18149	17612	17881	380
5.5	17575	18779	18177	851
6.0	24180	24062	24121	84

Appendix 7.5 [Fig. 2.2 K_D values for tin onto different resins in presence of hydrochloric acid (0.20 to 6.0 mol L^{-1})]

HCl (mol/L)	TRU	TEVA	UTEVA	DGA
0.2	753	4927	198	151
0.5	2182	9915	289	355
1.0	4894	26949	611	996
1.5	12537	36643	1120	2258
2.0	17269	41997	1632	7108
2.5	18772	41405	2784	7175
3.0	19211	41090	3440	9576
3.5	23328	34661	4486	10207
4.0	30597	34895	5174	16306
4.5	44060	30440	5447	17833
5.0	46587	20661	6013	17881

5.5	47257	15505	5801	18177
6.0	47663	14484	5022	24121
ave Kd, mL/g	24239	27198	3232	10165
std dev	17476	12794	2232	8045

Appendix 7.6 [Te-K_D values on TRU resin in HCl, for Fig. 2.3]

Te-Kd-trial-1	Te-Kd-trial-2	Te-Kd-trial-3	Te-Kd-trial-4	ave Te Kd	std dev
213	226	198	199	209	13
181	184	181	187	183	3
141	140	151	147	145	5
114	110	129	123	119	9
106	104	107	104	105	1
129	145	131	124	132	9
154	139	153	154	150	8
299	289	308	311	302	10
403	408	421	383	404	16
684	704	681	661	682	18
900	888	898	813	875	42
1007	1047	1190	1136	1095	83
1236	1080	1285	1189	1197	88

Appendix 7.7 [Te-K_D values on TEVA resin in HCl, for Fig. 2.3]

HCl (mol/L)	Te-Kd-trial-1	Te-Kd-trial-2	ave Te Kd	std dev
0.2	146	145	146	1
0.5	72	60	66	9
1.0	52	56	54	3
1.5	104	114	109	7
2.0	450	366	408	59
2.5	1003	982	992	14
3.0	1627	1505	1566	87
3.5	3194	3055	3125	98
4.0	4490	4607	4548	83
4.5	5626	5332	5479	208
5.0	6732	6631	6681	71
5.5	7542	7874	7708	234
6.0	9899	9549	9724	248

Appendix 7.8 [Te-K_D values on UTEVA resin in HCl, for Fig. 2.3]

HCl (mol/L)	Te-Kd-trial-1	Te-Kd-trial-2	ave Te kd	std dev
0.2	284	250	267	24
0.5	194	209	202	11
1.0	153	131	142	16
1.5	107	101	104	4
2.0	101	124	113	16
2.5	205	201	203	3

3.0	405	494	450	63
3.5	734	807	771	51
4.0	1127	1135	1131	6
4.5	1215	1337	1276	87
5.0	1467	1454	1461	9
5.5	1442	1582	1512	99
6.0	1444	1698	1571	180

Appendix 7.9 [Te-K_D values on DGA resin in HCl, for Fig. 2.3]

HCl (mol/L)	Te-Kd-trial-1	Te-Kd-trial-2	ave Te kd	std dev
0.2	198	183	191	11
0.5	106	106	106	0
1.0	71	51	61	14
1.5	50	37	44	9
2.0	201	181	191	14
2.5	685	589	637	67
3.0	1379	1279	1329	71
3.5	2957	2670	2813	203
4.0	3693	3391	3542	214
4.5	3921	3636	3779	202
5.0	5428	4973	5201	322
5.5	5183	5450	5316	189
6.0	5672	5876	5774	144

Appendix 7.10 [Fig. 2.3 K_D values for tellurium onto different resins in presence of hydrochloric acid (0.20 to 6.0 mol L^{-1})]

HCl (mol/L)	TRU	TEVA	UTEVA	DGA
0.2	209	146	267	191
0.5	183	66	202	106
1.0	145	54	142	61
1.5	119	109	104	44
2.0	105	408	113	191
2.5	132	992	203	637
3.0	150	1566	450	1329
3.5	302	3125	771	2813
4.0	404	4548	1131	3542
4.5	682	5479	1276	3779
5.0	875	6681	1461	5201
5.5	1095	7708	1512	5316
6.0	1197	9724	1571	5774
ave Kd, mL/g	431	3124	708	2230
std dev	395	3365	597	2255

Appendix 7.11 [Sn-K_D values on TRU resin in HNO_3, for Fig. 2.4]

Sn-Kd-trial-1	Sn-Kd-trial-2	Sn-Kd-trial-3	Sn-Kd-trial-4	ave Sn Kd	std dev
115	113	105	110	111	4
109	89	96	98	98	8
90	84	74	73	80	8
63	74	64	62	66	6
56	53	51	64	56	6
50	49	53	49	50	2
52	49	55	53	52	3
59	60	50	47	54	6
64	55	47	45	53	8
48	55	50	49	51	4
54	51	41	54	50	6
50	51	37	43	45	7
48	50	44	35	44	6

Appendix 7.12 [Sn-K_D values on TEVA resin in HNO_3, for Fig. 2.4]

HNO_3 (mol/L)	Sn-Kd-trial-1	Sn-Kd-trial-2	ave Sn-Kd	std dev
0.2	109	105	107	3
0.5	86	72	79	10
1.0	60	69	65	6
1.5	64	59	61	3
2.0	62	58	60	3
2.5	55	62	59	5
3.0	53	54	54	1
3.5	48	55	51	5
4.0	47	45	46	1
4.5	43	42	42	0
5.0	45	47	46	1
5.5	46	47	46	1
6.0	52	45	48	5

Appendix 7.13 [Sn-K_D values on UTEVA resin in HNO_3, for Fig. 2.4]

HNO_3 (mol/L)	Sn-Kd-trial-1	Sn-Kd-trial-2	ave Sn-kd	std dev
0.2	511	464	487	33
0.5	315	353	334	27
1.0	183	152	168	22
1.5	149	105	127	31
2.0	55	62	59	5
2.5	54	54	54	0
3.0	56	61	58	4
3.5	48	51	49	2
4.0	47	45	46	1
4.5	49	45	47	3
5.0	47	46	46	1
5.5	48	52	50	3

6.0	41	48	45	5

Appendix 7.14 [Sn-K_D values on DGA resin in HNO_3, for Fig. 2.4]

HNO_3 (mol/L)	Sn-Kd-trial-1	Sn-Kd-trial-2	ave sn-Kd	std dev
0.2	158	169	164	8
0.5	73	78	75	3
1.0	67	72	70	4
1.5	57	63	60	4
2.0	53	54	53	1
2.5	51	57	54	4
3.0	47	50	48	2
3.5	48	56	52	6
4.0	47	53	50	4
4.5	48	49	48	1
5.0	51	55	53	3
5.5	53	54	53	1
6.0	46	53	49	4

Appendix 7.15 [Fig. 2.4 K_D values for tin onto different resins in presence of nitric acid (0.20 to 6.0 mol L^{-1})]

HNO_3 (mol/L)	TRU	TEVA	UTEVA	DGA
0.2	111	107	487	164
0.5	98	79	334	75
1.0	80	65	168	70
1.5	66	61	127	60
2.0	56	60	59	53
2.5	50	59	54	54
3.0	52	54	58	48
3.5	54	51	49	52
4.0	53	46	46	50
4.5	51	42	47	48
5.0	50	46	46	53
5.5	45	46	50	53
6.0	44	48	45	49
ave Kd, mL/g	62	59	121	64
std dev	21	18	137	31

Appendix 7.16 [Te-K_D values on TRU resin in HNO_3, for Fig. 2.5]

Te-Kd-trial-1	Te-Kd-trial-2	Te-Kd-trial-3	Te-Kd-trial-4	ave Te Kd	std dev
262	249	243	253	252	8
197	189	177	195	190	9
180	171	157	163	168	10
129	123	134	113	125	9
101	98	95	92	96	4
89	82	89	71	83	9
77	72	87	86	80	7

72	81	76	72	75	4
83	73	64	67	72	8
57	70	60	73	65	8
63	66	62	59	63	3
66	66	50	55	59	8
65	73	60	54	63	8

Appendix 7.17 [Te-K_D on TEVA resin in HNO_3, for Fig. 2.5]

HNO_3 (mol/L)	Te-Kd-trial-1	Te-Kd-trial-2	ave Te Kd	std dev
0.2	230	240	235	7
0.5	105	104	104	1
1.0	65	72	69	5
1.5	55	49	52	4
2.0	35	38	36	2
2.5	23	30	27	5
3.0	23	31	27	6
3.5	22	30	26	6
4.0	33	26	29	5
4.5	16	17	17	1
5.0	20	26	23	5
5.5	27	27	27	0
6.0	30	22	26	5

Appendix 7.18 [Te-K_D values on UTEVA resin in HNO_3, for Fig. 2.5]

HNO_3 (mol/L)	Te-Kd-trial-1	Te-Kd-trial-2	ave Te Kd	std dev
0.2	317	330	323	9
0.5	222	210	216	9
1.0	167	180	174	9
1.5	110	115	113	3
2.0	77	86	81	7
2.5	73	82	77	6
3.0	74	70	72	2
3.5	73	71	72	1
4.0	68	56	62	9
4.5	55	59	57	3
5.0	50	53	51	2
5.5	53	54	54	1
6.0	46	53	49	5

Appendix 7.19 [Te-K_D values on DGA resin in HNO_3, for Fig. 2.5]

HNO_3 (mol/L)	Te-Kd-trial-1	Te-Kd-trial-2	ave Te kd	std dev
0.2	258	266	262	6
0.5	117	122	120	3
1.0	78	71	74	6
1.5	47	58	53	7
2.0	47	54	51	5

2.5	43	34	39	6
3.0	31	37	34	5
3.5	33	40	36	5
4.0	35	34	35	1
4.5	26	35	31	6
5.0	31	32	32	0
5.5	32	34	33	1
6.0	27	29	28	1

Appendix 7.20 [Fig. 2.5 K_D values for tellurium onto different resins in presence of nitic acid (0.20 to 6.0 mol L^{-1})]

HNO3 (mol/L)	TRU	TEVA	UTEVA	DGA
0.2	252	235	323	262
0.5	190	104	216	120
1.0	168	69	174	74
1.5	125	52	113	53
2.0	96	36	81	51
2.5	83	27	77	39
3.0	80	27	72	34
3.5	75	26	72	36
4.0	72	29	62	35
4.5	65	17	57	31
5.0	63	23	51	32
5.5	59	27	54	33
6.0	63	26	49	28
ave Kd, mL/g	107	54	108	64
std dev	60	59	82	65

Appendix 7.21 [Sn-K_D values on TRU resin in different pH solutions, for Fig. 2.6]

Sn-Kd-trial-1	Sn-Kd-trial-2	Sn-Kd-trial-3	pH	ave Sn-Kd	std dev
89	87	128	1.0	101	23
212	265	230	2.0	236	27
291	272	259	3.0	274	16
400	294	273	4.0	322	68
471	776	687	5.0	645	157
818	399	761	6.0	659	227
409	612	516	7.0	512	101

Appendix 7.22 [Sn-K_D values on TEVA resin in different pH solutions, for Fig. 2.6]

Sn-Kd-trial-1	Sn-Kd-trial-2	Sn-Kd-trial-3	pH	ave Sn-Kd	std dev
99	77	99	1.0	92	13
528	555	695	2.0	592	90
492	520	468	3.0	494	26
569	763	747	4.0	693	108
1621	875	1067	5.0	1188	388
887	1672	889	6.0	1150	453

823	972	908	7.0	901	75

Appendix 7.23 [Sn-K_D values on UTEVA resin in different pH solutions, for Fig. 2.6]

Sn-Kd-trial-1	Sn-Kd-trial-2	Sn-Kd-trial-3	pH	ave Sn-Kd	std dev
271	82	102	1.0	151	104
404	363	236	2.0	334	88
585	503	802	3.0	630	155
797	561	587	4.0	648	129
1330	1286	512	5.0	1043	460
768	528	471	6.0	589	158
490	561	1451	7.0	834	535

Appendix 7.24 [Sn-K_D values on DGA resin in different pH solutions, for Fig. 2.6]

Sn-Kd-trial-1	Sn-Kd-trial-2	Sn-Kd-trial-3	pH	ave Sn-Kd	std dev
276	165	231	1.0	224	56
318	287	341	2.0	316	27
563	424	875	3.0	621	231
836	649	521	4.0	669	158
484	381	754	5.0	540	193
380	485	325	6.0	397	82
891	562	869	7.0	774	184

Appendix 7.25 [Fig. 2.6 K_D values of tin in different pH solutions (pH 1.0–7.0)]

pH	TRU	TEVA	UTEVA	DGA
1.0	101	92	151	224
2.0	236	592	334	316
3.0	274	494	630	621
4.0	322	693	648	669
5.0	645	1188	1043	540
6.0	659	1150	589	397
7.0	512	901	834	774
ave Sn-Kd	393	730	604	506
std dev	215	387	296	200

Appendix 7.26 [Te-K_D values on TRU resin in different pH solutions, for Fig. 2.7]

Te-Kd-trial-1	Te-Kd-trial-2	Te-Kd-trial-3	pH	ave Te-Kd	std dev
70	70	71	1.0	70	1
90	99	65	2.0	85	18
110	99	96	3.0	102	7
86	86	87	4.0	86	1
104	109	113	5.0	108	5
113	105	110	6.0	109	4
92	99	133	7.0	108	22

Appendix 7.27 [Te-K_D values on TEVA resin in different pH solutions, for Fig. 2.7]

Te-Kd-trial-1	Te-Kd-trial-2	Te-Kd-trial-3	pH	ave Te-Kd	std dev
75	75	67	1.0	72	5
109	98	78	2.0	95	16
97	87	95	3.0	93	5
120	105	104	4.0	110	9
104	99	125	5.0	109	14
104	103	107	6.0	105	2
98	88	95	7.0	94	5

Appendix 7.28 [Te-K_D values on UTEVA resin in different pH solutions, for Fig. 2.7]

Te-Kd-trial-1	Te-Kd-trial-2	Te-Kd-trial-3	pH	ave Te-Kd	std dev
80	71	76	1.0	76	4
152	102	90	2.0	114	33
103	101	111	3.0	105	5
111	114	92	4.0	106	12
111	100	93	5.0	101	9
98	108	85	6.0	97	11
150	118	120	7.0	129	18

Appendix 7.29 [Te-K_D values on DGA resin in different pH solutions, for Fig. 2.7]

Te-Kd-trial-1	Te-Kd-trial-2	Te-Kd-trial-3	pH	ave Te-Kd	std dev
99	78	76	1.0	84	13
88	94	100	2.0	94	6
110	101	103	3.0	105	4
136	124	111	4.0	124	12
81	144	115	5.0	114	32
104	144	89	6.0	112	28
115	110	112	7.0	112	2

Appendix 7.30 [Fig. 2.7 K_D values of tellurium in different pH solutions (pH 1.0 – 7.0)]

pH	TRU	TEVA	UTEVA	DGA
1.0	70	72	76	84
2.0	85	95	114	94
3.0	102	93	105	105
4.0	86	110	106	124
5.0	108	109	101	114
6.0	109	105	97	112
7.0	108	94	129	112
ave Te-Kd	96	97	104	106
std dev	15	13	16	13

Appendix 7.31 [Fig. 2.8 K_D values of tin and tellurium onto different resins in presence of nitric acid (0.20 to 6.0 mol L^{-1}) solution]

ave.	Kd values	in HNO_3
	Sn	Te
TRU	62	107
TEVA	59	54
UTEVA	121	108
DGA	64	64

Appendix 7.32 [Fig. 2.9 A comparison of K_D values of tin and tellurium onto different resins in presence of hydrochloric acid (0.20 to 6.0 mol L^{-1}) solution]

ave.	Kd values	in HCl
	Sn	**Te**
TRU	24239	432
TEVA	27232	3124
UTEVA	3233	708
DGA	10166	2230

Appendix 7.33 [Fig. 2.10 Ratio of Sn and Te K_D values onto different resins in presence of hydrochloric acid (0.20 to 6.0 mol L^{-1}) solution]

Acid treatment	**Metal**	**Types of resin**	**Sn**	**Te**	**Ratio $K_{D(Sn)}/K_{D(Te)}$**
HCl	Sn/Te	TRU	24239	432	56.20
HCl	Sn/Te	TEVA	27232	3124	8.70
HCl	Sn/Te	UTEVA	3233	708	4.60
HCl	Sn/Te	DGA	10166	223	4.60

Appendix 7.34 [Fig. 2.11 Column packing with TRU resin and adsorptions of tin and tellurium]

Mass (mg) TRU resin	**Sn ads (%)**	**Te ads (%)**
50	98.62	60.75
75	99.54	57.69
100	99.80	58.47
125	99.85	56.89
150	99.91	58.69
175	99.93	58.51
200	99.95	60.99
225	99.98	59.40
250	99.99	60.68
275	99.99	60.29
300	99.99	60.10
ave.	99.78	59.31
std dev.	0.39	1.30

Appendix 7.35 [Fig. 2.12 Elution of tin and tellurium with hydrochloric acid (1.0 to 12.0 mol L^{-1})]

HCl, mol/L	% Sn wash	% Te wash
1.0	0.03	2.84
2.0	0.38	2.06
3.0	1.36	3.12
4.0	2.30	1.59
5.0	3.08	1.94
6.0	1.51	3.53
7.0	0.37	1.62
8.0	0.32	1.46
9.0	3.40	2.29
10.0	2.24	0.85
11.0	2.85	1.64
12.0	3.68	1.94
ave	1.79	2.07
std dev	1.31	0.76

Appendix 7.36 [Fig. 2.13 Elution of tin and tellurium with nitric acid solution (0.50 to 6.0 mol L^{-1})]

HNO_3, mol/L	% Sn wash	% Te wash
0.5	17.01	24.14
1.0	20.68	26.23
2.0	31.47	28.45
4.0	44.61	35.87
6.0	48.50	38.71
ave	32.45	30.68
std dev	13.99	6.30

Appendix 7.37 [Fig. 2.14 Elution of tin and tellurium from TRU column by hydrofluoric acid (0.20 to 6.0 mol L^{-1})]

HF (mol/L)	% Sn wash	% Te wash
0.2	88.91	4.54
0.5	92.37	5.14
1.0	94.52	7.40
1.5	95.08	11.29
2.0	95.35	12.11
2.5	95.50	13.36
3.0	95.59	15.16
3.5	95.95	15.37
4.0	96.17	15.82
4.5	96.36	16.01
5.0	96.48	16.46
5.5	96.74	17.12
6.0	97.21	19.46
ave.	95.09	13.02
std. dev.	2.22	4.71

Appendix 7.38 [Fig. 2.15 A comparison on the percentage of tin and tellurium wash by HCl, HNO_3, and HF]

washing media	% Sn wash	% Te wash
HCl	1.79	2.07
HNO_3	32.45	30.68
HF	95.09	13.12

Appendix 7.39 [Fig. 2.16 Percent of tin and tellurium elution with the number of wash treatment]

Metal elution with number of wash treatment

# of wash	% Sn wash	% Te wash
1-wash	85.50	6.09
2-wash	89.51	7.61
3-wash	92.94	10.43
4-wash	95.09	13.01

Appendix 7.40 [Fig. 2.17 Selectivity of tin and tellurium separation with increasing eluent concentration (0.005 to 6.0 mol L^{-1})]

HF conc vs ratio of % Sn wash over % Te wash

HF (mol/L)	Sn wash (%)	Te wash (%)	Ratio (Sn/Te)
0.005	68.80	3.33	20.66
0.01	71.43	3.40	21.03
0.05	75.83	3.59	21.11
0.10	77.42	3.62	21.41
0.20	88.91	4.54	19.60
0.50	92.37	5.14	17.96
1.0	94.52	7.40	12.77
1.5	95.08	11.29	8.42
2.0	95.35	12.11	7.88
2.5	95.50	13.36	7.15
3.0	95.59	15.16	6.30
3.5	95.95	15.37	6.24
4.0	96.17	15.82	6.08
4.5	96.36	16.01	6.02
5.0	96.48	16.46	5.86
5.5	96.74	17.12	5.65
6.0	97.21	19.46	5.00

Appendix 7.41 [Fig. 2.18 The drop of separation efficiency with the number of washing treatments]

drop of separation efficiency with number of wash treatment
ratio: % tin wash over % tellurium wash

# of wash	Ratio
1st wash	14.04
2nd wash	11.76
3rd wash	8.91
4th wash	7.31

Appendix 7.42 [Chloride and sulfate concentrations in surface and groundwaters]

Surface water					
Observed	**Cl^-**	**ave Cl^- ppm**	**std dev**	29.98 mg in 1000 mL	
14.97	29.94	29.99	0.09	1 mL = 0.0299867 mg	
15.05	30.10			2 mL = 0.0599 mg/10 mL	or 5.99 mg/L
14.96	29.92			3 mL = 0.0899 mg/10 mL	or 8.99 mg/L
				4 mL = 0.1199 mg/10 mL	or 11.99 mg/L
				5 mL = 0.1499 mg/10 mL	or 14.99 mg/L
Observed	**SO_4^{2-}**	**ave SO_4^{2-}ppm**	**std dev**	9.78 mg in 1000 mL	
4.88	9.76	9.78	0.03	1 mL = 0.00978 mg	
4.91	9.82			2 mL = 0.01956 mg/10 mL	or 1.96 mg/L
4.88	9.76			3 mL = 0.02934 mg/10 mL	or 2.93 mg/L
				4 mL = 0.03912 mg/10 mL	or 3.91 mg/L
				5 mL = 0.0489 mg/10 mL	or 4.89 mg/L

Groundwater					
Observed	**Cl^-**	**ave Cl^- ppm**	**std dev**	71.41666 mg in 1000 mL	
14.64	73.2	71.42	1.57	1 mL = 0.0714166 mg	
14.16	70.8			2 mL = 0.142833 mg/10 mL	or 14.28 mg/L
14.05	70.25			3 mL = 0.214249 mg/10 mL	or 21.42 mg/L
				4 mL = 0.285666 mg/10 mL	or 28.57 mg/L
				5 mL = 0.357083 mg/10 mL	or 35.71 mg/L
Observed	**SO_4^{2-}**	**ave SO_4^{2-}ppm**	**std dev**	69.95 mg in 1000 mL	
14.37	71.85	69.95	1.69	1 mL = 0.06995 mg	
13.88	69.4			2 mL = 0.1399 mg/10 mL	or 13.99 mg/L
13.72	68.6			3 mL = 0.2099 mg/10 mL	or 20.99 mg/L
				4 mL = 0.2798 mg/10 mL	or 27.98 mg/L
				5 mL = 0.3498 mg/10 mL	or 34.98 mg/L

Appendix 7.43 [Sn-K_D values on TRU resin in HCl, for Fig. 3.1]

Sn-Kd-trial-1	Sn-Kd-trial-2	Sn-Kd-trial-3	HCl (mol/L)	ave Sn-Kd	std dev
115	160	167	0.2	148	28
2343	2275	1960	0.5	2192	204
3885	4792	3694	1.0	4123	586
5502	6716	5322	1.5	5847	758
7072	6976	8314	2.0	7454	746
8285	8003	9763	2.5	8684	945
8383	8932	9130	3.0	8815	387
8281	7529	8138	3.5	7983	400
8060	7967	7055	4.0	7694	555
6925	6015	6472	4.5	6471	455
4465	5320	5610	5.0	5132	595
3900	3582	2760	5.5	3414	588
2282	2111	1791	6.0	2061	249

Appendix 7.44 [Sn-K_D (Cl^--spike) values on TRU resin in HCl, for Fig. 3.1]

Sn-Kd-trial-1	Sn-Kd-trial-2	Sn-Kd-trial-3	HCl (mol/L)	ave. Sn-kd	std dev
122	132	126	0.2	126	5
1134	1233	1490	0.5	1286	184
5158	5418	4533	1.0	5037	455
6607	8034	6455	1.5	7032	871
9658	8861	7650	2.0	8723	1011
9163	8452	9789	2.5	9134	669
9901	10451	8518	3.0	9623	996
9919	7840	9503	3.5	9087	1100
8144	7341	7202	4.0	7562	509
7382	6065	6725	4.5	6724	658
4973	5658	4965	5.0	5199	398
4576	4774	3821	5.5	4390	503
3922	3816	3697	6.0	3812	112

Appendix 7.45 [Sn-K_D (SO_4^{2-}-spike) values on TRU resin in HCl, for Fig. 3.1]

Sn-Kd-trial-1	Sn-Kd-trial-2	Sn-Kd-trial-3	HCl (mol/L)	ave. Sn-kd	std dev
104	119	99	0.2	107	10
909	803	704	0.5	805	102
2684	3438	3702	1.0	3275	528
5765	7039	7529	1.5	6778	910
8598	7157	9558	2.0	8438	1209
8998	8867	9075	2.5	8980	105
9744	8914	7849	3.0	8836	950
7593	8176	9811	3.5	8527	1150
7550	8376	7593	4.0	7840	465
7321	7032	7475	4.5	7276	225
6271	5637	7019	5.0	6309	692
4531	3667	4701	5.5	4300	554
2193	2215	2467	6.0	2292	152

Appendix 7.46 [Sn-K_D (Cl^- + SO_4^{2-}-spike) values on TRU resin in HCl, for Fig. 3.1]

Sn-Kd-trial-1	Sn-Kd-trial-2	Sn-Kd-trial-3	HCl (mol/L)	ave. Sn-kd	std dev
245	236	288	0.2	256	28
1282	1356	1611	0.5	1416	173
3205	3537	2586	1.0	3109	483
5317	5031	4943	1.5	5097	196
7108	6339	5979	2.0	6475	577
6824	7519	8187	2.5	7510	682
8708	7284	8902	3.0	8298	883
8533	8213	8799	3.5	8515	293
7896	8278	7536	4.0	7903	371
6504	7784	6010	4.5	6766	916
5856	4432	5006	5.0	5098	717
4186	3495	3739	5.5	3807	350

1006	1283	1079	6.0	1122	143

Appendix 7.47 [Fig. 3.1 K_D values of tin in presence of chloride and sulfate spikes in HCl medium]

HCl (mol/L)	Sn-Kd	Sn + Cl^-	Sn + SO_4^{2-}	Sn + Cl^- + SO_4^{2-}
0.2	148	126	107	256
0.5	2192	1286	805	1416
1.0	4123	5037	3275	3109
1.5	5847	7032	6778	5097
2.0	7454	8723	8438	6475
2.5	8684	9134	8980	7510
3.0	8815	9623	8836	8298
3.5	7983	9087	8527	8515
4.0	7694	7562	7840	7903
4.5	6471	6724	7276	6766
5.0	5132	5199	6309	5098
5.5	3414	4390	4300	3807
6.0	2061	3812	2292	1122
ave	5386	5980	5674	5029
std dev	2808	3022	3154	2867

Appendix 7.48 [Te-K_D values on TRU resin in HCl, for Fig. 3.2]

Te-Kd-trial-1	Te-Kd-trial-2	Te-Kd-trial-3	HCl (mol/L)	ave Te-Kd	std dev
249	256	223	0.2	243	17
188	205	138	0.5	177	35
139	118	141	1.0	132	13
112	111	109	1.5	111	1
103	127	130	2.0	120	15
143	185	178	2.5	169	22
314	395	280	3.0	330	59
813	843	945	3.5	867	69
1663	1537	1660	4.0	1620	72
2779	2642	2761	4.5	2727	75
3111	3097	3134	5.0	3114	19
3519	3624	3685	5.5	3609	84
3433	3433	3519	6.0	3461	50

Appendix 7.49 [Te-K_D (Cl^--spike) values on TRU resin in HCl, for Fig. 3.2]

Te-Kd-trial-1	Te-Kd-trial-2	Te-Kd-trial-3	HCl (mol/L)	ave. Te-kd	std dev
185	157	156	0.2	166	17
88	111	114	0.5	104	14
86	58	81	1.0	75	15
79	81	51	1.5	70	17
97	94	104	2.0	98	5
320	349	269	2.5	313	40
942	955	969	3.0	955	14
1903	1662	1775	3.5	1780	121

2937	2393	2540	4.0	2623	281
2769	2682	2937	4.5	2796	130
2810	2762	2960	5.0	2844	104
1934	2907	2907	5.5	2583	562
2916	2015	2226	6.0	2386	471

Appendix 7.50 [Te-K_D (SO_4^{2-}-spike) values on TRU resin in HCl, for Fig. 3.2]

Te-Kd-trial-1	Te-Kd-trial-2	Te-Kd-trial-3	HCl (mol/L)	ave. Te-kd	std dev
145	112	133	0.2	130	17
64	207	47	0.5	106	88
37	39	49	1.0	42	7
42	53	28	1.5	41	12
82	91	66	2.0	80	13
241	244	292	2.5	259	29
867	1009	919	3.0	932	72
1709	1905	1436	3.5	1683	235
2773	2234	2118	4.0	2375	349
2940	2643	2504	4.5	2696	223
2934	2902	2764	5.0	2867	91
2538	3236	3153	5.5	2975	381
2521	2541	2341	6.0	2468	110

Appendix 7.51 [Te-K_D (Cl^- + SO_4^{2-}-spike) values on TRU resin in HCl, for Fig. 3.2]

Te-Kd-trial-1	Te-Kd-trial-2	Te-Kd-trial-3	HCl (mol/L)	ave. Te-kd	std dev
149	139	118	0.2	135	16
167	118	116	0.5	134	29
76	85	88	1.0	83	7
43	89	82	1.5	71	25
103	112	130	2.0	115	14
300	283	208	2.5	264	49
832	842	649	3.0	775	109
1875	1707	1468	3.5	1683	204
2442	2217	2713	4.0	2457	249
3315	3702	2655	4.5	3224	530
3447	2974	3322	5.0	3248	245
2951	2936	3217	5.5	3034	158
3176	2733	2426	6.0	2778	377

Appendix 7.52 [Fig. 3.2 K_D values of tellurium in presence of chloride and sulfate spikes in HCl medium]

HCl (mol/L)	Te-Kd	Te + Cl^-	Te + SO_4^{2-}	Te + Cl^- + SO_4^{2-}
0.2	243	166	130	135
0.5	177	104	106	134
1.0	132	75	42	83
1.5	111	70	41	71
2.0	120	98	80	115
2.5	169	313	259	264
3.0	330	955	932	775
3.5	867	1780	1683	1683
4.0	1620	2623	2375	2457
4.5	2727	2796	2696	3224
5.0	3114	2844	2867	3248
5.5	3609	2583	2975	3034
6.0	3461	2386	2468	2778
ave	1283	1292	1281	1385
std dev	1426	1214	1243	1371

Appendix 7.53 [Fig. 3.3 A comparison of K_D values between tin and tellurium produced in HCl medium]

Sample type	Sn-Kd	Te-Kd
Unspiked	5386	1283
Cl-spiked	5980	1292
SO_4^{2-}-spiked	5674	1281
Cl^- + SO_4^{2-} mixed	5029	1385
ave	5517	1310
std dev	406	50

Appendix 7.54 [Sn-K_D (time) values on TRU resin in HCl, for Fig. 3.4]

Sn-Kd-trial-1	Sn-Kd-trial-2	Sn-Kd-trial-3	contact time, min	ave Sn-Kd	std dev
203	226	241	5	223	19
322	355	260	15	312	48
417	442	403	30	421	20
446	489	509	45	481	32
520	479	574	60	525	48
512	547	519	75	526	18
554	447	533	90	511	57
476	515	435	105	475	40
463	408	447	120	439	29
336	288	288	135	304	28
144	195	221	150	187	39
172	148	158	165	160	12
143	163	139	180	148	13

Appendix 7.55 [Sn-K_D (Cl^--time) values on TRU resin in HCl, for Fig. 3.4]

Sn-Kd-trial-1	Sn-Kd-trial-2	Sn-Kd-trial-3	Contact time, min	ave Sn-Kd	std dev
113	93	86	5	97	14
134	164	177	15	158	22
229	214	222	30	222	8
227	217	281	45	242	34
215	299	289	60	268	45
268	318	288	75	291	25
361	298	288	90	316	40
285	349	326	105	320	32
362	236	243	120	280	71
300	206	255	135	253	47
275	211	211	150	232	37
148	228	217	165	198	44
169	208	154	180	177	28

Appendix 7.56 [Sn-K_D (SO_4^{2-}-time) values on TRU resin in HCl, for Fig. 3.4]

Sn-Kd-trial-1	Sn-Kd-trial-2	Sn-Kd-trial-3	Contact time, min	ave Sn-Kd	std dev
126	98	128	5	117	17
184	175	159	15	172	13
292	213	252	30	253	39
391	258	284	45	311	70
370	319	374	60	354	30
354	392	323	75	356	35
378	303	388	90	357	47
395	343	284	105	341	56
313	386	289	120	329	51
308	342	316	135	322	18
310	296	328	150	311	16
269	261	243	165	258	13
274	213	223	180	237	33

Appendix 7.57 [Sn-K_D (Cl^- + SO_4^{2-}-time) values on TRU resin in HCl, for Fig. 3.4]

Sn-Kd-trial-1	Sn-Kd-trial-2	Sn-Kd-trial-3	Contact time, min	ave Sn-Kd	std dev
49	58	55	5	54	5
180	214	205	15	200	18
253	313	322	30	296	38
388	363	346	45	366	21
465	389	401	60	418	41
496	440	419	75	452	40
468	424	451	90	448	22
293	399	436	105	376	74
346	321	328	120	331	13
250	252	255	135	252	2
249	207	274	150	244	34
170	201	192	165	188	16

149	135	116	180	133	17

Appendix 7.58 [Fig. 3.4 K_D values of tin with respect to different contact times]

Contact time (min)	Sn-Kd	Sn + Cl^-	Sn + SO_4^{2-}	Sn + Cl^- + SO_4^{2-}
5	223	97	117	54
15	312	158	172	200
30	421	222	253	296
45	481	242	311	366
60	525	268	354	418
75	526	291	356	452
90	511	316	357	448
105	475	320	341	376
120	439	280	329	331
135	304	253	322	252
150	187	232	311	244
165	160	198	258	188
180	148	177	237	133
ave	363	235	286	289
std dev	146	65	75	124

Appendix 7.59 [Te-K_D values (time) on TRU resin in HCl, for Fig. 3.5]

Te-Kd-trial-1	Te-Kd-trial-2	Te-Kd-trial-3	contact time, min	ave Te-Kd	std dev
16.73	9.87	16.40	5	14.33	3.86
23.17	23.14	21.67	15	22.66	0.86
23.86	27.57	29.36	30	26.93	2.81
24.48	33.88	29.58	45	29.31	4.70
34.58	26.61	31.47	60	30.88	4.02
40.24	30.16	25.98	75	32.13	7.33
34.48	28.20	27.93	90	30.20	3.70
28.82	23.55	28.67	105	27.01	3.00
21.95	26.45	30.09	120	26.16	4.08
22.36	28.55	24.15	135	25.02	3.19
23.83	24.25	22.82	150	23.63	0.74
15.33	22.72	18.41	165	18.82	3.71
11.89	10.58	14.13	180	12.20	1.79

Appendix 7.60 [Te-K_D values (Cl^--time) on TRU resin in HCl, for Fig. 3.5]

Te-Kd-trial-1	Te-Kd-trial-2	Te-Kd-trial-3	Contact time, min	ave Te-Kd	std dev
20.09	22.03	18.86	5	20.33	1.60
22.48	30.20	32.28	15	28.32	5.16
32.56	31.26	44.59	30	36.14	7.35
39.85	37.41	34.66	45	37.31	2.60
39.81	45.34	33.54	60	39.57	5.90
39.69	41.20	34.03	75	38.30	3.78
29.15	36.47	38.99	90	34.87	5.11

25.22	36.33	33.64	105	31.73	5.80
31.31	23.59	26.78	120	27.23	3.88
26.63	27.14	18.45	135	24.07	4.88
20.85	19.49	22.43	150	20.92	1.47
15.34	13.01	9.07	165	12.47	3.17
7.68	11.12	5.39	180	8.06	2.89

Appendix 7.61 [Te-K_D values (SO_4^{2-}-time) on TRU resin in HCl, for Fig. 3.5]

Te-Kd-trial-1	Te-Kd-trial-2	Te-Kd-trial-3	Contact time, min	ave Te-Kd	std dev
7.18	11.86	10.23	5	9.76	2.37
12.23	10.01	15.22	15	12.49	2.61
11.78	14.76	15.14	30	13.89	1.84
15.17	13.66	17.38	45	15.40	1.87
23.08	19.28	18.23	60	20.20	2.55
21.95	19.88	32.79	75	24.87	6.93
28.99	25.61	23.11	90	25.90	2.95
30.80	30.26	29.27	105	30.11	0.78
27.14	25.17	23.16	120	25.16	1.99
15.22	24.11	22.61	135	20.65	4.76
16.19	16.91	15.23	150	16.11	0.84
19.23	13.01	12.70	165	14.98	3.69
18.73	10.06	12.00	180	13.60	4.55

Appendix 7.62 [Te-K_D values (Cl^- + SO_4^{2-}-time) on TRU resin in HCl, for Fig. 3.5]

Te-Kd-trial-1	Te-Kd-trial-2	Te-Kd-trial-3	Contact time, min	ave Te-Kd	std dev
13.78	17.88	19.56	5	17.07	2.97
20.68	23.21	18.38	15	20.76	2.42
23.56	25.40	21.53	30	23.50	1.93
26.09	27.73	31.80	45	28.54	2.94
35.65	30.47	28.56	60	31.56	3.67
35.83	31.73	32.88	75	33.48	2.11
35.42	31.92	36.97	90	34.77	2.59
33.93	34.58	30.22	105	32.91	2.35
28.95	32.11	26.30	120	29.12	2.91
23.72	24.34	30.86	135	26.31	3.96
28.85	24.81	19.53	150	24.40	4.67
23.18	20.50	21.76	165	21.81	1.34
21.73	13.76	17.04	180	17.51	4.00

Appendix 7.63 [Fig. 3.5 K_D values of tellurium with respect to different contact times]

Contact time (min)	Te-Kd	Te + Cl^-	Te + SO_4^{2-}	Te + Cl^- + SO_4^{2-}
5	14.33	20.33	9.76	17.07
15	22.66	28.32	12.49	20.76
30	26.93	36.14	13.89	23.50
45	29.31	37.31	15.40	28.54
60	30.88	39.57	20.20	31.56
75	32.13	38.30	24.87	33.48
90	30.20	34.87	25.90	34.77
105	27.01	31.73	30.11	32.91
120	26.16	27.23	25.16	29.12
135	25.02	24.07	20.65	26.31
150	23.63	20.92	16.11	24.40
165	18.82	12.47	14.98	21.81
180	12.20	8.06	13.60	17.51
ave	24.56	27.64	18.70	26.29
std dev	6.20	10.07	6.24	6.00

Appendix 7.64 [Sn-K_D values on TRU resin in different pH, for Fig. 3.6]

Sn-Kd-trial-1	Sn-Kd-trial-2	Sn-Kd-trial-3	pH	ave Sn-Kd	std dev
178	147	199	1.0	175	26
355	384	389	2.0	376	18
563	416	425	3.0	468	82
381	454	401	4.0	412	38
522	422	523	5.0	489	58
477	616	469	6.0	521	83
558	445	439	7.0	481	67

Appendix 7.65 [Sn-K_D (Cl^--spike) values on TRU resin in different pH, for Fig. 3.6]

Sn-Kd-trial-1	Sn-Kd-trial-2	Sn-Kd-trial-3	pH	ave Sn-Kd	std dev
146	164	157	1.0	156	9
428	406	453	2.0	429	24
384	489	354	3.0	409	71
356	259	219	4.0	278	71
592	455	649	5.0	565	100
513	780	**766**	6.0	686	150
662	476	405	7.0	515	133

Appendix 7.66 [Sn-K_D (SO_4^{2-}-spike) values on TRU resin in different pH, for Fig. 3.6]

Sn-Kd-trial-1	Sn-Kd-trial-2	Sn-Kd-trial-3	pH	ave Sn-Kd	std dev
51	147	160	1.0	120	59
228	191	135	2.0	185	47
265	241	319	3.0	275	40
269	258	266	4.0	264	5
406	495	444	5.0	448	45
311	248	230	6.0	263	43

422	141	517	7.0	360	196

Appendix 7.67 [Sn-K_D (Cl^- + SO_4^{2-}-spike) values on TRU resin in different pH, for Fig. 3.6]

Sn-Kd-trial-1	Sn-Kd-trial-2	Sn-Kd-trial-3	pH	ave Sn-Kd	std dev
128	165	161	1.0	151	20
318	287	341	2.0	316	27
563	386	475	3.0	475	89
389	399	521	4.0	436	74
484	381	754	5.0	540	193
380	485	325	6.0	397	82
447	558	865	7.0	623	217

Appendix 7.68 [Fig. 3.6 Effects of pH on the K_D values of tin in presence of chloride and sulfate ions]

pH	Sn-Kd	Sn + Cl^-	Sn + SO_4^{2-}	Sn + Cl^- + SO_4^{2-}
1.0	175	156	120	151
2.0	376	429	185	316
3.0	468	409	275	475
4.0	412	278	264	436
5.0	489	565	448	540
6.0	521	686	263	397
7.0	481	515	360	623

Appendix 7.69 [Fig. 3.7 Variation of the average K_D values of tin for all spiked and unspiked samples]

pH	ave Sn-Kd
1.0	150
2.0	326
3.0	407
4.0	348
5.0	511
6.0	467
7.0	495

Appendix 7.70 [Te-K_D values on TRU resin in different pH, for Fig. 3.8]

Te-Kd-trial-1	Te-Kd-trial-2	Te-Kd-trial-3	pH	ave Te-Kd	std dev
127	108	136	1.0	124	15
181	153	150	2.0	162	17
186	144	164	3.0	165	21
176	159	121	4.0	152	28
143	211	140	5.0	165	40
194	151	158	6.0	168	23
228	186	334	7.0	249	76

Appendix 7.71 [Te-K_D values (Cl^--spike) on TRU resin in different pH, for Fig. 3.8]

Te-Kd-trial-1	Te-Kd-trial-2	Te-Kd-trial-3	pH	ave Te-Kd	std dev
139	143	130	1.0	138	6
192	170	151	2.0	171	21
176	112	153	3.0	147	33
148	157	187	4.0	164	21
143	124	169	5.0	145	23
156	200	211	6.0	189	29
142	148	130	7.0	140	9

Appendix 7.72 [Te-K_D values (SO_4^{2-}-spike) on TRU resin in different pH, for Fig. 3.8]

Te-Kd-trial-1	Te-Kd-trial-2	Te-Kd-trial-3	pH	ave Te-Kd	std dev
160	143	153	1.0	152	8
304	203	180	2.0	229	66
207	202	223	3.0	211	11
223	228	185	4.0	212	24
221	201	187	5.0	203	17
196	216	171	6.0	194	23
292	229	252	7.0	257	32

Appendix 7.73 [Te-K_D values (Cl^- + SO_4^{2-}-spike) on TRU resin in different pH, for Fig. 3.8]

Te-Kd-trial-1	Te-Kd-trial-2	Te-Kd-trial-3	pH	ave Te-Kd	std dev
199	156	151	1.0	169	26
176	188	201	2.0	188	12
219	202	206	3.0	209	9
271	247	223	4.0	247	24
262	289	231	5.0	260	29
208	288	178	6.0	225	57
221	211	215	7.0	216	5

Appendix 7.74 [Fig. 3.8 Effects of pH on the K_D values of tellurium in presence of chloride and sulfate ions]

pH	Te-Kd	Te + Cl^-	Te + SO_4^{2-}	Te + Cl^- + SO_4^{2-}
1.0	124	138	152	169
2.0	162	171	229	188
3.0	165	147	211	209
4.0	152	164	212	247
5.0	165	145	203	260
6.0	168	189	194	225
7.0	249	140	257	216
ave	169	156	208	216
std dev	38	19	32	32

Appendix 7.75 [Sn-K_D values (vial) on TRU resin in HCl, for Fig. 3.9]

Sn-Kd-trial-1	Sn-Kd-trial-2	Sn-Kd-trial-3	HCl (mol/L)	ave Sn-Kd	std dev
92	70	102	0.2	88	16
312	351	342	0.5	335	20
798	882	725	1.0	802	79
1634	1821	1475	1.5	1643	173
1915	2291	2175	2.0	2127	193
2441	2211	2516	2.5	2389	159
2568	2575	2880	3.0	2674	179
2740	2550	2342	3.5	2544	199
2244	2411	2313	4.0	2323	83
2275	2220	2303	4.5	2266	42
2043	2138	2293	5.0	2158	127
1894	1672	1980	5.5	1849	159
1420	1743	1922	6.0	1695	255

Appendix 7.76 [Sn-K_D values (Cl^--vial) on TRU resin in HCl, for Fig. 3.9]

Sn-Kd-trial-1	Sn-Kd-trial-2	Sn-Kd-trial-3	HCl (mol/L)	ave Sn-Kd	std dev
995	1030	1205	0.2	1077	113
1755	1699	1530	0.5	1661	117
2158	2093	2323	1.0	2191	119
2812	2822	2693	1.5	2776	72
3917	3743	3537	2.0	3732	190
4059	4273	4307	2.5	4213	135
4640	4548	4266	3.0	4484	195
4563	4305	4444	3.5	4438	129
3802	3909	4107	4.0	3939	154
3442	3586	3694	4.5	3574	126
3367	3075	3187	5.0	3210	148
2732	3017	2627	5.5	2792	202
2443	2505	2319	6.0	2423	95

Appendix 7.77 [Sn-K_D values (SO_4^{2-}-vial) on TRU resin in HCl, for Fig. 3.9]

Sn-Kd-trial-1	Sn-Kd-trial-2	Sn-Kd-trial-3	HCl (mol/L)	ave Sn-Kd	std dev
511	436	496	0.2	481	40
713	651	661	0.5	675	33
840	976	982	1.0	933	80
1135	1232	1205	1.5	1191	50
1613	1758	1849	2.0	1740	119
2144	2407	2387	2.5	2313	146
2741	2610	2893	3.0	2748	142
3123	3427	3316	3.5	3289	154
3944	3873	4097	4.0	3971	115
4044	4210	3999	4.5	4084	111
3901	3946	4190	5.0	4012	156
3563	3594	3771	5.5	3643	112

2360	2451	2360	6.0	2390	53

Appendix 7.78 [Sn-K_D values (Cl^- + SO_4^{2-}-vial) on TRU resin in HCl, for Fig. 3.9]

Sn-Kd-trial-1	Sn-Kd-trial-2	Sn-Kd-trial-3	HCl (mol/L)	ave Sn-Kd	std dev
296	310	321	0.2	309	12
597	506	496	0.5	533	55
820	884	761	1.0	822	61
1401	1232	1526	1.5	1386	148
1755	2010	1972	2.0	1912	138
2630	2113	2520	2.5	2421	272
2801	3066	2837	3.0	2901	143
2922	2922	3165	3.5	3003	140
2959	2580	3048	4.0	2862	249
2614	2815	2482	4.5	2637	168
2489	2085	2332	5.0	2302	204
1911	2014	2152	5.5	2026	121
1865	1340	1595	6.0	1600	262

Appendix 7.79 [Fig. 3.9 K_D values of tin in different shaking orientations in presence of chloride and sulfate ions, 'h' stands for horizontal and 'v' for vertical alignments]

HCl (mol/L)	Sn-vial-v	Cl^--vial-v	SO_4^{2-}-vial-v	Cl^- + SO_4^{2-}-vial-v
0.2	88	1077	481	309
0.5	335	1661	675	533
1.0	802	2191	933	822
1.5	1643	2776	1191	1386
2.0	2127	3732	1740	1912
2.5	2389	4213	2313	2421
3.0	2674	4484	2748	2901
3.5	2544	4438	3289	3003
4.0	2323	3939	3971	2862
4.5	2266	3574	4084	2637
5.0	2158	3210	4012	2302
5.5	1849	2792	3643	2026
6.0	1695	2423	2390	1600
ave	1761	3116	2421	1901
std dev	841	1077	1325	915

Appendix 7.80 [Te-K_D values (vial) on TRU resin in HCl, for Fig. 3.10]

Te-Kd-trial-1	Te-Kd-trial-2	Te-Kd-trial-3	HCl (mol/L)	ave Te-Kd	std dev
96	150	103	0.2	116	29
74	136	119	0.5	109	32
81	94	68	1.0	81	13
42	47	16	1.5	35	16
57	62	46	2.0	55	8
124	125	195	2.5	148	41
244	294	269	3.0	269	25

954	748	765	3.5	822	115
1372	1713	1346	4.0	1477	205
2104	2204	2393	4.5	2234	147
2583	2501	2652	5.0	2579	76
2611	2563	2312	5.5	2495	160
2358	1990	2028	6.0	2125	203

Appendix 7.81 [Te-K_D values (Cl^--vial) on TRU resin in HCl, for Fig. 3.10]

Te-Kd-trial-1	Te-Kd-trial-2	Te-Kd-trial-3	HCl (mol/L)	ave Te-Kd	std dev
189	178	137	0.2	168	27
136	134	84	0.5	118	29
90	95	93	1.0	93	2
85	78	87	1.5	83	5
64	74	82	2.0	73	9
30	69	60	2.5	53	21
80	111	100	3.0	97	16
214	214	238	3.5	222	14
487	463	491	4.0	480	15
850	839	843	4.5	844	6
1033	1105	1158	5.0	1099	63
1345	1431	1340	5.5	1372	51
1181	1250	1267	6.0	1233	45

Appendix 7.82 [Te-K_D values (SO_4^{2-}-vial) on TRU resin in HCl, for Fig. 3.10]

Te-Kd-trial-1	Te-Kd-trial-2	Te-Kd-trial-3	HCl (mol/L)	ave Te-Kd	std dev
226	171	188	0.2	195	28
117	137	111	0.5	121	14
85	110	110	1.0	101	14
91	73	107	1.5	90	17
56	62	71	2.0	63	8
77	81	93	2.5	84	8
109	132	109	3.0	116	14
204	208	245	3.5	219	22
464	489	444	4.0	466	23
686	836	842	4.5	788	88
915	937	1069	5.0	974	83
987	1061	1019	5.5	1022	37
922	897	961	6.0	927	32

Appendix 7.83 [Te-K_D values (Cl^- + SO_4^{2-}-vial) on TRU resin in HCl, for Fig. 3.10]

Te-Kd-trial-1	Te-Kd-trial-2	Te-Kd-trial-3	HCl (mol/L)	ave Te-Kd	std dev
205	185	177	0.2	189	14
135	178	135	0.5	149	25
102	99	78	1.0	93	13
83	95	81	1.5	86	7
87	74	82	2.0	81	7

123	118	108	2.5	116	8
290	260	265	3.0	272	16
723	677	681	3.5	694	25
946	987	1099	4.0	1011	79
1488	1312	1375	4.5	1392	90
1524	1587	1626	5.0	1579	51
1675	1719	1593	5.5	1662	64
1406	1530	1567	6.0	1501	85

Appendix 7.84 [Fig. 3.10 K_D values of tellurium in different shaking orientations in presence of chloride and sulfate ions, 'h' stands for horizontal and 'v' for vertical alignments]

HCl (mol/L)	Te-vial-v	Cl^--vial-v	SO_4^{2-}-vial-v	Cl^- + SO_4^{2-}-vial-v
0.2	116	168	195	189
0.5	109	118	121	149
1.0	81	93	101	93
1.5	35	83	90	86
2.0	55	73	63	81
2.5	148	53	84	116
3.0	269	97	116	272
3.5	822	222	219	694
4.0	1477	480	466	1011
4.5	2234	844	788	1392
5.0	2579	1099	974	1579
5.5	2495	1372	1022	1662
6.0	2125	1233	927	1501
ave	965	457	397	679
std dev	1051	497	385	654

Appendix 7.85 [Sn-K_D values for surface water (0 mL-spike), for Fig. 3.11]

Sn-Kd-trial-1	Sn-Kd-trial-2	Sn-Kd-trial-3	HCl (mol/L)	ave Sn-Kd	std dev
2206	2157	2067	0.5	2143	70
6217	6248	5718	1.0	6061	297
14100	15946	14359	1.5	14801	999
21517	22485	22542	2.0	22181	576
25356	26040	25560	2.5	25652	351
28898	30652	29428	3.0	29660	899
31809	29887	31257	3.5	30984	989
31082	32571	31960	4.0	31871	748
32013	33217	31418	4.5	32216	916
31212	30177	29659	5.0	30349	790
29109	28516	29853	5.5	29160	670
23197	24799	24619	6.0	24205	878

Appendix 7.86 [Sn-K_D values for surface water (2 mL-spike), for Fig. 3.11]

Sn-Kd-trial-1	Sn-Kd-trial-2	Sn-Kd-trial-3	HCl (mol/L)	ave Sn-Kd	std dev
2927	2805	2764	0.5	2832	85
9749	10784	9442	1.0	9992	703
20805	19106	19511	1.5	19807	887
28426	26926	27875	2.0	27742	758
33423	34723	35167	2.5	34438	906
36256	37390	38414	3.0	37353	1080
41335	39744	40947	3.5	40675	830
41744	42026	41724	4.0	41831	169
40194	39548	38773	4.5	39505	711
36554	37184	35849	5.0	36529	668
34093	35120	33769	5.5	34328	705
30153	29843	28549	6.0	29515	851

Appendix 7.87 [Sn-K_D values for surface water (3 mL-spike), for Fig. 3.11]

Sn-Kd-trial-1	Sn-Kd-trial-2	Sn-Kd-trial-3	HCl (mol/L)	ave Sn-Kd	std dev
1508	2107	2113	0.5	1910	348
7245	7305	6990	1.0	7180	167
14112	12508	12802	1.5	13141	854
20010	18511	19569	2.0	19363	770
24062	25289	25506	2.5	24953	778
30345	33549	31088	3.0	31661	1677
36389	37807	39546	3.5	37914	1581
41218	42647	43907	4.0	42591	1345
42328	41512	43610	4.5	42484	1058
38091	39847	40651	5.0	39530	1309
35611	34329	37242	5.5	35727	1460
30446	31210	30219	6.0	30625	520

Appendix 7.88 [Sn-K_D values for surface water (4 mL-spike), for Fig. 3.11]

Sn-Kd-trial-1	Sn-Kd-trial-2	Sn-Kd-trial-3	HCl (mol/L)	ave Sn-Kd	std dev
2841	2791	3049	0.5	2894	137
9193	10265	9164	1.0	9541	628
17351	16680	17592	1.5	17208	473
24830	26353	23875	2.0	25019	1249
31567	29733	30538	2.5	30612	919
33560	32538	32560	3.0	32886	584
34129	35666	32869	3.5	34221	1401
35325	34101	36806	4.0	35411	1355
35142	33746	34081	4.5	34323	729
33516	32100	31244	5.0	32287	1148
29297	29673	28215	5.5	29062	757
25382	25291	24291	6.0	24988	605

Appendix 7.89 [Sn-K_D values for surface water (5 mL-spike), for Fig. 3.11]

Sn-Kd-trial-1	Sn-Kd-trial-2	Sn-Kd-trial-3	HCl (mol/L)	ave Sn-Kd	std dev
2227	2486	1600	0.5	2105	456
5373	6801	6408	1.0	6194	738
13890	12179	12095	1.5	12721	1013
16003	17217	16542	2.0	16587	608
24661	22889	23067	2.5	23539	975
28094	27095	27703	3.0	27631	504
28054	29933	28911	3.5	28966	941
31561	29957	30247	4.0	30588	855
27414	28931	29948	4.5	28764	1275
26547	25676	28613	5.0	26945	1508
23548	24671	22461	5.5	23560	1105
19940	20147	21215	6.0	20434	684

Appendix 7.90 [Fig. 3.11 K_D values of tin in presence of surface water, 'SW' stands for surface water]

HCl (mol/L)	Sn + 0 mL	Sn + 2 mL	Sn + 3 mL	Sn + 4 mL	Sn + 5 mL
0.5	2143	2832	1910	2894	2105
1.0	6061	9992	7180	9541	6194
1.5	14801	19807	13141	17208	12721
2.0	22181	27742	19363	25019	16587
2.5	25652	34438	24953	30612	23539
3.0	29660	37353	31661	32886	27631
3.5	30984	40675	37914	34221	28966
4.0	31871	41831	42591	35411	30588
4.5	32216	39505	42484	34323	28764
5.0	30349	36529	39530	32287	26945
5.5	29160	34328	35727	29062	23560
6.0	24205	29515	30625	24988	20434
ave	23274	29546	27256	25704	20670
std dev	10274	12521	13968	10557	9397

Appendix 7.91 [Fig. 3.12 The effect of surface water addition on the K_D values of tin]

Surface water	
mL-spike	**Sn-Kd**
0	23274
2	29546
3	27256
4	25704
5	20670

Appendix 7.92 [Te-K_D values for surface water (0 mL-spike), for Fig. 3.13]

Te-Kd-trial-1	Te-Kd-trial-2	Te-Kd-trial-3	HCl (mol/L)	ave Te-Kd	std dev
122	127	133	0.5	127	5
89	83	85	1.0	86	3
81	80	77	1.5	79	2
118	126	131	2.0	125	7
294	344	303	2.5	314	27
820	796	704	3.0	773	62
1118	1095	1298	3.5	1171	111
1738	1639	1738	4.0	1705	57
1838	1929	2228	4.5	1998	204
2339	2230	2037	5.0	2202	153
2040	2129	1999	5.5	2056	66
1853	1763	1640	6.0	1752	107

Appendix 7.93 [Te-K_D values for surface water (2 mL-spike), for Fig. 3.13]

Te-Kd-trial-1	Te-Kd-trial-2	Te-Kd-trial-3	HCl (mol/L)	ave Te-Kd	std dev
111	90	127	0.5	109	19
87	85	77	1.0	83	6
94	103	90	1.5	96	7
134	118	101	2.0	117	17
402	376	352	2.5	377	25
787	711	823	3.0	774	57
1536	1428	1434	3.5	1466	61
1841	1861	1773	4.0	1825	46
1936	2130	2031	4.5	2032	97
2331	2228	2140	5.0	2233	96
2139	1992	2237	5.5	2123	123
1830	1934	1731	6.0	1832	101

Appendix 7.94 [Te-K_D values for surface water (3 mL-spike), for Fig. 3.13]

Te-Kd-trial-1	Te-Kd-trial-2	Te-Kd-trial-3	HCl (mol/L)	ave Te-Kd	std dev
92	102	99	0.5	98	6
78	80	79	1.0	79	1
80	79	100	1.5	86	12
135	123	142	2.0	133	10
325	323	310	2.5	319	8
710	740	803	3.0	751	48
1379	1204	1222	3.5	1268	96
1851	1811	1881	4.0	1848	35
2532	2499	2333	4.5	2455	106
2528	2681	2495	5.0	2568	100
2434	2295	2382	5.5	2370	70
2098	1908	1985	6.0	1997	96

Appendix 7.95 [Te-K_D values for surface water (4 mL-spike), for Fig. 3.13]

Te-Kd-trial-1	Te-Kd-trial-2	Te-Kd-trial-3	HCl (mol/L)	ave Te-Kd	std dev
126	104	117	0.5	116	11
129	95	112	1.0	112	17
115	70	77	1.5	87	24
133	138	134	2.0	135	3
285	346	320	2.5	317	31
901	901	985	3.0	929	49
1385	1422	1355	3.5	1387	33
1627	1902	1676	4.0	1735	147
1909	2249	2154	4.5	2104	176
2395	2255	2139	5.0	2263	128
2100	2164	2067	5.5	2110	50
1687	1705	1841	6.0	1745	84

Appendix 7.96 [Te-K_D values for surface water (5 mL-spike), for Fig. 3.13]

Te-Kd-trial-1	Te-Kd-trial-2	Te-Kd-trial-3	HCl (mol/L)	ave Te-Kd	std dev
113	121	125	0.5	120	6
90	84	107	1.0	94	12
88	106	101	1.5	99	9
119	131	144	2.0	132	13
342	354	331	2.5	342	12
834	767	756	3.0	786	42
1341	1406	1225	3.5	1324	91
1965	2123	1818	4.0	1969	152
2466	2209	2322	4.5	2333	129
2388	2482	2317	5.0	2396	83
2138	2261	2310	5.5	2236	88
1823	1945	1791	6.0	1853	81

Appendix 7.97 [Fig. 3.13 K_D values of tellurium in presence of surface water, 'SW' stands for surface water]

HCl (mol/L)	Te + 0 mL	Te + 2 mL	Te + 3 mL	Te + 4 mL	Te + 5 mL
0.5	127	109	98	116	120
1.0	86	83	79	112	94
1.5	79	96	86	87	99
2.0	125	117	133	135	132
2.5	314	377	319	317	342
3.0	773	774	751	929	786
3.5	1171	1466	1268	1387	1324
4.0	1705	1825	1848	1735	1969
4.5	1998	2032	2455	2104	2333
5.0	2202	2233	2568	2263	2396
5.5	2056	2123	2370	2110	2236
6.0	1752	1832	1997	1745	1853
ave	886	936	998	941	986

std dev	872	905	1031	896	974

Appendix 7.98 [Sn-K_D values for groundwater (0 mL-spike), for Fig. 3.14]

Sn-Kd-trial-1	Sn-Kd-trial-2	Sn-Kd-trial-3	HCl (mol/L)	ave Sn-Kd	std dev
1256	1255	1228	0.5	1246	16
4163	4074	4183	1.0	4140	58
8178	7830	7197	1.5	7735	498
10753	12428	12346	2.0	11842	944
15874	13785	14371	2.5	14677	1078
16689	15663	14918	3.0	15757	889
15299	17782	18338	3.5	17140	1618
17569	18285	17185	4.0	17680	558
17011	18541	17315	4.5	17622	810
16915	16126	18001	5.0	17014	942
15549	14619	16915	5.5	15694	1155
13246	13459	14563	6.0	13756	707

Appendix 7.99 [Sn-K_D values for groundwater (2 mL-spike), for Fig. 3.14]

Sn-Kd-trial-1	Sn-Kd-trial-2	Sn-Kd-trial-3	HCl (mol/L)	ave Sn-Kd	std dev
1526	1817	1662	0.5	1668	145
5239	5175	4949	1.0	5121	152
8106	9000	9937	1.5	9014	915
15134	14663	16217	2.0	15338	797
19238	20940	19637	2.5	19938	890
23399	22585	21828	3.0	22604	785
25341	24399	23832	3.5	24524	762
26445	25795	25445	4.0	25895	507
24988	25397	26419	4.5	25601	737
24790	23002	24599	5.0	24130	982
21187	20697	20198	5.5	20694	494
17396	16098	17299	6.0	16931	723

Appendix 7.100 [Sn-K_D values for groundwater (3 mL-spike), for Fig. 3.14]

Sn-Kd-trial-1	Sn-Kd-trial-2	Sn-Kd-trial-3	HCl (mol/L)	ave Sn-Kd	std dev
1395	1340	1473	0.5	1403	67
4905	4774	4938	1.0	4872	87
9864	10012	11905	1.5	10594	1138
18106	19723	20017	2.0	19282	1029
22438	23248	21267	2.5	22318	996
28882	29296	27013	3.0	28397	1216
33882	32467	32629	3.5	32993	774
35449	36635	35196	4.0	35760	769
32517	35596	34998	4.5	34370	1632
28187	29396	31029	5.0	29537	1426
25189	26198	24599	5.5	25329	809
19196	20498	18099	6.0	19264	1201

Appendix 7.101 [Sn-K_D values for groundwater (4 mL-spike), for Fig. 3.14]

Sn-Kd-trial-1	Sn-Kd-trial-2	Sn-Kd-trial-3	HCl (mol/L)	ave Sn-Kd	std dev
1527	1513	1484	0.5	1508	22
5119	4993	5166	1.0	5093	89
10404	8736	10917	1.5	10019	1140
14007	16167	14504	2.0	14893	1131
21807	20703	21707	2.5	21406	610
23023	24561	25157	3.0	24247	1101
25503	27482	26262	3.5	26416	998
26710	26232	27958	4.0	26967	891
23018	24996	25498	4.5	24504	1311
21488	22696	21099	5.0	21761	833
18848	17498	19199	5.5	18515	898
14796	15498	13599	6.0	14631	960

Appendix 7.102 [Sn-K_D values for groundwater (5 mL-spike), for Fig. 3.14]

Sn-Kd-trial-1	Sn-Kd-trial-2	Sn-Kd-trial-3	HCl (mol/L)	ave Sn-Kd	std dev
1484	1455	1360	0.5	1433	65
4759	4943	4686	1.0	4796	133
9790	9980	10199	1.5	9989	205
14504	12802	14240	2.0	13849	916
19537	17907	18632	2.5	18692	817
23122	22163	24260	3.0	23181	1049
27944	26808	26312	3.5	27021	837
30215	31899	29668	4.0	30594	1163
28868	29256	28398	4.5	28841	430
23988	25496	24699	5.0	24727	754
20287	21998	21498	5.5	21261	880
17696	16248	15999	6.0	16648	916

Appendix 7.103 [Fig. 3.14 K_D values of tin in presence of groundwater, 'GW' stands for groundwater]

HCl (mol/L)	Sn + 0 mL	Sn + 2 mL	Sn + 3 mL	Sn + 4 mL	Sn + 5 mL
0.5	1246	1668	1403	1508	1433
1.0	4140	5121	4872	5093	4796
1.5	7735	9014	10594	10019	9989
2.0	11842	15338	19282	14893	13849
2.5	14677	19938	22318	21406	18692
3.0	15757	22604	28397	24247	23181
3.5	17140	24524	32993	26416	27021
4.0	17680	25895	35760	26967	30594
4.5	17622	25601	34370	24504	28841
5.0	17014	24130	29537	21761	24727
5.5	15694	20694	25329	18515	21261
6.0	13756	16931	19264	14631	16648
ave	12859	17622	22010	17497	18419

std dev	5562	8270	11420	8414	9394

Appendix 7.104 [Te-K_D values for groundwater (0 mL-spike), for Fig. 3.15]

Te-Kd-trial-1	Te-Kd-trial-2	Te-Kd-trial-3	HCl (mol/L)	ave Te-Kd	std dev
120	102	105	0.5	109	9
97	97	98	1.0	97	1
60	71	72	1.5	68	6
91	76	64	2.0	77	14
140	141	118	2.5	133	13
285	253	290	3.0	276	20
489	500	546	3.5	512	31
838	869	821	4.0	843	24
1017	932	926	4.5	959	51
1014	983	1031	5.0	1009	25
934	902	857	5.5	898	39
732	627	725	6.0	695	59

Appendix 7.105 [Te-K_D values for groundwater (2 mL-spike), for Fig. 3.15]

Te-Kd-trial-1	Te-Kd-trial-2	Te-Kd-trial-3	HCl (mol/L)	ave Te-Kd	std dev
107	114	98	0.5	106	8
72	66	72	1.0	70	4
69	70	76	1.5	71	4
68	84	87	2.0	79	10
147	131	138	2.5	139	8
307	355	366	3.0	342	31
832	898	911	3.5	880	42
1231	1244	1404	4.0	1293	96
1483	1562	1395	4.5	1480	83
1326	1581	1497	5.0	1468	130
1382	1277	1194	5.5	1285	94
1054	1192	987	6.0	1078	105

Appendix 7.106 [Te-K_D values for groundwater (3 mL-spike), for Fig. 3.15]

Te-Kd-trial-1	Te-Kd-trial-2	Te-Kd-trial-3	HCl (mol/L)	ave Te-Kd	std dev
97	87	123	0.5	103	18
87	68	80	1.0	78	10
70	57	60	1.5	62	7
73	77	66	2.0	72	5
153	160	155	2.5	156	4
325	326	293	3.0	314	19
805	880	816	3.5	833	40
1332	1461	1376	4.0	1390	66
1433	1425	1523	4.5	1460	54
1380	1492	1327	5.0	1400	85
1328	1266	1218	5.5	1271	55
990	1022	1125	6.0	1046	70

Appendix 7.107 [Te-K_D values for groundwater (4 mL-spike), for Fig. 3.15]

Te-Kd-trial-1	Te-Kd-trial-2	Te-Kd-trial-3	HCl (mol/L)	ave Te-Kd	std dev
128	115	130	0.5	124	8
93	83	88	1.0	88	5
79	68	83	1.5	77	8
103	76	84	2.0	88	14
117	129	111	2.5	119	9
467	384	421	3.0	424	41
835	967	896	3.5	899	66
1420	1420	1469	4.0	1436	29
1385	1509	1629	4.5	1508	122
1327	1431	1534	5.0	1430	104
1339	1218	1147	5.5	1235	97
1132	1025	930	6.0	1029	101

Appendix 7.108 [Te-K_D values for groundwater (5 mL-spike), for Fig. 3.15]

Te-Kd-trial-1	Te-Kd-trial-2	Te-Kd-trial-3	HCl (mol/L)	ave Te-Kd	std dev
134	122	120	0.5	125	8
75	78	86	1.0	80	6
76	72	68	1.5	72	4
96	82	85	2.0	88	7
162	169	156	2.5	162	7
369	404	429	3.0	401	30
743	820	882	3.5	815	70
1119	1020	922	4.0	1020	99
1272	1308	1212	4.5	1264	48
1398	1130	1032	5.0	1187	189
1037	828	1129	5.5	998	155
675	827	790	6.0	764	79

Appendix 7.109 [Fig. 3.15 K_D values of tellurium in presence of groundwater, 'GW' stands for groundwater]

HCl (mol/L)	Te + 0 mL	Te + 2 mL	Te + 3 mL	Te + 4 mL	Te + 5 mL
0.5	109	106	103	124	125
1.0	97	70	78	88	80
1.5	68	71	62	77	72
2.0	77	79	72	88	88
2.5	133	139	156	119	162
3.0	276	342	314	424	401
3.5	512	880	833	899	815
4.0	843	1293	1390	1436	1020
4.5	959	1480	1460	1508	1264
5.0	1009	1468	1400	1430	1187
5.5	898	1285	1271	1235	998
6.0	695	1078	1046	1029	764
ave	473	691	682	705	581

std dev	386	606	602	606	473

Appendix 7.110 [Fig. 3.16 A comparison of on the K_D values of tin and tellurium in presence of groundwater]

GW-mL	Gw-Sn-Kd	GW-Te-Kd
0	12859	473
2	17622	691
3	22010	682
4	17497	705
5	18419	581

Appendix 7.111 [Table 3.1: K_D values of tin and tellurium in presence of surface water]

Surface water	Cl^-: 1 mL = 0.02998 mg	Cl^-: mg/L	SO_4^{2-}: 1 mL = 0.00978	SO_4^{2-}: mg/L
2.0 mL	0.06/ 10 mL	5.99	0.02/ 10 mL	1.96
3.0 mL	0.09/ 10 mL	8.99	0.03/ 10 mL	2.93
4.0 mL	0.12/ 10 mL	11.99	0.04/ 10 mL	3.91
5.0 mL	0.15/ 10 mL	14.99	0.05/ 10 mL	4.89

SW-K_D

Cl^- (mg)	SO_4^{2-} (mg)	Sn-Kd
0.001	0.001	23274
5.99	1.96	29546
8.99	2.93	27257
11.99	3.91	25705
14.99	4.89	20670

Appendix 7.112 [Table 3.2: K_D values of tin and tellurium in presence of groundwater]

Groundwater	Cl^-: 1 mL = 0.07142 mg	Cl^-: mg/L	SO_4^{2-}: 1 mL = 0.06995	SO_4^{2-}: mg/L
2.0 mL	0.14284/ 10 mL	14.28	0.1399/ 10 mL	13.99
3.0 mL	0.21426/ 10 mL	21.43	0.20985/ 10 mL	20.99
4.0 mL	0.28568/ 10 mL	28.57	0.2798/ 10 mL	27.98
5.0 mL	0.3571/ 10 mL	35.71	0.34975/ 10 mL	34.98

GW-K_D

Cl^- (mg)	SO_4^{2-} (mg)	Sn-Kd
0.001	0.001	12858.53
14.28	13.99	17621.70
21.43	20.99	22009.95
28.57	27.98	17496.57
35.71	34.98	18419.44

Appendix 7.113 [Percent Sn-adsorption with standard Cl^--and SO_4^{2-}-spikes, for Fig. 3.17]

Types of spike	% Sn-trial-1	% Sn-trial-2	% Sn-trial-3	ave % Sn ads	std dev
Sn	98.816	98.74	98.68	98.74	0.07
Sn + Cl^-	99.03	99.12	99.20	99.12	0.09
Sn + SO_4^{2-}	99.62	99.90	99.27	99.59	0.32
Sn + Cl^- + SO_4^{2-}	99.14	99.28	99.21	99.21	0.07
			ave	99.17	

std dev	0.35	

Appendix 7.114 [Percent Te-adsorption with standard Cl^-- and SO_4^{2-}-spikes, for Fig. 3.17]

Types of spike	% Te-trial-1	% Te-trial-2	% Te-trial-3	ave % Te ads	std dev
Te	58.74	55.89	59.20	57.94	1.80
Te + Cl^-	60.55	63.93	64.64	63.04	2.18
Te + SO_4^{2-}	61.88	61.99	59.42	61.09	1.45
Te + Cl^- + SO_4^{2-}	70.02	65.78	67.78	67.87	2.12
			ave	62.48	
			std dev	4.15	

Appendix 7.115 [Fig. 3.17 Adsorptions of tin and tellurium in 3.0 mol L^{-1} of HCl solution in presence of chloride and sulfate ions]

Types of spike	% Sn ads	% Te ads
Sn + 0	98.74	57.94
Sn + Cl^-	99.12	63.04
Sn + SO_4^{2-}	99.59	61.09
Sn + Cl^- + SO_4^{2-}	99.21	67.86
Ave	99.17	62.48
std dev	0.35	4.15

Appendix 7.116 [Percent Sn-desorption (0 Cl^- + 0 SO_4^{2-}-spike), for Fig. 3.18]

Sn + 0 spike

TRU, mg	% Sn-des-1	% Sn-des-2	% Sn-des-3	HF (mol/L)	Ave % Sn desorp	std dev
100	81.90	79.72	69.64	0.50	77.09	6.54
100	78.44	75.31	82.89	1.0	78.88	3.81
100	77.69	84.67	75.87	2.0	79.41	4.65
100	78.58	86.62	73.88	3.0	79.69	6.44
100	74.86	96.74	69.15	4.0	80.25	14.56
100	83.98	84.52	75.62	5.0	81.37	4.99
100	86.02	81.61	84.76	6.0	84.13	2.27
				ave	80.12	
				std dev	2.20	

Appendix 7.117 [Percent Sn-desorption (Cl^--spike), for Fig. 3.18]

Sn + Cl^-

TRU, mg	% Sn-des-1	% Sn-des-2	% Sn-des-3	HF (mol/L)	Ave % Sn desorp	std dev
100	74.39	66.60	69.86	0.50	70.28	3.92
100	71.79	75.72	72.48	1.0	73.33	2.10
100	74.18	77.55	71.85	2.0	74.52	2.87
100	69.55	83.12	81.30	3.0	77.99	7.36
100	94.61	73.29	74.78	4.0	80.89	11.90
100	80.73	80.35	84.80	5.0	81.96	2.47
100	86.96	81.35	85.39	6.0	84.57	2.89
				ave	77.65	
				std dev	5.16	

Appendix 7.118 [Percent Sn-desorption (SO_4^{2-}-spike), for Fig. 3.18]

Sn + SO_4^{2-}

TRU, mg	% Sn-des-1	% Sn-des-2	% Sn-des-3	HF (mol/L)	Ave % Sn desorp	std dev
100	82.53	77.13	78.33	0.50	79.33	2.83
100	71.45	83.96	85.02	1.0	80.14	7.55
100	81.43	80.84	83.84	2.0	82.04	1.59
100	89.80	68.13	83.70	3.0	80.54	11.18
100	80.33	88.70	86.85	4.0	85.30	4.40
100	88.15	86.10	90.38	5.0	88.21	2.14
100	97.44	95.92	93.31	6.0	95.56	2.09
				ave	84.45	
				std dev	5.83	

Appendix 7.119 [Percent Sn-desorption (Cl^- + SO_4^{2-}-spike), for Fig. 3.18]

Sn + Cl^- + SO_4^{2-}

TRU, mg	% Sn-des-1	% Sn-des-2	% Sn-des-3	HF (mol/L)	Ave % Sn desorp	std dev
100	86.87	74.88	74.20	0.50	78.65	7.13
100	81.74	79.45	81.45	1.0	80.88	1.24
100	79.74	75.68	91.18	2.0	82.20	8.04
100	75.57	92.05	90.87	3.0	86.17	9.19
100	93.98	95.04	93.00	4.0	94.01	1.02
100	90.44	97.94	80.07	5.0	89.48	8.97
100	91.40	85.09	91.60	6.0	89.36	3.70
				ave	85.82	
				std dev	5.51	

Appendix 7.120 [Fig. 3.18 The desorption of tin by hydrofluoric acid treated at concentrations of 0.50 to 6.0 mol L^{-1}]

Sn desorption (%)	% des	% des	% des	% des
HF (mol/L)	Sn + 0	Sn + Cl^-	Sn + SO_4^{2-}	Sn + Cl^- + SO_4^{2-}
0.5	77.09	70.28	79.33	78.65
1.0	78.88	73.33	80.14	80.88
2.0	79.41	74.52	82.04	82.20
3.0	79.69	77.99	80.54	86.17
4.0	80.25	80.89	85.30	94.01
5.0	81.37	81.96	88.21	89.48
6.0	84.13	84.57	95.56	89.36
ave	80.12	77.65	84.45	85.82
std dev	2.20	5.16	5.83	5.51

Appendix 7.121 [Percent Te-desorption (0 Cl^- + 0 SO_4^{2-}-spike), for Fig. 3.19]

Te + 0 spike

TRU, mg	% Te-des-1	% Te-des-2	% Te-des-3	HF (mol/L)	Ave % Te desorp	std dev
100	13.93	19.19	11.53	0.50	14.88	3.92
100	18.14	18.44	19.26	1.0	18.61	0.58
100	25.50	15.06	20.69	2.0	20.41	5.23
100	19.11	24.37	23.62	3.0	22.37	2.84
100	19.34	24.97	23.17	4.0	22.49	2.88
100	17.84	23.47	23.92	5.0	21.74	3.39
100	26.10	26.25	26.10	6.0	26.15	0.09
				ave	20.95	
				std dev	3.53	

Appendix 7.122 [Percent Te-desorption (Cl^--spike), for Fig. 3.19]

Te + Cl^-

TRU, mg	% Te-des-1	% Te-des-2	% Te-des-3	HF (mol/L)	Ave % Te desorp	std dev
100	16.33	13.67	17.66	0.50	15.89	2.03
100	20.33	16.88	16.64	1.0	17.95	2.06
100	20.71	20.63	19.23	2.0	20.19	0.83
100	20.64	22.20	20.25	3.0	21.03	1.04
100	23.30	22.91	20.09	4.0	22.10	1.75
100	24.79	27.53	25.49	5.0	25.94	1.42
100	25.02	21.89	25.81	6.0	24.24	2.07
				ave	21.05	
				std dev	3.47	

Appendix 7.123 [Percent Te-desorption (SO_4^{2-}-spike), for Fig. 3.19]

Te + SO_4^{2-}

TRU, mg	% Te-des-1	% Te-des-2	% Te-des-3	HF (mol/L)	Ave % Te desorp	std dev
100	15.91	22.18	19.42	0.50	19.17	3.14
100	20.91	16.21	19.79	1.0	18.97	2.46
100	22.18	20.69	18.15	2.0	20.34	2.04
100	21.51	23.08	24.57	3.0	23.05	1.53
100	25.69	29.35	26.66	4.0	27.23	1.90
100	28.00	29.72	23.82	5.0	27.18	3.03
100	33.68	28.30	30.47	6.0	30.82	2.70
				ave	23.82	
				std dev	4.65	

Appendix 7.124 [Percent Te-desorption (Cl^- + SO_4^{2-}-spike), for Fig. 3.19]

Te + Cl^- + SO_4^{2-}

TRU, mg	% Te-des-1	% Te-des-2	% Te-des-3	HF (mol/L)	Ave % Te desorp	std dev
100	12.30	12.37	11.08	0.50	11.91	0.73
100	13.59	13.59	12.22	1.0	13.13	0.79
100	17.82	18.46	10.53	2.0	15.60	4.40
100	18.10	17.96	13.73	3.0	16.60	2.48
100	23.66	14.95	14.88	4.0	17.83	5.05
100	23.27	20.18	16.74	5.0	20.06	3.26
100	24.05	22.48	20.40	6.0	22.31	1.83
				ave	16.78	
				std dev	3.67	

Appendix 7.125 [Fig. 3.19 The desorption of tellurium by hydrofluoric acid treated at concentrations of 0.50 to 6.0 mol L^{-1}]

Te desorption (%)	% des	% des	% des	% des
HF (mol/L)	Te + 0	Te + Cl^-	Te + SO_4^{2-}	Te + Cl^- + SO_4^{2-}
0.5	14.88	15.89	19.17	11.91
1.0	18.61	17.95	18.97	13.13
2.0	20.41	20.19	20.34	15.60
3.0	22.37	21.03	23.05	16.60
4.0	22.49	22.10	27.23	17.83
5.0	21.74	25.94	27.18	20.06
6.0	26.15	24.24	30.82	22.31
ave	20.95	21.05	23.82	16.78
std dev	3.53	3.47	4.65	3.67

Appendix 7.126 [Percent Sn-adsorption with surface water, for Fig. 3.20]

Spikes	% Sn-ads-1	% Sn-ads-2	% Sn-ads-3	ave % Sn ads	std dev
0 mL	98.31	99.45	99.12	98.96	0.59
2 mL	99.24	97.45	99.20	99.48	1.02
4 mL	99.66	99.93	98.48	99.36	0.77
6 mL	99.35	99.46	99.35	99.39	0.06

Appendix 7.127 [Percent Te-adsorption with surface water, for Fig. 3.20]

Spikes	% Te-ads-1	% Te-ads-2	% Te-ads-3	ave % Te ads	std dev
0 mL	60.40	59.92	63.87	61.40	2.15
2 mL	64.73	64.06	59.45	62.74	2.88
4 mL	60.06	69.44	61.59	63.70	5.03
6 mL	68.66	59.32	67.77	65.25	5.15

Appendix 7.128 [Fig. 3.20 The adsorptions of tin and tellurium in 3.0 mol L^{-1} of HCl solution in presence of surface water]

Surface water		
Spike	**% Sn ads**	**% Te ads**
0 mL	98.96	61.40
2 mL	99.48	62.74
4 mL	99.36	63.70
6 mL	99.39	65.25
ave	99.29	63.27
std dev	0.23	1.62

Appendix 7.129 [Percent Sn-desorption with surface water (0 mL-spike), for Fig. 3.21]

0 mL spike

TRU, mg	% Sn-des-1	% Sn-des-2	% Sn-des-3	HF (mol/L)	Ave % Sn desorp	std dev
100	76.55	75.72	66.02	0.50	72.76	5.85
100	76.93	76.10	73.74	1.0	75.59	1.66
100	90.83	90.40	89.97	2.0	90.40	0.43
100	89.61	85.42	94.26	3.0	89.76	4.42
100	93.91	89.39	87.49	4.0	90.26	3.30
100	96.62	91.76	94.76	5.0	94.38	2.45
100	95.94	93.25	96.02	6.0	95.07	1.58
				ave	86.89	
				std dev	8.96	

Appendix 7.130 [Percent Sn-desorption with surface water (2 mL-spike), for Fig. 3.21]

2 mL spike

TRU, mg	% Sn-des-1	% Sn-des-2	% Sn-des-3	HF (mol/L)	Ave % Sn desorp	std dev
100	83.86	79.04	69.27	0.50	77.39	7.43
100	91.18	85.08	67.81	1.0	81.36	12.12
100	93.55	86.78	71.14	2.0	83.82	11.49
100	88.67	82.30	83.52	3.0	84.83	3.38
100	86.80	92.57	77.04	4.0	85.47	7.85
100	89.94	91.56	83.96	5.0	88.49	4.00
100	93.64	87.43	84.97	6.0	88.68	4.47
				ave	84.29	
				std dev	3.98	

Appendix 7.131 [Percent Sn-desorption with surface water (4 mL-spike), for Fig. 3.21]

TRU, mg	% Sn-des-1	% Sn-des-2	% Sn-des-3	HF (mol/L)	Ave % Sn desorp	std dev
100	83.64	78.76	79.98	0.50	80.79	2.54
100	72.96	85.10	86.39	1.0	81.48	7.41
100	80.89	94.16	85.19	2.0	86.75	6.77
100	91.70	69.56	95.68	3.0	85.65	14.07
100	92.03	80.36	88.47	4.0	86.95	5.98
100	91.59	97.49	91.86	5.0	93.65	3.33
100	92.49	97.94	95.28	6.0	95.24	2.72
				ave	87.22	

				std dev	5.52	

Appendix 7.132 [Percent Sn-desorption with surface water (6 mL-spike), for Fig. 3.21]

6 mL spike

TRU, mg	% Sn-des-1	% Sn-des-2	% Sn-des-3	HF (mol/L)	Ave % Sn desorp	std dev
100	67.67	87.21	76.60	0.50	77.16	9.78
100	64.39	92.34	85.15	1.0	80.63	14.51
100	72.60	87.93	81.85	2.0	80.79	7.72
100	95.84	82.63	73.62	3.0	84.03	11.18
100	84.36	85.31	83.48	4.0	84.38	0.92
100	89.18	87.91	88.87	5.0	88.65	0.66
100	82.04	93.25	92.22	6.0	89.17	6.20
				ave	83.54	
				std dev	4.39	

Appendix 7.133 [Fig. 3.21 The desorption of tin by hydrofluoric acid (0.50 to 6.0 mol L^{-1}) in presence of surface water]

% Sn desorption HF (mol/L)	% Sn des Sn + 0 mL	% Sn des Sn + 2 mL	% Sn des Sn + 4 mL	% Sn des Sn + 6 mL
0.50	72.76	77.39	80.79	77.16
1.0	75.59	81.36	81.48	80.63
2.0	90.40	83.82	86.75	80.79
3.0	89.76	84.83	85.65	84.03
4.0	90.26	85.47	86.95	84.38
5.0	94.38	88.49	93.65	88.65
6.0	95.07	88.68	95.24	89.17
ave	86.89	84.29	87.22	83.54
std dev	8.96	3.98	5.52	4.39

Appendix 7.134 [Percent Te-desorption with surface water (0 mL-spike), for Fig. 3.22]

0 mL spike

TRU, mg	% Te-des-1	% Te-des-2	% Te-des-3	HF (mol/L)	Ave % Te desorp	std dev
100	3.84	9.07	6.45	0.50	6.46	2.61
100	8.02	13.32	11.14	1.0	10.83	2.66
100	15.34	14.96	20.56	2.0	16.95	3.13
100	18.99	24.22	23.47	3.0	22.23	2.83
100	19.22	24.81	23.02	4.0	22.35	2.86
100	17.72	23.32	23.77	5.0	21.60	3.37
100	25.93	26.08	25.93	6.0	25.98	0.09
				ave	18.06	
				std dev	7.06	

Appendix 7.135 [Percent Te-desorption with surface water (2 mL-spike), for Fig. 3.22]

2 mL spike

TRU, mg	% Te-des-1	% Te-des-2	% Te-des-3	HF (mol/L)	Ave % Te desorp	std dev
100	5.07	4.55	7.33	0.50	5.65	1.48
100	3.84	10.59	4.14	1.0	6.19	3.81
100	7.97	7.90	12.81	2.0	9.56	2.81
100	10.13	15.61	13.77	3.0	13.17	2.79
100	16.64	11.28	14.62	4.0	14.18	2.71
100	13.05	10.63	18.71	5.0	14.13	4.15
100	18.27	15.32	19.01	6.0	17.53	1.95
				ave	11.49	
				std dev	4.46	

Appendix 7.136 [Percent Te-desorption with surface water (4 mL-spike), for Fig. 3.22]

4 mL spike

TRU, mg	% Te-des-1	% Te-des-2	% Te-des-3	HF (mol/L)	Ave % Te desorp	std dev
100	5.82	11.94	9.24	0.50	9.00	3.06
100	10.70	6.12	9.61	1.0	8.81	2.40
100	11.94	10.48	8.01	2.0	10.14	1.99
100	11.28	12.81	14.27	3.0	12.79	1.49
100	15.36	18.93	16.31	4.0	16.86	1.85
100	17.62	19.29	13.54	5.0	16.82	2.96
100	23.15	17.91	20.02	6.0	20.36	2.64
				ave	13.54	
				std dev	4.53	

Appendix 7.137 [Percent Te-desorption with surface water (6 mL-spike), for Fig. 3.22]

6 mL spike

TRU, mg	% Te-des-1	% Te-des-2	% Te-des-3	HF (mol/L)	Ave % Te desorp	std dev
100	12.86	12.93	11.58	0.50	12.46	0.76
100	14.21	14.21	12.78	1.0	13.73	0.82
100	18.63	19.31	19.38	2.0	19.11	0.41
100	18.93	18.78	14.36	3.0	17.36	2.60
100	14.28	15.63	15.56	4.0	15.16	0.76
100	24.33	21.11	17.51	5.0	20.98	3.41
100	25.16	23.51	21.33	6.0	23.33	1.92
				ave	17.45	
				std dev	3.95	

Appendix 7.138 [Fig. 3.22 The desorption of tellurium by hydrofluoric acid (0.50 to 6.0 mol L^{-1}) in presence of surface water]

% Te desorption HF (mol/L)	% Te des Te + 0 mL	% Te des Te + 2 mL	% Te des Te + 4 mL	% Te des Te + 6 mL
0.50	6.46	5.65	9.00	12.46
1.0	10.83	6.19	8.81	13.73
2.0	16.95	9.56	10.14	19.11
3.0	22.23	13.17	12.79	17.36
4.0	22.35	14.18	16.86	15.16
5.0	21.60	14.13	16.82	20.98
6.0	25.98	17.53	20.36	23.33
ave	18.06	11.49	13.54	17.45
std dev	7.06	4.46	4.53	3.95

Appendix 7.139 [Percent Sn-adsorption with groundwater, for Fig. 3.23]

Spikes	% Sn-ads-1	% Sn-ads-2	% Sn-ads-3	ave % Sn ads	std dev
0 mL	98.82	98.74	98.68	98.74	0.07
2 mL	99.03	99.12	99.20	99.12	0.09
4 mL	99.62	99.90	99.27	99.59	0.32
6 mL	99.14	99.28	99.21	99.21	0.07
			ave	99.17	
			std dev	0.35	

Appendix 7.140 [Percent Te-adsorption with groundwater, for Fig. 3.23]

Spikes	% Te-ads-1	% Te-ads-2	% Te-ads-3	ave % Te ads	std dev
0 mL	58.74	55.88	59.20	57.94	1.80
2 mL	60.55	63.93	64.64	63.04	2.18
4 mL	61.88	61.97	59.42	61.09	1.45
6 mL	70.02	65.78	67.77	67.86	2.12
			ave	62.48	
			std dev	4.15	

Appendix 7.141 [Fig. 3.23 The adsorptions of tin and tellurium in 3.0 mol L^{-1} of HCl solution in presence of groundwater]

Spikes	% Sn ads	% Te ads
0 mL	98.74	57.94
2 mL	99.12	63.04
4 mL	99.59	61.09
6 mL	99.21	67.86
ave	99.17	62.48
std dev	0.35	4.15

Appendix 7.142 [Percent Sn-desorption with groundwater (0 mL-spike), for Fig. 3.24]

0 mL spike

TRU, mg	% Sn-des-1	% Sn-des-2	% Sn-des-3	HF (mol/L)	Ave % Sn desorp	std dev
100	70.75	70.77	69.56	0.50	70.36	0.69
100	82.05	61.19	72.84	1.0	72.02	10.46
100	80.39	79.43	68.01	2.0	75.94	6.88
100	70.74	86.62	80.38	3.0	79.25	8.00
100	93.66	80.31	72.24	4.0	82.07	10.82
100	95.21	73.25	89.38	5.0	85.95	11.38
100	82.32	95.25	92.61	6.0	90.06	6.84
				ave	79.38	
				std dev	7.21	

Appendix 7.143 [Percent Sn-desorption with groundwater (2 mL-spike), for Fig. 3.24]

2 mL spike

TRU, mg	% Sn-des-1	% Sn-des-2	% Sn-des-3	HF (mol/L)	Ave % Sn desorp	std dev
100	72.91	84.27	79.28	0.50	78.82	5.69
100	73.11	93.83	81.65	1.0	82.86	10.41
100	76.69	89.71	71.53	2.0	79.31	9.37
100	78.43	86.85	84.46	3.0	83.24	4.34
100	89.72	83.03	87.00	4.0	86.58	3.36
100	92.25	82.72	86.86	5.0	87.28	4.78
100	83.82	86.35	92.28	6.0	87.48	4.34
				ave	83.65	
				std dev	3.64	

Appendix 7.144 [Percent Sn-desorption with groundwater (4 mL-spike), for Fig. 3.24]

4 mL spike

TRU, mg	% Sn-des-1	% Sn-des-2	% Sn-des-3	HF (mol/L)	Ave % Sn desorp	std dev
100	64.30	71.94	82.96	0.50	73.07	9.38
100	82.20	75.30	84.60	1.0	80.70	4.83
100	79.89	76.22	85.27	2.0	80.46	4.55
100	88.48	75.63	82.01	3.0	82.04	6.43
100	77.49	84.30	92.64	4.0	84.81	7.59
100	82.31	84.80	88.99	5.0	85.37	3.38
100	91.09	84.56	87.71	6.0	87.78	3.27
				ave	82.03	
				std dev	4.77	

Appendix 7.145 [Percent Sn-desorption with groundwater (6 mL-spike), for Fig. 3.24]

6 mL spike

TRU, mg	% Sn-des-1	% Sn-des-2	% Sn-des-3	HF (mol/L)	Ave % Sn desorp	std dev
100	65.08	63.81	76.20	0.50	68.36	6.82
100	76.83	69.41	75.29	1.0	73.84	3.91
100	69.62	79.18	85.66	2.0	78.15	8.07
100	82.81	85.12	74.89	3.0	80.94	5.37
100	82.91	78.30	95.01	4.0	85.41	8.63
100	88.41	78.41	92.49	5.0	86.44	7.25
100	84.38	88.99	91.03	6.0	88.13	3.41
				ave	80.18	
				std dev	7.24	

Appendix 7.146 [Fig. 3.24 The desorption of tin by hydrofluoric acid (0.50 to 6.0 mol L^{-1}) in presence of groundwater]

Desorption HF (mol/L)	% Sn desorp Sn + 0 mL	% Sn desorp Sn + 2 mL	% Sn desorp Sn + 4 mL	% Sn desorp Sn + 6 mL
0.50	70.36	78.82	73.07	68.36
1.0	72.02	82.86	80.70	73.84
2.0	75.94	79.31	80.46	78.15
3.0	79.25	83.24	82.04	80.94
4.0	82.07	86.58	84.81	85.41
5.0	85.95	87.28	85.37	86.44
6.0	90.06	87.48	87.78	88.13
ave	79.38	83.65	82.03	80.18
std dev	7.21	3.64	4.77	7.24

Appendix 7.147 [Percent Te-desorption with groundwater (0 mL-spike), for Fig. 3.25]

0 mL spike

TRU, mg	% Te-des-1	% Te-des-2	% Te-des-3	HF (mol/L)	Ave % Te desorp	std dev
100	4.31	3.75	2.79	0.50	3.62	0.77
100	8.02	6.72	3.58	1.0	6.11	2.29
100	10.61	7.83	6.15	2.0	8.20	2.25
100	14.03	14.19	8.63	3.0	12.28	3.16
100	10.03	19.36	23.72	4.0	17.70	6.99
100	20.15	13.34	23.20	5.0	18.90	5.04
100	15.49	13.66	24.51	6.0	17.89	5.80
				ave	12.10	
				std dev	6.25	

Appendix 7.148 [Percent Te-desorption with groundwater (2 mL-spike), for Fig. 3.25]

2 mL spike

TRU, mg	% Te-des-1	% Te-des-2	% Te-des-3	HF (mol/L)	Ave % Te desorp	std dev
100	1.40	10.57	4.80	0.50	5.59	4.64
100	1.40	11.44	6.11	1.0	6.31	5.02
100	5.67	13.91	2.95	2.0	7.51	5.71
100	8.11	9.31	12.82	3.0	10.08	2.45
100	6.11	15.76	6.72	4.0	9.53	5.40
100	4.54	15.70	11.17	5.0	10.47	5.62
100	21.58	13.96	17.19	6.0	17.57	3.82
				ave	9.58	
				std dev	4.00	

Appendix 7.149 [Percent Te-desorption with groundwater (4 mL-spike), for Fig. 3.25]

4 mL spike

TRU, mg	% Te-des-1	% Te-des-2	% Te-des-3	HF (mol/L)	Ave % Te desorp	std dev
100	2.71	6.35	3.75	0.50	4.27	1.88
100	3.92	8.47	4.16	1.0	5.52	2.56
100	4.70	4.78	12.12	2.0	7.20	4.26
100	7.67	13.33	12.99	3.0	11.33	3.17
100	10.11	12.98	14.77	4.0	12.62	2.35
100	17.21	20.39	19.96	5.0	19.19	1.73
100	23.76	24.37	29.09	6.0	25.74	2.92
				ave	12.27	
				std dev	7.81	

Appendix 7.150 [Percent Te-desorption with groundwater (6 mL-spike), for Fig. 3.25]

6 mL spike

TRU, mg	% Te-des-1	% Te-des-2	% Te-des-3	HF (mol/L)	Ave % Te desorp	std dev
100	2.22	2.73	3.21	0.50	2.72	0.49
100	3.48	4.00	3.74	1.0	3.74	0.26
100	4.28	4.30	4.32	2.0	4.30	0.02
100	5.68	4.92	7.59	3.0	6.07	1.38
100	11.47	3.14	3.82	4.0	6.14	4.63
100	14.94	14.28	18.60	5.0	15.94	2.33
100	21.25	21.10	25.59	6.0	22.64	2.55
				ave	8.79	
				std dev	7.53	

Appendix 7.151 [Fig. 3.25 The desorption of tellurium by hydrofluoric acid (0.50 to 6.0 mol L^{-1}) in presence of groundwater]

Desrption HF (mol/L)	% Te desorp Te + 0 mL	% Te desorp Te + 2 mL	% Te desorp Te + 4 mL	% Te desorp Te + 6 mL
0.50	3.62	5.59	4.27	2.72
1.0	6.11	6.31	5.52	3.74
2.0	8.20	7.51	7.20	4.30
3.0	12.28	10.08	11.33	6.07
4.0	17.70	9.53	12.62	6.14
5.0	18.90	10.47	19.19	15.94
6.0	17.89	17.57	25.74	22.64
ave	12.10	9.58	12.27	8.79
std dev	6.25	4.00	7.81	7.53

Appendix 7.152 [Fig. 3.26 A comparison on the desorption performance of tin in presence of field water, 'SW' stands for surface water, and 'GW' for groundwater]

% Sn desorption Spikes	Surface water % Sn desorp	Groundwater % Sn desorp
Sn + 0 mL	86.89	79.38
Sn + 2 mL	84.29	83.65
Sn + 4 mL	87.22	82.03
Sn + 6 mL	83.54	80.18
ave	85.48	81.31
std dev	1.84	1.92

Appendix 7.153 [Fig. 3.27 A comparison on the desorption profile of tellurium in presence of field water, 'SW' stands for surface water, and 'GW' for groundwater]

% Te desorption	Surface water	Groundwater
Te + 0 mL	18.06	12.09
Te + 2 mL	11.49	9.58
Te + 4 mL	13.54	12.27
Te + 6 mL	17.45	8.79
ave	15.13	10.68
std dev	315%	176%

Appendix 7.154 [Limit of detection (LOD) for ICP- MS in the detection of Sn]

Sample ID	Sn CPS	Blk CPS	Real CPS	Sn slope	Sn ppb	Ave Sn ppb	std dev	3*sd	LOD-ppb
P1	**122.23**	0.00	122.23	15302	0.008	0.008	0.001	0.004	0.004
P2	**137.04**	0.00	137.04	15302	0.009				
P3	**133.33**	0.00	133.33	15302	0.008				
P4	**148.15**	0.00	148.15	15302	0.009				
P5	**151.85**	0.00	151.85	15302	0.009				
P6	**137.04**	0.00	137.04	15302	0.008				
P7	**96.30**	0.00	96.30	15302	0.006				
P8	**118.52**	0.00	118.52	15302	0.008				
P9	**140.75**	0.00	140.75	15302	0.009				
P10	**92.597**	0.00	92.597	15302	0.006				

Appendix 7.155 [Limit of detection (LOD) for ICP-MS in the detection of Te]

Sample ID	Te CPS	Blk CPS	Real CPS	Te slope	Te ppb	Ave Te ppb	std dev	3*sd	LOD-ppb
P1	**33.33**	0.00	33.33	1019	0.032	0.029	0.015	0.046	0.046
P2	25.93	0.00	25.93	1019	0.025				
P3	25.92	0.00	25.92	1019	0.025				
P4	29.63	0.00	29.63	1019	0.029				
P5	18.52	0.00	18.52	1019	0.018				
P6	14.81	0.00	14.81	1019	0.015				
P7	25.93	0.00	25.93	1019	0.025				
P8	14.81	0.00	14.81	1019	0.015				
P9	44.45	0.00	44.45	1019	0.044				
P10	66.67	0.00	66.67	1019	0.065				

Appendix 7.156 [Concentration of Sn and Te in the field water detected by ICP-MS]

Sn + Te **Surface water** The limit of detection (LOD) for Sn was 0.004 ppb.

Sn	Sample ID	Sn CPS	Blk CPS	Real CPS	Sn slope	Sn ppb	Ave. Sn ppb
	P4 - SW1	**825.96**	0.00	825.96	16805	0.049	
	P5 - SW2	**633.36**	0.00	633.36	16805	0.038	0.04
	P6 - SW3	**629.65**	0.00	629.65	16805	0.038	

Te	Sample ID	Te CPS	Blk CPS	Real CPS	Te slope	Te ppb	Ave. Te ppb
	P4 - SW1	**7.41**	0.00	7.41	774.78	0.009	
	P5 - SW2	**0.00**	0.00	0.00	774.78	0.000	0.0064
	P6 - SW3	**7.41**	0.00	7.41	774.78	0.009	

Sn + Te **Groundwater** The limit of detection (LOD) for Te was 0.04611 ppb.

Sn	Sample ID	Sn CPS	Blk CPS	Real CPS	Sn slope	Sn ppb	Ave. Sn ppb
	P7 - GW1	**1111.17**	0.00	1111.17	16805	0.071	
	P8 - GW2	**1366.74**	0.00	1366.74	16805	0.080	0.07
	P9 - GW3	**1200.06**	0.00	1200.06	16805	0.072	

Te	Sample ID	Te CPS	Blk CPS	Real CPS	Te slope	Te ppb	Ave. Te ppb
	P7 - GW1	**7.41**	0.00	7.41	774.78	0.009	
	P8 - GW2	**11.11**	0.00	11.11	774.78	0.01	0.01
	P9 - GW3	**11.11**	0.00	11.11	774.78	0.01	

Chapter 8:

Manuscript for publication

Discovery, production and half-lives of tin isotopes†

Mohammad Majibur Rahman,[a,c] William Edward Kieser,[b] and Ian Doughlas Clark[*a]

[a)]Department of Earth and Environmental Sciences, University of Ottawa, Ontario, Canada, K1N 6N5
[b)]Department of Physics and A. E. Lalonde Accelerator Mass Spectrometry (AMS) Laboratory, Advanced Research Complex (ARC), University of Ottawa, Ontario, Canada, K1N 6N5
[a)]Department of Earth and Environmental Sciences, University of Ottawa, Ontario, Canada, K1N 6N5
[c)]Department of Environmental Sciences, Jahangirnagar University, Dhaka 1342, Bangladesh

Abstract
This article represents the production reaction and half-lives of fortyone tin isotopes identified so far, some common properties of elemental tin have also been tabulated.

Contents

Explanatory Notes
Atomic number: Z

Neutron number: N

Mass number: A

Reaction scheme: The reaction scheme of an isotope was reproduced either in the same order as appeared in the original paper, or the target material was kept within the parenthesis. The very similar reaction scheme of an isotope has been repeated to show the frequency of study over different time intervals.

……

*Corresponding author. Tel.: +1 613 562 5800 x 6834
Email address: idclark@uottawa.ca (I. D. Clark)

†Dedicated to Professor Robert Jack Cornett (1954–2017), Canada Research Chair in Radiochemistry and Environmental Health, University of Ottawa, for his life-long passion to science and innovation. Dr. Cornett died in Ottawa in a tragic bicycle accident while data collection for this article was in progress.

Half-lives: The unit of half-life was kept intact as appeared in the original article. Again, the same half-life value has been repeated to show the degree of consistencies among different study groups. The half-life symbol stands: *ns* for nano-second (10^{-9} s), *μs* for micro-second (10^{-6} s), *ms* for millisecond (10^{-3} s), *s* for second, *m* for minute, *h* for hour, *d* for day, *y* for year, and *ky* for kiloyear (10^3 y).

References: References were kept restricted, as much as possible, to peer review and open access journals; it will enable interested readers to look on the original paper for a greater detail. In the full reference list, an *et al.* follows the first name for more than six authors.

Abbreviations: ICAW, International Commission on Atomic Weight; IUPAC, Internatinal Union of Pure and Applied Chemistry; NMR, Nuclear Magnetic Resonance; RMS, Root Mean Square.

The symbol '#' represents not purely experimental value, additional explanatory notes are available in the source article.

Table 1: Some common properties of tin

Parameter	**Value**	Ref.
Atomic number, Z	50	[W14]
Atomic weight, observed in 1811 by Gay-Lussac	117.65	[B72]
Atomic weight, reported in 1991 by IUPAC	118.710(7)	[I12]
Abundance, relative to silicon = 1×10^6	3.6	[C5]
Boiling point	2270 °C	[W14]
Density, reported in 1902	7.300	[S44]
Electron affinity, eV	1.2	[M39]
Electronic configuration	$1s^2 2s^2 2p^6 3s^2 3p^6 3d^{10} 4s^2 4p^6 4d^{10} 5s^2 5p^2$	[W14]
Electronegativity	1.96	[A9]
First discovery of tin isotope, reported in 1922 by Aston	$^{119–122}$Sn, ^{124}Sn	[A30]
Last discovery of tin isotope, reported in 2015 by Lorusso	^{139}Sn	[L27]
Ionization potential, eV	7.3	[D15]
Melting point	231.9681 °C	[W14]
Main oxidation states	+2, +4	[C51]
Valence	2, 4	[O9]
Specific gravity	5.75 (gray), 7.31 (white)	[W14]
Number of isotopes	41	[W11]
Number of stable isotopes	10, the greatest number of stable isotopes among all elements in the periodic table	[L1], [R30], [Y10]
Self-conjugated nuclide ($N = Z$)	^{100}Sn$_{N = 50, Z = 50}$	[M34]
Doubly magic isotopes	^{100}Sn$_{N = 50}$, ^{132}Sn$_{N = 82}$	[B29]
Double shell closure	^{100}Sn ($N = 50$) & ^{132}Sn ($N = 82$)	[A8]
The most magic isotope among all heavy nuclide	^{132}Sn ($N = 82$)	[Z6]
Isotope with therapeutic application	^{117}Sn^m ($t_{½}$ = 13.6 d)	[L35]
Isotopes with spectroscopic applications	Stable isotopes possessing odd number of neutrons – ^{115}Sn, ^{117}Sn, ^{119}Sn (all three have a nuclear spin of one-half, $I = ½$)	[D32], [G55], [S81]
Isotope with the smallest mass unit	^{99}Sn (98.948530# ± 540#)	[W11]
Isotope with the largest mass unit	^{139}Sn (138.958730# ± 540#)	[W11]
Isotope with the shortest half-life	^{138}Sn (210 ± 45 ns)	[S52]
Isotope with the longest half-life	^{126}Sn ((2.5 ± 0.2) × 10^6 y))	[Z2]

Table 2: Nucleosynthesis of stable tin isotopes

Isotope $Z = 50$	N	A	*RMS* nuclear charge radii (*fm*)* [A15]	Produced by [L28]	Modes of nucleosynthesis [B83],[L2]	Abundance (per cent)		
						Aston (1936) [A33]	ICAW (1973) [B41]	IUPAC (1997) [R31]
^{112}Sn	62	112	4.5948	*p*–process	Proton capture	1.1	0.973(3)	0.97(1)
^{114}Sn	64	114	4.6099	*p*–process	Proton capture	0.8	0.652(3)	0.66(1)
^{115}Sn	65	115	4.6148	*p*–, *r*–, *s*–processes	Proton and neutron captures (rapid and slow)	0.4	0.359(3)	0.34(1)
^{116}Sn	66	116	4.6250	*s*–process	Slow neutron capture	15.5	14.532(36)	14.54(9)
^{117}Sn	67	117	4.6302	*r*–, *s*–processes	Slow and rapid neutron captures	9.1	7.675(23)	7.68(7)
^{118}Sn	68	118	4.6393	*r*–, *s*–processes	Slow and rapid neutron captures	22.5	24.218(36)	24.22(9)
^{119}Sn	69	119	4.6438	*r*–, *s*–processes	Slow and rapid neutron captures	9.8	8.583(13)	8.59(4)
^{120}Sn	70	120	4.6519	*r*–, *s*–processes	Slow and rapid neutron captures	28.5	32.590(33)	32.58(9)
^{122}Sn	72	122	4.6634	*r*–process	Rapid neutron capture	5.5	4.629(9)	4.63(3)
^{124}Sn	74	124	4.6735	*r*–process	Rapid neutron capture	6.8	5.789(18)	5.79(5)

*[1 fm = 10^{-15} m]

Table 3: Early events on the discovery of tin isotopes

Year	Events	Lab/City	Country
1922	Almost a century ago, Aston [**A30**], while working with tin tetramethide on the "Half Tone" photographic plate at the Cavendish Laboratory, surprisingly observed eight spectral lines on the newly installed (in 1919) [**A32**] mass-spectrograph which correspond atomic weights of 116 (c), 117 (f), 118 (b), 119 (e), 120 (a), 121 (h), 122 (g), and 124 (d). The letter in the bracket indicates intensity, corresponding to chemical weight of tin 118.7. He assumed that these lines might have been appeared due to the presence of tin isotopes. However, the assignment of the extremely faint line 121 (h) was uncertain.	Cambridge	UK
1924	Richards [**R26**], Harvard University, in the very first article in *Chemical Review* has organized these eight isotopes in decreasing order of abundances as 120, 118, 116, 124, 119, 117, 122 and 121.	Harvard	USA
1927	Aston [**A31**], Cavendish Laboratory, has mentioned that tin possesses at least 11 isotopes, which were arranged in order of intensity on the mass spectrogram as: 120, 118, 116, 124, 119, 117, 122, 121, 112, 114 and 115. In this publication, he has added three more isotopes (^{112}Sn, ^{114}Sn, ^{115}Sn) with the 1922-observation.	Cambridge	UK
1934	Fermi et al. [**F7**], in the Physical Laboratory at the University of Rome, have carried out an extensive study to observe the artificial radioactivity of more than sixty elements. The neutron bombardment on tin rather showed a very weak activity, presumably due to the presence of impurity. In the same time, they have mentioned the existence of 11 tin isotopes (112, 114, 115, 116, 117, 118, 119, 120, 121, 122, 124), but the abundances of two isotopes (118 and 120) have been reported as more than 20% of the element.	Rome	Italy

Table 3: Early events on the discovery of tin isotopes *(continued)*

Year	Events	Lab/City	Country
1934	Tolansky [**T16**], at Imperial College of Science, has mentioned the isotoic abundances of tin as (per cent): 112 (1.1), 114 (0.7), 115 (0.4), 116 (14.2), 117 (9.8), 118 (21.5), 119 (11.0), 120 (27.0), 121 (2.9), 122 (5.0) and 124 (6.2).	London	UK
1935	Amaldi et al. [**A10**], in the Physical Laboratory at the University of Rome, have also mentioned the same isotopic abundances of tin as reported by Fermi [**F7**].	Rome	Italy
1936	Aston [**A33**], Cavendish Laboratory, has arranged 10 tin isotopes with their abundances (in percent) as: ^{112}Sn (1.1), ^{114}Sn (0.8), ^{115}Sn (0.4), ^{116}Sn (15.5), ^{117}Sn (9.1), ^{118}Sn (22.5), ^{119}Sn (9.8), ^{120}Sn (28.5), ^{122}Sn (5.5), ^{124}Sn (6.8).	Cambridge	UK
1936	Livingood **[L22]**, at the University of California, has prepared ^{121}Sn isotope by the 5-MeV deuteron bombardment on a piece of antimony metal. The reaction follows as: $_{51}Sb^{123} + {}_1H^2 \rightarrow {}_{50}Sn^{121} + {}_2He^4$, $_{50}Sn^{121} \rightarrow {}_{51}Sb^{121} + e^-$	Berkeley	USA
1936	Livingood and Seaborg [**L23**], at the University of California, have carried out another experiment by the same 5-MeV deuteron bombardment on tin and have chemically analyzed the reaction products for transmutation into radioactive indium, tin and antimony isotopes.	Berkeley	USA
1937	Lawson and Cork [**L7**], at the University of Michigan, have reported the abundances of six tin isotopes (as percent): 112 (1.1), 114 (0.8), 115 (0.4), 116 (15.5), 117 (9.1), and 118 (22.5).	Michigan	USA
1938	Pool [**P27**], Ohi State University, has reported the abundances of five tin isotopes as 112 (1.1), 114 (0.8), 115 (0.4), 116 (15.5), and 117 (9.1 %)	Ohio	USA
1944	Seaborg [**S28**], University of California, in his article "Table of Isotopes" has reported 13 tin isotopes having atomic masses of 112–120, 122, 124–126; among these only one isotope (^{113}Sn) with definite elemental identity and mass assignment, one isotope (^{125}Sn) with definite elemental identity but probable mass assignment, one isotope (^{126}Sn) with definite elemental identity but no mass assignment, and one isotope (^{119}Sn) with no certain elemental identity. Also, it has been claimed that no sufficient evidence is available for ^{125}Sn isotope.	Berkeley	USA
1948	White and Cameron [**W19**], at Oak Ridge, have determined the isotopic abundances of tin, with a wider range of other elements, by mass spectrometric techniques, which follows as (in percent): 112 (0.90 ± 0.003), 114 (0.61 ± 0.01), 115 (0.35 ± 0.006), 116 (14.07 ± 0.08), 117 (7.54 ± 0.03), 118 (23.98 ± 0.03), 119 (8.62 ± 0.003), 120 (33.03 ± 0.12), 122 (4.78 ± 0.01), and 124 (6.11 ± 0.006).	Tennessee	USA
1950	Duckworth and Preston [**D28**], in the Scott Laboratory at Wesleyan University, on mass spectrographic analysis, have assigned the mass of ^{116}Sn isotope, along with other radionuclides, as 115.93794 ± 0.00058	Connecticut	USA
1962	Barber et al. [**B10**], at McMaster University, have presented the masses of seven tin isotopes: ^{116}Sn (115.901758), ^{117}Sn (116.902968), ^{118}Sn (117.901614), ^{119}Sn (118.903315), ^{120}Sn (119.902201), ^{122}Sn (121.903439), and ^{124}Sn (123.905264).	Hamilton	Canada
1962	The International Commission on Atomic Weights [C**4**] has reported ten isotopes of tin: ^{112}Sn, ^{114}Sn, ^{115}Sn, ^{116}Sn, ^{117}Sn, ^{118}Sn, ^{119}Sn, ^{120}Sn, ^{122}Sn & ^{124}Sn.	ICAW	***

Table 4: Early events of half-life measurement of tin isotopes.

Year	Isotope	Half-life	Events	Lab/City	Country
1934	Sn	Weak activity	Fermi et al. [**F7**], in the Physical Laboratory at the University of Rome, have carried out a thorough investigation to observe the artificial radioactivity on more than sixty elements. The neutron bombardment on tin, however, showed an extremely weak activity. They claimed that this might have caused due to impurity.	Rome	Italy
1936	Sn	8 m, 18 m	The half-life measurement of tin can be traced back to 1936, done by Naidu at the Birkbeck College [**N2**]. Geiger-Müller counters filled with air were irradiated with slow neutrons from a radon-beryllium source and the subsequent radioactivity of tin was measured. The slow neutron bombardment yields radiations of half-lives of 8 ± 2 minutes and 18 ± 2 minutes.	London	UK
1936	Sn	28 h	Livingood and Seaborg [**L23**], at the University of California, have irradiated tin with 5-MeV deuterons. The tin fraction showed an activity of 28 ± 2 hours.	Berkeley	USA
1937	Sn	47 m	Pool et al. [**P26**], at the University of Michigan, have observed that neutron bombardment on tin produces an activity of 47 minutes.	Michigan	USA
1937	^{123}Sn, ^{125}Sn	18 m 8 m	Grosse [**G40**] has tabulated all ten stable isotopes having mass number 112, 114, 115, 116, 117, 118, 119, 120, 122 and 124. Two radioactive isotopes, ^{123}Sn and ^{125}Sn, have been assigned a half-life of 18 minutes and 8 minutes, respectively.	Chicago	USA
1939	Sn	70 d	Livingood and Seaborg [**L24**], again with 5-MeV deuteron bombardment on tin at the University of California, have found that tin precipitate shows radioactivity with half-lives of 9 minutes, 40 minutes, 26 hours, 10 days, 70 days and at least 400 days. The 70-day activity, therefore, was assigned to ^{113}Sn, which decays to stable ^{113}In isotope by the *K*-electron capture.	Berkeley	USA
1949	^{124}Sn	~ 10^{16} y	Fireman [**F11**], at Princeton University, has reported that ^{124}Sn isotope with a double beta-decay produces a half-life of 0.4×10^{16} to 0.9×10^{16} years.	Princeton	USA
1949	^{111}Sn	35 m	Hinshaw and Pool [**H27**], at Ohio State University, have observed that the tin fraction of alpha-particle bombardment on cadmium produces ^{111}Sn isotope which decays with a half-life of 35.0 ± 0.5 minutes.	Ohio	USA
1949	^{125}Sn, ^{123}Sn, ^{121}Sn	9.8 m, 40 m, 1.1 d	Lee and Pool [**L9**], at Ohio State University, have observed that neutron bombardment on SnO_2 powder produces 9.8 minutes, 40 minutes, and 1.1-day activity, which are due to ^{125}Sn, ^{123}Sn and ^{121}Sn isotopes, respectively.	Ohio	USA
1949	^{108}Sn	4.5 h	Mallary and Pool [**M8**], at Ohio State University, have demonstrated that tin-108 isotope can be prepared by bombarding cadmium-106 isotope with 20-MeV alpha particles, which decays with a half-life of 4.5 h by *K*-electron capture.	Ohio	USA
1951	^{127}Sn, ^{126}Sn	1.5 h, 50 m	Barnes and Freedman [**B14**], at the Los Alamos Scientific Laboratory, have observed that the fission of ^{235}U produces 1.5-h Sn activity, which was assigned to ^{127}Sn. It was also assumed that the '70-min Sn' fraction consists, at least, a mixture of 50-min ^{126}Sn and 1.5-h ^{127}Sn. In 1962, Dropesky and Orth [**D25**] have reported that ^{126}Sn has a half-life of as high as 10^5 years.	Los Alamos	USA
1952	^{124}Sn	~ 0^{17} y	Fireman and Schwarzer [**F12**], at the Brookhaven National Laboratory, have re-investigated the double beta-decay of ^{124}Sn isotope and made conclusion that ^{124}Sn should possess a half-life of $(2–5) \times 10^{17}$ years.	New York	USA

Table 5: Nuclear properties of tin isotopes

Isotope $Z = 50$	N	A	**Atomic mass (amu)** [W11]		***RMS* nuclear charge radii (*fm*)** [A15]	**Mass excess (keV)** [W11]		**Binding energy per nucleon (keV)** [W11]		**Beta-decay energy (keV)** [W11]		
^{99}Sn	49	99	98.948530#	540#		–47940#	500#	8160#	5#	β^+	13430#	590#
^{100}Sn	50	100	99.938500	320		–57280	300	8253	3	β^+	7030	240
^{101}Sn	51	101	100.935260	320		–60310	300	8281.1	3.0	β^+	8310#	360#
^{102}Sn	52	102	101.930290	110		–64930	100	8324.4	1.0	β^+	5760	100
^{103}Sn	53	103	102.928100	82		–66970	70	8341.8	0.7	β^+	7660	70
^{104}Sn	54	104	103.923105	6		–71627	6	8383.91	0.06	β^+	4556	8
^{105}Sn	55	105	104.921268	4		–73338	4	8397.23	0.04	β^+	6303	11
^{106}Sn	56	106	105.916957	5		–77354	5	8432.04	0.05	β^+	3254	13
^{107}Sn	57	107	106.915714	6		–78512	5	8439.49	0.05	β^+	5052	12
^{108}Sn	58	108	107.911894	6	4.5605	–82070	5	8469.03	0.05	β^+	2050	10
^{109}Sn	59	109	108.911293	9	4.5679	–82630	8	8470.52	0.07	β^+	3859	9
^{110}Sn	60	110	109.907845	15	4.5785	–85842	14	8496.09	0.13	β^+	628	18
^{111}Sn	61	111	110.907741	6	4.5836	–85939	5	8493.13	0.05	β^+	2453	6
^{112}Sn	62	112	111.9048249	3	4.5948	–88655.06	0.29	8513.618	0.003			
^{113}Sn	63	113	112.9051758	17	4.6015	–88328.1	1.6	8506.811	0.014	β^+	1039.0	1.6
^{114}Sn	64	114	113.90278013	3	4.6099	–90559.723	0.029	8522.566				
^{115}Sn	65	115	114.903344697	16	4.6148	–90033.835	0.015	8514.069				
^{116}Sn	66	116	115.90174282	10	4.6250	–91525.97	0.01	8523.116	0.001			
^{117}Sn	67	117	116.9029540	5	4.6302	–90397.8	0.5	8509.611	0.004			
^{118}Sn	68	118	117.9016066	5	4.6393	–91652.9	0.5	8516.533	0.004			
^{119}Sn	69	119	118.9033112	8	4.6438	–90065.0	0.7	8499.449	0.006			
^{120}Sn	70	120	119.9022019	10	4.6519	–91098.4	0.9	8504.492	0.007	β^-	–2681	7
^{121}Sn	71	121	120.9042428	10	4.6566	–89197.3	1.0	8485.201	0.008	β^-	403.1	2.7
^{122}Sn	72	122	121.9034440	26	4.6634	–89941.3	2.4	8487.907	0.020	β^-	–1606	3
^{123}Sn	73	123	122.9057254	26	4.6665	–87816.2	2.4	8467.243	0.020	β^-	1407.9	2.7
^{124}Sn	74	124	123.9052767	11	4.6735	–88234.2	1.0	8467.421	0.008	β^-	–613.9	1.5
^{125}Sn	75	125	124.9077864	11	4.6765	–85896.4	1.0	8445.550	0.008	β^-	2359.9	2.6
^{126}Sn	76	126	125.907659	11	4.6833	–86015	10	8443.52	0.08	β^-	380	30
^{127}Sn	77	127	126.910390	11	4.6867	–83471	10	8420.56	0.08	β^-	3229	11
^{128}Sn	78	128	127.910507	19	4.6921	–83362	18	8416.98	0.14	β^-	1268	14
^{129}Sn	79	129	128.913482	19	4.6934	–80591	17	8392.82	0.13	β^-	4038	27
^{130}Sn	80	130	129.9139745	20	4.7019	–80132.2	1.9	8386.816	0.014	β^-	2153	14
^{131}Sn	81	131	130.917053	4	4.7078	–77265	4	8362.517	0.028	β^-	4717	4
^{132}Sn	82	132	131.9178239	21	4.7093	–76546.5	2.0	8354.872	0.015	β^-	3089	3
^{133}Sn	83	133	132.9239138	20		–70873.9	1.9	8310.088	0.014	β^-	8050	4
^{134}Sn	84	134	133.928680	3		–66434	3	8275.171	0.024	β^-	7587	4
^{135}Sn	85	135	134.934909	3		–60632	3	8230.687	0.023	β^-	9058	4
^{136}Sn	86	136	135.939990#	320#		–55900#	300#	8195#	2#	β^-	8610#	300#
^{137}Sn	87	137	136.946550#	430#		–49790#	400#	8149#	3#	β^-	10270#	400#
^{138}Sn	88	138	137.951840#	540#		–44860#	500#	8113#	4#	β^-	9360#	1180#
^{139}Sn	89	139	138.958730#	540#		–38440#	500#	8066#	4#	β^-	11350#	640#

Table 6: Discovery, production scheme and half-lives of tin isotopes.

Isotope	Year	Production scheme				Half-life value			
		Year	*Reaction*	*Principal method/condition*	*Ref*	*Year*	*Half-life*		*Ref*
^{99}Sn	2016	---	---	---	---	---	---	---	[C20]
		2016	$^{124}Xe^{52+}(Be)^{99}Sn$	Fragmentation	[C20]	1997	41.8 ms		[M33]
						2003	5# ms		[A42]
						2012	5# ms	>0.2 μs	[A43]
						2016	>760 ns		[C20]
						2017	5# ms	>0.2 μs	[A45]
						2017	>760 ns		[B82]
						2018	24 ms	4	[P7]
^{100}Sn	1994	---	---	---	---	---	---	---	[S19]
		1994	$^{112}Sn(^{58}Ni)^{100}Sn$	Fragmentation	[L11]	1994	0.53 s		[B80]
		1994	$^{124}Xe(Be)^{100}Sn$	Nuclear fragmentation	[S19]	1995	0.66 s		[S20]
		1995	$^{112}Sn(^{58}Ni)^{100}Sn$	Quasi-fragmentation	L12]	1995	0.66 s		[S21]
		1995	$^{112}Sn(^{nat}Ni)^{100}Sn$	Quasi-fragmentation	[R37]	1996	0.94 s		[K35]
		1995	$^{124}Xe(Be)^{100}Sn$	Nuclear fragmentation	[S20]	1997	1.1 s	0.4	[A41]
		1995	$^{124}Xe(Be)^{100}Sn$	Nuclear fragmentation	[S21]	1997	1.8113 s		[M33]
		1996	$^{50}Cr(^{58}Ni)^{100}Sn$	Fusion-evaporation	[C28]	1997	0.94		[S54]
		1996	$^{124}Xe(Be)^{100}Sn$	Fragmentation	[K35]	1997	0.94 s		[S74]
		1997	$^{50}Cr(^{58}Ni)^{100}Sn$	Fusion-evaporation	[L10]	2003	1.1 s	0.4	[A42]
		1997	$^{50}Cr(^{58}Ni)^{100}Sn$	Fusion-evaporation	[M25]	2005	0.94 s		[K7]
		1997	$^{124}Xe(Be)^{100}Sn$	High-energy projectile fragmentation	[S74]	2008	0.55 s		[B18]
		2001	$^{58}Ni(^{50}Cr)^{100}Sn$	Fusion-evaporation	[L19]	2008	1.0 s		[S56]
		2002	$^{112}Sn(Be)^{100}Sn$	Fragmentation	[F1]	2012	1.11 s	0.15	[A43]
		2005	$^{58}Ni(^{50}Cr, 2p6n)^{100}Sn$	Fusion-evaporation, ^{58}Ni beam on the ^{50}Cr target	[K7]	2012	1.16 s	0.20	[B26]
		2007	$^{104}Te(\alpha)^{100}Sn$	Alpha-decay	[M31]	2017	1.16 s	0.16	[A45]
		2008	$^{112}Sn(Be)^{100}Sn$	Nuclear fragmentation	[B18]				
		2008	$^{58}Ni(^{54}Fe)^{100}Sn$	Fusion-evaporation	[K48]				
		2012	$^{104}Te(\alpha)^{100}Sn$	Alpha-decay	[B30]				
		2012	$^{112}Sn(^{9}Be)^{100}Sn$	Fragmentation	[L26]				
		2014	$^{56}Ni(^{46}Ti, 2n)^{100}Sn$	Fusion-quasifission	[K2]				
		2014	$^{58}Ni(^{46}Ti, 4n)^{100}Sn$	Fusion-quasifission	[K2]				
		2014	$^{75}Rb(^{28}Si, p2n)^{100}Sn$	Fusion-quasifission	[K2]				
		2014	$^{58}Ni(^{50}Cr, \alpha4n)^{100}Sn$	Fusion-quasifission	[K2]				
		2014	$^{56}Ni(^{50}Cr, \alpha2n)^{100}Sn$	Fusion-quasifission	[K2]				
		2014	$^{56}Ni(^{58}Ni, ^{12}C2n)^{100}Sn$	Fusion-quasifission	[K2]				
		2014	$^{56}Ni(^{58}Ni, ^{14}C)^{100}Sn$	Fusion-quasifission	[K2]				

Table 6: Discovery, production scheme and half-lives of tin isotopes *(continued)*

Isotope	Year	Production scheme				Half-life value			
		Year	*Reaction*	*Principal method/condition*	*Ref*	*Year*	*Half-life*		*Ref*
^{100}Sn	1994	---	---	---	---	---	---	---	[S19]
		2014	^{58}Ni(^{58}Ni, ^{12}C4n)^{100}Sn	Fusion-quasifission	[K2]				
		2014	^{58}Ni(^{58}Ni, ^{14}C2n)^{100}Sn	Fusion-quasifission	[K2]				
		2014	^{72}Kr(^{40}Ca, ^{12}C)^{100}Sn	Fusion-quasifission	[K2]				
		2014	^{72}Kr(^{40}Ca, 3α)^{100}Sn	Fusion-quasifission	[K2]				
		2017	^{124}Xe(^{9}Be)^{100}Sn	Fragmentation reaction	[P6]				
^{101}Sn	1994	---	---	---	---	---	---	---	[S19]
		1981	^{50}Cr(^{58}Ni, 2p5n)^{101}Sn	Fusion-evaporation	[T10]	1994	1.5 s		[B80]
		1994	^{112}Sn(^{58}Ni)^{101}Sn	Fragmentation	[L11]	1995	3 s	1	[J3]
		1994	^{124}Xe(Be)^{101}Sn	Nuclear fragmentation	[S19]	1997	3.4883 s		[M33]
		1995	^{50}Cr(^{58}Ni, 2p5n)^{101}Sn	Fusion-evaporation	[J3]	2003	3 s	1	[A42]
		1995	^{124}Xe(Be)^{101}Sn	Nuclear fragmentation	[S20]	2007	1.9 s	0.3	[K22]
		1995	^{124}Xe(Be)^{101}Sn	Nuclear fragmentation	[S21]	2012	1.97 s	0.16	[A43]
		1997	^{124}Xe(Be)^{101}Sn	High-energy projectile fragmentation	[S74]	2012	2.1 s	0.2	[L26]
		2000	^{58}Ni(^{50}Cr, α3n)^{101}Sn	Heavy-ion induced fusion	[C41]	2016	3 s		[C7]
		2000	^{58}Ni(^{58}Ni, ^{12}C3n)^{101}Sn	Heavy-ion induced fusion	[C41]	2017	1.97 s	0.16	[A45]
		2006	^{105}Te(α)^{101}Sn	Alpha-decay	[L14]				
		2006	^{105}Te(α)^{101}Sn	Alpha-decay	[S40]				
		2007	^{50}Cr(^{58}Ni, α3n)^{101}Sn	Fusion-evaporation	[K22]				
		2007	^{105}Te(α)^{101}Sn	Alpha-decay	[M17]				
		2007	^{105}Te(α)^{101}Sn	Alpha-decay	[M31]				
		2007	^{58}Ni(^{46}Ti)^{101}Sn	^{58}Ni beam on the ^{46}Ti target followed by the 3-neutron evaporation from the ^{104}Sn compound nucleus	[S41]				
		2010	^{54}Fe(^{58}Ni, α)^{101}Sn	Heavy-ion fusion-evaporation	[D9]				
		2012	^{112}Sn(^{9}Be)^{101}Sn	Fragmentation	[L26]				
		2014	^{56}Ni(^{46}Ti, n)^{101}Sn	Fusion-quasifission	[K2]				
		2014	^{58}Ni(^{46}Ti, 3n)^{101}Sn	Fusion-quasifission	[K2]				
		2014	^{75}Rb(^{28}Si, pn)^{101}Sn	Fusion-quasifission	[K2]				
		2014	^{58}Ni(^{50}Cr, α3n)^{101}Sn	Fusion-quasifission	[K2]				

Table 6: Discovery, production scheme and half-lives of tin isotopes *(continued)*

Isotope	Year	Production scheme				Half-life value			
		Year	*Reaction*	*Principal method/condition*	*Ref*	*Year*	*Half-life*		*Ref*
^{101}Sn	1994	---	---	---	---	---	---	---	[S19]
		2014	^{56}Ni(^{50}Cr, αn)^{101}Sn	Fusion-quasifission	[K2]				
		2014	^{56}Ni(^{58}Ni, ^{12}C1n)^{101}Sn	Fusion-quasifission	[K2]				
		2014	^{58}Ni(^{58}Ni, ^{12}C3n)^{101}Sn	Fusion-quasifission	[K2]				
		2014	^{58}Ni(^{58}Ni, 3α3n)^{101}Sn	Fusion-quasifission	[K2]				
		2014	^{58}Ni(^{58}Ni, ^{14}C1n)^{101}Sn	Fusion-quasifission	[K2]				
^{102}Sn	1994	---	---	---	---	---	---	---	[L11]
		1981	^{106}Te(α)^{102}Sn	Alpha-decay	[S8]	1995	4.5 s	0.7	[S20]
		1994	^{112}Sn(^{58}Ni)^{102}Sn	Fragmentation	[L11]	1997	4.6 s	1.4	[A41]
		1994	^{124}Xe(Be)^{102}Sn	Nuclear fragmentation	[S19]	1998	4.5 s	0.7	[F40]
		1995	^{114}Ba(^{12}C)^{102}Sn	Cluster radioactive decay	[G51]	2003	4.6 s	1.4	[A42]
		1995	^{112}Sn(^{58}Ni)^{102}Sn	Quasi-fragmentation	[L12]	2006	3.8 s	0.2	[K8]
		1995	^{129}Xe(Al)^{102}Sn	Nuclear fragmentation	[S20]	2009	3.8 s	0.2	[F43]
		1995	^{124}Xe(Be)^{102}Sn	Nuclear fragmentation	[S21]	2002	3.8 s	0.2	[F1]
		1996	^{50}Cr(^{58}Ni, 1α2n)^{102}Sn	^{58}Ni beam on the ^{50}Cr target	[L17]	2012	3.8 s	0.2	[A43]
		1998	^{50}Cr(^{58}Ni, α2n)^{102}Sn	^{58}Ni beam on the ^{50}Cr target	[L18]	2016	3.8 s		[C7]
		2001	^{58}Ni(^{50}Cr, 1α2n)^{102}Sn	^{58}Ni beam on the ^{50}Cr target	[L19]	2017	3.8 s	0.2	[A45]
		2002	^{112}Sn(Be)^{102}Sn	Fragmentation	[F1]				
		2005	^{58}Ni(^{50}Cr, 2p4n)^{102}Sn	Fusion-evaporation	[K7]				
		2006	^{58}Ni(^{50}Cr, 2p6n)^{102}Sn	Fusion-evaporation	[K8]				
		2007	^{106}Te(α)^{102}Sn	Alpha-decay	[M31]				
		2014	^{58}Ni(^{46}Ti, 2n)^{102}Sn	Fusion-quasifission	[K2]				
		2014	^{58}Ni(^{50}Cr, α2n)^{102}Sn	Fusion-quasifission	[K2]				
		2014	^{56}Ni(^{50}Cr, α)^{102}Sn	Fusion-quasifission	[K2]				
		2014	^{56}Ni(^{58}Ni, ^{12}C)^{102}Sn	Fusion-quasifission	[K2]				
		2014	^{58}Ni(^{58}Ni, ^{12}C2n)^{102}Sn	Fusion-quasifission	[K2]				
		2014	^{58}Ni(^{58}Ni, ^{14}C)^{102}Sn	Fusion-quasifission	[K2]				
		2016	^{106}Te(α)^{102}Sn		[C7]				
^{103}Sn	1981	---	---	---	---	---	---	---	[T10]
		1965	^{107}Te(α)^{103}Sn	Alpha-decay	[M1]	1981	7 s	3	[T10]
		1979	^{107}Te(α)^{103}Sn	Alpha-decay	[S7]	1997	7 s	3	[A41]
		1981	^{107}Te(α)^{103}Sn	Alpha-decay	[S8]	2001	7 s	3	[F41]

Table 6: Discovery, production scheme and half-lives of tin isotopes *(continued)*

Isotope	Year	Production scheme				Half-life value			
		Year	*Reaction*	*Principal method/condition*	*Ref*	*Year*	*Half-life*		*Ref*
^{103}Sn	1981	---	---	---	---	---	---	---	[T10]
		1981	^{58}Ni(^{50}Cr, 2p3n)^{103}Sn	Fusion-evaporation	[T10]	2003	7 s	3	[A42]
		1991	^{107}Te(α)^{103}Sn	Alpha-decay	[H21]	2004	7.0 s	0.6	[M37]
		1994	^{112}Sn(^{58}Ni)^{103}Sn	Fragmentation	[L11]	2005	7.0 s	0.2	[K19]
		2001	^{58}Ni(^{54}Fe, 2α1n)^{103}Sn	^{54}Fe target undergoes evaporation treatment	[F3]	2009	7.5 s	1.5	[F44]
		2001	^{58}Ni(^{50}Cr, 1α1n)^{103}Sn	^{58}Ni beam on the ^{50}Cr target	[L19]	2012	7.0 s	0.2	[A43]
		2001	^{107}Te(γ, α)^{103}Sn		[S9]	2016	7.0 s		[C7]
		2002	^{107}Te(α)^{103}Sn	Alpha-decay	[S39]	2017	7.0 s	0.2	[A45]
		2004	^{107}Te(γ, α)^{103}Sn		[H43]				
		2004	^{50}Cr(^{58}Ni, αn)^{103}Sn	Fusion-evaporation	[M37]				
		2005	^{50}Cr(^{58}Ni, αn)^{103}Sn	Fission-evaporation	[K19]				
		2005	^{50}Cr(^{58}Ni, αn)^{103}Sn	Fission-evaporation	[K20]				
		2007	^{107}Te(α)^{103}Sn	Alpha-decay	[M17]				
		2009	^{54}Fe(^{58}Ni, 2αnγ)^{103}Sn		[F43]				
		2014	^{58}Ni(^{46}Ti, n)^{103}Sn	Fusion-quasifission	[K2]				
		2014	^{58}Ni(^{50}Cr, αn)^{103}Sn	Fusion-quasifission	[K2]				
		2014	^{56}Ni(^{50}Cr, 2p1n)^{103}Sn	Fusion-quasifission	[K2]				
^{104}Sn	1985	---	---	---	---	---	---	---	[D13]
		1965	^{108}Te(α)^{104}Sn	Alpha-decay	[M1]	1985	23 s	2	[D13]
		1979	^{108}Te(α)^{104}Sn	Alpha-decay	[S7]	1985	21 s	1	[R20]
		1981	^{108}Te(α)^{104}Sn	Alpha-decay	[S8]	1988	21 s		[B11]
		1985	^{92}Mo(^{20}Ne, pn)^{104}Sn	^{20}Ne beam bombardment on the ^{92}Mo target	[D13]	1991	20.8 s	0.5	[B48]
		1985	^{50}Cr(^{58}Ni, 2p2n)^{104}Sn	Fusion-evaporation	[R20]	2000	20.8 s	0.5	[B49]
		1987	^{92}Mo(^{16}O, 4n)^{104}Sn	Fusion-evaporation	[K52]	2003	20.8 s	0.5	[A42]
		1988	^{58}Ni(^{50}Cr, 2p2n)^{104}Sn	Fusion-evaporation	[B11]	2006	20.8 s	0.5	[K8]
		1990	^{58}Ni(^{50}Cr, 2p2n)^{104}Sn	Fusion-evaporation	[S78]	2007	20.8 s	0.5	[B50]
		1991	^{108}Te(α)^{104}Sn	Alpha-decay	[H21]	2012	20.8 s	0.5	[A43]
		1991	^{50}Cr(^{58}Ni, 2p2n)^{104}Sn	Fusion-evaporation	[S22]	2016	20.8 s		[C7]
		1994	^{112}Sn(^{58}Ni)^{104}Sn	Fragmentation	[L11]	2017	20.8 s	0.5	[A45]
		1994	^{105}Sb(p)^{104}Sn	Proton-decay	[T11]				
		1995	^{58}Ni(^{50}Cr, 2p2n)^{104}Sn	Fusion-evaporation	[G35]				
		1995	^{58}Ni(^{50}Cr, 2p2n)^{104}Sn	Fusion-evaporation	[S24]				
		1996	^{58}Ni(^{50}Cr, 2p2n)^{104}Sn	Particle evaporation	[C18]				

Table 6: Discovery, production scheme and half-lives of tin isotopes *(continued)*

Isotope	Year	Production scheme				Half-life value			
		Year	*Reaction*	*Principal method/condition*	*Ref*	*Year*	*Half-life*		*Ref*
^{104}Sn	1985	---	---	---	---	---	---	---	[D13]
		1996	^{58}Ni(^{46}Ti)^{104}Sn	Ni beam on the Ti target	[G32]				
		1997	^{58}Ni(^{50}Cr, 2p2n)^{104}Sn	Fusion-evaporation	[G36]]				
		1998	^{58}Ni(^{50}Cr, 2p2n)^{104}Sn		[G33]				
		2001	^{58}Ni(^{50}Cr, 2p2n)^{104}Sn	^{58}Ni beam on the ^{50}Cr target	[L19]				
		2001	^{108}Te(γ, α)^{104}Sn		[S9]				
		2005	^{105}Sb(p)^{104}Sn	Direct proton-decay	[L20]				
		2006	^{58}Ni(^{50}Cr, 2p4n)^{104}Sn	Fusion-evaporation, ^{58}Ni beam on the ^{50}Cr target	[K8]				
		2013	^{124}Xe(^{9}Be)^{104}Sn	Fragmentation	[B1]				
		2013	^{46}Ti(^{58}Ni)^{104}Sn	Fusion-evaporation	[F2]				
		2013	^{124}Xe(^{9}Be)^{104}Sn	Nuclear fragmentation	[G43]				
		2014	^{124}Xe(Be)^{104}Sn	Fragmentation	[D24]				
		2018	^{124}Xe(Be)^{104}Sn	Fragmentation	[C45]				
^{105}Sn	1981	---	---	---	---	---	---	---	[T10]
		1979	^{109}Te(α)^{105}Sn	Alpha-decay	[P23]	1981	31 s	0.6	[T10]
		1979	^{109}Te(α)^{105}Sn	Alpha-decay	[S7]	1985	27 s	3	[D13]
		1981	^{109}Te(α)^{105}Sn	Alpha-decay	[S8]	1995	34 s	1	[P17]
		1981	^{58}Ni(^{54}Fe, 2p5n)^{105}Sn	Fusion-evaporation	[T10]	2003	34 s	1	[A42]
		1991	^{109}Te(α)^{105}Sn	Alpha-decay	[H21]	2005	34 s	1	[F42]
		1991	^{50}Cr(^{58}Ni, 2p1n)^{105}Sn	Fusion-evaporation	[S22]	2006	32.6 s	0.6	[K21]
		1992	^{58}Ni(^{50}Cr, 2p1n)^{105}Sn	^{58}Ni beam on the gold backed ^{50}Cr target	[S23]	2012	34 s	1	[A43]
		1994	^{112}Sn(^{58}Ni)^{105}Sn	Fragmentation	[L11]	2016	34 s		[C7]
		1994	^{105}Sb(β^{+})^{105}Sn		[T11]	2017	34 s	1	[A45]
		1995	^{58}Ni(^{50}Cr, 2p1n)^{105}Sn	Fusion-evaporation	[A16]				
		1995	^{58}Ni(^{50}Cr, 2p1n)^{105}Sn	Fusion-evaporation	[G35]				
		1995	^{54}Fe(^{54}Fe, 2p1n)^{105}Sn	Recoil of heavy-ion beams	[I8]				
		1995	^{54}Fe(^{54}Fe, 2p1n)^{105}Sn	Recoil of heavy-ion beams	[O2]				
		1995	^{50}Cr(^{58}Ni, 2p1n)^{105}Sn	^{58}Ni beam on the ^{50}Cr target	[P17]				
		1995	^{58}Ni(^{50}Cr)^{105}Sn	The target consisted self-supporting foils of isotopically enriched ^{50}Cr	[P25]				
		1995	^{58}Ni(^{50}Cr, 2p1n)^{105}Sn	Fusion-evaporation	[S24]				
		1996	^{58}Ni(^{50}Cr, 2p1n)^{105}Sn	Particle evaporation	[C18]				

Table 6: Discovery, production scheme and half-lives of tin isotopes *(continued)*

Isotope	Year	Production scheme				Half-life value			
		Year	*Reaction*	*Principal method/condition*	*Ref*	*Year*	*Half-life*		*Ref*
^{105}Sn	1981	---	---	---	---	---	---	---	[T10]
		1997	^{50}Cr(^{58}Ni, 2p1n)^{105}Sn		[G6]				
		1997	^{58}Ni(^{50}Cr, 2p1n)^{105}Sn	Fusion-evaporation	[G36]				
		2001	^{58}Ni(^{50}Cr, 2p1n)^{105}Sn	^{58}Ni beam on the ^{50}Cr target	[L19]				
		2005	^{50}Cr(^{58}Ni, 2p1n)^{105}Sn	Fusion-evaporation	[K20]				
		2006	^{50}Cr(^{58}Ni, 2p1n)^{105}Sn	Fusion-evaporation	[K21]				
		2015	^{106}Sn(^{9}Be)^{105}Sn	One-neutron knockout reaction	[J16]				
^{106}Sn	1975	---	---	---	---	---	---	---	[B84]
		1975	^{106}Cd(^{3}He, 3n)^{106}Sn	^{3}He ions on the metallic cadmium target	[B84]	1975	1.9 m	0.3	[B84]
		1977	^{58}Ni(^{58}Ni)^{106}Sn	Fusion-evaporation	[K37]	1978	2.10 m	0.15	[V5]
		1978	^{96}Ru(^{14}N, p3n)^{106}Sn	Isotopically enriched ^{96}Ru target backed on gold	[V5]	1988	115 s	5	[B11]
		1978	^{96}Ru(^{16}O, 2p4n)^{106}Sn	Isotopically enriched ^{96}Ru target backed on gold	[V5]	1997	1.92 m	0.08	[A41]
		1979	^{58}Ni(^{58}Ni, 6p4n)^{106}Sn	^{58}Ni beam on the ^{58}Ni target	[P28]	2003	1.92 m	0.08	[A42]
		1979	^{110}Te(α)^{106}Sn	Alpha-decay	[P28]	2008	115 s	5	[E3]
		1979	^{110}Te(α)^{106}Sn	Alpha-decay	[S7]	2012	1.92 m	0.08	[A43]
		1980	^{106}Cd(^{3}He, 3n)^{106}Sn		[A46]	2017	1.92 m	0.08	[A45]
		1980	^{58}Ni(^{54}Fe)^{106}Sn	^{58}Ni bombardment on the ^{54}Fe target	[A47]				
		1981	^{110}Te(α)^{106}Sn	Alpha-decay	[S8]				
		1988	^{58}Ni(^{58}Ni, 6p4n)^{106}Sn	Fusion-evaporation	[B11]				
		1989	^{106}Cd(^{3}He, 3n)^{106}Sn	^{3}He bombardment	[A14]				
		1989	^{58}Ni(^{54}Fe, α2p)^{106}Sn	Ni beam on the tantalum backed ^{54}Fe target	[A51]				
		1994	^{54}Fe(^{58}Ni, α2p)^{106}Sn	Fusion	[M7]				
		1994	^{51}V(^{58}Ni, p2n)^{106}Sn		[M7]				
		1994	^{54}Fe(^{58}Ni, α2p)^{106}Sn	Enriched ^{54}Fe foil backed on thick Au	[W2]				
		1995	^{54}Fe(^{58}Ni, α2p)^{106}Sn	Recoil of heavy-ion beams	[I8]				
		1995	^{58}Ni(^{54}Fe, α2p)^{106}Sn	Fusion-evaporation	[P9]				
		1997	^{58}Ni(^{50}Cr, 2p)^{106}Sn	Fusion-evaporation	[G36]				

Table 6: Discovery, production scheme and half-lives of tin isotopes *(continued)*

Isotope	Year	Production scheme				Half-life value			
		Year	*Reaction*	*Principal method/condition*	*Ref*	*Year*	*Half-life*		*Ref*
^{106}Sn	1975	---	---	---	---	---	---	---	[B84]
		1997	^{54}Fe(^{58}Ni, α2p)^{106}Sn	^{58}Ni beam on the ^{54}Fe target	[J19]				
		1998	^{54}Fe(^{58}Ni, α2p)^{106}Sn	^{54}Fe beam on the ^{58}Ni target backed on gold	[J5]				
		1999	^{54}Fe(^{58}Ni, α2p)^{106}Sn	^{54}Fe beam on the ^{58}Ni target backed on gold	[J6]				
		2001	^{58}Ni(^{50}Cr, 2p)^{106}Sn	^{58}Ni beam on the ^{50}Cr target	[L19]				
		2007	^{124}Xe(Be)^{106}Sn	Projectile fragmentation, ^{124}Xe beams on the Be target	[V1]				
		2012	^{108}Sn(p, t)^{106}Sn		[P31]				
^{107}Sn	1976	---	---	---	---	---	---	---	[H36]
		1969	^{106}Cd(α, 3n)^{107}Sn	Alpha-particle bombardment	[Y6]	1976	2.90 m	0.05	[H36]
		1976	^{106}Cd(^{3}He, 2n)^{107}Sn	^{3}He beam on the ^{106}Cd target	[H36]	1997	2.90 m	0.05	[A41]
		1976	^{106}Cd(^{3}He, 2nγ)^{107}Sn	^{3}He bombardment on the ^{106}Cd target	[H36]	2003	2.90 m	0.05	[A42]
		1977	^{58}Ni(^{58}Ni)^{107}Sn	Fusion-evaporation	[K37]	2012	2.90 m	0.05	[A43]
		1978	^{96}Ru(^{14}N, p2n)^{107}Sn		[V5]	2017	2.90 m	0.05	[A45]
		1980	^{58}Ni(^{54}Fen)^{107}Sn	^{58}Ni bombardment on the ^{54}Fe target	[A47]				
		1984	^{106}Cd(^{3}He, 2nγ)^{107}Sn	^{3}He beam on the isotopically enriched and self-supported ^{106}Cd target	[A48]				
		1993	^{54}Fe(^{56}Fe, 2p1n)^{107}Sn	Fusion, ^{54}Fe target backed on evaporated gold layer	[I7]				
		1995	^{56}Fe(^{54}Fe, 2p1n)^{107}Sn	Recoil of heavy-ion beams	[I8]				
		1995	^{54}Fe(^{56}Fe, 2p1n)^{107}Sn	Recoil of heavy-ion beams	[O2]				
		1997	^{107}Sb(β^{+}/EC)^{107}Sn	^{107}Sb preparation by fusion-evaporation using ^{58}Ni beam on ^{50}Cr, ^{58}Cr and ^{58}Ni targets	[S50]				
		2002	^{107}Sb(β^{+}/EC)^{107}Sn	^{107}Sb production from ^{58}Ni(^{54}Fe, 3p2n) heavy-ion reaction	[R25]				
		2015	^{108}Sn(^{9}Be)^{107}Sn	One-neutron knockout reaction	[J16]				
		2016	^{108}Sn(^{9}Be)^{107}Sn	One-neutron knockout reaction	[C21]				

Table 6: Discovery, production scheme and half-lives of tin isotopes *(continued)*

Isotope	Year	Production scheme				Half-life value			
		Year	*Reaction*	*Principal method/condition*	*Ref*	*Year*	*Half-life*		*Ref*
^{108}Sn	1949	---	---	---	---	---	---	---	[M8]
		1949	^{106}Cd(α, 2nγ)^{108}Sn	^{106}Cd bombardment with alpha-particle	[M8]	1949	4.5 h		[M8]
		1968	^{106}Cd(α, 2n)^{108}Sn	Alpha-particle bombardment	[Y5]	1964	9 m		[N5]
		1969	^{106}Cd(α, 2n)^{108}Sn	Alpha-particle bombardment	[Y6]	1977	10.8 m	0.3	[V4]
		1969	^{100}Ru(^{12}C, 4nγ)^{108}Sn		[B49]	1978	10.30 m		[H37]
		1976	^{108}Sb(β$^+$)^{108}Sn	^{108}Sb production from ^{112}Sn(p, 5n) reaction	[O11]	1982	10.30 m	0.08	[H2]
		1977	^{106}Cd(^{3}He, n)^{108}Sn	Two-neutron transfer reaction, target preparation by rolling or evaporation	[F10]	1988	623 s	15	[B11]
		1977	^{58}Ni(^{58}Ni)^{108}Sn	Fusion-evaporation	[K37]	1997	10.30 m	0.08	[A41]
		1977	^{106}Cd(α, 2n)^{108}Sn	^{106}Cd target preparation by electroplating	[V4]	2007	10.3 m		[O12]
		1979	^{58}Ni(^{58}Ni, 6p2n)^{108}Sn	^{58}Ni beam on the ^{58}Ni target	[P23]	2008	10.30 m	0.08	[E3]
		1980	^{106}Cd(α, 2n)^{108}Sn		[A46]	2003	10.30 m	0.08	[A42]
		1980	^{58}Ni(^{54}Fe)^{108}Sn	^{58}Ni beam on the ^{54}Fe target	[A47]	2011	10.3 m		[R36]
		1981	^{92}Mo(^{19}F, p2nγ)^{108}Sn	Isotopically enriched ^{92}Mo target backed on lead	[A12]	2012	10.30 m	0.08	[A43]
		1983	^{92}Mo(^{19}F, p2n)^{108}Sn	^{19}F beam impinging on the ^{92}Mo target sputtered onto Au foil	[H15]	2017	10.30 m	0.08	[A45]
		1984	^{92}Mo(^{16}O, γ)^{108}Sn		[G1]				
		1984	^{96}Ru(^{12}C, γ)^{108}Sn		[G1]				
		1987	^{98}Mo(^{16}O, 6n)^{108}Sn	Fusion-evaporation	[E1]				
		1988	^{58}Ni(^{58}Ni, 6p2n)^{108}Sn	Fusion-evaporation	[B11]				
		1989	^{58}Ni(^{54}Fe, 4p)^{108}Sn	Ni beam on the tantalum backed ^{54}Fe target	[A51]				
		1993	^{54}Fe(^{58}Ni, 4p)^{108}Sn	Target consists of self-supporitng ^{54}Fe foil	[W1]				
		1994	^{54}Fe(^{58}Ni, 4p)^{108}Sn	Fusion	[M7]				
		1995	^{54}Fe(^{58}Ni, 4p)^{108}Sn	Recoil of heavy-ion beams	[I8]				
		1995	^{58}Ni(^{54}Fe, 4p)^{108}Sn	Fusion-evaporation	[P9]				

Table 6: Discovery, production scheme and half-lives of tin isotopes *(continued)*

Isotope	Year	Production scheme				Half-life value			
		Year	*Reaction*	*Principal method/condition*	*Ref*	*Year*	*Half-life*		*Ref*
^{108}Sn	1949	---	---	---	---	---	---	---	[M8]
		1995	^{18}O(^{92}Mo, 2n)^{108}Sn	Fusion-evaporation followed by the heavy-ion collision	[T7]				
		1995	^{50}Ti(^{60}Ni, 2n)^{108}Sn	Fusion-evaporation followed by the heavy-ion collision	[T7]				
		1996	^{54}Fe(^{58}Ni, 4p)^{108}Sn	Target consists of ^{54}Fe foil	[W3]				
		1997	^{54}Fe(^{58}Ni, 4p)^{108}Sn	^{58}Ni beam on the ^{54}Fe target	[J19]				
		1997	^{108}Sb(β^+/EC)^{108}Sn	^{108}Sb preparation by fusion-evaporation using ^{58}Ni beam on ^{50}Cr, ^{58}Cr and ^{58}Ni targets	[S50]				
		1998	^{54}Fe(^{58}Ni, 4p)^{108}Sn	^{54}Fe beam on the ^{58}Ni target backed on gold	[J5]				
		1998	^{54}Fe(^{58}Ni, 4p)^{108}Sn	^{54}Fe target backed on gold	[W4]				
		1999	^{54}Fe(^{58}Ni, 4p)^{108}Sn	^{54}Fe beam on the ^{58}Ni target backed on gold	[J6]				
		2007	^{124}Xe(Be)^{108}Sn	Projectile fragmentation, ^{124}Xe beams on the Be target	[V1]				
		2008	^{108}Cd(β^- β^-)^{108}Sn	Double-beta decay experiment using the low-background $CdWO_4$ crystal scintillator	[B23]				
^{109}Sn	1965	---	---	---	---	---	---	---	[A11]
		1962	^{109}In(β^-)^{109}Sn	^{109}In production by bombarding natural silver foils with alpha-particles	[N16]	1964	18 m		[N5]
		1969	^{108}Cd(α, 3n)^{109}Sn	Alpha-particle bombardment	[Y6]	1969	1.5 m	0.2	[H8]
		1974	^{113}In(p, 5n)^{109}Sn	Proton beam on natural indium	[H30]	1970	18 m	1	[S42]
		1976	^{106}Cd(α, n)^{109}Sn	Alpha-irradiation	[M4]	1974	18.0 m		[H30]
		1976	^{109}Sb(β^+)^{109}Sn	^{109}Sb production from ^{112}Sn(p, 4n) reaction	[O11]	1978	18.0 m	0.2	[B28]
		1977	^{58}Ni(^{58}Ni)^{109}Sn	Fusion-evaporation	[K37]	1987	18 m		[E1]
		1978	^{112}Sn(^{3}He, ^{6}He)^{109}Sn	^{3}He beam on the ^{112}Sn target	[P5]	1997	18.0 m	0.2	[A41]
		1979	^{108}Cd(α, 3n)^{109}Sn	Alpha-particle on metal foils enriched of Cd	[H12]	2003	18.0 m	0.2	[A42]

Table 6: Discovery, production scheme and half-lives of tin isotopes *(continued)*

Isotope	Year	Production scheme				Half-life value			
		Year	*Reaction*	*Principal method/condition*	*Ref*	*Year*	*Half-life*		*Ref*
^{109}Sn	1965	---	---	---	---	---	---	---	[A11]
		1982	^{109}Sb(β^+)^{109}Sn	^{109}Sb production from ^{92}Mo + ^{20}Ne reaction	[J10]	2005	18.0 m	0.2	[G53]
		1987	^{98}Mo(^{16}O, 5n)^{109}Sn	Fusion-evaporation	[E1]	2012	18.0 m	0.2	[A43]
		1987	^{97}Mo(^{16}O, 4n)^{109}Sn	Fusion-evaporation	[E1]	2016	18.1 m	0.2	[K54]
		1992	^{61}Ni(^{48}Ti, γ)^{109}Sn	Bombardment of ^{61}Ni target with ^{48}Ti beam	[C3]	2017	18.0 m	0.2	[A45]
		1995	^{55}Mn(^{58}Ni, 3p1n)^{109}Sn	Heavy-ion and light particle-induced reaction	[K14]				
		1995	^{106}Cd(α, n)^{109}Sn	Heavy-ion and light particle-induced reaction	[K14]				
		1995	^{106}Cd(α, n)^{109}Sn	Alpha-particle on the ^{106}Cd target	[K15]				
		1995	^{55}Mn(^{58}Ni, 3p1n)^{109}Sn		[K15]				
		1995	^{18}O(^{92}Mo, 1n)^{109}Sn	Fusion-evaporation followed by the heavy-ion collision	[T7]				
		1995	^{50}Ti(^{60}Ni, 1n)^{109}Sn	Fusion-evaporation followed by the heavy-ion collision	[T7]				
		1996	^{94}Mo(^{19}F, p3n)^{109}Sn	Vacuum annealed ^{94}Mo target	[C25]				
		1996	^{54}Fe(^{59}Co, 3p1n)^{109}Sn	Bombardment of self-supporting ^{54}Fe foil with ^{59}Co beam	[K16]				
		1999	^{106}Cd(α, nγ)^{109}Sn	Alpha-particle bombardment, target preparation by evaporation	[D8]				
		1999	^{106}Cd(α, nγγ)^{109}Sn	Alpha-particle bombardment, target preparation by evaporation	[D8]				
		2002	^{109}Sb(β^+/EC)^{109}Sn	^{109}Sb production from ^{58}Ni(^{54}Fe, 3p) heavy-ion reaction	[R25]				
		2005	^{106}Cd(α, n)^{109}Sn	Target preparation by evaporating isotopically enriched ^{106}Cd	[G53]				
		2006	^{106}Cd(α, n)^{109}Sn	Target preparation by evaporating highly enriched ^{106}Cd onto Al	[G54]				

Table 6: Discovery, production scheme and half-lives of tin isotopes *(continued)*

Isotope	Year	Production scheme				Half-life value			
		Year	*Reaction*	*Principal method/condition*	*Ref*	*Year*	*Half-life*		*Ref*
^{110}Sn	1964	---	---	---	---	---	---	---	[N5]
		1964	In(p)^{110}Sn	Proton bombardment on natural indium	[N5]	1964	4 h		[N5]
		1968	^{108}Cd(α, 2n)^{110}Sn	Alpha-particle bombardment	[Y5]	1974	4 h		[B69]
		1969	^{108}Cd(α, 2n)^{110}Sn	Alpha-particle bombardment	[Y6]	1974	4.0 h		[H30]
		1970	^{112}Sn(p, t)^{110}Sn	Target preparation by SnO_2 evaporation	[F14]	1983	4.11 h	0.10	[G19]
		1972	^{110}Sb(ε)^{110}Sn		[M27]	1991	4.15 h		[L33]
		1972	^{110}Sb(β^+)^{110}Sn		[A40]	1997	4.11 h	0.10	[A41]
		1972	^{110}Sb(β^+ + EC)^{110}Sn	Positron emission accompanied by electron capture	[S53]	2003	4.11 h	0.10	[A42]
		1974	^{113}In(p, 4n)^{110}Sn	Proton beam on natural indium	[H30]	2005	4.173 h	0.023	[G53]
		1976	^{110}Sb(β^+)^{110}Sn	^{110}Sb production from ^{112}Sn(p, 3n) reaction	[O11]	2007	4.1 h		[C19]
		1977	^{58}Ni(^{58}Ni)^{110}Sn	Fusion-evaporation	[K37]	2007	4.11 h		[O12]
		1980	^{112}Sn(p, t)^{110}Sn		[C48]	2009	4.156 h		[R21]
		1980	^{108}Cd(α, 2n)^{110}Sn	Alpha-particle bombardment on the self-supporting cadmium target	[P24]	2012	4.154 h	0.004	[A43]
		1981	^{112}Sn(p, t)^{110}Sn		[C50]	2012	4.154 h	0.004	[G52]
		1985	^{113}In(p, 4nγ)^{110}Sn		[G52]	2015	4.11 h		[D5]
		1985	^{112}Sn(p, p2nγ)^{110}Sn		[G52]	2015	4.15 h		[K6]
		1986	Cd(α)^{110}Sn	Alpha-irradiation on the cadmium target	[A17]	2017	4.154 h	0.004	[A45]
		1986	^{98}Mo(^{16}O, 4nγ)^{110}Sn	Thin gold supported ^{98}Mo target	[K11]				
		1987	^{94}Mo(^{16}O, γ)^{110}Sn	Heavy-ion fusion reaction	[C23]				
		1987	^{98}Mo(^{16}O, 4n)^{110}Sn	Fusion-evaporation	[E1]				
		1987	^{40}Ar(^{70}Ge, γ)^{110}Sn	Bombardment of ^{70}Ge target by ^{40}Ar beam	[G3]				
		1987	^{45}Sc(^{65}Cu, γ)^{110}Sn	Bombardment of self-supporting ^{65}Cu foil with ^{45}Sc beam	[M5]				
		1987	^{94}Mo(^{19}F, p2nγ)^{110}Sn	^{94}Mo target backed on lead	[V10]				
		1988	^{98}Mo(^{16}O, 4n)^{110}Sn	Lead-backed isotopically-enriched ^{98}Mo target	[H9]				

Table 6: Discovery, production scheme and half-lives of tin isotopes *(continued)*

Isotope	Year	Production scheme				Half-life value			
		Year	*Reaction*	*Principal method/condition*	*Ref*	*Year*	*Half-life*		*Ref*
^{110}Sn	1964	---	---	---	---	---	---	---	[N5]
		1989	^{110}Cd(^{3}He, 3n)^{110}Sn	^{3}He bombardment on the cadmium target	[A14]				
		1989	^{104}Pd(^{12}C, α2n)^{110}Sn		[A14]				
		1989	^{40}Ar(^{70}Ge, γ)^{110}Sn	Bombardment of ^{70}Ge target by ^{40}Ar beam	[B70]				
		1990	^{40}Ar(^{70}Ge, γ)^{110}Sn	Collision (fusion), bombardment of ^{70}Ge target by ^{40}Ar beam	[B71]				
		1991	^{115}In(p, 4n)^{110}Sn		[L33]				
		1991	^{113}In(p, 6n)^{110}Sn		[L33]				
		1992	^{62}Ni(^{48}Ti, γ)^{110}Sn	Bombarding of ^{62}Ni target with ^{48}Ti beam	[C3]				
		1995	^{18}O(^{92}Mo, γ)^{110}Sn	Fusion-evaporation followed by the heavy-ion collision	[T7]				
		1995	^{50}Ti(^{60}Ni, γ)^{110}Sn	Fusion-evaporation followed by the heavy-ion collision	[T7]				
		2003	^{110}Sb(β^{+})^{110}Sn		[W13]				
		2003	^{98}Mo(^{16}O, 4n)^{110}Sn		[W28]				
		2003	^{98}Mo(^{16}O, 4n)^{110}Sn	^{16}O beam on the ^{98}Mo target followed by neutron evaporation from ^{114}Sn	[W27]				
		2005	^{112}Sn(d, p3n)^{110}Sn	Deuteron beam on the enriched Sn target	[B5]				
		2005	^{118}Sn(d, p9n)^{110}Sn	Deuteron beam on the enriched Sn target	[B5]				
		2005	^{120}Sn(d, p11n)^{110}Sn	Deuteron beam on the enriched Sn target	[B5]				
		2005	^{124}Sn(d, p15n)^{110}Sn	Deuteron beam on the enriched Sn target	[B5]				
		2005	^{106}Cd(α, γ)^{110}Sn	Target preparation by evaporating isotopically-enriched ^{106}Cd	[G53]				
		2005	^{98}Mo(^{16}O, 4n)^{110}Sn	^{16}O beam on the ^{98}Mo target	[W29]				
		2006	^{112}Sn(p, t)^{110}Sn		[G47]				

Table 6: Discovery, production scheme and half-lives of tin isotopes *(continued)*

Isotope	Year	Production scheme				Half-life value			
		Year	*Reaction*	*Principal method/condition*	*Ref*	*Year*	*Half-life*		*Ref*
^{110}Sn	1964	---	---	---	---	---	---	---	[N5]
		2006	^{106}Cd(α, γ)^{110}Sn	Target preparation by evaporating highly enriched ^{106}Cd onto Al	[G54]				
		2007	^{124}Xe(Be)^{110}Sn	Projectile fragmentation, ^{124}Xe beams on the Be target	[V1]				
		2014	^{112}Sn(γ, 2n)^{110}Sn	Photonuclear reaction	[D4]				
		2015	^{112}Sn(γ, 2n)^{110}Sn	Photonuclear reaction	[D5]				
		2015	^{112}Sn(γ, 2n)^{110}Sn	Bremsstrahlung irradiation	[K6]				
		2016	^{12}C(^{106}Cd, ^{8}Be)^{110}Sn	Alpha-particle transfer	[K56]				
		2016	^{12}C(^{106}Cd, ^{8}Be)^{110}Sn	Alpha-particle transfer	[K57]				
^{111}Sn	1949	---	---	---	---	---	---	---	[H27]
		1949	^{108}Cd(α, n)^{111}Sn	Alpha bombardment	[H27]	1949	35.0 m	0.5	[H27]
		1951	Cd(α)^{111}Sn	Alpha bombardment	[M19]	1951	35 m		[F6]
		1960	^{112}Sn(γ, n)^{111}Sn	Bremsstrahlung reaction	[Y8]	1951	35 m	1	[M19]
		1969	^{110}Cd(α, 3n)^{111}Sn	Alpha-particle bombardment	[Y6]	1964	35 m		[N5]
		1970	^{112}Sn(p, d)^{111}Sn	Proton bombardment	[C17]	1967	35.5 m	0.8	[C46]
		1970	^{112}Sn(n, 2n)^{111}Sn		[L34]	1971	38.8 m	0.8	[R8]
		1972	^{108}Cd(α, nγ)^{111}Sn		[B75]	1974	35.3 m		[H30]
		1972	^{111}Cd(^{3}He, 3n)^{111}Sn		[B75]	1997	35.3 m	0.6	[A41]
		1972	^{110}Cd(^{3}He, 2n)^{111}Sn		[B75]	2003	35.3 m	0.6	[A42]
		1972	^{111}Sb(β^{+} + EC)^{111}Sn	Positron emission accompanied by electron capture	[S53]	2012	35.3 m	0.6	[A43]
		1974	^{107}Ag(^{7}Li, 3n)^{111}Sn	Lithium beam on the ^{107}Ag target	[B73]	2014	35 m		[D4]
		1974	^{113}In(p, 3n)^{111}Sn	Proton beam on natural indium	[H30]	2015	35 m		[K6]
		1974	^{112}Sn(d, t)^{111}Sn	Neutron pickup reaction	[W15]	2017	35.3 m	0.6	[A45]
		1975	^{112}Sn(d, t)^{111}Sn	Deuteron beams on the thin tin target	[B21]				
		1976	^{108}Cd(α, n)^{111}Sn	Alpha-irradiation	[M4]				
		1976	^{112}Sn(p, d)^{111}Sn		[W23]				
		1976	^{111}Sb(ε)^{111}Sn	^{111}Sb production from natural tin using ^{112}Sn(p, 2n)^{111}Sb reaction	[W23]				

Table 6: Discovery, production scheme and half-lives of tin isotopes *(continued)*

Isotope	Year	Production scheme				Half-life value			
		Year	*Reaction*	*Principal method/condition*	*Ref*	*Year*	*Half-life*		*Ref*
^{111}Sn	1949	---	---	---	---	---	---	---	[H27]
		1977	^{58}Ni(^{58}Ni)^{111}Sn	Fusion-evaporation	[K37]				
		1977	^{112}Sn(d, t)^{111}Sn	Single-neutron pickup reaction	[W16]				
		1978	^{112}Sn(d, t)^{111}Sn	Deuteron bombardment	[K43]				
		1978	^{109}Cd(^{3}He, nγ)^{111}Sn		H32]				
		1979	^{110}Cd(α, 3n)^{111}Sn	Alpha-particle on enriched Cd metal foil	[H12]				
		1980	^{112}Sn(^{3}He, α)^{111}Sn	Neutron pickup	[G23]				
		1980	^{112}Sn(p, d)^{111}Sn	Proton bombardment on Sn foil	[T2]				
		1981	^{112}Sn(p, d)^{111}Sn	Proton bombardment	[B55]				
		1982	^{112}Sn(p, d)^{111}Sn	Target preparation by SnO_2 evaporation	[F16]				
		1982	^{112}Sn(d, t)^{111}Sn	Vector-polarized deuteron beam on the tin target	[G9]				
		1984	^{108}Cd(α, n)^{111}Sn	Alpha-particle bombardment	[P32]				
		1984	^{111}Cd(^{3}He, 3n)^{111}Sn	^{3}He beam on the cadmium target	[P32]				
		1984	^{109}Ag(^{6}Li, 4n)^{111}Sn	^{6}Li beam on the silver target	[P32]				
		1985	^{112}Sn(^{3}He, αγ)^{111}Sn	Neutron-pickup reaction, ^{3}He beam on self-supporting metallic ^{112}Sn foil	[A50]				
		1986	Cd(α)^{111}Sn	Alpha-irradiation on the cadmium target	[A17]				
		1986	^{20}Ne(^{91}Zr, γ)^{111}Sn	Thick self-supporting target	[G2]				
		1987	^{100}Mo(^{16}O, 5n)^{111}Sn	Fusion-evaporation	[E1]				
		1995	^{103}Rh(^{12}C, p3n)^{111}Sn	Thick self-supporting rhodium target	[G11]				
		1995	^{96}Ru(^{19}F, 3p1n)^{111}Sn	^{96}Ru target backed by ^{208}Pb	[L4]				
		1995	^{64}Ni(^{56}Fe, αp4n)^{111}Sn	Thin self-supporting ^{64}Ni target	[L4]				
		1996	^{112}Sn(n, 2n)^{111}Sn		[A21]				
		2003	^{98}Mo(^{16}O, 3n)^{111}Sn	^{16}O beam on the ^{98}Mo target followed by neutron evaporation from ^{114}Sn	[W27]				

Table 6: Discovery, production scheme and half-lives of tin isotopes *(continued)*

Isotope	Year	Production scheme				Half-life value			
		Year	*Reaction*	*Principal method/condition*	*Ref*	*Year*	*Half-life*		*Ref*
^{111}Sn	1949	---	---	---	---	---	---	---	[H27]
		2005	^{98}Mo(^{16}O, 3n)^{111}Sn	^{16}O beam on the ^{98}Mo target	[W29]				
		2007	^{112}Sn(α, αn)^{111}Sn		[R23]				
		2008	^{100}Mo(^{20}Ne, α5n)^{111}Sn	Isotopically enriched ^{100}Mo evaporation on aluminium backing	[G13]				
		2014	^{112}Sn(γ, n)^{111}Sn	Photonuclear reaction	[D4]				
		2015	^{112}Sn(γ, n)^{111}Sn	Photonuclear reaction	[D5]				
		2015	^{112}Sn(γ, n)^{111}Sn	Bremsstrahlung irradiation	[K6]				
^{112}Sn	1927	---	---	---	---	---	---	---	[A31]
		1939	^{112}In(β$^-$)^{112}Sn		[C44]	1937	STABLE		[G40]
		1952	^{112}In(β$^-$)^{112}Sn	Beta-decay	[G30]	1947	105 d		[S34]
		1953	^{112}In(β$^-$)^{112}Sn		[57]	1961	32.1 m	2	[R22]
		1961	^{114}Sn(p, t)^{112}Sn	Proton bombardment	[C35]	2003	STABLE		[A42]
		1962	^{112}In(β$^-$)^{112}Sn	^{112}In production from ^{113}In(γ, n)^{112}In and ^{112}Cd(d, 2n)^{112}In reactions	[R33]	2003	STABLE		[L3]
		1963	^{112}In(β$^-$)^{112}Sn	Beta-decay	[D3]	2005	3.8×10^{24} y		[D22]
		1965	^{114}Sn(p, t)^{112}Sn	Proton bombardment	[B16]	2007	1.3×10^{20} y		[K36]
		1967	^{112}Cd(^{3}He, 3nγ)^{112}Sn	^{3}He projectile hitting	[B31]	2008	9.2×10^{19} y		[B8]
		1967	^{110}Cd(α, 2n)^{112}Sn	Alpha-particle bombardment	[Y3]	2008	$>1.5\times10^{18}$ y		[D11]
		1968	^{110}Cd(α, 2n)^{112}Sn	Alpha-particle bombardment	[Y5]	2008	1.8×10^{19} y	1.3	[D12]
		1969	^{110}Cd(α, 2n)^{112}Sn	Alpha-particle bombardment	[Y6]	2008	$>2.7\times10^{19}$ y	1.3	[K33]
		1969	^{113}In(p, 2n)^{112}Sn	Proton bombardment	[Y6]	2008	$\sim10\times10^{23-24}$ y		[K33]
		1970	^{114}Sn(p, t)^{112}Sn	Target preparation by SnO_2 evaporation	[F14]	2009	4.7×10^{20} y		[B9]
		1972	^{112}Sb(β$^+$ + EC)^{112}Sn	$^{112}SnO_2$ target enriched with ^{112}Sn, ^{112}Sb production by (p, n) reaction	[M28]	2012	STABLE		[A43]
		1972	^{112}Sb(β$^+$ + EC)^{112}Sn	Positron emission accompanied by electron capture	[S53]	2017	STABLE		[A45]
		1975	^{110}Cd(α, 2n)^{112}Sn	Alpha beam on cadmium foil	[V7]				

Table 6: Discovery, production scheme and half-lives of tin isotopes *(continued)*

Isotope	Year	Production scheme				Half-life value			
		Year	*Reaction*	*Principal method/condition*	*Ref*	*Year*	*Half-life*		*Ref*
^{112}Sn	1927	---	---	---	---	---	---	---	[A31]
		1976	^{112}Sb(ε)^{112}Sn	^{112}Sb production from natural tin using ^{112}Sn(p, n)^{112}Sb reaction	[W23]				
		1977	^{110}Cd(^{3}He, n)^{112}Sn	Two-neutron transfer reaction, target preparation by rolling or evaporation	[F10]				
		1979	^{110}Cd(α, 2nγ)^{112}Sn	Alpha bombardment	[B79]				
		1980	^{114}Sn(p, t)^{112}Sn		[B54]				
		1994	^{100}Mo(^{18}O, 6n)^{112}Sn		[A3]				
		1997	^{19}F(^{93}Nb)^{112}Sn	Fusion-evaporation	[J8]				
		2003	^{98}Mo(^{16}O, 2n)^{112}Sn	^{16}O beam on the ^{98}Mo target followed by neutron evaporation from ^{114}Sn	[W27]				
		2005	^{116}Te(γ, α)^{112}Sn		[G8]				
		2005	^{98}Mo(^{16}O, 2n)^{112}Sn	^{16}O beam on the ^{98}Mo target	[W29]				
		2007	^{100}Mo(^{20}Ne, α4n)^{112}Sn	Isotopically enriched ^{100}Mo evaporated on aluminium backing	[G12]				
		2012	^{114}Sn(p, t)^{112}Sn	Proton beam on the Sn target	[G50]				
		2015	^{108}Cd(α, γ)^{112}Sn		[N11]				
		2017	^{114}Sn(γ, 2n)^{112}Sn		[B4]				
^{113}Sn	1936	---	---	---	---	---	---	---	[L23]
		1936	^{113}In(p, n)^{113}Sn	Proton bombardment	[L23]	1939	105 d	15	[B13]
		1938	^{113}In(p, n)^{113}Sn	Proton-induced reaction	[D27]	1939	~70 d		[L24]
		1939	^{113}In(p, n)^{113}Sn	Proton bombardment	[B12]	1947	105 d		[C40]
		1947	Cd(α, n)^{113}Sn	Alpha bombardment	[C40]	1947	105 d		[S34]
		1947	^{113}In(d, 2n)^{113}Sn	Deuteron bombardment	[S34]	1948	~100 d		[M30]
		1948	^{114}Sn(γ, n)^{113}Sn	Neutron removal	[M30]	1950	104 d		[M24]
		1948	^{112}Sn(n, γ)^{113}Sn		[S29]	1951	118 d	2	[C43]
		1951	^{112}Sn(n)^{113}Sn	Neutron capture	[C43]	1951	112 d		[T8]
		1959	^{112}Sn(n, γ)^{113}Sn	Neutron-irradiation	[B86]	1952	112 d		[G30]
		1961	^{112}Sn(n, γ)^{113}Sn	Neutron irradiation on ^{112}Sn enriched tin	[G37]	1956	130 d	3	[G14]

Table 6: Discovery, production scheme and half-lives of tin isotopes *(continued)*

Isotope	Year	Production scheme				Half-life value			
		Year	*Reaction*	*Principal method/condition*	*Ref*	*Year*	*Half-life*		*Ref*
^{113}Sn	1936	---	---	---	---	---	---	---	[L23]
		1961	^{112}Sn(n)^{113}Sn	Thermal-neutron irradiation	[S16]	1957	130 d		[B35]
		1964	^{112}Sn(d, p)^{113}Sn	Deuteron bombardment	[C37]	1959	112 d		[B86]
		1964	^{114}Sn(d, t)^{113}Sn	Deuteron bombardment	[C37]	1961	~119 d		[G37]
		1966	^{112}Sn(d, p)^{113}Sn	Neutron stripping	[R27]	1961	118 d	3	[S16]
		1967	^{112}Sn(d, p)^{113}Sn	Stripping reaction	[S17]	1961	20 m	1	[S16]
		1967	^{114}Sn(d, t)^{113}Sn	Stripping reaction	[S17]	1965	118 d		[S60]
		1968	^{112}Sn(n, γ)^{113}Sn	Neutron capture	[S3]	1967	119 d		[B68]
		1969	^{112}Sn(n, γ)^{113}Sn	Irradiation of stable Sn metal	[P33]	1969	118 d		[P33]
		1969	^{112}Cd(α, 3n)^{113}Sn	Alpha-particle bombardment	[Y6]	1971	112 d	1	[R7]
		1970	^{114}Sn(p, d)^{113}Sn	Proton bombardment	[C17]	1972	115.07 d	0.30	[L5]
		1970	^{114}Sn(n, 2n)^{113}Sn		[L34]				
		1971	^{115}Sn(p, t)^{113}Sn	Target preparation by SnO_2 evaporation	[F15]	1974	115 d		[B87]
		1972	^{111}Cd(α, 2nγ)^{113}Sn		[B75]	1975	115 d		[D20]
		1972	^{113}Sb(β^+ + EC)^{113}Sn	Positron emission accompanied by electron capture	[S53]	1976	118 d		[F47]
		1973	^{112}Sn(n, γ)^{113}Sn		[R9]	1977	115 d		[B88]
		1973	^{112}In(p, n)^{113}Sn		[R9]	1977	115.07 d	0.3	[P21]
		1974	^{109}Ag(^{7}Li, 3n)^{113}Sn	Lithium beam on the ^{107}Ag target	[B73]	1978	115.1 d		[H23]
		1974	^{111}Cd(α, 2n)^{113}Sn	Alpha-beam on the ^{111}Cd target	[B73]	1980	115.09 d	0.04	[H35]
		1974	^{113}In(p, n)^{113}Sn		[D19]	1987	115 d		[A18]
		1975	^{112}Sn(d, p)^{113}Sn	Deuteron beams on the thin tin target	[B21]	1992	115.079 d	0.080	[U4]
		1975	^{112}Sn(n, γ)^{113}Sn		[D20]	1993	115.1 d		[F17]
		1975	^{114}Sn(d, t)^{113}Sn	Deuteron beams on the thin tin target	[B21]	1995	115.1 d		[G31]
		1975	^{113}In(p, n)^{113}Sn		[D20]	1997	115.09 d	0.04	[A41]
		1975	^{115}In(p, 3n)^{113}Sn		[D20]	2003	115.09 d	0.03	[A42]
		1975	^{113}In(d, 2n)^{113}Sn		[D20]	2003	115.09 d	1.00	[P28]
		1975	^{115}In(d, 4n)^{113}Sn		[D20]	2008	115 d		[K33]
		1975	^{110}Cd(α, n)^{113}Sn		[D20]	2009	115.09 d		[B9]
		1975	^{111}Cd(α, 2n)^{113}Sn		[D20]	2012	115.09 d	0.03	[A43]
		1975	^{112}Cd(α, 3n)^{113}Sn		[D20]	2014	115.09 d	0.03	[R32]
		1975	^{113}Cd(α, 4n)^{113}Sn		[D20]	2017	115.09 d	0.03	[A45]

Table 6: Discovery, production scheme and half-lives of tin isotopes *(continued)*

Isotope	Year	Production scheme				Half-life value			
		Year	***Reaction***	***Principal method/condition***	***Ref***	***Year***	***Half-life***		***Ref***
^{113}Sn	1936	---	---	---	---	---	---	---	[L23]
		1975	^{113}Cd(α, 4n)^{113}Sn		[V7]	2018	115.09 d		[A6]
		1976	^{110}Cd(α, n)^{113}Sn	Alpha-irradiation	[M4]	2018	115.1 d		[A27]
		1976	^{113}Sb(ε)^{113}Sn	^{113}Sb production from natural tin using ^{112}Sn(d, n)^{113}Sb reaction	[W23]				
		1977	^{114}Sn(d, t)^{113}Sn	Single-neutron pickup reaction	[W16]				
		1978	^{114}Sn(d, t)^{113}Sn	Deuteron bombardment	[K43]				
		1978	^{114}Sn(^{3}He, α)^{113}Sn	Neutron pickup reaction	[T6]				
		1979	^{112}Sn(t, d)^{113}Sn	Triton bombardment	[C27]				
		1979	^{112}Cd(α, 3n)^{113}Sn	Alpha-particle on enriched Cd	[H12]				
		1980	^{114}Sn(p, d)^{113}Sn	Proton bombardment on Sn foil	[T2]				
		1982	^{114}Sn(p, d)^{113}Sn	Target preparation by SnO_2 evaporation	[F16]				
		1991	^{112}Sn(α, ^{3}He)^{113}Sn	Stripping reaction	[M13]				
		1995	^{114}Sn(n, 2n)^{113}Sn		[G31]				
		1996	^{112}Sn(n, γ)^{113}Sn		[A21]				
		1997	^{113}In(p, n)^{113}Sn	Proton-induced reaction	[K17]				
		1997	^{115}In(p, 3n)^{113}Sn	Proton-induced reaction	[K17]				
		1997	^{110}Cd(α, n)^{113}Sn	Alpha-particle-induced reaction	[K17]				
		1997	^{111}Cd(α, 2n)^{113}Sn	Alpha-particle-induced reaction	[K17]				
		1998	^{100}Mo(^{18}O, 5n)^{113}Sn	Thick ^{100}Mo target backed onto Au backing	[C26]				
		2005	^{98}Mo(^{16}O, n)^{113}Sn	^{16}O beam on the ^{98}Mo target	[W29]				
		1998	^{100}Mo(^{18}O, 5n)^{113}Sn	^{18}O beam on self-supporting ^{100}Mo foil	[S31]				
		2005	^{112}Sn(d, p)^{113}Sn	Deuteron beam on the enriched Sn target	[B5]				
		2005	^{118}Sn(d, p6n)^{113}Sn	Deuteron beam on the enriched Sn target	[B5]				

Table 6: Discovery, production scheme and half-lives of tin isotopes *(continued)*

Isotope	Year	Production scheme				Half-life value			
		Year	*Reaction*	*Principal method/condition*	*Ref*	*Year*	*Half-life*		*Ref*
^{113}Sn	1936	---	---	---	---	---	---	---	[L23]
		2005	^{120}Sn(d, p8n)^{113}Sn	Deuteron beam on the enriched Sn target	[B5]				
		2005	^{124}Sn(d, p12n)^{113}Sn	Deuteron beam on the enriched Sn target	[B5]				
		2006	^{112}Sn(n, γ)^{113}Sn	Thermal-neutron capture by natural Sn foil	[K50]				
		2015	^{114}Sn(γ, n)^{113}Sn	Bremsstrahlung irradiation	[K6]				
		2016	^{100}Mo(^{19}F, p5n)^{113}Sn	Isotopically enriched ^{100}Mo target, evaporated on gold backing	[B6]				
		2017	^{113m}In(β$^-$)^{113}Sn		[C39]				
		2018	^{115}In(α, t3n)^{113}Sn		[A6]				
		2018	^{113}In(α, tn)^{113}Sn		[A6]				
		2018	^{110}Cd(α, n)^{113}Sn		[A27]				
		2018	^{111}Cd(α, 2n)^{113}Sn		[A27]				
		2018	^{112}Cd(α, 3n)^{113}Sn		[A27]				
		2018	^{113}Cd(α, 4n)^{113}Sn		[A27]				
		2018	^{114}Cd(α, 5n)^{113}Sn		[A27]				
		2018	^{112}Sn(^{7}Li, ^{6}Li)^{113}Sn	One-neutron stripping	[C29]				
^{114}Sn	1927	---	---	---	---	---	---	---	[A31]
		1939	^{114}In(β$^-$)^{114}Sn		[C44]	1937	STABLE		[G40]
		1940	^{114}In(β$^-$)^{114}Sn		[L8]	2003	STABLE		[A42]
		1952	^{114}In(β$^-$)^{114}Sn	Beta-decay	[G30]	2003	STABLE		[L3]
		1952	^{114}In(β$^-$)^{114}Sn	Beta-decay	[J9]	2012	STABLE		[A43]
		1953	^{114}In(β$^-$)^{114}Sn	Beta-decay	[H33]	2017	STABLE		[A45]
		1956	^{114}In(β$^-$)^{114}Sn	Beta-decay	G39]				
		1961	^{114}In(β$^-$)^{114}Sn		[D7]				
		1961	^{114}In(β$^-$)^{114}Sn		[N12]				
		1963	^{114}In(β$^-$)^{114}Sn	Beta-decay	[D3]				
		1964	^{113}Sn(d, p)^{114}Sn	Deuteron bombardment	[C37]				
		1964	^{115}Sn(d, t)^{114}Sn	Deuteron bombardment	[C37]				
		1965	^{116}Sn(p, t)^{114}Sn	Proton bombardment	[B16]				
		1967	^{114}Cd(^{3}He, 3nγ)^{114}Sn	^{3}He projectile hitting	[B31]				
		1967	^{112}Cd(α, 2n)^{114}Sn	Alpha-particle bombardment	[Y3]				

Table 6: Discovery, production scheme and half-lives of tin isotopes *(continued)*

Isotope	Year	Production scheme				Half-life value			
		Year	*Reaction*	*Principal method/condition*	*Ref*	*Year*	*Half-life*		*Ref*
^{114}Sn	1927	---	---	---	---	---	---	---	[A31]
		1968	^{113}Sn(d, p)^{114}Sn	Deuteron bombardment	[C38]				
		1968	^{114}Sb(β^+)^{114}Sn		[R6]				
		1968	^{112}Cd(α, 2n)^{114}Sn	Alpha-particle bombardment	[Y5]				
		1969	^{112}Sn(t, p)^{114}Sn	^{112}Sn target preparation by vacuum evaporation	[B44]				
		1969	^{112}Cd(α, 2n)^{114}Sn	Alpha-particle bombardment	[Y6]				
		1969	^{115}In(p, 2n)^{114}Sn	Proton bombardment	[Y6]				
		1970	^{116}Sn(p, t)^{114}Sn	Target preparation by SnO_2 evaporation	[F14]				
		1971	^{116}Sn(p, t)^{114}Sn		[F15]				
		1972	^{113}In(^{3}He, d)^{114}Sn	^{3}He ions on enriched targets of ^{113}In supported on carbon foil backings	[C2]				
		1972	^{114}Sb(β^+ + EC)^{114}Sn	$^{114}SnO_2$ target enriched with ^{114}Sn, ^{114}Sb production by (p, n) reaction	[M28]				
		1972	^{114}Sb(β^+ + EC)^{114}Sn	Positron emission accompanied by electron capture	[S53]				
		1973	^{112}Sn(^{18}O, ^{16}O)^{114}Sn	Two-neutron transfer	[A23]				
		1973	^{116}Sn(p, t)^{114}Sn		[Y2]				
		1975	^{112}Sn(^{18}O, ^{16}O)^{114}Sn	*2n*-transfer reaction	[B61]				
		1976	^{114}Sb(ε)^{114}Sn	^{114}Sb production from natural tin using ^{114}Sn(p, n)^{114}Sb reaction	[W23]				
		1977	^{116}Sn(p, t)^{114}Sn	Proton bombardment	[C47]				
		1977	^{112}Cd(^{3}He, n)^{114}Sn	Two-neutron transfer reaction, target preparation by rolling or evaporation	[F10]				
		1979	^{112}Cd(α, 2nγ)^{114}Sn	Alpha bombardment	[B79]				
		1980	^{116}Sn(p, t)^{114}Sn	Proton beam on isotopically enriched metal foils	[C48]				

Table 6: Discovery, production scheme and half-lives of tin isotopes *(continued)*

Isotope	Year	Production scheme				Half-life value			
		Year	*Reaction*	*Principal method/condition*	*Ref*	*Year*	*Half-life*		*Ref*
^{114}Sn	1927	---	---	---	---	---	---	---	[A31]
		1980	^{112}Cd(α, 2n)^{114}Sn	Alpha-particle bombardment on self-supporting cadmium target	[P24]				
		1981	^{116}Sn(p, t)^{114}Sn	Proton beam on self-supporting metal foils	[C50]				
		1982	^{115}Sn(p, d)^{114}Sn	Target preparation by SnO_2 evaporation	[F16]				
		1982	^{116}Sn(α, ^{6}He)^{114}Sn		[G24]				
		1989	^{116}Sn(p, t)^{114}Sn		[G25]				
		1989	^{116}Sn(α, ^{6}He)^{114}Sn		[G25]				
		1989	^{100}Mo(^{18}O, 4n)^{114}Sn		[H10]				
		1991	^{100}Mo(^{18}O, 4n)^{114}Sn	Compound nucleus reaction	[S10]				
		1991	^{112}Cd(α, 2n)^{114}Sn	Compound nucleus reaction	[S10]				
		1992	^{100}Mo(^{18}O, 4n)^{114}Sn	Compound nucleus reaction	[S11]				
		1992	^{112}Cd(α, 2n)^{114}Sn	Compound nucleus reaction	[S11]				
		1994	^{112}Cd(α, 2n)^{114}Sn	Compound nucleus reaction on self-supporting ^{112}Cd foil	[S12]				
		1995	^{103}Rh(^{12}C, p)^{114}Sn	Self-supporting natural Rh evaporated on gold backing	[C24]				
		1995	^{112}Cd(α, 2n)^{114}Sn	Compound-nucleus reaction	[W26]				
		1997	^{110}Pb(^{9}Be, 5n)^{114}Sn	Heavy-ion fusion, ^{110}Pb target backing on natural lead	[S30]				
		2001	^{100}Mo(^{18}O, 4n)^{114}Sn	Self-supporting ^{100}Mo foil rolled onto bismuth backing	[G4]				
		2003	^{98}Mo(^{16}O, γ)^{114}Sn	^{16}O beam on the ^{98}Mo target	[W27]				
		2004	^{116}Sn(p, t)^{114}Sn		[G45]				
		2005	^{98}Mo(^{16}O, γ)^{114}Sn	^{16}O beam on the ^{98}Mo target	[W29]				
		2006	^{115}Sn(n, 2n)^{114}Sn		[F33]				

Table 6: Discovery, production scheme and half-lives of tin isotopes *(continued)*

Isotope	Year	Production scheme				Half-life value			
		Year	*Reaction*	*Principal method/condition*	*Ref*	*Year*	*Half-life*		*Ref*
^{114}Sn	1927	---	---	---	---	---	---	---	[A31]
		2008	^{114}Cd(β^- β^-)^{114}Sn	Double-beta decay experiment using a low-background $CdWO_4$ crystal scintillator	[B23]				
		2010	^{117}Sn(γ, 3n)^{114}Sn	Photoneutron reactions	[V3]				
		2014	^{48}Ca(^{238}U)^{114}Sn		[I9]				
		2016	^{113}In(p, γ)^{114}Sn	Target preparation by evaporating of natural indium	[H11]				
^{115}Sn	1927	---	---	---	---	---	---	---	[A31]
		1939	^{115}In(β^-)^{115}Sn		[C44]	1937	STABLE		[G40]
		1949	^{115}In(β^-)^{115}Sn		[B22]	2003	STABLE		[A42]
		1950	^{115}In(β^-)^{115}Sn		[M12]	2003	STABLE		[L3]
		1952	^{115}In(β^-)^{115}Sn	Beta-decay	[G30]	2012	STABLE		[A43]
		1953	^{115}In(β^-)^{115}Sn	Beta-decay	[H33]	2017	STABLE		[A45]
		1960	^{115}In(β^-)^{115}Sn		[Y8]				
		1961	^{115}In(β^-)^{115}Sn		[B19]				
		1961	^{116}Sn(d, t)^{115}Sn	Deuteron bombardment	[C35]				
		1962	^{115}Sb(β^+)^{115}Sn	Electron capture and positron emission	[S32]				
		1964	^{114}Sn(d, p)^{115}Sn	Deuteron bombardment	[C37]				
		1964	^{115}In(p, nγ)^{115}Sn		[I13]				
		1964	^{116}Sn(d, t)^{115}Sn	Deuteron bombardment	[C37]				
		1966	^{115}In(p, n)^{115}Sn		[M18]				
		1966	^{114}Sn(d, p)^{115}Sn	Neutron stripping	[R27]				
		1966	^{115}In(p, n)^{115}Sn	Irradiation with proton beam	[T9]				
		1967	^{115m}In(β^-)^{115}Sn		[M38]				
		1967	^{115}Sb(β^+)^{115}Sn		[M38]				
		1967	^{114}Sn(d, p)^{115}Sn	Stripping reaction	[S17]				
		1967	^{116}Sn(d, t)^{115}Sn	Stripping reaction	[S17]				
		1969	^{116}Sn(γ, n)^{115}Sn	Photonuclear reaction	[F48]				
		1969	^{114}Cd(α, 3n)^{115}Sn	Alpha-particle bombardment	[Y6]				
		1970	^{116}Sn(p, d)^{115}Sn	Proton bombardment	[C17]				
		1971	^{117}Sn(p, t)^{115}Sn	Target preparation by SnO_2 evaporation	[F15]				
		1973	^{116}Sn(p, d)^{115}Sn	Neutron pickup reaction	[I6]				
		1974	^{115}In(β^-)^{115}Sn	Natural indium enriched with ^{115}In	[H7]				
		1974	^{116}Sn(d, t)^{115}Sn	Neutron pickup reaction	[W15]				

Table 6: Discovery, production scheme and half-lives of tin isotopes *(continued)*

Isotope	Year	Production scheme				Half-life value			
		Year	*Reaction*	*Principal method/condition*	*Ref*	*Year*	*Half-life*		*Ref*
^{115}Sn	1927	---	---	---	---	---	---	---	[A31]
		1975	^{116}Sn(d, t)^{115}Sn	Deuteron beams on the thin tin target	[B21]				
		1975	^{114}Sn(d, p)^{115}Sn	Deuteron beams on the thin tin target	[B21]				
		1975	^{115}In(p, n)^{115}Sn	^{115}In target preparation by evaporation	[M3]				
		1975	^{112}Cd(α, n)^{115}Sn	^{112}Cd target preparation by evaporation	[M3]				
		1975	^{115}In(d, 2n)^{115}Sn	^{115}In target preparation by evaporation	[M3]				
		1975	^{113}Cd(α, 2n)^{115}Sn	^{113}Cd target preparation by evaporation	[M3]				
		1976	^{115}In(β$^-$)^{115}Sn	Beta-decay	[R3]				
		1976	^{115}Sb(ε)^{115}Sn	^{115}Sb production from natural tin using ^{114}Sn(d, n)^{115}Sb reaction	[W23]				
		1977	^{116}Sn(d, t)^{115}Sn	^{116}Sn target preparation by vacuum evaporation	[B26]				
		1977	^{116}Sn(d, t)^{115}Sn	Neutron pickup reaction	[B27]				
		1977	^{116}Sn(^{3}He, α)^{115}Sn	Neutron pickup reaction	[S33]				
		1977	^{116}Sn(p, d)^{115}Sn	Neutron pickup reaction	[S33]				
		1977	^{116}Sn(d, t)^{115}Sn	Single-neutron pickup reaction	[W16]				
		1978	^{112}Cd(α, nγ)^{115}Sn		[H32]				
		1978	^{116}Sn(d, t)^{115}Sn	Deuteron bombardment	[K43]				
		1978	^{115}In(β$^-$)^{115}Sn	Beta-emission	[P15]				
		1978	^{114}Sn(n, γ)^{115}Sn	Neutron capture	[R12]				
		1978	^{116}Sn(^{3}He, α)^{115}Sn	Neutron pickup reaction	[T6]				
		1979	^{114}Sn(t, d)^{115}Sn	Triton bombardment	[C27]				
		1979	^{116}Cd(α, 5n)^{115}Sn	Alpha-particle on enriched Cd metal foil	[H12]				
		1979	^{117}Sn(p, t)^{115}Sn		[R18]				
		1980	^{116}Sn(^{3}He, α)^{115}Sn	Neutron pickup	[G23]				
		1980	^{116}Sn(p, d)^{115}Sn	Proton bombardment on Sn foil	[T2]				

Table 6: Discovery, production scheme and half-lives of tin isotopes *(continued)*

Isotope	Year	Production scheme				Half-life value			
		Year	*Reaction*	*Principal method/condition*	*Ref*	*Year*	*Half-life*		*Ref*
^{115}Sn	1927	---	---	---	---	---	---	---	[A31]
		1981	^{116}Sn(d, t)^{115}Sn	Neutron pickup reaction with vector-polarized deuteron beam	[P14]				
		1982	^{116}Sn(p, d)^{115}Sn	Target preparation by SnO_2 evaporation	[F16]				
		1985	^{115}In(p, n)^{115}Sn	Proton beam on isotopically enriched ^{115}In target	[R19]				
		1990	^{116}Cd(α, 5n)^{115}Sn	Alpha-bombardment on carbon-backed ^{116}Cd metal	[C52]				
		1994	^{116}Sn(d, t)^{115}Sn	Polarized deuteron beam on ^{116}Sn	[W20]				
		1996	^{114}Sn(n, γ)^{115}Sn	Neutron capture	[W24]				
		1997	^{110}Pb(^{9}Be, 4n)^{115}Sn	Heavy-ion fusion, ^{110}Pb target backing on natural lead	[S30]				
		1998	^{104}Ru(^{18}O, α3n)^{115}Sn	Fusion-evaporation	[S5]				
		1999	^{113}Cd(α, 2nγ)^{115}Sn	Alpha-bombardment on self-supporting ^{113}Cd target	[L25]				
		2000	^{116}Sn(d, ^{3}He)^{115}Sn	Nucleon pickup pion transfer	[U1]				
		2003	^{116}Sn(d, ^{3}He)^{115}Sn	Pion-transfer reaction under recoil-free condition	[S76]				
		2004	^{116}Sn(d, ^{3}He)^{115}Sn	Pion-transfer reaction under recoil-free condition	[S77]				
		2005	^{115}In(β^-)^{115}Sn	Beta-decay	[C13]				
		2006	^{116}Sn(n, 2n)^{115}Sn		[F33]				
		2007	^{115}In(β^-)^{115}Sn	Beta-decay	[C14]				
		2008	^{115m}In(β^-)^{115}Sn	Beta-decays of *r*-process	[D18]				
		2009	^{115}In^{m}(β^-)^{115}Sn	Beta-decay	[H19]				
		2009	^{115}In(β^-)^{115}Sn		[M36]				
		2009	^{116}Sn(γ, n)^{115}Sn	Photoneutron capture	[U5]				
		2009	^{115}In(β^-)^{115}Sn	Natural indium enriched with ^{115}In isotope	[W22]				

Table 6: Discovery, production scheme and half-lives of tin isotopes *(continued)*

Isotope	Year	Production scheme				Half-life value			
		Year	*Reaction*	*Principal method/condition*	*Ref*	*Year*	*Half-life*		*Ref*
^{115}Sn	1927	---	---	---	---	---	---	---	[A31]
		2011	^{115}In(β$^-$)^{115}Sn	Ultrapure natural indium enriched with ^{115}In	[A13]				
		2012	^{100}Mo(^{18}O, 3n)^{115}Sn		[B51]				
		2013	^{115}In(β$^-$)^{115}Sn	Thermal beta-decay	[K44]				
		2016	^{114}Sn(n, γ)^{115}Sn	Neutron capture	[U3]				
		2018	^{115}In(β$^-$)^{115}Sn	Beta-decay	[Z5]				
^{116}Sn	1922	---	---	---	---	---	---	---	[A30]
		1937	^{116}In(β$^-$)^{116}Sn	Beta-decay	[L7]	1937	STABLE		[G40]
		1939	^{116}In(β$^-$)^{116}Sn	Beta-particle emission	[C44]	2003	STABLE		[A42]
		1952	^{116}In(β$^-$)^{116}Sn	Beta-decay	[G30]	2003	STABLE		[L3]
		1954	^{116}In(β$^-$)^{116}Sn	Beta-radiation	[B62]	2012	STABLE		[A43]
		1955	^{116}Sb(β$^+$)^{116}Sn	Positron-emission	[S67]	2017	STABLE		[A45]
		1956	^{116}In(β$^-$)^{116}Sn	Beta-radiation	[S6]				
		1960	^{116}Sb(β$^+$)^{116}Sn	Positron-emission	[J7]				
		1960	^{116}In(β$^-$)^{116}Sn		[J7]				
		1961	^{117}Sn(d, t)^{116}Sn	Deuteron bombardment	[C35]				
		1962	^{116}In(β$^-$)^{116}Sn	^{116}In production by thermal-neutron capture	[F9]				
		1963	^{116}In(β$^-$)^{116}Sn	Beta-decay	[D3]				
		1964	^{113}Sn(d, p)^{116}Sn	Deuteron bombardment	[C37]				
		1964	^{117}Sn(d, t)^{116}Sn	Deuteron bombardment	[C37]				
		1966	^{115}In(^{3}He, d)^{116}Sn		[C42]				
		1967	^{115}In(^{3}He, d)^{116}Sn		[B38]				
		1967	^{116}Cd(^{3}He, 3nγ)^{116}Sn	^{3}He projectile hitting	[B31]				
		1967	^{115}In(^{3}He, d)^{116}Sn		[B38]				
		1967	^{114}Cd(α, 2n)^{116}Sn	Alpha-particle bombardment	[Y3]				
		1968	^{115}Sn(d, p)^{116}Sn	Deuteron bombardment	[C38]				
		1968	^{117}Sn(d, t)^{116}Sn	Deuteron bombardment	[C38]				
		1968	^{116}Sb(β$^+$)^{116}Sn		[R6]				
		1968	^{117}Sn(p, d)^{116}Sn	Proton irradiation	[Y1]				
		1968	^{118}Sn(p, t)^{116}Sn	Proton irradiation	[Y1]				
		1968	^{114}Cd(α, 2n)^{116}Sn	Alpha-particle bombardment	[Y5]				
		1969	^{114}Cd(α, 2nγ)^{116}Sn	Alpha bombardment	[C22]				
		1969	^{117}Sn(γ, n)^{116}Sn	Photonuclear reaction	[F48]				

Table 6: Discovery, production scheme and half-lives of tin isotopes *(continued)*

Isotope	Year	Production scheme				Half-life value			
		Year	*Reaction*	*Principal method/condition*	*Ref*	*Year*	*Half-life*		*Ref*
^{116}Sn	1922	---	---	---	---	---	---	---	[A30]
		1969	^{115}In(^{3}He, d)^{116}Sn	^{3}He bombardment on natural indium	[S51]				
		1969	^{114}Cd(α, 2n)^{116}Sn	Alpha-particle bombardment	[Y6]				
		1970	^{118}Sn(p, t)^{116}Sn	Target preparation by SnO_2 evaporation	[F14]				
		1970	^{116}In(β$^-$)^{116}Sn		[R2]				
		1971	Sn(C)^{116}Sn	^{116}Sn preparation from isotopically enriched Sn metal by vacuum evaporation using niobium boat and carbon backing	[R28]				
		1972	^{115}Sn(n, γ)^{116}Sn	Radiative capture of thermal neutron	[M22]				
		1972	^{116m}In(β$^-$)^{116}Sn	Target preparation by vacuum evaporation of natural indium onto mylar backing	[P22]				
		1973	^{117}Sn(p, d)^{116}Sn	Neutron pickup	[I6]				
		1973	^{116}In(β$^-$)^{116}Sn	^{116}In^{g} production from $^{115}In_2O_3$	[O7]				
		1973	^{118}Sn(p, t)^{116}Sn		[Y2]				
		1975	^{116m}In(β$^-$)^{116}Sn	^{116m}In preparation by ^{115}In(n, γ)^{116m}In reaction	[Y4]				
		1977	^{118}Sn(p, t)^{116}Sn	Proton bombardment	[C47]				
		1977	^{114}Cd(^{3}He, n)^{116}Sn	Two-neutron transfer reaction, target preparation by rolling or evaporation	[F10]				
		1979	^{114}Cd(α, 2nγ)^{116}Sn	Alpha bombardment	[B79]				
		1979	^{118}Sn(p, t)^{116}Sn	Polarized proton beam on the target	[Y9]				
		1980	^{118}Sn(p, t)^{116}Sn	Proton beam on isotopically enriched metal foil	[C48]				
		1980	^{114}Cd(α, 2n)^{116}Sn	Alpha-particle bombardment on self-supporting cadmium target	[P24]				
		1981	^{117}Sn(p, d)^{116}Sn	Proton beam on self-supporting metal foils	[C50]				

Table 6: Discovery, production scheme and half-lives of tin isotopes *(continued)*

Isotope	Year	Production scheme				Half-life value			
		Year	*Reaction*	*Principal method/condition*	*Ref*	*Year*	*Half-life*		*Ref*
^{116}Sn	1922	---	---	---	---	---	---	---	[A30]
		1981	^{118}Sn(p, t)^{116}Sn	Proton beam on self-supporting metal foils	[C50]				
		1981	^{116}Sb(ε)^{116}Sn		[J17]				
		1982	^{117}Sn(p, d)^{116}Sn	Target preparation by SnO_2 evaporation	[F16]				
		1985	^{118}Sn(p, t)^{116}Sn	Two-nuclear transfer reaction	[M26]				
		1986	^{115}In(^{3}He, d)^{116}Sn	Proton-stripping	[W17]				
		1986	^{115}In(α, t)^{116}Sn	Proton-stripping	[W17]				
		1987	^{112}Cd(^{7}Li)^{116}Sn	^{7}Li-pulsed beam hitting on the ^{112}Cd target	[L30]				
		1987	^{115}In(α, t)^{116}Sn		[W18]				
		1990	^{116}Cd(α, 4n)^{116}Sn	Alpha-bombardment on carbon-backed ^{116}Cd metal	[C52]				
		1990	^{117}Sn(d, t)^{116}Sn	Neutron pickup reaction	[S13]				
		1990	^{117}Sn(^{3}He, α)^{116}Sn	Neutron pickup reaction	[S13]				
		1990	^{115}In(^{3}He, d)^{116}Sn	Proton stripping reaction	[S13]				
		1990	^{115}In(α, t)^{116}Sn	Proton stripping reaction	[S13]				
		1991	^{115}Sn(n, γ)^{116}Sn	Thermal-neutron capture	[R14]				
		1992	^{115}In(^{3}He, d)^{116}Sn	Proton stripping reaction	[S14]				
		1992	^{115}In(α, t)^{116}Sn	Proton stripping reaction	[S14]				
		1993	^{115}Sn(n, γ)^{116}Sn	Neutron capture	[I1]				
		1994	^{116}Sb(β^{+} + ε)^{116}Sn	^{116}Sb preparation from ^{116}Sn target by proton bombardment	[G5]				
		1996	^{115}Sn(n, γ)^{116}Sn	Neutron capture	[W24]				
		1997	^{110}Pb(^{9}Be, 3n)^{116}Sn	Heavy-ion fusion, ^{110}Pb target backing on natural lead	[S30]				
		1998	^{117}Sn(p, np)^{116}Sn		[B89]				
		1998	^{104}Ru(^{18}O, α2n)^{116}Sn	Fusion-evaporation	[S5]				

Table 6: Discovery, production scheme and half-lives of tin isotopes *(continued)*

Isotope	Year	Production scheme				Half-life value			
		Year	*Reaction*	*Principal method/condition*	*Ref*	*Year*	*Half-life*		*Ref*
^{116}Sn	1922	---	---	---	---	---	---	---	[A30]
		2003	^{116}Cd(β⁻ β⁻)^{116}Sn	Double beta-decay experiment using a low-background cadmium tungstate ($^{116}CdWO_4$) crystal scintillator	[D6]				
		2003	^{116}Cd(β⁻ β⁻)^{116}Sn	Double beta transitions	[K34]				
		2006	^{116}Cd(β⁻ β⁻)^{116}Sn	Double beta decay	[R29]				
		2007	^{116}Cd(β⁻ β⁻)^{116}Sn	Double beta-decay	[B59]				
		2009	^{117}Sn(^{3}He, αγ)^{116}Sn	^{3}He beam on the self-supporting ^{117}Sn target	[A4]				
		2009	^{117}Sn(γ, n)^{116}Sn	Neutron capture	[U5]				
		2011	^{118}Sn(p, t)^{116}Sn		[G49]				
		2011	^{116}Cd(β⁻ β⁻)^{116}Sn	Double-beta decay	[R5]				
		2011	^{115}In(p)^{116}Sn	*s*-Process	[T19]				
		2014	^{48}Ca(^{238}U)^{116}Sn	Fusion-fission	[I9]				
		2014	^{64}Ni(^{238}U)^{116}Sn	Fusion-fission	[I9]				
		2014	^{48}Ca(^{208}Pb)^{116}Sn	Fusion-fission	[I9]				
		2015	^{116}Cd(β⁻ β⁻)^{116}Sn	Double beta-decay	[N7]				
		2016	^{115}In(p, γ)^{116}Sn	Target preparation by natural indium evaporation	[H11]				
		2017	^{116m}In(β⁻)^{116}Sn	Beta-decay	[P29]				
		2018	^{116}Cd(^{20}Ne, ^{20}O)^{116}Sn	Heavy-ion induced double charge exchange reaction	[C8]				
^{117}Sn	1922	---	---	---	---	---	---	---	[A30]
		1939	^{117}In(β⁻)^{117}Sn	Beta-particle emission	[C44]	1937	STABLE		[G40]
		1950	^{114}Cd(α, n)^{117}Sn	Alpha-particle bombardment on enriched cadmium	[M9]	1950	14 d		[H18]
		1950	^{116}Sn(d, p)^{117}Sn	Deuteron bombardment on enriched tin	[M9]	1950	14 d		[M9]
		1950	^{118}Sn(n^{f}, 2n)^{117}Sn	Fast neutron bombardment on enriched tin	[M9]	1951	14.0 d	0.5	[C43]
		1951	^{116}Sn(n)^{117}Sn	Neutron capture	[C43]	1956	14.5 d		[G29]
		1952	^{117}In(β⁻)^{117}Sn	Beta-decay	[G30]	2003	STABLE		[A42]
		1952	^{117}Sb(ε)^{117}Sn		[G30]	2003	STABLE		[L3]
		1955	^{117}In(β⁻)^{117}Sn		[M20]	2012	STABLE		[A43]
		1955	^{117}Sb(ε)^{117}Sn		[M20]	2017	STABLE		[A45]
		1960	^{117}In(β⁻)^{117}Sn		[Y8]				
		1961	^{116}Sn(d, p)^{117}Sn	Deuteron bombardment	[C35]				

Table 6: Discovery, production scheme and half-lives of tin isotopes *(continued)*

Isotope	Year	Production scheme				Half-life value			
		Year	*Reaction*	*Principal method/condition*	*Ref*	*Year*	*Half-life*		*Ref*
^{117}Sn	1922	---	---	---	---	---	---	---	[A30]
		1961	^{118}Sn(d, t)^{117}Sn	Deuteron bombardment	[C35]				
		1961	^{117}In(β^-)^{117}Sn		[H41]				
		1963	^{117}In(β^-)^{117}Sn	Beta-decay	[D3]				
		1963	^{117}Sb(β^+)^{117}Sn		[D3]				
		1963	^{117}In(β^-)^{117}Sn		[N9]				
		1966	^{116}Sn(d, p)^{117}Sn	Neutron stripping	[R27]				
		1967	^{116}Sn(d, p)^{117}Sn	Stripping reaction	[S17]				
		1967	^{118}Sn(d, t)^{117}Sn	Stripping reaction	[S17]				
		1968	^{117m}Sn(IC)^{117}Sn	Internal-conversion	[B60]				
		1968	^{116}Sn(n, γ)^{117}Sn	Neutron capture	[S3]				
		1968	^{116}Sn(d, p)^{117}Sn		[V6]				
		1968	^{118}Sn(p, d)^{117}Sn	Proton irradiation	[Y1]				
		1969	^{118}Sn(γ, n)^{117}Sn	Photonuclear reaction	[F48]				
		1969	^{116}Cd(α, 3n)^{117}Sn	Alpha-particle bombardment	[Y6]				
		1970	^{117}In(β^-)^{117}Sn		[B2]				
		1970	^{116}Sn(α, ^{3}He)^{117}Sn	Alpha bombardment	[B39]				
		1970	^{118}Sn(p, d)^{117}Sn	Proton bombardment	[C17]				
		1971	^{119}Sn(p, t)^{117}Sn	Target preparation by SnO_2 evaporation	[F15]				
		1972	^{116}Sn(d, p)^{117}Sn	^{116}Sn target preparation by vacuum evaporation	[C9]				
		1972	^{118}Sn(p, d)^{117}Sn	Neutron pickup reaction	[S1]				
		1972	^{119}Sn(p, t)^{117}Sn		[S68]				
		1973	^{118}Sn(p, d)^{117}Sn	Neutron pickup reaction	[I6]				
		1974	^{118}Sn(p, d)^{117}Sn	Neutron pickup reaction	[S2]				
		1974	^{118}Sn(^{3}He, α)^{117}Sn	Neutron pickup reaction	[S2]				
		1974	^{118}Sn(p, d)^{117}Sn		[S2]				
		1974	^{118}Sn(d, t)^{117}Sn	Neutron pickup reaction	[W15]				
		1975	^{116}Sn(d, p)^{117}Sn	Deuteron beams on the thin tin target	[B21]				
		1975	^{118}Sn(d, t)^{117}Sn	Deuteron beams on the thin tin target	[B21]				
		1975	^{116}Sn(n, γ)^{117}Sn	Neutron capture	[B34]				
		1975	^{118}Sn(^{3}He, α)^{117}Sn	Neutron pickup reaction	[G22]				

Table 6: Discovery, production scheme and half-lives of tin isotopes *(continued)*

Isotope	Year	Production scheme				Half-life value			
		Year	*Reaction*	*Principal method/condition*	*Ref*	*Year*	*Half-life*		*Ref*
^{117}Sn	1922	---	---	---	---	---	---	---	[A30]
		1975	^{118}Sn(d, t)^{117}Sn	Vector-polarized deuteron beam on self-supporting metallic ^{118}Sn foil	[V9]				
		1976	^{116}Sn(d, p)^{117}Sn		[M4]				
		1976	^{114}Cd(α, n)^{117}Sn	Alpha-irradiation	[M4]				
		1977	^{118}Sn(^{3}He, α)^{117}Sn	Neutron pickup reaction	[S33]				
		1977	^{118}Sn(p, d)^{117}Sn	Neutron pickup reaction	[S33]				
		1977	^{118}Sn(d, t)^{117}Sn	Single-neutron pickup reaction	[W16]				
		1978	^{118}Sn(d, t)^{117}Sn	Deuteron bombardment	[K43]				
		1978	^{116}Sn(n, γ)^{117}Sn	Neutron capture	[R12]				
		1978	^{118}Sn(^{3}He, α)^{117}Sn	Neutron pickup reaction	[T6]				
		1978	^{118}Sn(^{3}He, α)^{117}Sn	Neutron pickup reaction	[W21]				
		1979	^{116}Sn(t, d)^{117}Sn	Triton bombardment	[C27]				
		1979	^{116}Cd(α, 3n)^{117}Sn	Alpha-particle on enriched Cd metal foil	[H12]				
		1979	^{119}Sn(p, t)^{117}Sn		[R17]				
		1980	^{118}Sn(p, d)^{117}Sn	Proton bombardment on Sn foil	[T2]				
		1982	^{118}Sn(p, d)^{117}Sn	Target preparation by SnO_2 evaporation	[F16]				
		1984	^{116}Sn(α, ^{3}He)^{117}Sn	Neutron stripping reaction	[G10]				
		1986	^{117}In(β^-)^{117}Sn	Beta-decay	[B64]				
		1990	^{116}Cd(α, 3n)^{117}Sn	Alpha-bombardment on carbon-backed ^{116}Cd metal	[C52]				
		1991	^{116}Sn(α, ^{3}He)^{117}Sn	Stripping reaction	[M13]				
		1996	^{116}Sn(n, γ)^{117}Sn	Neutron capture	[W24]				
		1996	^{116}Sn(n, γ)^{117}Sn		[W25]				
		2006	^{116}Sn(n, γ)^{117}Sn	Thermal-neutron capture by natural Sn foil	[K50]				
		2007	^{116}Sn(n, γ)^{117}Sn	Neutron capture	[E2]				
		2007	^{115}Sn(α, 2p)^{117}Sn		[R23]				
		2007	^{116}Sn(α, n2p)^{117}Sn		[R23]				
		2007	^{117}Sn(α, 2n2p)^{117}Sn		[R23]				

Table 6: Discovery, production scheme and half-lives of tin isotopes *(continued)*

Isotope	Year	Production scheme				Half-life value			
		Year	*Reaction*	*Principal method/condition*	*Ref*	*Year*	*Half-life*		*Ref*
^{117}Sn	1922	---	---	---	---	---	---	---	[A30]
		2007	^{118}Sn(α, 3n2p)^{117}Sn		[R23]				
		2010	^{120}Sn(γ, 3n)^{117}Sn	Photoneutron reactions	[V3]				
		2011	^{124}Sn(n, 8nγ)^{117}Sn	Fusion-fission reaction	[F34]				
		2011	^{118}Sn(γ, n)^{117}Sn	Radiative neutron apture	[U6]				
		2018	^{116}Sn(n)^{117}Sn		[P4]				
		2018	^{118}Sn(n, 2n)^{117}Sn		[P4]				
^{118}Sn	1922	---	---	---	---	---	---	---	[A30]
		1960	^{118}Sb(β$^+$)^{118}Sn	Positron-emission	[J7]	1937	STABLE		[G40]
		1961	^{118}Sb(β$^+$)^{118}Sn	Positron-emission	[B63]	2003	STABLE		[A42]
		1961	^{119}Sn(d, t)^{118}Sn	Deuteron bombardment	[C35]	2003	STABLE		[L3]
		1961	^{117}Sn(d, p)^{118}Sn	Deuteron bombardment	[C35]	2012	STABLE		[A43]
		1961	^{117}Sn(d, p)^{118}Sn	Deuteron bombardment	[C36]	2017	STABLE		[A45]
		1961	^{118}Sb(β$^+$/ε)^{118}Sn		[I3]				
		1961	^{118}Sb(ε)^{118}Sn		[R15]				
		1961	^{118}In(β$^-$)^{118}Sn		[G27]				
		1962	^{117}Sn(n, γ)^{118}Sn		[B10]				
		1964	^{118}In(β$^-$)^{118}Sn		[K5]				
		1964	^{118}Sb(β$^+$ + EC)^{118}Sn	Positron emission accompanied by electron capture	[K5]				
		1964	^{117}Sn(d, p)^{118}Sn	Deuteron beam on ^{117}Sn oxide	[N15]				
		1965	^{120}Sn(p, t)^{118}Sn	Proton bombardment	[B16]				
		1967	^{116}Cd(α, 2n)^{118}Sn	Alpha-particle bombardment	[Y3]				
		1968	^{117}Sn(n, γ)^{118}Sn		[B33]				
		1968	^{117}Sn(d, p)^{118}Sn		[B33]				
		1968	^{116}Sn(t, p)^{118}Sn	^{116}Sn target preparation by vacuum evaporation	[B43]				
		1968	^{116}Sn(t, p)^{118}Sn		[B77]				
		1968	^{116}Sn(t, p)^{118}Sn		[B77]				
		1968	^{119}Sn(d, t)^{118}Sn	Deuteron bombardment	[C38]				
		1968	^{118}Sb(β$^+$)^{118}Sn		[R6]				
		1968	^{117}Sn(n, γ)^{118}Sn	Neutron capture	[S3]				
		1968	^{116}Cd(α, 2n)^{118}Sn	Alpha-particle bombardment	[Y5]				
		1969	^{119}Sn(γ, n)^{118}Sn	Photonuclear reaction	[F48]				

Table 6: Discovery, production scheme and half-lives of tin isotopes *(continued)*

Isotope	Year	Production scheme				Half-life value			
		Year	*Reaction*	*Principal method/condition*	*Ref*	*Year*	*Half-life*		*Ref*
^{118}Sn	1922	---	---	---	---	---	---	---	[A30]
		1969	^{116}Cd(α, 2n)^{118}Sn	Alpha-particle bombardment	[Y6]				
		1970	^{120}Sn(p, t)^{118}Sn	Target preparation by SnO_2 evaporation	[F14]				
		1970	^{118}In(β$^-$)^{118}Sn	^{118}In production from metallic ^{118}Sn isotope	[H16]				
		1970	^{118}Sb(EC)^{118}Sn	Electron capture, ^{118g}Sb production from ^{118}Te isotope	[H16]				
		1972	^{116}Sn(t, p)^{118}Sn		[I15]				
		1973	^{119}Sn(p, d)^{118}Sn	Neutron pickup	[I6]				
		1975	^{116}Sn(^{18}O, ^{16}O)^{118}Sn	*2n*-transfer reaction	[B61]				
		1975	^{117}Sn(d, p)^{118}Sn	Vector-polarized deuteron bombardment	[K41]				
		1976	^{120}Sn(^{18}O, ^{20}O)^{118}Sn	Two-neutron stripping and pickup reaction	[S66]				
		1977	^{120}Sn(p, t)^{118}Sn		[C47]				
		1977	^{116}Cd(^{3}He, n)^{118}Sn	Two-neutron transfer reaction, target preparation by rolling or evaporation	[F10]				
		1977	^{118}In^g(β$^-$)^{118}Sn	^{118}In preparation by bremsstrahlung on ^{238}U isotope	[F38]				
		1979	^{116}Cd(α, 2nγ)^{118}Sn	Alpha bombardment	[B79]				
		1979	^{117}Sn(t, d)^{118}Sn	Triton bombardment	[C27]				
		1979	^{122}Te(d, ^{6}Li)^{118}Sn	Alpha-cluster pickup *via* (d, ^{6}Li) pathway	[J4]				
		1979	^{120}Sn(p, t)^{118}Sn		[J4]				
		1980	^{120}Sn(p, t)^{118}Sn	Proton beam on rolled ^{120}Sn foil	[C48]				
		1980	^{116}Cd(α, 2n)^{118}Sn	Alpha-particle bombardment on the self-supporting cadmium target	[P24]				
		1981	^{119}Sn(p, d)^{118}Sn	Proton beam on self-supporting metal foils	[C50]				
		1981	^{120}Sn(p, t)^{118}Sn	Proton beam on self-supporting metal foils	[C50]				

Table 6: Discovery, production scheme and half-lives of tin isotopes *(continued)*

Isotope	Year	Production scheme				Half-life value			
		Year	*Reaction*	*Principal method/condition*	*Ref*	*Year*	*Half-life*		*Ref*
^{118}Sn	1922	---	---	---	---	---	---	---	[A30]
		1982	^{119}Sn(p, d)^{118}Sn	Target preparation by SnO_2 evaporation	[F16]				
		1982	^{118}Sb(ε)^{118}Sn	*K*-capture	[K23]				
		1983	^{117}Sn(d, p)^{118}Sn	Deuteron bombardment	[F46]				
		1985	^{120}Sn(p, t)^{118}Sn	Two-nuclear transfer reaction	[M26]				
		1988	^{118}In(β$^-$)^{118}Sn	^{118}In production by Sn(n, p) reaction	[R13]				
		1995	^{116}Cd(^{7}Li, p4nγ)^{118}Sn		[K39]				
		1996	^{117}Sn(n, γ)^{118}Sn	Neutron capture	[W24]				
		2002	^{117}Sn(n, γ)^{118}Sn	Thermal neutron radiative capture	[B67]				
		2004	^{117}Sn(n, 2γ)^{118}Sn	Thermal neutron capture followed by two-step gamma cascades	[K32]				
		2008	^{120}Sn(p, t)^{118}Sn		[G48]				
		2008	^{117}Sn(n, γ)^{118}Sn	Neutron capture	[N14]				
		2009	^{116}Cd(^{7}Li, 4n1p)^{118}Sn	Fusion-evaporation reaction	[W7]				
		2010	^{119}Sn(^{3}He, αγ)^{118}Sn	^{3}He beam on the ^{119}Sn target	[T14]				
		2010	^{116}Cd(^{7}Li, 1p4n)^{118}Sn	Fusion-evaporation reaction	[W8]				
		2011	^{124}Sn(n, 7nγ)^{118}Sn	Fusion-fission reaction	[F34]				
		2011	^{120}Sn(p, t)^{118}Sn	Proton beam on the isotopically enriched ^{120}Sn target	[M35]				
		2011	^{117}Sn(n, γ)^{118}Sn	Radiative neutron capture	[U6]				
		2011	^{119}Sn(γ, n)^{118}Sn		[U6]				
		2014	^{48}Ca(^{238}U)^{118}Sn	Fusion-fission	[I9]				
		2014	^{64}Ni(^{238}U)^{118}Sn	Fusion-fission	[I9]				
		2014	^{48}Ca(^{208}Pb)^{118}Sn	Fusion-fission	[I9]				
		2014	^{120}Sn(p, t)^{118}Sn	Proton beam on the thick ^{120}Sn target	[N6]				
		2015	^{48}Ca(^{208}Pb)^{118}Sn	Fusion-fission	[I10]				
		2015	^{48}Ca(^{238}U)^{118}Sn	Fusion-fission	[I10]				
		2015	^{64}Ni(^{238}U)^{118}Sn	Fusion-fission	[I10]				

Table 6: Discovery, production scheme and half-lives of tin isotopes *(continued)*

Isotope	Year	Production scheme				Half-life value			
		Year	*Reaction*	*Principal method/condition*	*Ref*	*Year*	*Half-life*		*Ref*
^{119}Sn	1922	---	---	---	---	---	---	---	[A30]
		1948	^{118}Sn(n, γ)^{119}Sn		[S29]	1937	STABLE		[G40]
		1948	^{121}Sb(d, α)^{119}Sn		[S29]	1948	25 m		[S29]
		1948	Cd(α, n)^{119}Sn		[S29]	1948	3 h		[S29]
		1952	^{119}In(β$^-$)^{119}Sn	Beta-decay	[G30]	1949	4.5 m	0.5	[D29]
		1952	^{119}Sb(ε)^{119}Sn		[G40]	2003	STABLE		[A42]
		1957	^{119}In(β$^-$)^{119}Sn		[O8]	2003	STABLE		[L3]
		1957	^{119}Sb(ε)^{119}Sn	Electron capture	[O8]	2012	STABLE		[A43]
		1960	^{119}In(β$^-$)^{119}Sn		[Y8]	2017	STABLE		[A45]
		1961	^{118}Sn(d, p)^{119}Sn	Deuteron bombardment	[C35]				
		1961	^{119}In(β$^-$)^{119}Sn		[G28]				
		1963	^{119}Sb(ε)^{119}Sn		[D3]				
		1964	^{119}Sb(EC)^{119}Sn	Electron capture	[B24]				
		1966	^{118}Sn(d, p)^{119}Sn	Neutron stripping	[R27]				
		1967	^{118}Sn(d, p)^{119}Sn	Stripping reaction	[S17]				
		1967	^{120}Sn(d, t)^{119}Sn	Stripping reaction	[S17]				
		1968	^{118}Sn(n, γ)^{119}Sn		[B33]				
		1968	^{118}Sn(d, p)^{119}Sn		[B33]				
		1968	^{119m}Sn(IC)^{119}Sn	Internal-conversion	[B60]				
		1968	^{118}Sn(n, γ)^{119}Sn	Neutron capture	[S3]				
		1968	^{118}Sn(d, p)^{119}Sn		[V6]				
		1969	^{120}Sn(γ, n)^{119}Sn	Photonuclear reaction	[F48]				
		1969	^{116}Cd(α, n)^{119}Sn	Alpha-particle bombardment	[Y6]				
		1970	^{120}Sn(p, d)^{119}Sn	Proton bombardment	[C17]				
		1972	^{119}In(β$^-$)^{119}Sn	^{119}In preparation from ^{120}Sn(γ, p) reaction on the enriched SnO_2 target	[J1]				
		1973	^{118}Sn(n, γ)^{119}Sn		[R10]				
		1973	^{119}In(β$^-$)^{119}Sn	^{119g}In production by ^{120}Sn(γ, p) and ^{119}Sn(n, p) reactions	[R10]				
		1974	^{120}Sn(d, t)^{119}Sn	Neutron pickup reaction	[W15]				
		1975	^{118}Sn(d, p)^{119}Sn	Deuteron beams on the thin tin target	[B21]				
		1975	^{120}Sn(d, t)^{119}Sn	Deuteron beams on the thin tin target	[B21]				
		1975	^{118}Sn(^{18}O, ^{17}O)^{119}Sn	*2n*-transfer reaction	[B61]				
		1975	^{118}Sn(d, p)^{119}Sn	Deuteron bombardment	[B65]				
		1976	^{119}In(β$^-$)^{119}Sn	^{119}In preparation by ^{235}U(n, *f*) and ^{238}U(α, *f*) reactions	[F20]				
		1976	^{118}Sn(d, p)^{119}Sn		[M4]				

Table 6: Discovery, production scheme and half-lives of tin isotopes *(continued)*

Isotope	Year	Production scheme				Half-life value			
		Year	*Reaction*	*Principal method/condition*	*Ref*	*Year*	*Half-life*		*Ref*
^{119}Sn	1922	---	---	---	---	---	---	---	[A30]
		1976	^{116}Cd(α, n)^{119}Sn	Alpha-irradiation	[M4]				
		1977	^{120}Sn(^{3}He, α)^{119}Sn	Neutron pickup reaction	[S33]				
		1977	^{120}Sn(p, d)^{119}Sn	Neutron pickup reaction	[S33]				
		1977	^{120}Sn(d, t)^{119}Sn	Single-neutron pickup reaction	[W16]				
		1978	^{120}Sn(d, t)^{119}Sn	Deuteron bombardment	[K43]				
		1978	^{118}Sn(n, γ)^{119}Sn	Neutron capture	[R12]				
		1978	^{120}Sn(^{3}He, α)^{119}Sn	Neutron pickup reaction	[T6]				
		1979	^{118}Sn(t, d)^{119}Sn	Triton bombardment	[C27]				
		1980	^{120}Sn(^{3}He, α)^{119}Sn	Neutron pickup	[G23]				
		1980	^{120}Sn(p, d)^{119}Sn	Proton bombardment on Sn foil	[T2]				
		1981	^{120}Sn(p, d)^{119}Sn	Polarized beam on the ^{120}Sn target	[C49]				
		1982	^{120}Sn(p, d)^{119}Sn	Proton beam on self-supported ^{120}Sn foil	[D16]				
		1982	^{120}Sn(p, d)^{119}Sn	Target preparation by SnO_2 evaporation	[F16]				
		1984	^{118}Sn(α, ^{3}He)^{119}Sn	Neutron stripping reaction	[G10]				
		1990	^{119}Sb(ε/β^{+})^{119}Sn		[M29]				
		1991	^{118}Sn(α, ^{3}He)^{119}Sn	Stripping reaction	[M13]				
		1992	^{122}Sn(^{80}Se)^{119}Sn	^{80}Se pulse beam on lead backed ^{122}Sn target	[M15]				
		1992	^{124}Sn(^{80}Se)^{119}Sn	^{80}Se pulse beam on lead backed ^{124}Sn target	[M15]				
		1994	^{124}Sn(^{80}Se)^{119}Sn	Heavy-ion collision	[M16]				
		1994	^{120}Sn(d, t)^{119}Sn	Polarized deuteron beam on the ^{120}Sn target	[W20]				
		1995	^{124}Sn(^{80}Se)^{119}Sn	Heavy-ion collision	[D2]				
		1996	^{118}Sn(n, γ)^{119}Sn	Neutron capture	[W25]				
		1996	^{118}Sn(n, γ)^{119}Sn	Neutron capture	[W24]				
		2003	^{120}Sn(d, ^{3}He)^{119}Sn	Pion-transfer reaction under recoil-free condition	[S76]				

Table 6: Discovery, production scheme and half-lives of tin isotopes *(continued)*

Isotope	Year	Production scheme				Half-life value			
		Year	*Reaction*	*Principal method/condition*	*Ref*	*Year*	*Half-life*		*Ref*
^{119}Sn	1922	---	---	---	---	---	---	---	[A30]
		2004	^{120}Sn(d, ^{3}He)^{119}Sn	Pion-transfer reaction under recoil-free condition	[S77]				
		2007	^{118}Sn(n, γ)^{119}Sn	Neutron capture	[E2]				
		2010	^{119}Sn(^{3}He, ^{3}He′γ)^{119}Sn	^{3}He beam on the ^{119}Sn target	[T14]				
		2011	^{120}Sn(γ, n)^{119}Sn		[U6]				
		2011	^{118}Sn(n, γ)^{119}Sn	Radiative neutron capture	[U6]				
		2012	^{12}C(^{238}U)^{119}Sn	Fission fragmentation	[A28]				
		2012	^{18}O(^{208}Pb)^{119}Sn	Fission fragmentation	[A28]				
		2012	^{119}Sb(ε)^{119}Sn		[W9]				
		2013	^{12}C(^{238}U)^{119}Sn	Fusion-fission	[A29]				
		2013	^{18}O(^{208}Pb)^{119}Sn	Fusion-fission	[A29]				
		2017	^{120}Sn(^{6}Li, ^{7}Li)^{119}Sn	One-neutron stripping	[F13]				
		2018	^{120}Sn(^{10}B, ^{11}B)^{119}Sn	One-neutron transfer	[G16]				
		2018	^{120}Sn(n, 2n)^{119}Sn		[P4]				
^{120}Sn	1922	---	---	---	---	---	---	---	[A30]
		1946	^{235}Un(n)^{120}Sn	Thermal neutron fission	[G41]	1937	STABLE		[G40]
		1948	U(α)^{120}Sn		[S29]	1946	7.0 d		[G41]
		1948	U(n)^{120}Sn		[S29]	1946	136 d		[G41]
		1950	^{120}Sb(ε)^{120}Sn	*K*-capture	[B56]	1946	17.5 d		[G41]
		1953	^{120}Sb(β^{+})^{120}Sn		[H33]	1948	~ 80 h		[S29]
		1958	^{120}Sb(β^{+})^{120}Sn	Positron-emission	[M21]	1948	60 h		[S29]
		1958	^{120}In(β^{-})^{120}Sn		[M21]	1949	17.5 m	1	[D29]
		1960	^{120}Sb(β^{+})^{120}Sn		[I2]	1960	2.3 m	0.3	[Y8]
		1960	^{120}Sb(β^{+})^{120}Sn	Positron-emission	[J7]	2003	STABLE		[A42]
		1961	^{120}Sb(β^{+})^{120}Sn	Positron emission	[B63]	2003	STABLE		[L3]
		1961	^{119}Sn(d, p)^{120}Sn	Deuteron bombardment	[C35]	2012	STABLE		[A43]
		1961	^{119}Sn(d, p)^{120}Sn	Deuteron bombardment	[C36]	2017	STABLE		[A45]
		1961	^{120}Sb(β^{+}/ε)^{120}Sn		[I3]				
		1961	^{120}Sb(ε)^{120}Sn		[R15]				
		1962	^{118}Sn(t, p)^{120}Sn	Two-neutron stripping reaction	[Y7]				
		1963	^{120}Sb(β^{+})^{120}Sn		[D3]				
		1964	^{120}In(β^{-})^{120}Sn	Beta-decay	[K5]				
		1964	^{119}Sn(d, p)^{120}Sn	Deuteron beam on ^{119}Sn oxide	[N15]				
		1966	^{121}Sn(γ, n)^{120}Sn		[A1]				

Table 6: Discovery, production scheme and half-lives of tin isotopes *(continued)*

Isotope	Year	Production scheme				Half-life value			
		Year	*Reaction*	*Principal method/condition*	*Ref*	*Year*	*Half-life*		*Ref*
^{120}Sn	1922	---	---	---	---	---	---	---	[A30]
		1968	^{118}Sn(t, p)^{120}Sn	^{118}Sn target preparation by vacuum evaporation	[B43]				
		1968	^{118}Sn(t, p)^{120}Sn		[B77]				
		1968	^{118}Sn(t, p)^{120}Sn		[B77]				
		1968	^{120}Sb(β^+)^{120}Sn		[R6]				
		1968	^{119}Sn(n, γ)^{120}Sn	Neutron capture	[S3]				
		1968	^{118}Cd(α, 2n)^{120}Sn	Alpha-particle bombardment	[Y5]				
		1970	^{122}Sn(p, t)^{120}Sn	Target preparation by SnO_2 evaporation	[F14]				
		1970	^{120}Sb(β^+)^{120}Sn	Positron emission, ^{120}Sb preparation from ^{121}Sb with bremsstrahlung beam	[P2]				
		1971	^{120}In(β^-)^{120}Sn	^{120}In preparation by ^{120}Sn(n, p)^{120}In reaction	[L21]				
		1971	^{120}Sb(EC)^{120}Sn	Electron capture, ^{120}Sb preparation from ^{121}Sb(n, 2n)^{120}Sb reaction	[L21]				
		1971	Sn(C)^{120}Sn	^{120}Sn preparation from the isotopically enriched Sn metal by vacuum evaporation using niobium boat and carbon backing	[R28]				
		1972	^{118}Sn(t, p)^{120}Sn		[C15]				
		1972	^{118}Sn(t, p)^{120}Sn		[I15]				
		1972	^{121}Sb(d, ^{3}He)^{120}Sn		[K40]				
		1973	^{118}Sn(^{120}Sn, ^{118}Sn)^{120}Sn	Two-nucleon transfer reaction	[B78]				
		1973	^{120}In(β^-)^{120}Sn	^{120}In preparation from ^{120}Cd and Cd by Sn(p, 3pxn)Cd spallation	[S18]				
		1975	^{118}Sn(^{18}O, ^{16}O)^{120}Sn	*2n*-transfer reaction	[B61]				
		1975	^{122}Sn(^{16}O, ^{18}O)^{120}Sn	Two-neutron transfer reaction	[S27]				
		1975	^{120}Sb(β^+ + EC)^{120}Sn	Positron emission and electron capture, ^{120}Sb preparation from ^{121}Sb(γ, n) reaction	[C6]				

Table 6: Discovery, production scheme and half-lives of tin isotopes *(continued)*

Isotope	Year	Production scheme				Half-life value			
		Year	***Reaction***	***Principal method/condition***	***Ref***	***Year***	***Half-life***		***Ref***
^{120}Sn	1922	---	---	---	---	---	---	---	[A30]
		1975	^{123}Te(n, α)^{120}Sn		[H38]				
		1975	^{119}Sn(d, p)^{120}Sn	Vector-polarized deuteron bombardment	[K41]				
		1976	^{120}Sb(ε)^{120}Sn		[K42]				
		1976	^{122}Sn(^{16}O, ^{18}O)^{120}Sn	Two-neutron stripping and pickup reactions	[S66]				
		1977	^{122}Sn(p, t)^{120}Sn	Proton bombardment	[C47]				
		1978	^{120}In(β$^-$)^{120}Sn	Indium isotope preparation by the thermal-neutron induced fission of ^{235}U	[A5]				
		1978	^{121}Sb(t, α)^{120}Sn	Triton bombardment	[B15]				
		1978	^{121}Sb(d, ^{3}He)^{120}Sn		[B15]				
		1978	^{120}In(β$^-$)^{120}Sn	^{120}In preparation from ^{238}U(p, *f*) reaction	[C31]				
		1979	^{119}Sn(t, d)^{120}Sn	Triton bombardment	[C27]				
		1979	^{120}In(β$^-$)^{120}Sn	Indium isotope preparation by the neutron-induced fission of ^{235}U	[F21]				
		1979	^{124}Te(d, ^{6}Li)^{120}Sn	Alpha-cluster pickup *via* (d, ^{6}Li) reaction	[J4]				
		1980	^{122}Sn(p, t)^{120}Sn	Proton beam on the rolled ^{122}Sn foil	[C48]				
		1981	^{122}Sn(p, t)^{120}Sn	Proton beam on self-supporting metal foils	[C50]				
		1983	^{123}Sb(p, α)^{120}Sn	Neutron pickup	[G7]				
		1983	^{121}Sb(d, ^{3}He)^{120}Sn	Neutron stripping	[G7]				
		1984	^{120}Sb(ε)^{120}Sn	Electron capture (EC)	[I14]				
		1985	^{122}Sn(p, t)^{120}Sn	Two-nuclear transfer reaction	[M26]				
		1986	^{116}Cd(^{7}Li, p2n)^{120}Sn	^{7}Li beam on the ^{116}Cd target	[D1]				
		1987	^{116}Cd(^{7}Li)^{120}Sn	^{7}Li ion beam on the ^{116}Cd target	[L30]				
		1988	^{120}In(β$^-$)^{120}Sn	^{120}In production by Sn(n, p) reaction	[R13]				
		1999	^{122}Sn(p, t)^{120}Sn		[G44]				

Table 6: Discovery, production scheme and half-lives of tin isotopes *(continued)*

Isotope	Year	Production scheme				Half-life value			
		Year	*Reaction*	*Principal method/condition*	*Ref*	*Year*	*Half-life*		*Ref*
^{120}Sn	1922	---	---	---	---	---	---	---	[A30]
		2003	^{120}Te(β^+ β^+)^{120}Sn	Double beta transitions	[K34]				
		2005	^{123}Sb(p, α)^{120}Sn	Polarized proton beam on the Sb target	[G46]				
		2007	^{120}Te(β^+ + EC)^{120}Sn	Electron capture and positron emission	[B7]				
		2007	^{119}Sn(n, γ)^{120}Sn	Neutron capture	[E2]				
		2008	^{119}Sn(n, γ)^{120}Sn	Neutron capture	[N14]				
		2009	^{120}Te(ε ε)^{120}Sn	Double-electron capture	[S26]				
		2009	^{120}Te(ε β^+)^{120}Sn	Electron capture and positron emission	[S26]				
		2011	^{124}Sn(n, 5nγ)^{120}Sn	Fusion-fission reaction	[F34]				
		2011	^{119}Sn(n, γ)^{120}Sn	Radiative neutron capture	[U6]				
		2012	^{12}C(^{238}U)^{120}Sn	Fission fragmentation	[A28]				
		2012	^{18}O(^{208}Pb)^{120}Sn	Fission fragmentation	[A28]				
		2013	^{12}C(^{238}U)^{120}Sn	Fusion-fission	[A29]				
		2013	^{18}O(^{208}Pb)^{120}Sn	Fusion-fission	[A29]				
		2014	^{48}Ca(^{238}U)^{120}Sn	Fusion-fission	[I9]				
		2014	^{64}Ni(^{238}U)^{120}Sn	Fusion-fission	[I9]				
		2014	^{48}Ca(^{208}Pb)^{120}Sn	Fusion-fission	[I5]				
		2015	^{48}Ca(^{208}Pb)^{120}Sn	Fusion-fission	[I10]				
		2015	^{48}Ca(^{238}U)^{120}Sn	Fusion-fission	[I10]				
		2015	^{64}Ni(^{238}U)^{120}Sn	Fusion-fission	[I10]				
		2017	^{119}Sn(^{7}Li, ^{6}Li)^{120}Sn	One-neutron stripping	[F13]				
		2018	^{120}Te(β^+ + EC)^{120}Sn	β^+EC decay	[A52]				
		2018	^{238}U(^{12}C)^{120}Sn	Fission-fragmentation, uranium beam impinging on the ^{12}C target	[R16]				
^{121}Sn	1936	---	---	---	---	---	---	---	[L22]
		1936	^{123}Sb(d, α)^{121}Sn	Deuteron bombardment	[L22]	1936	24 h	2	[L22]
		1936	^{123}Sb(d, α)^{121}Sn	Deuteron bombardment	[L23]	1939	26 h		[L24]
		1948	^{120}Sn(d, p)^{121}Sn	Deuteron irradiation	[L16]	1948	28 h		[L16]
		1948	Th(α)^{121}Sn		[S29]	1948	130 d		[S29]
		1948	U(n)^{121}Sn		[S29]	1949	28 h		[D30]
		1948	^{233}U(n)^{121}Sn		[S29]	1949	1.1 d	0.05	[L9]
		1948	Th(α)^{121}Sn		[S29]	1951	28 h		[F6]

Table 6: Discovery, production scheme and half-lives of tin isotopes *(continued)*

Isotope	Year	Production scheme				Half-life value			
		Year	*Reaction*	*Principal method/condition*	*Ref*	*Year*	*Half-life*		*Ref*
^{121}Sn	1936	---	---	---	---	---	---	---	[L22]
		1949	^{120}Sn(d, p)^{121}Sn	Deuteron bombardment	[L9]	1951	36 m		[F6]
		1959	^{120}Sn(d, p)^{121}Sn	Deuteron bombardment	[P11]	1952	27.5 h		[G30]
		1960	^{122}Sn(γ, n)^{121}Sn	Bremsstrahlung reaction	[Y8]	1957	~28 h		[B83]
		1960	^{121}In(β$^-$)^{121}Sn		[Y8]	1963	27.0 h	0.6	[M6]
		1961	^{120}Sn(d, p)^{121}Sn	Deuteron bombardment	[C35]	1963	27.5 h		[W5]
		1962	^{120}Sn(d, p)^{121}Sn		[B10]	1966	26.85 h	0.20	[L6]
		1963	^{120}Sn(d, p)^{121}Sn		[D3]	1968	27.06 h	0.04	[E5]
		1963	^{124}Te(n, α)^{121}Sn		[M6]	1968	27.06 h	0.03	[E5]
		1963	^{235}U(n)^{121}Sn	Thermal-neutron fission	[W5]	1968	27.0 h	0.1	[E5]
		1964	^{120}Sn(d, p)^{121}Sn		[N8]	1968	25.5 h	0.1	[S61]
		1965	^{120}Sn(n, γ)^{121}Sn	Neutron irradiation onto ^{120}Sn enriched SnO_2	[S60]	1969	27 h		[E6]
		1966	^{121}Sb(μ$^-$, ν)^{121}Sn		[A1]	1969	27 h		[P33]
		1966	U(*f*)^{125}Sn	Fission	[L6]	1971	27.5 h	0.5	[H34]
		1966	^{120}Sn(d, p)^{121}Sn	Neutron stripping	[R27]	1976	27 h		[F47]
		1967	^{120}Sn(d, p)^{121}Sn	Stripping reaction	[S17]	1977	27 h		[B88]
		1967	^{122}Sn(d, t)^{121}Sn	Stripping reaction	[S17]	1989	27.1 h		[R4]
		1968	^{120}Sn(n, γ)^{121}Sn		[B33]	1991	27.06 h	0.04	[T4]
		1968	^{235}U(*f*)^{121}Sn	Fission	[E5]	1997	27.06 h	0.04	[A41]
		1968	^{120}Sn(n, γ)^{121}Sn	Neutron irradiation onto ^{120}Sn enriched SnO_2	[S61]	2000	27.03 h	0.04	[T5]
		1968	^{120}Sn(d, p)^{121}Sn		[V6]	2002	27.06 h		[R24]
		1969	^{119}Sn(t, p)^{121}Sn		[B44]	2003	27.03 h	0.04	[A42]
		1969	^{120}Sn(n, γ)^{121}Sn	Irradiation on stable Sn metal	[P33]	2012	27.03 h	0.04	[A43]
		1970	^{122}Sn(p, d)^{121}Sn	Proton bombardment	[C17]	2016	27 h		[H20]
		1972	^{119}Sn(t, p)^{121}Sn	^{119}Sn preparation by vacuum evaporation	[C15]	2017	27.03 h	0.04	[A45]
		1972	^{120}Sn(t, d)^{121}Sn	^{120}Sn preparation by vacuum evaporation	[C15]				
		1973	^{121}In(β$^-$)^{121}Sn	$^{121g+m}$In production by ^{122}Sn(γ, p) reaction	[F37]				
		1974	^{122}Sn(d, t)^{121}Sn	Neutron pickup reaction	[W15]				
		1975	^{120}Sn(d, p)^{121}Sn	Deuteron bombardment	[B20]				
		1975	^{120}Sn(d, p)^{121}Sn	Deuteron beams on the thin tin target	[B21]				

Table 6: Discovery, production scheme and half-lives of tin isotopes *(continued)*

Isotope	Year	Production scheme				Half-life value			
		Year	*Reaction*	*Principal method/condition*	*Ref*	*Year*	*Half-life*		*Ref*
^{121}Sn	1936	---	---	---	---	---	---	---	[L22]
		1975	^{122}Sn(d, t)^{121}Sn	Deuteron beams on the thin tin target	[B21]				
		1976	^{120}Sn(n, γ)^{121}Sn	Neutron capture	[C10]				
		1976	^{121}In(β$^-$)^{121}Sn	^{121}In preparation by ^{235}U(n, *f*) and ^{238}U(α, *f*) reactions	[F20]				
		1976	^{120}Sn(d, pγ)^{121}Sn	^{120}Sn preparation by evaporation	[M4]				
		1977	^{122}Sn(p, d)^{121}Sn	Neutron pickup reaction	[S33]				
		1977	^{122}Sn(d, t)^{121}Sn	Single-neutron pickup reaction	[W16]				
		1978	^{121}In(β$^-$)^{121}Sn	Indium isotope preparation by the thermal-neutron induced fission of ^{235}U	[A5]				
		1978	^{121m}Sn(IT)^{121g}Sn	Internal-conversion	[H42]				
		1978	^{122}Sn(d, t)^{121}Sn	Deuteron bombardment	[K43]				
		1980	^{122}Sn(p, d)^{121}Sn	Proton bombardment on Sn foil	[T2]				
		1982	^{122}Sn(p, d)^{121}Sn	Target preparation by SnO_2 evaporation	[F16]				
		1984	^{120}Sn(α, ^{3}He)^{121}Sn	Neutron stripping reaction	[G10]				
		1986	Sn(n)^{121}Sn	Neutron activation on enriched stable Sn	[A17]				
		1991	^{120}Sn(α, ^{3}He)^{121}Sn	Stripping reaction	[M13]				
		1992	^{122}Sn(^{80}Se)^{121}Sn	Bombarding of lead backed ^{122}Sn target with ^{80}Se pulse beam	[M15]				
		1992	^{124}Sn(^{80}Se)^{121}Sn	Bombarding of lead backed ^{124}Sn target with ^{80}Se pulse beam	[M15]				
		1994	^{124}Sn(^{80}Se)^{121}Sn	Heavy-ion collision	[M16]				
		1995	^{124}Sn(^{80}Se)^{121}Sn	Heavy-ion collision	[D2]				
		1995	^{124}Sn(^{80}Se, ^{80}Se3nγ)^{121}Sn		[O6]				
		1996	^{120}Sn(n, γ)^{121}Sn	Neutron capture	[W25]				
		1996	^{120}Sn(n, γ)^{121}Sn	Neutron capture	[W24]				
		2004	^{120}Sn(^{7}Li, ^{6}Li)^{121}Sn	^{120}Sn(^{7}Li, ^{6}Li* → α + d)^{121}Sn transfer breakup reaction	[D10]				

Table 6: Discovery, production scheme and half-lives of tin isotopes *(continued)*

Isotope	Year	Production scheme				Half-life value			
		Year	*Reaction*	*Principal method/condition*	*Ref*	*Year*	*Half-life*		*Ref*
^{121}Sn	1936	---	---	---	---	---	---	---	[L22]
		2006	^{122}Sn(n, 2n)^{121}Sn		[F33]				
		2007	^{120}Sn(n, γ)^{121}Sn	Neutron capture	[E2]				
		2010	^{120}Sn(^{6}He, ^{5}He)^{121}Sn	One-neutron stripping reaction	[F4]				
		2010	^{120}Sn(^{7}Li, ^{6}Li)^{121}Sn	^{7}Li nuclear break-up process	[S64]				
		2011	^{122}Sn(^{3}He, αγ)^{121}Sn	^{3}He beam on the ^{122}Sn target	[T15]				
		2011	^{122}Sn(γ, n)^{121}Sn		[U6]				
		2012	^{12}C(^{238}U)^{121}Sn	Fission fragmentation	[A28]				
		2012	^{18}O(^{208}Pb)^{121}Sn	Fission fragmentation	[A28]				
		2012	^{122}Sn(d, ^{3}He)^{121}Sn	Pionic reaction	[I11]				
		2013	^{12}C(^{238}U)^{121}Sn	Fusion-fission	[A29]				
		2013	^{18}O(^{208}Pb)^{121}Sn	Fusion-fission	[A29]				
		2017	^{120}Sn(^{7}Li, ^{6}Li)^{121}Sn	One-nucleaon transfer reaction	[K58]				
		2017	^{120}Sn(^{7}Li, ^{6}Li)^{121}Sn	One-neutron transfer reaction	[Z1]				
		2018	^{122}Sn(d, ^{3}He)^{121}Sn	Pionic-reaction	[N13]				
^{122}Sn	1922	---	---	---	---	---	---	---	[A30]
		1955	^{122}Sb(ε)^{122}Sn	Electron capture	[F5]	1937	STABLE		[G40]
		1955	^{122}Sb(ε)^{122}Sn	*K*-capture	[G26]	1960	3.1 m	0.3	[Y8]
		1958	^{122}Sb(EC + β^{+})^{122}Sn	Electron capture and positron emission	[P13]	1968	40 m		[T17]
		1963	^{122}Sb(β^{+})^{122}Sn		[D3]	2003	STABLE		[A42]
		1964	^{122}In(β^{-})^{122}Sn		[K5]	2003	STABLE		[L3]
		1968	^{120}Cd(α, 2n)^{122}Sn	Alpha-particle bombardment	[Y5]	2012	STABLE		[A43]
		1970	^{124}Sn(p, t)^{122}Sn	Target preparation by SnO_2 evaporation	[F14]	2017	STABLE		[A45]
		1971	^{122}In(β^{-})^{122}Sn		[T1]				
		1972	^{120}Sn(t, p)^{122}Sn		[C15]				
		1973	^{120}Sn(^{18}O, ^{16}O)^{122}Sn	Two-neutron transfer reaction	[A23]				
		1973	^{120}Sn(^{18}O, ^{16}O)^{122}Sn	Two-neutron transfer reaction	[A24]				
		1973	^{122}In(β^{-})^{122}Sn	^{122}In preparation from ^{122}Cd by Sn(p, 3pxn)Cd spallation	[S18]				
		1974	^{120}Sn(^{18}O, ^{16}O)^{122}Sn	Two-nucleon transfer	[A25]				
		1975	^{120}Sn(^{18}O, ^{16}O)^{122}Sn	Two-neutron transfer reaction	[S27]				

Table 6: Discovery, production scheme and half-lives of tin isotopes *(continued)*

Isotope	Year	Production scheme				Half-life value			
		Year	*Reaction*	*Principal method/condition*	*Ref*	*Year*	*Half-life*		*Ref*
^{122}Sn	1922	---	---	---	---	---	---	---	[A30]
		1976	^{120}Sn(^{18}O, ^{16}O)^{122}Sn	Two-neutron stripping and pickup reaction	[S66]				
		1977	^{124}Sn(p, t)^{122}Sn		[C47]				
		1978	^{122}In(β^-)^{122}Sn	In preparation from thermal-neutron induced ^{235}U fission	[A5]				
		1978	^{123}Sb(t, α)^{122}Sn	Triton bombardment	[B15]				
		1979	^{122}In(β^-)^{122}Sn	^{122}In separation from ^{238}U(p, *f*) products	[C32]				
		1979	^{122}In(β^-)^{122}Sn	Indium isotope preparation by neutron-induced fission of ^{235}U	[F21]				
		1979	^{126}Te(d, ^{6}Li)^{122}Sn	Alpha-cluster pickup *via* (d, ^{6}Li) reaction	[J4]				
		1979	^{124}Sn(p, t)^{122}Sn		[K53]				
		1980	^{124}Sn(p, t)^{122}Sn	Proton beam on the rolled ^{124}Sn foil	[C48]				
		1981	^{124}Sn(p, t)^{122}Sn	Proton beam on self-supporting metal foils	[C50]				
		1983	^{124}Sn(p, t)^{122}Sn	Proton beam on ^{124}Sn enriched metal target	[M14]				
		1985	^{124}Sn(p, t)^{122}Sn	Two-nuclear transfer reaction	[M26]				
		1988	^{122}In(β^-)^{122}Sn	^{122}In production by Sn(n, p) reaction	[R13]				
		1992	^{124}Sn(^{76}Ge)^{122}Sn	Heavy-ion collision	[B76]				
		2010	^{120}Sn(^{6}He, α)^{122}Sn	Two-neutron stripping reaction	[F4]				
		2011	^{124}Sn(n, 3nγ)^{122}Sn	Fusion-fission reaction	[F34]				
		2011	^{124}Sn(p, t)^{122}Sn		[G49]				
		2011	^{121}Sn(n, γ)^{122}Sn	Radiative neutron capture	[U6]				
		2012	^{12}C(^{238}U)^{122}Sn	Fission fragmentation	[A28]				
		2012	^{18}O(^{208}Pb)^{122}Sn	Fission fragmentation	[A28]				
		2013	^{12}C(^{238}U)^{122}Sn	Fusion-fission	[A29]				
		2013	^{18}O(^{208}Pb)^{122}Sn	Fusion-fission	[A29]				
		2013	^{238}U(^{12}C)^{122}Sn	Fusion-induced fission	[C1]				
		2014	^{48}Ca(^{238}U)^{122}Sn	Fusion-fission	[I9]				
		2014	^{64}Ni(^{238}U)^{122}Sn	Fusion-fission	[I9]				

Table 6: Discovery, production scheme and half-lives of tin isotopes *(continued)*

Isotope	Year	Production scheme				Half-life value			
		Year	*Reaction*	*Principal method/condition*	*Ref*	*Year*	*Half-life*		*Ref*
^{123}Sn	1939	---	---	---	---	---	---	---	[L24]
		2014	^{48}Ca(^{208}Pb)^{122}Sn	Fusion-fission	[I9]				
		2015	^{48}Ca(^{208}Pb)^{122}Sn	Fusion-fission	[I10]				
		2015	^{48}Ca(^{238}U)^{122}Sn	Fusion-fission	[I10]				
		2015	^{64}Ni(^{238}U)^{122}Sn	Fusion-fission	[I10]				
		2016	^{122}Sb(ε)^{122}Sn	Electron-capture	[T21]				
^{123}Sn	1939	---	---	---	---	---	---	---	[L24]
		1939	^{120}Cd(α, n)^{123}Sn	Alpha bombardment	[L24]	1937	18 m		[G40]
		1939	^{122}Sn(d, p)^{123}Sn	Deuteron bombardment	[L24]	1939	10 d		[L24]
		1948	^{124}Sn(γ, n)^{123}Sn	Neutron removal	[M30]	1948	41.5 m	0.5	[M30]
		1948	^{233}U(n)^{123}Sn	Thermal neutron fission	[G42]	1948	136 d		[G42]
		1948	Th(α)^{123}Sn		[S29]	1948	~ 18 d		[G42]
		1948	U(n)^{123}Sn		[S29]	1948	9 d		[S29]
		1948	^{233}U(n)^{123}Sn		[S29]	1948	11 d		[S29]
		1948	Sn(d, p)^{123}Sn		[S29]	1949	39.5 m		[D30]
		1948	Sn(n, γ)^{123}Sn		[S29]	1949	40 m	1	[L9]
		1948	^{224}Sn(d, t)^{123}Sn		[S29]	1949	130 d	5	[L9]
		1949	^{122}Sn(d, p)^{123}Sn	Deuteron bombardment	[L9]	1950	130 d		[M24]
		1949	^{122}Sn(n, γ)^{123}Sn	Neutron irradiation	[L9]	1951	125 d	3	[C43]
		1949	^{124}Sn(n, 2n)^{123}Sn	Neutron capture	[L9]	1951	136 d		[F6]
		1951	^{122}Sn(n)^{123}Sn	Neutron capture	[C43]	1951	39.5 m		[F6]
		1960	^{124}Sn(γ, n)^{123}Sn	Bremsstrahlung reaction	[Y8]	1952	126 d		[G30]
		1960	^{123}In(β^-)^{123}Sn		[Y8]	1953	136 d		[H33]
		1961	^{124}Sn(α, αn)^{123}Sn	Alpha irradiation	[H4]	1960	40 m		[Y8]
		1961	^{122}Sn(α, 2p1n)^{123}Sn	Alpha irradiation	[H4]	1961	130 d		[H4]
		1962	^{122}Sn(d, p)^{123}Sn		[B10]	1961	40 m		[S16]
		1962	^{128}Te(n, 2p4n)^{123}Sn		[H3]	1963	39.7 m	1.0	[M6]
		1962	^{130}Te(n, 2p6n^{123}Sn		[H3]	1963	41 m		[S80]
		1963	^{126}Te(n, α)^{123}Sn		[M6]	1964	40 m		[K9]
		1964	^{124}Sn(n, 2n)^{123}Sn		[K9]	1965	125 d		[S60]
		1964	^{122}Sn(d, p)^{123}Sn	Monoenergetic deuteron bombardment	[N8]	1966	129.0 d	0.5	[L6]
		1966	^{123}Sb(μ^-, ν)^{123}Sn		[A1]	1968	126.4 d	0.3	[E5]
		1966	U(*f*)^{123}Sn	Fission	[L6]	1968	129.6 d	0.6	[E5]
		1966	^{122}Sn(d, p)^{123}Sn	Neutron stripping	[R27]	1968	129.3 h	0.5	[E5]
		1967	^{122}Sn(d, p)^{123}Sn	Striping reaction	[S17]	1968	40.1 m	0.2	[E5]
		1967	^{124}Sn(d, t)^{123}Sn	Stripping reaction	[S17]	1969	40.1 m		[E6]
		1968	^{235}U(*f*)^{123}Sn	Fission	[E5]	1969	129.3 d	0.5	[E6]
		1968	^{122}Sn(n, γ)^{123}Sn	Radiative-neutron capture	[T17]	1969	40.1 m		[E6]

Table 6: Discovery, production scheme and half-lives of tin isotopes *(continued)*

Isotope	Year	Production scheme				Half-life value			
		Year	*Reaction*	*Principal method/condition*	*Ref*	*Year*	*Half-life*		*Ref*
^{123}Sn	1939	---	---	---	---	---	---	---	[L24]
		1969	^{235}U(n, *f*)^{123}Sn	Thermal neutron-fission	[E6]	1972	129.2 d	0.4	[A36]
		1970	^{124}Sn(p, d)^{123}Sn	Proton bombardment	[C17]	1972	125 d		[L5]
		1972	^{122}Sn(d, p)^{123}Sn	^{122}Sn preparation by vacuum evaporation	[C9]	1974	40 m		[B87]
		1972	^{122}Sn(n, γ)^{123}Sn		[L5]	1974	129.2 d		[R11]
		1973	^{124}Sn(p, d)^{123}Sn	Neutron pickup	[I6]	1976	40 m		[F47]
		1973	^{123}In(β$^-$)^{123}Sn	^{123}In preparation from ^{124}Sn(γ, p) reaction	[J2]	1993	129.2 d	0.4	[O4]
		1974	^{122}Sn(n, γ)^{123}Sn		[R11]	1997	129.2 d	0.4	[A41]
		1974	^{124}Sn(d, t)^{123}Sn	Neutron pickup reaction	[W15]	2003	129.2 d	0.4	[A42]
		1975	^{122}Sn(d, p)^{123}Sn	Deuteron beams on the thin tin target	[B21]	2004	129.2 d	0.4	[O5]
		1975	^{124}Sn(d, t)^{123}Sn	Deuteron beams on the thin tin target	[B21]	2012	129.2 d	0.4	[A43]
		1975	^{122}Sn(n, γ)^{123}Sn	Neutron capture	[B34]	2014	129.2 d		[D21]
		1975	^{124}Sn(^{3}He, α)^{123}Sn	Neutron pickup reaction	[G22]	2017	129.2 d	0.4	[A45]
		1976	^{123}In(β$^-$)^{123}Sn	^{123}In preparation by ^{235}U(n, *f*) and ^{238}U(α, *f*) reactions	[F20]				
		1976	^{122}Sn(d, pγ)^{123}Sn	^{122}Sn preparation by evaporation	[M4]				
		1977	^{122}Sn(n, γ)^{123}Sn		[C11]				
		1977	^{124}Sn(^{3}He, α)^{123}Sn	Neutron pickup reaction	[S33]				
		1977	^{124}Sn(p, d)^{123}Sn	Neutron pickup reaction	[S33]				
		1977	^{124}Sn(d, t)^{123}Sn	Single-neutron pickup reaction	[W16]				
		1978	^{123}In(β$^-$)^{123}Sn	Indium isotope preparation by the thermal-neutron induced fission of ^{235}U	[A5]				
		1978	^{124}Sn(d, t)^{123}Sn	Deuteron bombardment	[K43]				
		1978	^{124}Sn(^{3}He, α)^{123}Sn	Neutron pickup reaction	[W21]				
		1980	^{124}Sn(p, d)^{123}Sn	Proton bombardment on Sn foil	[T2]				
		1982	^{124}Sn(p, d)^{123}Sn	Target preparation by SnO_2 evaporation	[F16]				
		1986	Sn(n)^{123}Sn	Neutron activation on enriched stable Sn	[A17]				

Table 6: Discovery, production scheme and half-lives of tin isotopes *(continued)*

Isotope	Year	Production scheme				Half-life value			
		Year	*Reaction*	*Principal method/condition*	*Ref*	*Year*	*Half-life*		*Ref*
^{123}Sn	1939	---	---	---	---	---	---	---	[L24]
		1987	^{123}In(β^-)^{123}Sn	Indium isotope preparation by the neutron-induced fission of ^{235}U	[S65]				
		1991	^{122}Sn(α, ^{3}He)^{123}Sn	Stripping reaction	[M13]				
		1992	^{122}Sn(^{80}Se)^{123}Sn	^{122}Sn target, backed with lead, bombarding with the pulse beam of ^{80}Se	[M15]				
		1992	^{124}Sn(^{80}Se)^{123}Sn	^{80}Se pulse beam on lead backed ^{124}Sn target	[M15]				
		1994	^{124}Sn(^{80}Se)^{123}Sn	Heavy-ion collision	[M16]				
		1995	^{122}Sn(n, γ)^{123}Sn		[C12]				
		1995	^{124}Sn(^{136}Xe)^{123}Sn	Heavy-ion collision	[D2]				
		2003	^{124}Sn(d, ^{3}He)^{123}Sn	Pion-transfer reaction under recoil-free condition	[S76]				
		2004	^{124}Sn(d, ^{3}He)^{123}Sn	Pion-transfer reaction under recoil-free condition	[S77]				
		2005	^{124}Sn(d, p2n)^{123}Sn	Deuteron beam on the enriched Sn target	[B5]				
		2006	^{122}Sn(n, γ)^{123}Sn	Thermal-neutron capture on natural Sn foil	[K50]				
		2007	^{122}Sn(n, γ)^{123}Sn	Neutron capture	[E2]				
		2008	^{122}Sn(n, γ)^{123}Sn	Neutron capture	[C33]				
		2011	^{124}Sn(γ, n)^{123}Sn	Radiative neutron transfer	[U6]				
		2012	^{12}C(^{238}U)^{123}Sn	Fission fragmentation	[A28]				
		2012	^{18}O(^{208}Pb)^{123}Sn	Fission fragmentation	[A28]				
		2013	^{12}C(^{238}U)^{123}Sn	Fusion-fission	[A29]				
		2013	^{18}O(^{208}Pb)^{123}Sn	Fusion-fission	[A29]				
		2014	^{124}Sn(n, 2n)^{123}Sn	Neutron capture by natural ^{124}Sn	[D21]				
		2014	^{122}Sn(n, γ)^{123}Sn	Neutron capture	[D21]				
		2018	^{124}Sn(n, 2n)^{123}Sn		[P4]				
		2018	^{124}Sn(^{7}Li, ^{8}Li)^{123}Sn	One neutron pickup reaction	[P8]				

Table 6: Discovery, production scheme and half-lives of tin isotopes *(continued)*

Isotope	Year	Production scheme				Half-life value			
		Year	*Reaction*	*Principal method/condition*	*Ref*	*Year*	*Half-life*		*Ref*
^{124}Sn	1922	---	---	---	---	---	---	---	[A30]
		1964	^{123}Sn(d, p)^{124}Sn	Deuteron bombardment	[C37]	1937	STABLE		[G40]
		1968	^{124}Sn(n, γ)^{125}Sn	Radiative-neutron capture	[T17]	1949	(0.4–0.9)×10^{16} y		[F11]
		1968	^{122}Cd(α, 2n)^{124}Sn	Alpha-particle bombardment	[Y5]	1952	(2–5)×10^{17} y		[F12]
		1970	^{122}Sn(t, p)^{124}Sn		[F14]	1952	2×10^{17} y		[F36]
		1970	^{122}Sn(t, p)^{124}Sn		[F19]	1952	>2.1×10^{17} y	0.3	[H31]
		1970	^{122}Sn(t, p)^{124}Sn	Target preparation by evaporation	[F18]	1952	~10^{17} y		[K1]
		1975	^{122}Sn(^{18}O, ^{16}O)^{124}Sn	*2n*-transfer reaction	[B61]	1952	>2×10^{17} y		[P10]
		1978	^{124}In(β$^-$)^{124}Sn	In preparation by thermal-neutron induced ^{235}U fission	[A5]	1968	9.4 m		[T17]
		1979	^{124}In(β$^-$)^{124}Sn	In preparation by the neutron-induced fission of ^{235}U	[F21]	2003	STABLE		[A42]
		1979	^{128}Te(d, ^{6}Li)^{124}Sn	Alpha-cluster pickup *via* (d, ^{6}Li) reaction	[J4]	2003	STABLE		[L3]
		1987	^{124}In(β$^-$)^{124}Sn	Indium isotope preparation by the neutron-induced fission of ^{235}U	[S65]	2008	(0.8–1.2)×10^{21} y		[B8]
		1992	^{124}Sn(^{76}Ge)^{124}Sn	Heavy-ion collision	[B76]	2008	>(3.1–7.7)×10^{18} y		[D11]
		2011	^{123}Sn(n, γ)^{124}Sn	Nuetron capture	[A49]	2008	>8.7 × 10^{19} y		[D12]
		2011	^{124}Sn(n, nγ)^{124}Sn	Fusion-fission reaction	[F34]	2012	STABLE		[A43]
		2011	^{123}Sn(n, γ)^{124}Sn	Radiative neutron capture	[U6]	2017	STABLE		[A45]
		2012	^{12}C(^{238}U)^{124}Sn	Fission fragmentation	[A28]				
		2012	^{18}O(^{208}Pb)^{124}Sn	Fission fragmentation	[A28]				
		2013	^{12}C(^{238}U)^{124}Sn	Fusion-fission	[A29]				
		2013	^{18}O(^{208}Pb)^{124}Sn	Fusion-fission	[A29]				
		2014	^{48}Ca(^{238}U)^{124}Sn	Fusion-fission	[I9]				
		2014	^{64}Ni(^{238}U)^{124}Sn	Fusion-fission	[I9]				
		2014	^{48}Ca(^{208}Pb)^{124}Sn	Fusion-fission	[I9]				
		2015	^{48}Ca(^{208}Pb)^{124}Sn	Fusion-fission	[I10]				
		2015	^{48}Ca(^{238}U)^{124}Sn	Fusion-fission	[I10]				
		2015	^{64}Ni(^{238}U)^{124}Sn	Fusion-fission	[I10]				
		2016	^{235}U(n_{th}, f)^{124}Sn	Neutron-induced fission	[S15]				

Table 6: Discovery, production scheme and half-lives of tin isotopes *(continued)*

Isotope	Year	Production scheme				Half-life value			
		Year	*Reaction*	*Principal method/condition*	*Ref*	*Year*	*Half-life*		*Ref*
^{124}Sn	1922	---	---	---	---	---	---	---	[A30]
		2016	^{124}Sb(ε)^{124}Sn	Electron-capture	[T21]				
		2018	^{238}U(^{12}C)^{124}Sn	Fission-fragmentation, uranium beam impinging on ^{12}C target	[R16]				
^{125}Sn	1939	---	---	---	---	---	---	---	[L24]
		1948	U(n)^{125}Sn		[S29]	1937	8 m		[G40]
		1949	^{124}Sn(d, p)^{125}Sn	Deuteron bombardment	[L9]	1939	9 m		[L24]
		1949	^{124}Sn(n, γ)^{125}Sn	Slow neutron irradiation	[L9]	1947	9 m		[S34]
		1953	^{124}Sn(d, p)^{125}Sn		[W6]	1948	~ 20 m		[S29]
		1961	^{124}Sn(d, p)^{125}Sn	Deuteron bombardment	[C35]	1949	9.8 m	0.2	[L9]
		1961	^{124}Sn(α, 2p1n)^{125}Sn	Alpha irradiation	[H4]	1950	9.9 d		[H17]
		1962	^{128}Te(n, α)^{125}Sn		[H3]	1951	9.9 d		[F6]
		1962	^{130}Te(n, 2p4n)^{125}Sn		[H3]	1951	9.8 m		[F6]
		1963	^{124}Sn(d, p)^{125}Sn		[D3]	1952	9.4 d		[G30]
		1964	^{124}Sn(d, p)^{125}Sn	Deuteron bombardment	[C37]	1952	10 d		[M10]
		1964	^{124}Sn(d, p)^{125}Sn	Monoenergetic deuteron bombardment	[N8]	1956	10 d		[D26]
		1966	U(*f*)^{125}Sn	Fission	[L6]	1957	9.7 d		[B85]
		1966	^{124}Sn(d, p)^{125}Sn	Neutron stripping	[R27]	1961	9 m		[S16]
		1967	^{124}Sn(d, p)^{125}Sn	Stripping reaction	[S17]	1963	9.7 m		[M6]
		1968	^{124}Sn(n, γ)^{125}Sn		[B33]	1963	9.6 d		[W5]
		1968	^{235}U(*f*)^{125}Sn	Fission	[E5]	1964	9.4 m		[D14]
		1968	^{124}Sn(n, γ)^{125}Sn	Neutron capture	[S3]	1964	9.7 d		[D14]
		1969	^{235}U(n, *f*)^{125}Sn	Thermal neutron-fission	[E6]	1965	9.7 m		[K18]
		1972	^{124}Sn(d, p)^{125}Sn	^{124}Sn preparation by vacuum evaporation	[C9]	1966	9.625 d	0.025	[L6]
		1973	^{124}Sn(α, ^{3}He)^{125}Sn	Alpha bombardment	[B40]	1968	9.64 d	0.03	[E5]
		1973	^{124}Sn(d, p)^{125}Sn	Deuteron bombardment	[B40]	1968	9.6 m	0.1	[E5]
		1974	^{235}U(n)^{125}Sn	Fission	[G34]	1969	9.7 d		[E6]
		1975	^{124}Sn(d, p)^{125}Sn	Deuteron beams on the thin tin target	[B21]	1969	9.6 m		[E6]
		1975	^{124}Sn(^{18}O, ^{17}O)^{125}Sn	*2n*-transfer reaction	[B61]	1974	9.7 d		[A20]
		1976	^{125}In(β^{-})^{125}Sn	^{125}In preparation by ^{235}U(n, *f*) and ^{238}U(α, *f*) reactions	[F20]	1974	576 s		[A20]
		1976	^{124}Sn(d, pγ)^{125}Sn	^{124}Sn preparation by evaporation	[M4]	1974	9.65 d		[B69]

Table 6: Discovery, production scheme and half-lives of tin isotopes *(continued)*

Isotope	Year	Production scheme				Half-life value			
		Year	*Reaction*	*Principal method/condition*	*Ref*	*Year*	*Half-life*		*Ref*
^{125}Sn	1939	---	---	---	---	---	---	---	[L24]
		1977	^{124}Sn(n, γ)^{125}Sn		[C11]	1974	9.7 m		[B87]
		1977	^{124}Sn(d, p)^{125}Sn	Deuteron bombardment	[S73]	1974	576 s		[G34]
		1978	^{125}In(β$^-$)^{125}Sn	In preparation by thermal-neutron induced fission of ^{235}U	[A5]	1981	9.64 d	0.03	[T3]
		1986	Sn(n)^{125}Sn	Neutron activation on enriched stable Sn	[A17]	1997	9.64 d	0.03	[A41]
		1987	^{125}In(β$^-$)^{125}Sn	In preparation by neutron-induced fission of ^{235}U	[S65]	2003	9.64 d	0.03	[A42]
		1991	^{124}Sn(α, ^{3}He)^{125}Sn	Stripping reaction	[M13]	2009	9.64 d		[H6]
		1996	^{124}Sn(n, γ)^{125}Sn		[A21]	2011	9.64 d	0.03	[K13]
		2000	^{233}U(n)^{125}Sn	Thermal neutron-induced fission	[P19]	2012	9.64 d	0.03	[A43]
		2000	^{239}Pu(n)^{125}Sn	Thermal neutron-induced fission	[P19]	2014	9.64 d		[D21]
		2000	^{124}Sn(^{238}U)^{125}Sn	Heavy-ion reaction	[Z3]	2016	9.6 d		[H20]
		2004	U(p)^{125}Sn	Fission on the UC_2 target	[B52]	2017	9.64 d	0.03	[A45]
		2004	^{124}Sn(d, p)^{125}Sn	^{124}Sn beam on deuterated polyethylene (CD_2) target	[J11]	2018	9.64 d		[P8]
		2005	U(p)^{125}Sn	Fission on the UC_2 target	[B53]				
		2005	^{2}H(^{124}Sn, p)^{125}Sn	Single-neutron transfer reaction on deuterated polyethylene target	[J12]				
		2006	^{124}Sn(n, γ)^{125}Sn	Thermal-neutron capture by natural Sn foil	[K50]				
		2007	^{124}Sn(n, γ)^{125}Sn	Neutron capture	[E2]				
		2008	^{238}U(^{9}Be)^{125}Sn	Fission	[L29]				
		2010	^{124}Sn(^{9}Be, ^{8}Be)^{125}Sn	One-nuetron transfer reaction	[P34]				
		2011	^{124}Sn(n, γ)^{125}Sn		[T18]				
		2011	^{124}Sn(d, p^{125}Sn		[T18]				
		2012	^{12}C(^{238}U)^{125}Sn	Fission fragmentation	[A28]				
		2012	^{18}O(^{208}Pb)^{125}Sn	Fission fragmentation	[A28]				
		2013	^{12}C(^{238}U)^{125}Sn	Fusion-fission	[A29]				
		2013	^{18}O(^{208}Pb)^{125}Sn	Fusion-fission	[A29]				
		2014	^{124}Sn(n, γ)^{125}Sn	Neutron capture	[[D21]				
		2018	^{124}Sn(^{7}Li, ^{6}Li)^{125}Sn	One-neutron stripping reaction	[P8]				

Table 6: Discovery, production scheme and half-lives of tin isotopes *(continued)*

Isotope	Year	Production scheme				Half-life value			
		Year	*Reaction*	*Principal method/condition*	*Ref*	*Year*	*Half-life*		*Ref*
^{126}Sn	1951	---	---	---	---	---	---	---	[B14]
		1948	U(n)^{126}Sn		[S29]	1948	70 m		[S29]
		1962	^{235}U(n)^{126}Sn	Fission	[D25]	1948	80 m		[S29]
		1969	^{124}Sn(t, p)^{126}Sn	^{124}Sn preparation by vacuum evaporation	[B44]	1951	50 m		[B14]
		1970	^{124}Sn(t, p)^{126}Sn		[F14]	1951	70 m		[F6]
		1970	^{124}Sn(t, p)^{126}Sn	Target preparation by evaporation	[F18]	1962	~10^5 y		[D25]
		1973	^{124}Sn(t, p)^{126}Sn		[A38]	1971	~10^5 y		[O10]
		1975	^{124}Sn(^{18}O, ^{16}O)^{126}Sn	*2n*-transfer reaction	[B61]	1973	~10^5 y		[A38]
		1976	^{235}U(n, f)^{126}Sn	Fission	[S59]	1976	10^5 y		[S59]
		1978	^{126}In(β^-)^{126}Sn	In preparation by neutron-induced fission of ^{235}U	[A5]	1996	2.07×10^5 y	0.21	[G15]
		1979	^{126}In(β^-)^{126}Sn	In preparation by neutron-induced fission of ^{235}U	[F21]	1996	2.07×10^5 y	0.21	[H1]
		1979	^{130}Te(d, ^{6}Li)^{126}Sn	Alpha-cluster pickup *via* (d, ^{6}Li) reaction	[J4]	1996	2.5×10^5 y	0.2	[Z2]
		1985	^{124}Sn(^{14}C, ^{12}C)^{126}Sn	Two-neutron transfer reaction	[V8]	1997	~10^5 y		[K60]
		1987	^{126}In(β^-)^{126}Sn	In preparation by neutron-induced fission of ^{235}U	[S65]	1998	1.14×10^5 y		[Q1]
		1996	^{235}U(n)^{126}Sn	Fission	[Z2]	1999	2.345×10^5 y	0.071	[O1]
		1997	^{235}U(*f*)	Fission	[K60]	2003	230 ky	14	[A42]
		2000	^{124}Sn(^{238}U)^{126}Sn	Heavy-ion reaction	[Z3]	2005	2.33×10^5 y	0.10	[C16]
		2000	^{238}U(Xγ)^{126}Sn		[K12]	2006	2.42×10^5 y		[F33]
		2004	U(p)^{126}Sn	Fission	[B52]	2006	2.4×10^5 y		[F33]
		2006	^{125}Sn(n, γ)^{126}Sn		[F33]	2009	1.980×10^5 y	0.057	[B32]
		2006	^{126}Sb(n, p)^{126}Sn		[F33]	2010	2×10^5 y		[F8]
		2006	^{129m}Te(n, α)^{126}Sn		[F33]	2012	230 ky	14	[A43]
		2010	^{238}U(^{9}Be)^{126}Sn	Fission	[I4]	2012	10^5 y		[I5]
		2012	^{12}C(^{238}U)^{126}Sn	Fission fragmentation	[A28]	2012	2.3×10^5 y		[K55]
		2012	^{18}O(^{208}Pb)^{126}Sn	Fission fragmentation	[A28]	2013	2.17×10^5 y	0.14	[K59]
		2013	^{12}C(^{238}U)^{126}Sn	Fusion-fission	[A29]	2016	2.3×10^5 y		[H20]
		2013	^{18}O(^{208}Pb)^{126}Sn	Fusion-fission	[A29]	2017	230 ky	14	[A45]
		2013	^{238}U(*f*)^{126}Sn	Fission	[A54]	2017	2.35×10^5 y		[B74]

Table 6: Discovery, production scheme and half-lives of tin isotopes *(continued)*

Isotope	Year	Production scheme				Half-life value			
		Year	*Reaction*	*Principal method/condition*	*Ref*	*Year*	*Half-life*		*Ref*
^{126}Sn	1951	---	---	---	---	---	---	---	[B14]
		2014	^{48}Ca(^{238}U)^{126}Sn	Fusion-fission	[I9]				
		2014	^{64}Ni(^{238}U)^{126}Sn	Fusion-fission	[I9]				
		2014	^{48}Ca(^{208}Pb)^{126}Sn	Fusion-fission	[I9]				
		2015	^{48}Ca(^{208}Pb)^{126}Sn	Fusion-fission	[I10]				
		2015	^{48}Ca(^{238}U)^{126}Sn	Fusion-fission	[I10]				
		2015	^{64}Ni(^{238}U)^{126}Sn	Fusion-fission	[I10]				
		2016	^{235}U(n_{th}, f)^{126}Sn	Neutron-induced fission	[S15]				
^{127}Sn	1951	---	---	---	---	---	---	---	[B14]
		1951	^{235}U(n, *f*)^{127}Sn	Fission	[B14]	1951	1.5 h		[B14]
		1962	^{235}U(n)^{127}Sn	Fission	[D25]	1962	2.15 h	0.10	[D25]
		1962	^{130}Te(n, α)^{127}Sn		[H3]	1962	4.6 m	0.4	[H3]
		1962	^{128}Te(3n, α)^{127}Sn		[H3]	1962	2.2 h	0.2	[H3]
		1965	^{130}Te(n, α)^{127}Sn	Neutron irradiation	[K18]	1963	2.45 h	0.30	[M6]
		1974	^{235}U(n, *f*)^{127}Sn	Thermal-neutron fission	[A20]	1964	2.15 h		[T20]
		1974	^{130}Te(n, α)^{127}Sn		[A20]	1965	4.1 m	0.3	[K18]
		1974	^{235}U(n)^{127}Sn	Fission	[G34]	1969	2.1 h		[E6]
		1978	^{127}In(β$^-$)^{127}Sn	In preparation by neutron-induced fission of ^{235}U	[A5]	1972	2.10 h	0.04	[A37]
		1980	^{127}In(β$^-$)^{127}Sn	^{127}In preparation by ^{235}U(n, *f*) reaction	[G18]	1974	2.2 h		[A20]
		1987	^{127}In(β$^-$)^{127}Sn	In preparation by neutron-induced fission of ^{235}U	[S65]	1974	2.12 h		[B69]
		1993	^{252}Cf(*f*)^{127}Sn	Spontaneous fission	[X1]	1974	248 s	2	[G34]
		2000	^{233}U(n)^{127}Sn	Thermal neutron-induced fission	[P19]	1977	2.2 h		[S25]
		2000	^{239}Pu(n)^{127}Sn	Thermal neutron-induced fission	[P19]	1993	2.10 h		[X1]
		2004	U(p)^{127}Sn	Fission on the UC_2 target	[B52]	1997	2.10 h	0.04	[A41]
		2004	^{127}In(β$^-$)^{127}Sn	In preparation by thermal-neutron induced fission of ^{235}U carbide	[G17]	2003	2.10 h	0.04	[A42]
		2005	U(p)^{127}Sn	Fission on the UC_2 target	[B53]	2011	2.10 h	0.04	[H14]
		2007	^{136}Xe(Be)^{127}Sn	Projectile fragmentation	[A34]	2012	2.10 h	0.04	[A43]
		2008	U(p)^{127}Sn	Proton-induced fission on the uranium carbide target	[D31]	2017	2.10 h	0.04	[A45]
		2008	^{238}U(^{9}Be)^{127}Sn	Fission	[L29]				

Table 6: Discovery, production scheme and half-lives of tin isotopes *(continued)*

Isotope	Year	Production scheme				Half-life value			
		Year	*Reaction*	*Principal method/condition*	*Ref*	*Year*	*Half-life*		*Ref*
^{127}Sn	1951	---	---	---	---	---	---	---	[B14]
		2016	^{126}Sn(n, γ)^{127}Sn		[A19]				
		2016	^{126}Sn(d, p)^{127}Sn	Deuteron breakup *via* (d, p) transfer reaction	[T13]				
^{128}Sn	1956	---	---	---	---	---	---	---	[A11]
		1962	^{235}U(n)^{128}Sn	Fission	[D25]	1962	58 m	5	[D25]
		1962	^{235}U(n)^{128}Sn	Thermal neutron fission	[M11]	1962	57 m	4	[H3]
		1968	^{235}U(*f*)^{128}Sn	Fission	[E5]	1962	62 m		[M11]
		1974	^{235}U(n, *f*)^{128}Sn	Fission	[F35]	1962	57 m		[M11]
		1976	^{235}U(n)^{128}Sn	Thermal neutron-induced fission	[N18]	1962	57 m	4	[H3]
		1978	^{128}In(β$^-$)^{128}Sn	Indium production by thermal-neutron-induced fission of ^{235}U	[A5]	1964	59.8 m	0.8	[S70]
		1979	^{128}In(β$^-$)^{128}Sn	Indium preparation by neutron-induced fission of ^{235}U	[F21]	1968	60.0 m	0.4	[E5]
		1981	^{128}In(β$^-$)^{128}Sn	^{128}In preparation from ^{235}U(n, *f*) reaction	[F22]	1968	59.3m	0.5	[E5]
		1987	^{128}In(β$^-$)^{128}Sn	Indium preparation by neutron-induced fission of ^{235}U	[S65]	1972	58.3 m	1.5	[I16]
		1990	^{128}In(β$^-$)^{128}Sn	Indium production from thermal-neutron-induced fission of ^{235}U	[S69]	1973	60.0 m	4	[A55]
		1993	^{252}Cf(*f*)^{128}Sn	Spontaneous fission	[X1]	1974	1 h		[A20]
		2000	^{124}Sn(^{238}U)^{128}Sn	Fission and neutron transfer	[Z3]	1974	59.3 m	0.5	[F35]
		2004	U(p)^{128}Sn	Fission	[B52]	1976	59.1 m	0.5	[N18]
		2010	^{136}Xe(Be)^{128}Sn	Projectile fragmentation	[A35]	1983	59.1 m	0.5	[K38]
		2011	^{136}Xe(^{9}Be)^{128}Sn	Fragmentation	[P18]	1993	59.1 m		[X1]
		2012	^{128}In(β$^-$)^{128}Sn		[A44]	1997	59.1 m	0.5	[A41]
		2013	^{238}U(γ, f)^{128}Sn	Bremsstrahlung-induced fission	[N3]	2001	59.07 m	0.14	[K3]
		2014	^{48}Ca(^{238}U)^{128}Sn	Fusion-fission	[I9]	2003	59.07 m	0.14	[A42]
		2014	^{64}Ni(^{238}U)^{128}Sn	Fusion-fission	[I9]	2012	59.07 m	0.14	[A43]
		2015	Pu(α)^{128}Sn	Alpha-accompanied ternary fission reactions on $^{238-244}$Pu isotopes	[S79]	2013	59.07 m		[N3]

Table 6: Discovery, production scheme and half-lives of tin isotopes *(continued)*

Isotope	Year	Production scheme				Half-life value			
		Year	*Reaction*	*Principal method/condition*	*Ref*	*Year*	*Half-life*		*Ref*
^{128}Sn	1956	---	---	---	---	---	---	---	[A11]
		2016	^{235}U(n_{th}, f)^{128}Sn	Neutron-induced fission	[S15]	2015	59.07 m	0.14	[E4]
		2017	^{238}U(n, f)^{128}Sn	Electromagnetically-induced fission	[P12]	2017	59.07 m	0.14	[A45]
		2018	^{232}Th(γ, f)^{128}Sn	Bremsstrahlung-induced fission	[N4]	2018	59.07 m		[N4]
^{129}Sn	1962	---	---	---	---	---	---	---	[D25]
		1962	^{235}U(n)^{129}Sn	Fission	[D25]	1962	6.2 m	1.2	[D25]
		1972	U(n)^{129}Sn	Fission	[I16]	1962	8.8 m	0.6	[H3]
		1974	^{235}U(n, *f*)^{129}Sn	Fission	[F35]	1962	1.0 h	0.1	[H3]
		1974	^{235}U(n)^{129}Sn	Fission	[G34]	1966	2 m		[C34]
		1978	^{129}In(β^-)^{129}Sn	Indium isotope from thermal-neutron induced fission of ^{235}U	[A5]	1967	2.5 m		[B42]
		1980	^{129}In(β^-)^{129}Sn	^{129}In preparation by ^{235}U(n, *f*) reaction	[G18]	1967	7.5 m		[B42]
		1982	^{235}U(n, *f*)^{129}Sn	Thermal-neutron fission	[H40]	1972	2.52 m	0.12	[I16]
		1984	^{235}U(n_{th}, *f*)^{129}Sn	Photofission	[F39]	1974	2.5 m	0.2	[F35]
		1984	^{238}U(n_{th}, *f*)^{129}Sn	Photofission	[F39]	1974	134 s	2	[G34]
		1987	^{129}In(β^-)^{129}Sn	Indium isotope from neutron-induced fission of ^{235}U	[S65]	1974	8.9 m	0.6	[G34]
		1993	^{136}Xe(^{27}Al)^{129}Sn	Projectile fragmentation	[F45]	1974	135 s		[G34]
		2000	^{233}U(n)^{129}Sn	Thermal-neutron induced fission	[P19]	1974	456 s		[G34]
		2000	^{239}Pu(n)^{129}Sn	Thermal-neutron induced fission	[P19]	1974	7.4 m	0.3	[F35]
		2002	^{239}Pu(n)^{129}Sn	Thermal neutron-induced fission	[G20]	1980	6.7 m	0.4	[G18]
		2002	^{241}Pu(n)^{129}Sn	Thermal neutron-induced fission	[G20]	1982	2.5 m	0.1	[H40]
		2003	^{129}In(β^-)^{129}Sn	^{129}In isotope from thermal-neutron-induced fission of ^{241}Pu	[G21]	1982	6.9 m	0.1	[H40]
		2004	U(p)^{129}Sn	Fission on UC_2 target	[B52]	1983	2.16 m	0.04	[H13]
		2004	^{129}In(β^-)^{129}Sn	Indium isotope from thermal-neutron induced fission of ^{235}U carbide	[G17]	1997	2.23 m	0.04	[A41]
		2005	U(p)^{129}Sn	Fission on the UC_2 target	[B53]	2003	2.23 m	0.04	[A42]
		2008	^{238}U(^{9}Be)^{129}Sn	Fission	[L29]	2012	2.23 m	0.04	[A43]
		2009	^{128}Sn(n, γ)^{129}Sn	Neutron capture	[S75]	2014	2.23 m	0.04	[T12]
		2011	^{136}Xe(^{9}Be)^{129}Sn	Fragmentation	[P18]	2017	2.23 m	0.04	[A45]

Table 6: Discovery, production scheme and half-lives of tin isotopes *(continued)*

Isotope	Year	Production scheme				Half-life value			
		Year	*Reaction*	*Principal method/condition*	*Ref*	*Year*	*Half-life*		*Ref*
^{129}Sn	1962	---	---	---	---	---	---	---	[D25]
		2016	^{129}In(β$^-$)^{129}Sn	^{129}In production by impinging proton beam on the uranium carbide (UC_x) target	[L13]				
		2017	^{238}U(n, f)^{129}Sn	Electromagnetically-induced fission	[P12]				
		2017	^{238}U(^{9}Be)^{129}Sn	Fission of U followed by the fragmentation of ^{136}Xe isotope	[W12]				
^{130}Sn	1956	---	---	---	---	---	---	---	[P3]
		1956	U(n)^{130}Sn	Thermal-neutron fission	[P3]	1956	2.6 m	0.3	[P3]
		1972	U(n)^{130}Sn	Fission	[I16]	1962	2.6 m		[H3]
		1973	^{235}U(n, *f*)^{130}Sn	Thermal-neutron-induced fission	[K28]	1972	3.69 m	0.07	[I16]
		1973	^{130}In(β$^-$)^{130}Sn	^{130}In production from ^{235}U fission	[K26]	1974	3.7 m	0.2	[F35]
		1974	^{235}U(n, *f*)^{130}Sn	Fission	[F35]	1974	221 s		[G34]
		1974	^{235}U(n)^{130}Sn	Fission	[G34]	1974	1.7 m		[G34]
		1974	^{235}U(n)^{130}Sn	Fission	[K27]	1974	3.6 m	0.8	[G34]
		1981	^{130}In(β$^-$)^{130}Sn	^{130}In preparation from ^{235}U(n, *f*) reaction	[F22]	1974	3.72 m	0.11	[H24]
		1985	^{130}In(β$^-$)^{130}Sn	^{130}In production from thermal-neutron fission of ^{235}U	[F24]	1974	3.8 m	0.1	[K27]
		1987	^{130}In(β$^-$)^{130}Sn	Indium isotope from neutron-induced fission of ^{235}U	[S65]	1974	1.7 m	0.1	[K27]
		1990	^{130}In(β$^-$)^{130}Sn	Indium production from hermal-neutron-induced fission of ^{235}U	[S69]	1989	3.72 m	0.04	[S37]
		1993	^{136}Xe(^{27}Al)^{130}Sn	Projectile fragmentation	[F45]	1997	3.72 m	0.04	[A41]
		2000	^{124}Sn(^{238}U)^{130}Sn	Fission and neutron transfer	[Z3]	2001	3.72 m	0.07	[S55]
		2004	U(p)^{130}Sn	Fission	[B52]	2003	3.72 m	0.07	[A42]
		2005	U(p)^{130}Sn	Fission	[B53]	2009	162 s		[B32]
		2009	^{12}Sn(n, γ)^{130}Sn	Neutron capture	[S75]	2012	3.72 m	0.07	[A43]
		2011	^{136}Xe(^{9}Be)^{130}Sn	Fragmentation	[P18]	2013	3.72 m	0.07	[K4]
		2011	^{132}Sn(p, t)^{130}Sn		[P30]	2017	3.72 m	0.07	[A45]
		2012	U(p)^{130}Sn	Proton-induced fission reaction on natural uranium target	[H5]				

Table 6: Discovery, production scheme and half-lives of tin isotopes *(continued)*

Isotope	Year	Production scheme				Half-life value			
		Year	*Reaction*	*Principal method/condition*	*Ref*	*Year*	*Half-life*		*Ref*
^{130}Sn	1956	---	---	---	---	---	---	---	[P3]
		2013	U(p)^{130}Sn	Fission on natural uranium target	[K4]				
		2015	Pu(α)^{130}Sn	Alpha-accompanied ternary fission reactions on $^{238-244}$Pu isotopes	[S79]				
		2017	^{238}U(n, *f*)^{130}Sn	Electromagnetically-induced fission	[P12]				
^{131}Sn	1956	---	---	---	---	---	---	---	[P3]
		1956	U(n)^{131}Sn	Thermal-neutron fission	[P3]	1956	3.4 m	0.5	[P3]
		1963	^{235}U(n)^{131}Sn	Fission	[G38]	1963	65 s	10	[G38]
		1966	^{235}U(n)^{131}Sn	Thermal-neutron fission	[S72]	1966	1.32 m	0.23	[S72]
		1972	U(n)^{131}Sn	Fission	[I16]	1972	62.9 s	2.5	[I16]
		1974	^{235}U(n, *f*)^{131}Sn	Fission	[F35]	1972	62.9 s	0.8	[I16]
		1974	^{235}U(n)^{131}Sn	Fission	[G34]	1972	59.7 s	0.8	[I16]
		1978	^{232}Th(n)^{131}Sn	Neutron-induced fission	[I17]	1974	1.05 m	0.10	[F35]
		1980	^{131}In(β$^-$)^{131}Sn	^{131}In preparation by ^{235}U(n, *f*) reaction	[G18]	1974	55 s	4	[G34]
		1981	^{235}U(n)^{131}Sn	Thermal-neutron fission	[H39]	1974	61 s		[G34]
		1984	^{131}In(β$^-$)^{131}Sn		[F23]	1976	61 s	3	[A39]
		1984	^{131}In(β$^-$)^{131}Sn		[F25]	1977	39 s	2	[S25]
		1984	^{235}U(n_{th}, *f*)^{131}Sn	Photofission	[F39]	1977	50 s	2	[S25]
		1984	^{238}U(n_{th}, *f*)^{131}Sn	Photofission	[F39]	1981	61 s	1	[H38]
		1988	^{131}In(β$^-$)^{131}Sn		[F26]	1997	56.0 s	0.5	[A41]
		1988	^{131}In(β$^-$)^{131}Sn		[K51]	2003	56.0 s	0.5	[A42]
		1995	^{131}In(β$^-$)^{131}Sn		[M23]	2006	56.0 s	0.5	[K30]
		1999	^{131}In(β$^-$)^{131}Sn		[F31]	2008	56 s		[D31]
		2001	^{248}Cm(*f*)^{131}Sn	Spontaneous fission	[B36]	2009	53.1 s		[B32]
		2004	U(p)^{131}Sn	Fission on the UC_2 target	[B52]	2012	56.0 s	0.5	[A43]
		2004	^{131}In(β$^-$)^{131}Sn		[F32]	2013	56.0 s	0.5	[K4]
		2005	U(p)^{131}Sn	Fission on the UC_2 target	[B53]	2017	56.0 s	0.5	[A45]
		2007	^{130}Sn(d, p)^{131}Sn		[P1]				
		2008	U(p)^{131}Sn	Proton-induced fission on the uranium carbide target	[D31]				
		2009	^{130}Sn(n, γ)^{131}Sn		[B32]				
		2009	^{130}Sn(n, γ)^{131}Sn	Neutron capture	[S75]				
		2012	^{130}Sn(d, p)^{131}Sn	^{130}Sn beam on $(CD_2)_n$ foil	[K49]				
		2012	U(p)^{131}Sn	Proton-induced fission	[H5]				
		2012	^{130}Sn(n, γ)^{131}Sn	Neutron capture	[M32]				
		2012	^{130}Sn(n, γ)^{131}Sn	Neutron capture	[Z4]				

Table 6: Discovery, production scheme and half-lives of tin isotopes *(continued)*

Isotope	Year	Production scheme				Half-life value			
		Year	*Reaction*	*Principal method/condition*	*Ref*	*Year*	*Half-life*		*Ref*
^{131}Sn	1956	---	---	---	---	---	---	---	[P3]
		2013	U(p)^{131}Sn	Fission on the natural uranium	[K4]				
		2014	^{132}Sn(^{9}Be, ^{10}Beγ)^{131}Sn	One-neutron transfer reaction	[A7]				
		2015	^{130}Sn(^{9}Be, ^{8}Beγ)^{131}Sn	One-neutron transfer reaction	[J16]				
		2017	^{238}U(n, f)^{131}Sn	Electromagnetically-induced fission	[P12]				
^{132}Sn	1956	---	---	---	---	---	---	---	[P3]
		1956	U(n)^{132}Sn	Thermal-neutron fission	[P3]	1956	2.2 m	0.3	[P3]
		1963	^{235}U(n)^{132}Sn	Fission	[G38]	1963	50 s	10	[G38]
		1966	^{235}U(n)^{132}Sn	Thermal-neutron fission	[S72]	1966	1.00 m	0.17	[S72]
		1970	^{235}U(n)^{132}Sn	Thermal-neutron irradiation	[L15]	1970	2.1 m	0.2	[L15]
		1972	U(n)^{132}Sn	Fission	[I16]	1972	41.1 s	1.3	[I16]
		1972	^{235}U(n)^{132}Sn	Fission	[K24]	1972	31.5 s	6.4	[I16]
		1972	^{233}U(n_{th}, f)^{132}Sn	Thermal-neutron fission	[N1]	1972	40 s	1	[K24]
		1972	^{235}U(n_{th}, f)^{132}Sn	Thermal-neutron fission	[N1]	1972	39.0 s	1.0	[N1]
		1972	^{235}U(f)^{132}Sn	Fission	[N17]	1972	42.3 s	5.5	[N1]
		1973	^{132}In(β^-)^{132}Sn		[K25]	1972	40.9 s	3.0	[N1]
		1974	^{235}U(n, f)^{132}Sn	Fission	[F35]	1972	40.6 s	0.8	[N17]
		1974	^{235}U(n)^{132}Sn	Fission	[G34]	1973	40 s		[K25]
		1975	^{235}U(n, f)^{132}Sn	Fission-fragmentation	[B3]	1974	40 s	1	[F35]
		1978	^{232}Th(n)^{132}Sn	Neutron-induced fission	[I17]	1974	40.2 s		[G34]
		1980	^{132}In(β^-)^{132}Sn		[B45]	1974	41.0 s	1.5	[G34]
		1982	^{132}In(β^-)^{132}Sn		[B46]	1975	38.0 s	0.8	[B3]
		1986	^{132}In(β^-)^{132}Sn	^{132}In preparation by U(p) fission	[B47]	1976	40 s	1	[H25]
		1992	^{235}U(C)^{132}Sn	Fission-diffusion	[F28]	1978	40.0 s	1.0	[I17]
		1993	^{136}Xe(^{27}Al)^{132}Sn	Projectile fragmentation	[F45]	1989	40 s		[S71]
		1994	^{238}U(Pb)^{132}Sn	Projectile fission	[B25]	1992	39.7 s	0.5	[S38]
		1994	^{132}In(β^-)^{132}Sn	^{132}In production from neutron-induced fission of ^{235}U	[F29]	1995	39.7 s		[M2]
		1995	^{132}In(β^-)^{132}Sn	^{132}In isotope from neutron-induced fission of ^{235}U	[F30]	1997	39.7 s	0.5	[A41]
		1995	^{132}In(β^-)^{132}Sn		[M23]	2003	39.7 s	0.5	[A42]
		1999	^{132}In(β^-)^{132}Sn		[F31]	2005	39.7 s	0.8	[K29]
		2001	^{248}Cm(f)^{132}Sn	Spontaneous fission	[B26]	2009	34.4 s		[B32]
		2002	^{132}In(β^-)^{132}Sn	^{132}In isotope from proton-induced fission of ^{238}U	[D17]	2010	39.7 s		[J14]

Table 6: Discovery, production scheme and half-lives of tin isotopes *(continued)*

Isotope	Year	Production scheme				Half-life value			
		Year	*Reaction*	*Principal method/condition*	*Ref*	*Year*	*Half-life*		*Ref*
^{132}Sn	1956	---	---	---	---	---	---	---	[P3]
		2004	U(p)^{132}Sn	Fission	[B52]	2011	40 s		[J15]
		2004	^{238}U(Be)^{132}Sn	Projectile fission	[P20]	2012	39.7 s	0.8	[A43]
		2005	U(p)^{132}Sn	Fission	[B53]	2017	39.7 s	0.8	[A45]
		2005	^{238}U(Be)^{132}Sn	In-flight fission	[A2]				
		2008	U(p)^{132}Sn	Proton-induced fission reaction on uranium carbide target	[D31]				
		2009	^{131}Sn(n, γ)^{132}Sn		[B32]				
		2009	^{131}Sn(n, γ)^{132}Sn	Neutron capture	[S75]				
		2011	^{131}Sn(n, γ)^{132}Sn	Nuetron capture	[A49]				
		2011	^{nat}U(p)^{132}Sn	Fission	[J15]				
		2011	^{134}Sn(p, t)^{132}Sn	Two-nucleon transfer reaction	[P30]				
		2012	U(p)^{132}Sn	Proton-induced fission reaction on natural uranium target	[H5]				
		2013	U(p)^{132}Sn	Fission with proton beam on the natural uranium target	[K4]				
		2015	Pu(α)^{132}Sn	Alpha-accompanied ternary fission reactions on $^{238-244}$Pu isotopes	[S79]				
		2016	^{235}U(n_{th}, *f*)^{132}Sn	Neutron-induced fission	[S15]				
		2017	^{238}U(n, *f*)^{132}Sn	Electromagnetically-induced fission	[P12]				
^{133}Sn	1963	---	---	---	---	---	---	---	[G38]
		1963	^{235}U(n)^{133}Sn	Fission	[G38]	1963	39 s	15	[G38]
		1966	^{235}U(n)^{133}Sn	Thermal-neutron fission	[S72]	1966	55 s		[S72]
		1973	^{235}U(n)^{133}Sn	Fission	[B66]	1973	34 s		[B66]
		1974	^{235}U(n, *f*)^{133}Sn	Fission	[F35]	1973	1.47 s	0.04	[B66]
		1974	^{235}U(n)^{133}Sn	Fission	[G34]	1974	~2 s		[F35]
		1978	^{235}U(n)^{133}Sn	Thermal neutron-induced fission	[S58]	1974	1.7 s		[G34]
		1988	^{133}In(β$^-$)^{133}Sn		[K51]	1974	1.7 s	0.3	[H22]
		1996	^{133}In(β$^-$)^{133}Sn		[H28]	1976	1.47 s	0.07	[L31]
		1999	^{235}U(n)^{133}Sn	Thermal neutron-induced fission	[S4]	1976	1.47 s		[R34]
		1999	^{248}Cm(*f*)^{133}Sn	Spontaneous fission	[U2]	1978	1.47 s		[S58]
		2000	^{133}In(β$^-$)^{133}Sn		[H29]	1978	1.42 s		[S58]
		2002	^{133}In(β$^-$)^{133}Sn	^{133}In production from proton-induced fission of ^{238}U	[D17]	1978	1.37 s	0.07	[S58]
		2007	^{132}Sn(d, p)^{133}Sn	Neutron transfer reaction	[J13]	1983	1.5 s		[B58]
		2007	^{132}Sn(n, γ)^{133}Sn		[K10]	1986	1.44 s	0.04	[S36]

Table 6: Discovery, production scheme and half-lives of tin isotopes *(continued)*

Isotope	Year	Production scheme				Half-life value			
		Year	*Reaction*	*Principal method/condition*	*Ref*	*Year*	*Half-life*		*Ref*
^{133}Sn	1963	---	---	---	---	---	---	---	[G38]
		2007	^{132}Sn(d, p)^{133}Sn	Neutron transfer reaction	[P1]	1993	1.20 s	0.05	[R35]
		2008	^{132}Sn(n, γ)^{133}Sn	Neutron capture	[C33]	1993	1.20 s	0.05	[R35]
		2008	U(p)^{133}Sn	Proton-induced fission on the uranium carbide target	[D31]	1995	1.45 s	0.03	[R1]
		2009	^{132}Sn(n, γ)^{133}Sn		[B32]	1997	1.45 s	0.03	[A41]
		2009	^{132}Sn(n, γ)^{133}Sn	Neutron capture	[S75]	1999	1.37 s		[S4]
		2010	^{132}Sn(d, p)^{133}Sn	Target preparation by uranium carbide fission	[J14]	2002	1450 ms	30	[P16]
		2011	^{132}Sn(d, p)^{133}Sn		[J15]	2003	1.45 s	0.03	[A42]
		2012	U(p)^{133}Sn	Proton-induced fission reaction on natural uranium target	[H5]	2011	1.46 s	0.03	[K31]
		2012	^{132}Sn(n, γ)^{133}Sn	Direct neutron capture	[M32]	2012	1.46 s	0.03	[A43]
		2012	^{132}Sn(n, γ)^{133}Sn	Neutron capture	[Z4]	2017	1.46 s	0.03	[A45]
		2013	U(p)^{133}Sn	Fission with proton beam on the natural uranium target	[K4]				
		2014	^{132}Sn(^{9}Be, ^{8}Beγ)^{133}Sn	One-neutron transfer reaction	[A7]				
		2014	^{132}Sn(^{9}Be, ^{8}Be)^{133}Sn	One-neutron transfer through ^{132}Sn(^{9}Be, ^{8}Be → 2α)^{133}Sn pathway	[A53]				
		2016	^{132}Sn(d, p)^{133}Sn	Deuteron breakup *via* (d, p) transfer reaction	[T13]				
		2017	^{134}Sn(γ, n)^{133}Sn	One-neutron knockout from the ^{134}Sn target	[V2]				
^{134}Sn	1963	---	---	---	---	---	---	---	[G38]
		1963	^{235}U(n)^{134}Sn	Fission	[G38]	1963	20 s		[G38]
		1974	^{235}U(n, *f*)^{134}Sn	Fission	[S43]	1974	~1 s		[S43]
		1975	^{235}U(n, *f*)^{134}Sn	Fission	[A36]	1975	0.7 s	0.2	[A26]
		1988	^{133}Sn(n, γ)^{134}Sn		[K51]	1976	1.04 s	0.02	[L31]
		1996	^{134}In(β$^-$)^{134}Sn		[H28]	1976	1.04 s		[R34]
		1998	^{238}U(^{208}Pb)^{134}Sn	Projectile fission, ^{238}U impinging on the Pb target	[D23]	1980	0.85 s		[L32]
		2000	^{248}Cm(n)^{134}Sn	Fission	[K45]	1981	1.04 s	0.02	[S35]
		2002	^{134}In(β$^-$)^{134}Sn	^{134}In production from the proton-induced fission of ^{238}U	[D17]	1990	1.20 s	0.10	[F27]
		2005	U(n)^{134}Sn	Fast-neutron-induced fission on the UC_2 target	[S47]	1993	0.70 s		[R35]

Table 6: Discovery, production scheme and half-lives of tin isotopes *(continued)*

Isotope	Year	Production scheme				Half-life value			
		Year	*Reaction*	*Principal method/condition*	*Ref*	*Year*	*Half-life*		*Ref*
^{134}Sn	1963	---	---	---	---	---	---	---	[G38]
		2008	U(p)^{134}Sn	Proton-induced fission on the uranium carbide target	[D31]	1993	1.050 s	0.011	[R35]
		2009	^{133}Sn(n, γ)^{134}Sn	Neutron capture	[S75]	1997	1.12 s	0.08	[A41]
		2009	^{133}Sn(n, γ)^{134}Sn	Neutron capture	[S75]	2002	1120 ms	80	[P16]
		2012	U(p)^{134}Sn	Proton-induced fission reaction on natural uranium target	[H5]	2003	1.12 s	0.08	[A42]
		2013	U(p)^{134}Sn	Fission with proton beam on natural uranium target	[K4]	2004	1.050 s	0.11	[S63]
		2014	^{136}Sn(p, t)^{134}Sn	Two-neutron transfer reaction	[B17]	2005	1.04 s		[S47]
		2016	^{235}U(n_{th}, *f*)^{134}Sn	Neutron-induced fission	[S15]	2012	1.050 s	0.011	[A43]
		2017	^{238}U(Be)^{134}Sn	Projectile fission	[V2]	2015	890 ms	20	[L27]
						2017	890 ms	20	[A45]
^{135}Sn	1994	---	---	---	---	---	---	---	[B25]
		1994	^{238}U(Pb)^{135}Sn	Projectile fission	[B25]	1997	>150 ns		[A41]
		2001	^{238}U(n)^{135}Sn	Neutron-induced fission	[K46]	2001	0.6 s	0.1	[K46]
		2002	^{135}In(β^-)^{135}Sn	^{135}In isotope production from proton-induced fission of ^{238}U	[D17]	2001	450 ms	50	[S45]
		2002	U(p)^{135}Sn	Spallation on the UC_2 target	[S46]	2002	530 ms	20	[S46]
		2005	U(n)^{135}Sn	Fast-neutron-induced fission of UC_2 target	[S47]	2003	530 ms	20	[A42]
		2005	U(n)^{135}Sn	High-energy neutron-induced fission of UC_2 target	[S48]	2005	0.6 s	0.1	[K47]
		2009	^{134}Sn(n, γ)^{135}Sn	Neutron capture	[S75]	2005	530 ms		[S47]
		2012	U(p)^{135}Sn	Proton-induced fission reaction on natural uranium target	[H5]	2005	525 ms		[S49]
		2013	U(p)^{135}Sn	Fission with proton beam on the natural uranium target	[K4]	2008	530 ms	20	[S57]
						2012	530 ms	20	[A43]
						2015	515 ms	5	[L27]
						2017	515 ms	5	[A45]

Table 6: Discovery, production scheme and half-lives of tin isotopes *(continued)*

Isotope	Year	Production scheme				Half-life value			
		Year	*Reaction*	*Principal method/condition*	*Ref*	*Year*	*Half-life*		*Ref*
^{136}Sn	1994	---	---	---	---	---	---	---	[B25]
		1994	^{238}U(Pb)^{136}Sn	Projectile fission reaction	[B25]	1997	>150 ns		[A41]
		2002	U(p)^{136}Sn	Spallation on the UC_2 target	[S46]	2002	450 ms	50	[P16]
		2009	^{135}Sn(n, γ)^{136}Sn	Neutron capture	[S75]	2002	250 ms	30	[S46]
		2014	^{134}Sn(t, p)^{136}Sn	Two-neutron transfer reaction	[B17]	2002	0.25 s	0.03	[S62]
		2014	^{238}U(Be)^{136}Sn	Projectile fission, ^{238}U beam impinging on the Be target	[S52]	2003	250 ms	30	[A42]
		2014	^{9}Be(^{137}Sb)^{136}Sn	One-proton knockout reaction, ^{137}Sb beam production by an in-flight fission reaction of ^{238}U on the tungsten target	[W10]	2011	300 ms	15	[A22]
						2012	290 ms	13	[A43]
						2014	46 ns	7	[S52]
						2015	350 ms	5	[L27]
						2017	350 ms	5	[A45]
^{137}Sn	1994	---	---	---	---	---	---	---	[B25]
		1994	^{238}U(Pb)^{137}Sn	Projectile fission	[B25]	1997	>150 ns		[A41]
		2002	U(p)^{137}Sn	Spallation on the UC_2 target	[S46]	2002	190 ms	60	[S46]
		2009	^{136}Sn(n, γ)^{137}Sn	Neutron capture	[S75]	2003	190 ms	60	[A43]
						2007	190 ms	60	[B81]
						2011	273 ms	7	[A22]
						2012	273 ms	7	[A43]
						2015	230 ms	30	[L27]
						2017	273 ms	7	[A45]
^{138}Sn	2010	---	---	---	---	---	---	---	[O3]
		2010	^{238}U(Pb)^{138}Sn	Fission, $^{238}U^{86+}$ beam on the lead target	[O3]	2012	100# ms	>400 ns	[A43]
		2014	^{238}U(Be)^{138}Sn	Projectile fission on ^{238}U beam, impinging on the Be target	[S52]	2014	210 ns	45	[S52]
						2015	140 ms	30	[L27]
						2017	150 ms	30	[A45]
						2017	140 ms		[C30]
^{139}Sn	2015	---	---	---	---	---	---	---	[L27]
		2015	^{238}U(Be)^{139}Sn	Fission, ^{238}U beam collision with the beryllium target	[L27]	2015	130 ms	60	[L27]
						2016	130 ms	60	[J18]

Acknowledgements
MMR thanks the NSERC CREATE-REACT Program for providing financial support.

References

[A1] H. L. Acker, G. Backenstoss, C. Daum, J. C. Sens & S. A. De Wit. *Nucl Phys,* **87**: 1 (1966).
[A2] P. Adrich et al. *Phys Rev Lett,* **95**: 132501 (2005).
[A3] A. V. Afanasjev, D. B. Fossan, G. J. Lane & I. Ragnarsson. *Phys Rep,* **322**: 1 (1999).
[A4] U. Agvaanluvsan et al. *Phys Rev C,* **79**: 014320 (2009).
[A5] K. Aleklett, E. Lund & G. Rudstam. *Phys Rev C,* **18**: 462 (1978).
[A6] M. Aikawa, M. Saito, N. Ukon, Y. Komori & H. Haba. *Nucl Instr Methods Phys Res B,* **426**: 18 (2018).
[A7] J. M. Allmond et al. *Phys Rev Lett,* **112**: 172701 (2014).
[A8] J. M. Allmond et al. *Phys Rev C,* **92**: 041303 (2015).
[A9] A. L. Allred. *J Inorg Nucl Chem,* **17**: 215 (1961).
[A10] E. Amaldi, O. D'Agostino, E. Fermi, B. Pontecorvo, F. Rasetti & E. Segrè. *Proc Roy Soc,* **A149**: 522 (1935).
[A11] S. Amos, J. L. Gross & M. Thoennessen. *At Data Nucl Data Tables,* **97**: 383 (2011).
[A12] E. Andersson, P. Herges, H. V. Klapdor & I. N. Wischnewski. *Z Phys A,* **299**: 105 (1981).
[A13] E. Andreotti, M. Hult, R. G. de Orduña, G. Marissens, J. S. E. Wieslander & M. Misiaszek. *Phys Rev C,* **84**: 044605 (2011).
[A14] W. Andrejtscheff et al. *Nucl Phys A,* **505**: 397 (1989).
[A15] I. Angeli & K. P. Marinova. *At Data Nucl Data Tables,* **99**: 69 (2013).
[A16] G. de Angelis et al. *Nucl Phys A,* **583**: 231 (1995).
[A17] M. Anselment et al. *Phys Rev C,* **34**: 1052 (1986).
[A18] V. A. Anufriev, S. I. Babich, S. M. Masyanov & V. N. Nefedov. *Sov At Energy,* **63**: 912 (1987).
[A19] V. A. Apse, G. G. Kulikov & E. G. Kulikov. *Phys At Nucl,* **79**: 1513 (2016).
[A20] K. E. Apt & W. B. Walters. *Phys Rev C,* **9**: 310 (1974).
[A21] M. Arif, J. H. Zaidi, I. H. Qureshi & M. Z. Iqbal. *Radiochim Acta,* **75**: 175 (1996).
[A22] O. Arndt et al. *Phys Rev C,* **84**: 061307(R) (2011).
[A23] R. J. Ascuitto & N. K. Glendenning. *Phys Lett B,* **45**: 85 (1973).
[A24] R. J. Ascuitto & K. Glendenning. *Phys Lett B,* **47**: 332 (1973).
[A25] R. J. Ascuitto & N. K. Glendenning. *Phys Lett B,* **48**: 6 (1974).
[A26] M. Asghar et al. *Nucl Phys A,* **247**: 359 (1975).
[A27] M. N. Aslam, K. Zubia & S. M. Qaim. *Appl Radiat Isot,* **132**: 181 (2018).
[A28] A. Astier et al. *Phys Rev C,* **85**: 054316 (2012).
[A29] A. Astier. *EPJ Web Conf,* **62**: 01008 (2013).
[A30] F. W. Aston. *Nature,* **109**: 813 (1922).
[A31] F. W. Aston. *Proc Roy Soc,* **A115**: 487 (1927).
[A32] F. W. Aston. *Nature*, **120**: 956 (1927).
[A33] F. W. Aston. *Nature,* 137: 613 (1936).
[A34] L. Atanasova et al. *Prog Part Nucl Phys,* **59**: 355 (2007).
[A35] L. Atanasova et al. *Eur Phys Lett,* **91**: 42001 (2010).
[A36] R. L. Auble. *Nucl Data Sheets,* **7**: 363 (1972).
[A37] R. L. Auble. *Nucl Data Sheets,* 8: 77 (1972).

[A38] R. L. Auble. *Nucl Data Sheets,* **9**: 125 (1973).
[A39] R. L. Auble, H. R. Hiddleston & C. P. Browne. *Nucl Data Sheets,* **17**: 573 (1976).
[A40] G. Audi & A. H. Wapstra. *Nucl Phys A,* **565**: 1 (1993).
[A41] G. Audi, O. Bersillon, J. Blachot & A. H. Wapstra. *Nucl Phys A,* **624**: 1 (1997).
[A42] G. Audi, O. Bersillon, J. Blachot & A. H. Wapstra. *Nucl Phys A,* **729**: 3 (2003).
[A43] G. Audi et al. *Chin Phys C,* **36**: 1157 (2012).
[A44] G. Audi et al. *Chin Phys C,* **36**: 1287 (2012).
[A45] G. Audi, F. G. Kondev, M. Wang, W. J. Huang & S. Naimi. *Chin Phys C,* **41**: 030001 (2017).
[A46] G. Auger, J. M. Lagrange, M. Pautrat & J. Vanhorenbeeck. *J Phys G,* **6**: L95 (1980).
[A47] G. Auger, G. Albouy, C. Roulet, H. Sergolle, A. Kerek & T. Lindblad. *Z Phys A,* **296**: 319 (1980).
[A48] G. Auger, J. M. Lagrange, M. Pautrat & J. Vanhorenbeeck. *Nucl Phys A,* **426**: 109 (1984).
[A49] A. Avdeenkov, S. Goriely, S. Kamerdzhiev & S. Krewald. *Phys Rev C,* **83**: 064316 (2011).
[A50] F. Azaiez et al. *Nucl Phys A,* **444**: 373 (1985).
[A51] F. Azaiez et al. *Nucl Phys A,* **501**: 401 (1989).
[A52] C. Alduino et al. *Phys Rev C,* **97**: 055502 (2018).
[A53] J. M. Allmond et al. *Phys Rev C,* **90**: 014322 (2014).
[A54] S. Asai et al. *J Nucl Sci Technol,* **50**: 556 (2013).
[A55] R. L. Auble. *Nucl Data Sheets,* **9**: 157 (1973).
[B1] V. M. Bader et al. *Phys Rev C,* **88**: 051301(R) (2013).
[B2] P. A. Baedecker, A. Pakkanen & W. B. Walters. *Nucl Phys A,* **158**: 607 (1970).
[B3] G. Bailleul et al. *Z Phys A*, **273**: 283 (1975).
[B4] A. Bajpeyi, A. Shukla, A. J. Koning & S. Åberg. *Phys At Nucl*, **80**: 402 (2017).
[B5] A. R. Balabekyan et al. *Phys At Nucl*, **68**: 171 (2005).
[B6] P. Banerjee et al. *Phys Rev C*, **94**: 014316 (2016).
[B7] A. S. Barabash, F. Hubert, P. Hubert & V. Umatov. *J Phys G*, **34**: 1721 (2007).
[B8] A. S. Barabash, P. Hubert, A. Nachab, S. I. Konovalov, I. A. Vanyushin & V. Umatov. *Nucl Phys A*, **807**: 269 (2008).
[B9] A. S. Barabash, P. Hubert, A. Nachab, S. I. Konovalov & V. Umatov. *Phys Rev C*, **80**: 035501 (2009).
[B10] R. C. Barber, R. L. Bishop, L. A. Cambey, W. McLatchie & H. E. Duckworth. *Can J Phys,* **40**: 1496 (1962).
[B11] R. Barden et al. *Z Phys A,* 329: 319 (1988).
[B12] S. W. Barnes & P. W. Aradine. *Phys Rev,* **55**: 50 (1939).
[B13] S. W. Barnes. *Phys Rev,* **56**: 414 (1939).
[B14] J. W. Barnes & A. J. Freedman. *Phys Rev,* **84**: 365 (1951).
[B15] Z. Basrak, N. Cindro & M. Turk. *Nucl Phys A,* **299**: 381 (1978).
[B16] G. Bassani, N. M. Hintz, C. D. Kavaloski, J. R. Maxwell & G. M. Reynolds. *Phys Rev,* **139**: B830 (1965).
[B17] B. F. Bayman, A. Covello, A. Gargano, P. Guazzoni & L. Zetta. *Phys Rev C,* **90**: 044322 (2014).
[B18] D. Bazin et al. *Phys Rev Lett,* **101**: 252501 (2008).
[B19] G. B. Beard & W. H. Kelly. *Phys Rev,* **122**: 1576 (1961).
[B20] M. J. Bechara & O. Dietzsch. *Phys Rev C,* **12**: 90 (1975).
[B21] M. J. Bechara & O. Dietzsch. *Z Naturforsch A,* **30**: 356 (1975a).

[B22] P. R. Bell, B. H. Ketelle & J. M. Cassidy. *Phys Rev,* **76**: 574 (1949).
[B23] P. Belli et al. *Eur Phys J A,* **36**: 167 (2008).
[B24] N. Benzcer-Koller. *Phys Rev,* **134**: B1205 (1964).
[B25] M. Bernas et al. *Phys Lett B,* **331**: 19 (1994).
[B26] G. Berrier-Ronsin et al. *Nucl Phys A,* **288**: 279 (1977).
[B27] G. Berrier-Ronsin et al. *Phys Lett B,* **67**: 16 (1977).
[B28] F. E. Bertrand. *Nucl Data Sheets,* **23**: 229 (1978).
[B29] O. V. Bespalova, E. A. Romanovsky, T. I. Spasskaya & A. A. Klimochkina. *Phys At Nucl,* **78**: 881 (2015).
[B30] R. I. Betan & W. Nazarewicz. *Phys Rev C*, 86: 034338 (2012).
[B31] M. G. Betigeri & H. Morinaga. *Nucl Phys A*, **95**: 176 (1967).
[B32] J. Beun, J. C. Blackmon, W. R. Hix, G. C. McLaughlin, M. S. Smith & R. Surman. *J Phys G*, **36**: 025201 (2009).
[B33] M. R. Bhat, R. E. Chrien, O. A. Wasson, M. Beer & M. A. Lone. *Phys Rev,* **166**: 1111 (1968).
[B34] M. R. Bhat, R. E. Chrien, G. W. Cole & O. A. Wasson. *Phys Rev C,* **12**: 1457 (1975).
[B35] K. S. Bhatki, R. K. Gupta, S. Jha & B. K. Madan. *Nuovo Cimento,* **6**: 1461 (1957).
[B36] P. Bhattacharyya et al. *Phys Rev Lett,* **87**: 062502 (2001).
[B37] P. Bienvenu et al. *Radiochim Acta,* **97**: 687 (2009).
[B38] J. A. Biggerstaff, C. Bingham, P. D. Miller, J. Solomon & K. K. Seth. *Phys Lett B,* **25**: 273 (1967).
[B39] C. R. Bingham & M. L. Halbert. *Phys Rev C,* **1**: 244 (1970).
[B40] C. R. Bingham & D. L. Hillis. *Phys Rev C,* **8**: 729 (1973).
[B41] P. de Bièvre & I. L. Barnes. *Intl J Mass Spec Ion Process,* **65**: 211 (1985).
[B42] O. Birgül & S. J. Lyle. *Radiochim Acta,* **8**: 9 (1967).
[B43] J. H. Bjerregaard, O. Hansen, O. Nathan, L. Vistisen, R. Chapman & S. Hinds. *Nucl Phys A,* **110**: 1 (1968).
[B44] J. H. Bjerregaard, O. Hansen, O. Nathan, R. Chapman & S. Hinds. *Nucl Phys A,* **131**: 481 (1969).
[B45] T. Björnstad et al. *Phys Lett B*, **91**: 35 (1980).
[B46] T. Björnstad et al. *Z Phys A*, **306**: 95 (1982).
[B47] T. Björnstad et al. *Nucl Phys A*, **453**: 463 (1986).
[B48] J. Blachot. *Nucl Data Sheets*, **64**: 1 (1991).
[B49] J. Blachot. *Nucl Data Sheets*, **90**: 135 (2000).
[B50] J. Blachot. *Nucl Data Sheets*, **108**: 2035 (2007).
[B51] J. Blachot. *Nucl Data Sheets*, **113**: 2391 (2012).
[B52] F. Le Blanc et al. *Nucl Phys A*, **734**: 437 (2004).
[B53] F. Le Blanc et al. *Phys Rev C*, **72**: 034305 (2005).
[B54] P. J. Blankert, H. P. Blok & J. Blok. *Nucl Phys A*, **333**: 116 (1980).
[B55] P. J. Blankert, H. P. Blok & J. Blok. *Nucl Phys A*, **356**: 74 (1981).
[B56] J. P. Blaser, F. Boehm & P. Marmier. *Helvetic Phys Acta*, **23**: 623 (1950).
[B57] E. Bleuler, J. W. Blue, S. A. Chowdary, A. C. Johnson & D. J. Tendam. *Phys Rev*, **90**: 464 (1953).
[B58] J. Blomqvist, A. Kerek & B. Fogelberg. *Z Phys A*, **314**: 199 (1983).
[B59] T. Bloxham et al. *Phys Rev C*, **76**: 025501 (2007).
[B60] J.-P. Bocquet, Y. Y. Chu, G. T. Emery & M. L. Perlman. *Phys Rev*, **167**: 1117 (1968).

[B61] H. G. Bohlen, K. D. Hildenbrand, A. Gobbi & K. I. Kubo. *Z Phys A,* **273**: 211 (1975).
[B62] F. I. Boley. *Phys Rev,* **94**: 1078 (1954).
[B63] H. H. Bolotin, A. C. Li & A. Schwarzschild. *Phys Rev,* **124**: 213 (1961).
[B64] E. Bodenstedt, B. Gemünden, J. van den Hoff, S. Piel & R. Sajok. *Z Phys A,* **325**: 281 (1986).
[B65] T. Borello-Lewin, C. Q. Orsini, O. Dietzsch & E. W. Hamburger. *Nucl Phys A,* **249**: 284 (1975).
[B66] S. Borg, G. B. Holm & B. Rydberg. *Nucl Phys A*, **212**: 197 (1973).
[B67] S. B. Borzakov et al. *Nucl Instr Methods Phys Res A*, **480**: 696 (2002).
[B68] H. E. Bosch, M. C. Simon, E. Szichman, L. Gatto & S. M. Abecasis. *Phys Rev*, **159**: 1029 (1967).
[B69] W. W. Bowman & K. W. MacMurdo. *At Data Nucl Data Tables*, **13**: 89 (1974).
[B70] A. Bracco et al. *Phys Rev Lett*, **62**: 2080 (1989).
[B71] A. Bracco, F. Camera, J. J. Gaardhøje, B. Herskind & M. Pignanelli. *Nucl Phys A*, **519**: 47c (1990).
[B72] B. Brauner & H. Krepelka. *J Am Chem Soc*, **42**: 917 (1920).
[B73] R. Brenn, S. K. Bhattacherjee, G. D. Sprouse & L. E. Young. *Phys Rev C*, **10**: 1414 (1974).
[B74] G. A. Brennecka et al. *Geochim Cosmochim Acta*, **201**: 331 (2017).
[B75] H. F. Brinckmann et al. *Nucl Phys A*, **193**: 236 (1972).
[B76] R. Broda et al. *Phys Rev Lett*, **68**: 1671 (1992).
[B77] R. A. Broglia, C. Riedel, B. Sorensen & T. Udagawa. *Nucl Phys A*, **115**: 273 (1968).
[B78] R. A. Broglia, U. Götz, M. Ichimura, T. Kammuri & A. Winther. *Phys Lett B*, **45**: 23 (1973).
[B79] J. Bron et al. *Nucl Phys A*, **318**: 335 (1979).
[B80] B. A. Brown & K. Rykaczewski. *Phys Rev C*, **50**: R2270 (1994).
[B81] E. Browne & J. K. Tuli. *Nucl Data Sheets*, **108**: 2173 (2007).
[B82] E. Browne & J. K. Tuli. *Nucl Data Sheets*, **145**: 25 (2017).
[B83] E. M. Burbidge, G. R. Burbidge, W. A. Fowler & F. Hoyle. *Rev Mod Phys,* **29**: 547 (1957).
[B84] V. N. Burminskiĭ, I. V. Grebenshchikov, O. D. Kovrigin & G. I. Sychikov. *JETP Lett,* **22**: 54 (1975).
[B85] S. B. Burson, J. M. LeBlanc & D. W. Martin. *Phys Rev,* **105**: 625 (1957).
[B86] S. B. Burson, H. A. Grench & L. C. Schmid. *Phys Rev,* **115**: 188 (1959).
[B87] A. R. Byrne. *J Radioanal Chem,* **20**: 627 (1974).
[B88] A. R. Byrne. *J Radioanal Chem,* **37**: 591 (1977).
[B89] J. Blachot. *Nucl Data Sheets,* **84**: 277 (1998).
[C1] M. Caamaño et al. *Phys Rev C,* **88**: 024605 (2013).
[C2] M. E. Cage, P. D. Kunz, R. R. Johnson & D. A. Lind. *J Phys A,* **5**: 1529 (1972).
[C3] F. Camera et al. *Phys Lett B,* **293**: 18 (1992).
[C4] A. E. Cameron & E. Wichers. *J Am Chem Soc,* **84**: 4175 (1962).
[C5] A. G. W. Cameron. *Space Sci Rev*, **15**: 121 (1970).
[C6] M. Campbell, K. W. D. Ledingham, A. D. Baillie, M. L. Fitzpatrick, J. Y. Gourlay & J. G. Lynch. *Nucl Phys A*, **249**: 349 (1975).
[C7] L. Capponi et al. *Phys Rev C*, **94**: 024314 (2016).
[C8] D. Carbone et al. *J Phys: Conf Ser*, **1023**: 012006 (2018).
[C9] P. L. Carson & L. C. McIntyre, Jr. *Nucl Phys A*, **198**: 289 (1972).

[C10] R. F. Carlton, S. Raman, J. A. Harvey & G. G. Slaughter. *Phys Rev C*, **14**: 1439 (1976).
[C11] R. F. Carlton, S. Raman & G. G. Slaughter. *Phys Rev C*, **15**: 883 (1977).
[C12] R. F. Carlton, J. A. Harvey & N. W. Hill. *Phys Rev C*, **52**: 1498 (1995).
[C13] C. M. Cattadori, M. de Deo, M. Laubenstein, L. Pandola & V. I. Tretyak. *Nucl Phys A*, **748**: 333 (2005).
[C14] C. M. Cattadori, M. de Deo, M. Laubenstein, L. Pandola & V. I. Tretyak. *Phys At Nucl*, **70**: 127 (2007).
[C15] R. F. Casten, E. R. Flynn, O. Hansen & T. J. Mulligan. *Nucl Phys A*, **180**: 49 (1972).
[C16] S. A. Catlow, G. L. Troyer, D. R. Hansen & R. A. Jones. *J Radioanal Nucl Chem*, **263**: 599 (2005).
[C17] P. E. Cavanagh, C. F. Coleman, A. G. Hardacre, G. A. Gard & J. F. Turner. *Nucl Phys A*, **141**: 97 (1970).
[C18] J. Cederkäll et al. *Phys Rev C*, **53**: 1955 (1996).
[C19] J. Cederkäll et al. *Phys Rev Lett*, **98**: 172501 (2007).
[C20] I. Čeliković et al. *Phys Rev Lett,* **116**: 162501 (2016).
[C21] G. Cerizza et al. *Phys Rev C,* **93**: 021601(R) (2016).
[C22] C.-H. Chang, G. B. Hagemann & T. Yamazaki. *Nucl Phys A*, **134**: 110 (1969).
[C23] D. R. Chakrabarty et al. *Phys Rev C*, **36**: 1886 (1987).
[C24] D. R. Chakrabarty, V. M. Datar, S. Kumar, E. T. Mirgule, H. H. Oza & U. K. Das. *Phys Rev C*, **51**: 2942 (1995).
[C25] R. S. Chakrawarthy & R. G. Pillay. *Phys Rev C*, **54**: 2771 (1996).
[C26] R. S. Chakrawarthy et al. *Eur Phys J A*, **2**: 323 (1998).
[C27] R. Chapman et al. *Nucl Phys A*, **316**: 40 (1979).
[C28] M. Chartier et al. *Phys Rev Lett,* **77**: 2400 (1996).
[C29] D. Chattopadhyay et al. *Phys Rev C,* **97**: 051601(R) (2018).
[C30] J. Chen. *Nucl Data Sheets,* **146**: 1 (2017).
[C31] H. C. Cheung, H. Huang, B. N. S. Rao, L. Lessard & J. K. P. Lee. *J Phys G,* **4**: 1501 (1978).
[C32] H. C. Cheung, H. Huang & J. K. P. Lee. *Can J Phys,* **57**: 460 (1979).
[C33] S. Chiba, H. Koura, T. Hayakawa, T. Maruyama, T. Kawano & T. Kajino. *Phys Rev C,* **77**: 015809 (2008).
[C34] P. Chu & J. A. Marinsky. *J Inorg Nucl Chem*, **28**: 1339 (1966).
[C35] B. L. Cohen & R. E. Price. *Phys Rev*, **121**: 1441 (1961).
[C36] B. L. Cohen & R. E. Price. *Phys Rev*, **123**: 283 (1961).
[C37] B. L. Cohen, R. Patell, A. Prakash & E. J. Schneid. *Phys Rev*, **135**: B383 (1964).
[C38] B. L. Cohen, R. A. Moyer, J. B. Moorhead, L. H. Goldman & R. C. Diehl. *Phys Rev*, **176**: 1401 (1968).
[C39] I. M. Cohen. *J Radioanal Nucl Chem*, **312**: 29 (2017).
[C40] K. D. Coleman & M. L. Pool. *Phys Rev*, **72**: 1070 (1947).
[C41] M. La Commara et al. *Nucl Phys A*, **669**: 43 (2000).
[C42] M. Conjeaud, S. Harar & J. Picard. *Phys Lett*, **23**: 104 (1966).
[C43] J. M. Cork, A. E. Stoddard, C. E. Branyan, W. J. Childs, D. W. Martin & J. M. LeBlanc. *Phys Rev*, **84**: 596 (1951).
[C44] J. M. Cork & J. L. Lawson. *Phys Rev*, **56**: 291 (1939).
[C45] A. Corsi et al. *Phys Rev C*, **97**: 044321 (2018).
[C46] N. L. da Costa, C. V. de Barros Leite, A. G. de Pinho, D. Goldman, Y. Miyao & I. C. Nascimento. *Nuovo Cimento B*, **50**: 345 (1967).

[C47] G. M. Crawley, W. Benenson, D. Weber & B. Zwieglinski. *Phys Rev Lett*, **39**: 1451 (1977).
[C48] G. M. Crawley et al. *Phys Rev C*, **22**: 316 (1980).
[C49] G. M. Crawley, J. Kasagi, S. Gales, E. Gerlic, D. Friesel & A. Bacher. *Phys Rev C*, **23**: 1818 (1981).
[C50] G. M. Crawley, W. Benenson, G. Bertsch, S. Gales, D. Weber & B. Zwieglinski. *Phys Rev C*, **23**: 589 (1981).
[C51] J. B. Creech, F. Moynier & N. Badullovich. *Chem Geol,* **457**: 61 (2017).
[C52] M. B. Chatterjee, P. Banerjee, B. K. Sinha, S. Bose, R. Bhattacharya & S. K. Basu. *Phys Rev C,* **42**: 2737 (1990).
[D1] P. J. Daly et al. *Z Phys A,* **323**: 245 (1986).
[D2] P. J. Daly et al. *Phys Scr,* **T56**: 94 (1995).
[D3] R. A. Damerow, R. R. Ries & W. H. Johnson, Jr. *Phys Rev,* **132**: 1673 (1963).
[D4] A. S. Danagulyan et al. *Phys At Nucl*, **77**: 1313 (2014).
[D5] A. S. Danagulyan et al. *Phys At Nucl*, **78**: 447 (2015).
[D6] F. A. Danevich et al. *Phys Rev C*, **68**: 035501 (2003).
[D7] H. Daniel & P. Panussi. *Z Phys A*, **164**: 303 (1961).
[D8] I. Dankó et al. *Nucl Phys A,* **646**: 3 (1999).
[D9] I. G. Darby et al. *Phys Rev Lett,* **105**: 162502 (2010).
[D10] N. J. Davis et al. *Phys Rev C,* **69**: 064605 (2004).
[D11] J. Dawson, R. Ramaswamy, C. Reeve, J. R. Wilson & K. Zuber. *Nucl Phys A,* **799**: 167 (2008).
[D12] J. Dawson et al. *Phys Rev C,* **78**: 035503 (2008).
[D13] K. Deneffe et al. *J Phys G,* **11**: L59 (1985).
[D14] S. H. Devare & H. G. Devare. *Phys Rev,* **133**: B568 (1964).
[D15] C. Devillers, T. Lecomte & R. Hagemann. *Intl J Mass Spec Ion Phys,* **50**: 205 (1983).
[D16] S. A. Dickey, J. J. Kraushaar, R. A. Ristinen & M. A. Rumore. *Nucl Phys A,* **377**: 137 (1982).
[D17] I. Dillmann et al. *Eur Phys J A,* **13**: 281 (2002).
[D18] I. Dillmann, T. Rauscher, M. Heil, F. Käppeler, W. Rapp & F.-K. Thielemann. *J Phys G,* **35**: 014029 (2008).
[D19] F. Dimmling, N. Bräuer, B. Focke, T. Kornrumpf, K. Nishiyama & D. Riegel. *Z Phys,* **271**: 103 (1974).
[D20] P. P. Dmitriev, M. V. Panarin, G. A. Molin & Z. P. Dmitrieva. *Sov At Energy,* **39**: 734 (1975).
[D21] N. Dokania et al. *J Intr,* **9**: P11002 (2014).
[D22] P. Domin, S. Kovalenko, F. Šimkovic & S.V. Semenov. *Nucl Phys A,* **753**: 337 (2005).
[D23] C. Donzaud et al. *Eur Phys J A,* **1**: 407 (1998).
[D24] P. Doornenbal et al. *Phys Rev C,* **90**: 061302(R) (2014).
[D25] B. J. Dropesky & C. J. Orth. *J Inorg Nucl Chem,* **24**: 1301 (1962).
[D26] V. S. Dubey, C. E. Mandeville & M. A. Rothman. *Phys Rev,* **103**: 1430 (1956).
[D27] L. A. DuBridge, S. W. Barnes, J. H. Buck & C. V. Strain. *Phys Rev,* **53**: 447 (1938).
[D28] H. E. Duckworth & R. S. Preston. *Phys Rev*, **79**: 402 (1950).
[D29] R. B. Duffield & J. D. Knight. *Phys Rev*, **75**: 1967 (1949).
[D30] R. B. Duffield & L. M. Langer. *Phys Rev*, **76**: 1272 (1949).
[D31] M. Dworschak et al. *Phys Rev Lett*, **100**: 072501 (2008).

[D32] C. T. Dewberry et al. *J Mol Spec*, **248**: 20 (2008).
[E1] J. Eberz et al. *Z Phys A*, **326**: 121 (1987).
[E2] A. I. Egorov, Y. E. Loginov & S. E. Malyutenkova. *Appl Radiat Isot*, **65**: 1290 (2007).
[E3] A. Ekström et al. *Phys Rev Lett*, **101**: 012502 (2008).
[E4] Z. Elekes & J. Timar. *Nucl Data Sheets*, **129**: 191 (2015).
[E5] B. R. Erdal & A. C. Wahl. *J Inorg Nucl Chem*, **30**: 1985 (1968).
[E6] B. R. Erdal, A. C. Wahl & B. J. Dropesky. *J Inorg Nucl Chem*, **31**: 3005 (1969).
[F1] T. Faestermann et al. *Eur Phys J A*, **15**: 185 (2002).
[F2] T. Faestermann, M. Górska & H. Grawe. *Prog Part Nucl Phys*, **69**: 85 (2013).
[F3] C. Fahlander et al. *Phys Rev C*, **63**: 021307(R) (2001).
]F4] P. N. de Faria et al. *Phys Rev C*, **82**: 034602 (2010).
[F5] B. Farrelly, L. Koerts, N. Benczer, R. van Lieshout & C. S. Wu. *Phys Rev*, **99**: 1440 (1955).
[F6] A. M. Feingold. *Rev Mod Phys*, **23**: 10 (1951).
[F7] E. Fermi, E. Amaldi, O. D'Agostino, F. Rasetti & E. Segrè. *Proc Roy Soc,* **A146**: 483 (1934).
[F8] L. Ferreux, M.-C. Lépy, M.-M. Bé, P. Cassette, P. Bienvenu & G. Andreoletti. *Appl Radiat Isot*, **68**: 1571 (2010).
[F9] P. Fettweis & J. Vervier. *Phys Lett*, **3**: 36 (1962).
[F10] H. W. Fielding et al. *Nucl Phys A*, **281**: 389 (1977).
[F11] E. L. Fireman. *Phys Rev*, **75**: 323 (1949).
[F12] E. L. Fireman & D. Schwarzer. *Phys Rev*, **86**: 451 (1952).
[F13] M. Fisichella et al. *Phys Rev C*, **95**: 034617 (2017).
[F14] D. G. Fleming, M. Blann, H. W. Fulbright & J. A. Robbins. *Nucl Phys A*, **157**: 1 (1970).
[F15] D. G. Fleming, M. Blann & H. W. Fulbright. *Nucl Phys A*, 163: 401 (1971).
[F16] D. G. Fleming. *Can J Phys*, **60**: 428 (1982).
[F17] S. L. Flower, B. R. S. Babu, K. Neelakandan, R. N. Mukherjee & B. B. Baliga. *Nuovo Cimento A*, **106**: 163 (1993).
[F18] E. R. Flynn, J. G. Beery & A. G. Blair. *Nucl Phys A*, **154**: 225 (1970).
[F19] E. R. Flynn & J. G. Beery. *Phys Rev Lett*, **24**: 143 (1970).
[F20] B. Fogelberg, L.-E. De Geer, K. Fransson & M. af Ugglas. *Z Phys A*, **276**: 381 (1976).
[F21] B. Fogelberg & P. Carlé. *Nucl Phys A*, **323**: 205 (1979).
[F22] B. Fogelberg, K. Heyde & J. Sau. *Nucl Phys A*, **352**: 157 (1981).
[F23] B. Fogelberg & J. Blomqvist. *Phys Lett B*, **137**: 20 (1984).
[F24] B. Fogelberg, A. Aprahamian, R. L. Gill, H. Mach & D. Rehfield. *Phys Rev C*, **31**: 1026 (1985).
[F25] B. Fogelberg & J. Blomqvist. *Nucl Phys A*, **429**: 205 (1984).
[F26] B. Fogelberg, Y. Zongyuan & L. Spanier. *Phys Lett B*, **209**: 173 (1988).
[F27] B. Fogelberg, B. Ekström, L. Sihver & G. Rudstam. *Phys Rev C*, **41**: R1890 (1990).
[F28] B. Fogelberg, M. Hellström, L. Jacobsson, D. Jerrestam, L. Spanier & G. Rudstam. *Nucl Instr Methods Phys Res B*, **70**: 137 (1992).
[F29] B. Fogelberg et al. *Phys Rev Lett*, **73**: 2413 (1994).
[F30] B. Fogelberg et al. *Phys Scr*, **T56**: 79 (1995).
[F31] B. Fogelberg, K. A. Mezilev, H. Mach, V. I. Isakov & J. Slivova. *Phys Rev Lett*, **82**: 1823 (1999).

[F32] B. Fogelberg et al. *Phys Rev C*, **70**: 034312 (2004).
[F33] R. A. Forrest. *Fusion Eng Design*, **81**: 2143 (2006).
[F34] N. Fotiades et al. *Phys Rev C*, **84**: 054310 (2011).
[F35] M. M. Fowler, G. W. Goth, C.-C. Lin & A. C. Wahl. *J Inorg Nucl Chem*, **36**: 1191 (1974).
[F36] J. H. Fremlin & M. C. Walters. *Proc Phys Soc A,* **65**: 911 (1952).
[F37] D. de Frenne & E. Jacobs. *Z Phys*, **258**: 38 (1973).
[F38] D. de Frenne et al. *Phys Rev C*, **15**: 1440 (1977).
[F39] D. de Frenne, B. Proot, H. Thierens, P. de Gelder, E. Jacobs & A. de Clercq. *Phys Rev C*, **29**: 1777 (1984).
[F40] D. de Frenne & E. Jacobs. *Nucl Data Sheets*, **83**: 535 (1998).
[F41] D. de Frenne & E. Jacobs. *Nucl Data Sheets*, **93**: 447 (2001).
[F42] D. de Frenne & E. Jacobs. *Nucl Data Sheets*, **105**: 775 (2005).
[F43] D. de Frenne. *Nucl Data Sheets*, **110**: 1745 (2009).
[F44] D. de Frenne. *Nucl Data Sheets*, **110**: 2081 (2009).
[F45] J. Friese et al. *Nucl Phys A*, **553**: 753c (1993).
[F46] E. Frota-Pessôa. *Nuovo Cimento*, **77**: 369 (1983).
[F47] G. H. Fuller. *J Phys Chem Ref Data*, **5**: 835 (1976).
[F48] S. C. Fultz, B. L. Berman, J. T. Caldwell, R. L. Bramblett & M. A. Kelly. *Phys Rev*, **186**: 1255 (1969).
[G1] J. J. Gaardhøje, C. Ellegaard, B. Herskind & S. G. Steadman. *Phys Rev Lett*, **53**: 148 (1984).
[G2] J. J. Gaardhøje et al. *Phys Rev Lett*, **56**: 1783 (1986).
[G3] J. J. Gaardhøje et al. *Phys Rev Lett*, **59**: 1409 (1987).
[G4] J. Gableske et al. *Nucl Phys A*, **691**: 551 (2001).
[G5] Z. Gácsi & S. Raman. *Phys Rev C*, **49**: 2792 (1994).
[G6] A. Gadea et al. *Phys Rev C*, **55**: R1 (1997).
[G7] E. Gadioli et al. *Z Phys A*, **310**: 43 (1983).
[G8] D. Galaviz et al. *Phys Rev C*, **71**: 065802 (2005).
[G9] S. Galès, E. Gerlic, G. Duhamel, G. Perrin, C. Perrin & V. Comparat. *Nucl Phys A*, **381**: 40 (1982).
[G10] S. Galès et al. *Phys Lett B*, **144**: 323 (1984).
[G11] G. Gangopadhyay et al. *Z Phys A*, **351**: 1 (1995).
[G12] S. Ganguly et al. *Nucl Phys A*, **789**: 1 (2007).
[G13] S. Ganguly et al. *Phys Rev C*, **78**: 037301 (2008).
[G14] G. Gardner & J.I. Hopkins. *Phys Rev*, **101**: 999 (1956).
[G15] P. Gartenmann et al. *Nucl Instr Methods Phys Res B*, **114**: 125 (1996).
[G16] L. R. Gasques et al. *Phys Rev C*, **97**: 034629 (2018).
[G17] H. Gausemel et al. *Phys Rev C*, **69**: 054307 (2004).
[G18] L.-E. De Geer & G. B. Holm. *Phys Rev C*, **22**: 2163 (1980).
[G19] P. De Gelder, E. Jacobs & D. De Frenne. *Nucl Data Sheets*, **38**: 545 (1983).
[G20] J. Genevey, J. A. Pinston, C. Foin, M. Rejmund, H. Faust & B. Weiss. *Phys Rev C*, **65**: 034322 (2002).
[G21] J. Genevey et al. *Phys Rev C*, **67**: 054312 (2003).
[G22] E. Gerlic, J. Källne, H. Langevin-Joliot, J. van de Wiele & G. Duhamel. *Phys Lett B*, **57**: 338 (1975).
[G23] E. Gerlic et al. *Phys Rev C*, **21**: 124 (1980).
[G24] E. Gerlic et al. *Phys Lett B*, **117**: 20 (1982).
[G25] E. Gerlic et al. *Phys Rev C*, **39**: 2190 (1989).

[G26] M. J. Glaubman. *Phys Rev*, **98**: 645 (1955).
[G27] C. E. Gleit & C. D. Coryell. *Phys Rev*, **122**: 229 (1961).
[G28] C. E. Gleit & C. D. Coryell. *Phys Rev*, **124**: 1914 (1961).
[G29] R. K. Golden & S. Frankel. *Phys Rev*, **102**: 1053 (1956).
[G30] M. Goldhaber & R. D. Hill. *Rev Mod Phys*, **24**: 179 (1952).
[G31] P. M. Gopych, M. N. Demchenko, I. I. Zalyubovskii & P. S. Kizim. *At Energy*, **78**: 323 (1995).
[G32] M. Gorska et al. *Acta Phys Pol B*, **27**: 165 (1996).
[G33] M. Górska et al. *Phys Rev C*, **58**: 108 (1998).
[G34] B. Grapengiesser, E. Lund & G. Rudstam. *J Inorg Nucl Chem*, **36**: 2409 (1974).
[G35] H. Grawe et al. *Phys Scr*, **T56**: 71 (1995).
[G36] H. Grawe et al. *Z Phys A*, **358**: 185 (1997).
[G37] R. C. Greenwood & E. Brannen. *Phys Rev*, **122**: 1849 (1961).
[G38] A. E. Greendale & D. L. Love. *Anal Chem*, **35**: 1712 (1963).
[G39] L. Grodzins & H. Motz. *Phys Rev*, **102**: 761 (1956).
[G40] A. V. Grosse. *J Chem Edu*, **14**: 433 (1937).
[G41] W. E. Grummitt & G. Wilkinson. *Nature*, **158**: 163 (1946).
[G42] W. E. Grummitt & G. Wilkinson. *Nature*, **161**: 520 (1948).
[G43] G. Guastalla et al. *Phys Rev Lett*, **110**: 172501 (2013).
[G44] P. Guazzoni et al. *Phys Rev C*, **60**: 054603 (1999).
[G45] P. Guazzoni et al. *Phys Rev C*, **69**: 024619 (2004).
[G46] P. Guazzoni et al. *Phys Rev C*, **72**: 044604 (2005).
[G47] P. Guazzoni et al. *Phys Rev C*, **74**: 054605 (2006).
[G48] P. Guazzoni et al. *Phys Rev C*, **78**: 064608 (2008).
[G49] P. Guazzoni et al. *Phys Rev C*, **83**: 044614 (2011).
[G50] P. Guazzoni et al. *Phys Rev C*, **85**: 054609 (2012).
[G51] A. Guglielmetti et al. *Nucl Phys A*, **583**: 867 (1995).
[G52] G. Gürdal & F. G. Kondev. *Nucl Data Sheets*, **113**: 1315 (2012).
[G53] G. Gyürky et al. *Phys Rev C*, **71**: 057302 (2005).
[G54] G. Gyürky et al. *Phys Rev C*, **74**: 025805 (2006).
[G55] C. George & N. Chandrakumar. *Magn Reson Chem*, **48**: 912 (2010).
[H1] P. Haas et al. *Nucl Instr Methods Phys Res B*, **114**: 131 (1996).
[H2] R. L. Haese, F. E. Bertrand, B. Harmatz & M. J. Martin. *Nucl Data Sheets*, **37**: 289 (1982).
[H3] E. Hagebø, A. Kjelberg & A. C. Pappas. *J Inorg Nucl Chem,* **24**: 117 (1962).
[H4] R. L. Hahn & J. M. Miller. *Phys Rev*, **124**: 1879 (1961).
[H5] J. Hakala et al. *Phys Rev Lett*, **109**: 032501 (2012).
[H6] C. Y. Han, M. Saito & H. Sagara. *J Nucl Sci Technol*, **46**: 60 (2009).
[H7] H. H. Hansen, E. de Roost, W. van der Eijk & R. Vaninbroukx. *Z Phys*, **269**: 155 (1974).
[H8] P. G. Hansen et al. *Phys Lett B*, **28**: 415 (1969).
[H9] H. Harada, T. Murakami, K. Yoshida, J. Kasagi, T. Inamura & T. Kubo. *Phys Lett B*, **207**: 17 (1988).
[H10] H. Harada et al. *Phys Rev C*, **39**: 132 (1989).
[H11] S. Harissopulos, A. Spyrou, V. Foteinou, M. Axiotis, G. Provatas & P. Demetriou. *Phys Rev C*, **93**: 025804 (2016).
[H12] O. Hashimoto, Y. Shida, G. C. Madueme, N. Yoshikawa, M. Sakai & S. Ohya. *Nucl Phys A*, **318**: 145 (1979).
[H13] A. Hashizume, Y. Tendow & M. Ohshima. *Nucl Data Sheets*, **39**: 551 (1983).

[H14] A. Hashizume. *Nucl Data Sheets*, **112**: 1647 (2011).
[H15] M. Hass et al. *Nucl Phys A*, **410**: 317 (1983).
[H16] J. Hattula, E. Liukkonen & J. Kantele. *Z Phys*, **231**: 203 (1970).
[H17] R. W. Hayward. *Phys Rev*, **79**: 409 (1950).
[H18] R. W. Hayward. *Phys Rev*, **79**: 542 (1950).
[H19] T. Hayakawa et al. *Astrophys J,* **707**: 859 (2009).
[H20] T. Hayakawa et al. *J Nucl Sci Technol,* **53**: 2064 (2016).
[H21] F. Heine, T. Faestermann, A. Gillitzer, J. Homolka, M. Köpf & W. Wagner. *Z Phys A,* **340**: 225 (1991).
[H22] E. A. Henry. *Nucl Data Sheets*, **11**: 495 (1974).
[H23] K. Heyde, M. Waroquier & R. A. Meyer. *Phys Rev C*, **17**: 1219 (1978).
[H24] H. R. Hiddleston & C. P. Browne. *Nucl Data Sheets,* **13**: 133 (1974).
[H25] H. R. Hiddleston & C. P. Browne. *Nucl Data Sheets,* **17**: 225 (1976).
[H26] C. B. Hinke et al. *Nature,* **486**: 341 (2012).
[H27] R. A. Hinshaw & M. L. Pool. *Phys Rev,* **76**: 358 (1949).
[H28] P. Hoff et al. *Phys Rev Lett,* **77**: 1020 (1996).
[H29] P. Hoff et al. *Hyperfine Interact,* **129**: 141 (2000).
[H30] W. Hogervorst, C. Ekström, S. Ingelman & G. Wannberg. *Phys Scr,* **9**: 317 (1974).
[H31] B. G. Hogg & H. E. Duckworth. *Phys Rev,* **86**: 567 (1952).
[H32] R. E. Holland, F. J. Lynch & B. D. Belt. *Phys Rev C,* **17**: 2076 (1978).
[H33] J. M. Hollander, I. Perlman & G. T. Seaborg. *Rev Mod Phys,* **25**: 469 (1953).
[H34] D. J. Horen. *Nucl Data Sheets,* **6**: 75 (1971).
[H35] H. Houtermans, O. Milosevic & F. Reichel. *Intl J Appl Radiat Isot,* **31**: 153 (1980).
[H36] H.-C. Hseuh & E. S. Macias. *Phys Rev C,* **14**: 345 (1976).
[H37] H.-C. Hseuh & E. S. Macias. *Phys Rev C,* **17**: 272 (1978).
[H38] W. J. Huang, G. Audi, M. Wang, F. G. Kondev, S. Naimi & X. Xu. *Chin Phys C,* **41**: 030002 (2017).
[H39] H. Huck, M. L. Pérez, J. J. Rossi & H. M. Sofía. *Phys Rev C,* **24**: 2227 (1981).
[H40] H. Huck, M. L. Pérez & J. J. Rossi. *Phys Rev C,* **26**: 621 (1982).
[H41] J. P. Hummel. *Phys Rev,* **123**: 950 (1961).
[H42] J. M. R. Hutchinson, F. J. Schima & B. M. Coursey. *Phys Rev C,* **18**: 408 (1978).
[H43] B. Hadinia et al. *Phys Rev C,* **70**: 064314 (2004).
[I1] A. V. Ignatyuk, J. L. Weil, S. Raman & S. Kahane. *Phys Rev C,* **47**: 1504 (1993).
[I2] H. Ikegami. *Phys Rev,* **120**: 2185 (1960).
[I3] H. Ikegami & T. Udagawa. *Phys Rev,* **124**: 1518 (1961).
[I4] G. Ilie et al. *Phys Lett B,* **687**: 305 (2010).
[I5] E. Irani, S. K. Sadighi, S. Zare & R. Sadighi-Bonabi. *Energy Convers Manage,* **64**: 466 (2012).
[I6] T. Ishimatsu, S. Hayashibe, T. Awaya & H. Ohmura. *J Phys Soc Jap,* **35**: 1579 (1973).
[I7] T. Ishii, A. Makishima, K. Koganemaru, Y. Saito, M. Ogawa & M. Ishii. *Z Phys A,* **347**: 41 (1993).
[I8] M. Ishii, T. Ishii, A. Makishima, M. Ogawa, G. Momoki & K. Ogawa. *Phys Scr,* **T56**: 89 (1995).
[I9] Ł. W. Iskra et al. *Phys Rev C,* **89**: 044324 (2014).
[I10] Ł. W. Iskra et al. *J Phys: Conf Ser,* **580**: 012037 (2015).
[I11] K. Itahashi et al. *Hyperfine Interact,* **209**: 51 (2012).

[I12] IUPAC. *Pure Appl Chem,* **63**: 975 (1991).
[I13] E. Ivanov, A. Alevra, D. Plostinaru, N. Martalogu & R. Dumitrescu. *Nucl Phys,* **54**: 177 (1964).
[I14] Y. Iwata, M. Yasuhara, K. Maeda & Y. Yoshizawa. *Nucl Instr Methods Phys Res,* **219**: 123 (1984).
[I15] H. Iwe, R. Reif & C. Riedel. *Nucl Phys A,* **183**: 105 (1972).
[I16] T. Izak & S. Amiel. *J Inorg Nucl Chem,* **34**: 1469 (1972).
[I17] T. Izak-Biran & S. Amiel. *J Inorg Nucl Chem,* **40**: 937 (1978).
[J1] E. Jacobs & D. De Frenne. *Z Phys,* **257**: 402 (1972).
[J2] E. Jacobs & D. De Frenne. *Z Phys,* **258**: 329 (1973).
[J3] Z. Janas et al. *Phys Scr,* **T56**: 262 (1995).
[J4] J. Janecke, F. D. Becchetti & C. E. Thorn. *Nucl Phys A*, **325**: 337 (1979).
[J5] D. G. Jenkins et al. *Phys Lett B*, **428**: 23 (1998).
[J6] D. G. Jenkins et al. *Phys Rev Lett*, **83**: 500 (1999).
[J7] B. S. Jensen, O. B. Nielsen & O. Skilbreid. *Nucl Phys*, **19**: 654 (1960).
[J8] B. John, S. K. Kataria, B. S. Tomar, A. Goswami, G. K. Gubbi & S. B. Manohar. *Phys Rev C*, **56**: 2582 (1997).
[J9] M. W. Johns, C. D. Cox, R. J. Donnelly & C. C. McMullen. *Phys Rev*, **87**: 1134 (1952).
[J10] M. G. Johnston et al. *J Phys G*, **8**: 1405 (1982).
[J11] K. L. Jones et al. *Phys Rev C*, **70**: 067602 (2004).
[J12] K. L. Jones et al. *Eur Phys J A*, **25**: s283 (2005).
[J13] K. L. Jones et al. *Acta Phys Pol B*, **38**: 1205 (2007).
[J14] K. L. Jones et al. *Nature*, **465**: 454 (2010).
[J15] K. L. Jones et al. *Phys Rev C*, **84**: 034601 (2011).
[J16] K. L. Jones et al. *Acta Phys Polo B*, **46**: 537 (2015).
[J17] N.-G. Jonsson, A. Bäcklin, J. Kantele, R. Julin, M. Luontama & A. Passoja. *Nucl Phys A*, **371**: 333 (1981).
[J18] P. K. Joshi, B. Singh, S. Singh & A. K. Jain. *Nucl Data Sheets*, **138**: 1 (2016).
[J19] S. Juutinen et al. *Nucl Phys A*, **617**: 74 (1997).
[K1] M. I. Kalkstein & W. F. Libby. *Phys Rev*, **85**: 368 (1952).
[K2] S. A. Kalandarov, G. G. Adamian, N. V. Antonenko & J. P. Wieleczko. *Phys Rev C*, **90**: 024609 (2014).
[K3] M. Kanbe & K. Kitao. *Nucl Data Sheets*, **94**: 227 (2001).
[K4] A. Kankainen et al. *Phys Rev C*, **87**: 024307 (2013).
[K5] J. Kantele & M. Karras. *Phys Rev*, **135**: B9 (1964).
[K6] S. A. Karamian et al. *Phys At Nucl*, **78**: 757 (2015).
[K7] M. Karny et al. *Eur Phys J A*, **25**: 135 (2005).
[K8] M. Karny et al. *Eur Phys J A*, **27**: 129 (2006).
[K9] M. Karras. *Phys Rev*, **135**: B1301 (1964).
[K10] M. P. Kartamyshev, T. Engeland, M. Hjorth-Jensen & E. Osnes. *Phys Rev C*, **76**: 024313 (2007).
[K11] J. Kasagi, H. Harada, T. Murakami, K. Yoshida, H. Tachibanaki & T. Inamura. *Phys Lett B,* **176**: 307 (1986).
[K12] J. Katakura & K. Kitao. *Nucl Data Sheets*, **97**: 765 (2002).
[K13] J. Katakura. *Nucl Data Sheets*, **112**: 495 (2011).
[K14] L. Käubler et al. *Phys Scr,* **T56**: 266 (1995).
[K15] L. Käubler et al. *Z Phys A,* **351**: 123 (1995).
[K16] L. Käubler et al. *Z Phys A,* **356**: 235 (1996).

[K17] L. Käubler et al. *Z Phys A,* **358**: 303 (1997).
[K18] P. Kauranen. *J Inorg Nucl Chem*, **27**: 1713 (1965).
[K19] O. Kavatsyuk et al. *Eur Phys J A,* **25**: 211 (2005).
[K20] M. Kavatsyuk et al. *Eur Phys J A*, **25**: 139 (2005).
[K21] M. Kavatsyuk et al. *Eur Phys J A*, **29**: 183 (2006).
[K22] O. Kavatsyuk et al. *Eur Phys J A*, **31**: 319 (2007).
[K23] H. Kawakami, N. Yoshikawa, K. Komura, M. Koike & H. Yamada. *Phys Rev C*, **25**: 2013 (1982).
[K24] A. Kerek, G. B. Holm, P. Carlé & J. McDonald. *Nucl Phys A*, **195**: 159 (1972).
[K25] A. Kerek, G. B. Holm, L.-E. De Geer & S. Borg. *Phys Lett B*, **44**: 252 (1973).
[K26] A. Kerek, G. B. Holm, S. Borg & P. Carlé. *Nucl Phys A*, **209**: 520 (1973).
[K27] A. Kerek, P. Carlé & S. Borg. *Nucl Phys A*, **224**: 367 (1974).
[K28] T. A. Khan, D. Hofmann & F. Horsch. *Nucl Phys A*, **205**: 488 (1973).
[K29] Y. Khazov, A. A. Rodionov, S. Sakharov & B. Singh. *Nucl Data Sheets*, **104**: 497 (2005).
[K30] Y. Khazov, I. Mitropolsky & A. Rodionov. *Nucl Data Sheets*, **107**: 2715 (2006).
[K31] Y. Khazov, A. Rodionov & F. G. Kondev. *Nucl Data Sheets*, **112**: 855 (2011).
[K32] V. A. Khitrov, C. Panteleev, A. M. Sukhovoj, J. Honzatko & I. Tomandl. *Phys At Nucl*, **67**: 1818 (2004).
[K33] M. F. Kidd, J. H. Esterline & W. Tornow. *Phys Rev C*, **78**: 035504 (2008).
[K34] H. Kiel, D. Münstermann & K. Zuber. *Nucl Phys A*, **723**: 499 (2003).
[K35] P. Kienle. *Hyperfine Interact*, **103**: 49 (1996).
[K36] H. J. Kim et al. *Nucl Phys A,* **793**: 171 (2007).
[K37] R. Kirchner et al. *Phys Lett B*, **70**: 150 (1977).
[K38] K. Kitao, M. Kanbe & Z. Matumoto. *Nucl Data Sheets*, **38**: 191 (1983).
[K39] K. Kitao. *Nucl Data Sheets*, **75**: 99 (1995).
[K40] K. Kitao, Y. Tendow & A. Hashizume. *Nucl Data Sheets*, **96**: 241 (2002).
[K41] D. C. Kocher & W. Haeberli. *Nucl Phys A*, **252**: 381 (1975).
[K42] D. C. Kocher. *Nucl Data Sheets*, **17**: 39 (1976).
[K43] T. Koeling & F. Iachello. *Nucl Phys A*, **295**: 45 (1978).
[K44] I. V. Kopytin & I. A. Hussain. *Phys At Nucl*, **76**: 476 (2013).
[K45] A. Korgul et al. *Eur Phys J A*, **7**: 167 (2000).
[K46] A. Korgul, H. Mach, B. Fogelberg, W. Urban, W. Kurcewicz & V.I. Isakov. *Phys Rev C*, **64**: 021302 (2001).
[K47] A. Korgul et al. *Eur Phys J A*, **25**: s123 (2005).
[K48] A. Korgul et al. *Phys Rev C*, **77**: 034301 (2008).
[K49] R. L. Kozub et al. *Phys Rev Lett*, **109**: 172501 (2012).
[K50] K. S. Krane & J. Sylvester. *Phys Rev C*, **73**: 054312 (2006).
[K51] K.-L. Kratz et al. *J Phys G*, **14**: S331 (1988).
[K52] T. Kuehl et al. *Nucl Instr Methods Phys Res B*, **26**: 419 (1987).
[K53] I. Kumabe et al. *J Phys Soc Jap*, **47**: 673 (1979).
[K54] S. Kumar, J. Chen & F. G. Kondev. *Nucl Data Sheets*, **137**: 1 (2016).
[K55] G. J. Kumbartzki et al. *Phys Rev C,* **86**: 034319 (2012).
[K56] G. J. Kumbartzki et al. *Phys Rev C,* **93**: 044316 (2016).
[K57] G. J. Kumbartzki. *J Phys: Conf Ser,* **724**: 012027 (2016).
[K58] A. Kundu et al. *Phys Rev C,* **95**: 034615 (2017).
[K59] W. Kutschera. *Intl J Mass Spec,* **349-350**: 203 (2013).
[K60] W. F. Kinard, N. E. Bibler, C. J. Coleman & R. A. Dewberry. *J Radioanal Nucl Chem,* **219**: 197 (1997).

[L1] J. R. de Laeter & P. M. Jeffery. *J Geochem Res,* **70**: 2895 (1965).
[L2] J. R. de Laeter & P. M. Jeffery. *Geochim Cosmochim Acta,* **31**: 969 (1967).
[L3] J. R. de Laeter et al. *Pure Appl Chem*, **75**: 683 (2003).
[L4] D. R. LaFosse et al. *Phys Rev C,* **51**: R2876 (1995).
[L5] F. Lagoutine, J. Legrand, C. Perrot, J. P. Brethon & J. Morel. *Intl J Appl Radiat Isot,* **23**: 219 (1972).
[L6] F. O. Lawrence, W. R. Daniels & D. C. Hoffman. *J Inorg Nucl Chem,* **28**: 2477 (1966).
[L7] J. L. Lawson & J. M. Cork. *Phys Rev,* **52**: 531 (1937).
[L8] J. L. Lawson & J. M. Cork. *Phys Rev,* **57**: 982 (1940).
[L9] J. C. Lee & M. L. Pool. *Phys Rev,* **76**: 606 (1949).
[L10] A. Lépine-Szily et al. *Heavy Ion Phys,* **6**: 157 (1997).
[L11] M. Lewitowicz et al. *Phys Lett B,* **332**: 20 (1994).
[L12] M. Lewitowicz et al. *Nucl Phys A,* **588**: 197c (1995).
[L13] R. Lică et al. *Phys Rev C,* **93**: 044303 (2016).
[L14] S. N. Liddick et al. *Phys Rev Lett,* **97**: 082501 (2006).
[L15] C.-C. Lin & A. C. Wahl. *J Inorg Nucl Chem,* **32**: 2501 (1970).
[L16] M. Lindner & I. Perlman. *Phys Rev,* **73**: 1124 (1948).
[L17] M. Lipoglavšek et al. *Z Phys A,* **356**: 239 (1996).
[L18] M. Lipoglavšek et al. *Phys Lett B,* **440**: 246 (1998).
[L19] M. Lipoglavšek et al. *Nucl Phys A,* **682**: 399c (2001).
[L20] Z. Liu et al. *Phys Rev C,* **72**: 047301 (2005).
[L21] E. Liukkonen & J. Hattula. *Z Phys,* **241**: 150 (1971).
[L22] J. J. Livingood. *Phys Rev,* **50**: 425 (1936).
[L23] J. J. Livingood & G. Seaborg. *Phys Rev,* **50**: 435 (1936).
[L24] J. J. Livingood & G. T. Seaborg. *Phys Rev,* **55**: 667 (1939).
[L25] Y. N. Lobach, L. Käubler, R. Schwengner & A. A. Pasternak. *Phys Rev C,* **59**: 1975 (1999).
[L26] G. Lorusso et al. *Phys Rev C,* **86**: 014313 (2012).
[L27] G. Lorusso et al. *Phys Rev Lett,* **114**: 192501 (2015).
[L28] R. D. Loss, K. J. R. Rosman & J. R. de Laeter. *Geochim Cosmochim Acta,* **54**: 3525 (1990).
[L29] R. L. Lozeva et al. *Phys Rev C,* **77**: 064313 (2008).
[L30] S. Lunardi et al. *Z Phys A,* **328**: 487 (1987).
[L31] E. Lund & G. Rudstam. *Phys Rev C,* **13**: 1544 (1976).
[L32] E. Lund, P. Hoff, K. Aleklett, O. Glomset & G. Rudstam. *Z Phys A,* **294**: 233 (1980).
[L33] H. Lundqvist, S. Scott-Robson, L. Einarsson & P. Malmborg. *Appl Radiat Isot,* **42**: 447 (1991).
[L34] W.-D. Lu, N. R. Kumar & R. W. Fink. *Phys Rev C,* **1**: 350 (1970).
[L35] V. J. Lewington. *Phys Med Biol,* **41**: 2027 (1996).
[M1] R. D. Macfarlane & A. Siivola. *Phys Rev Lett,* **14**: 114 (1965).
[M2] H. Mach et al. *Phys Rev C,* **51**: 500 (1995).
[M3] G. C. Madueme, L. Westerberg, L. O. Edvardson & M. Migahed. *Phys Scr,* **12**: 189 (1975).
[M4] G. C. Madueme, L. O. Edvardson & L. Westerberg. *Phys Scr,* **13**: 17 (1976).
[M5] Z. Majka et al. *Phys Rev Lett,* **58**: 322 (1987).
[M6] N. K. Majumdar & A. Chatterjee. *Nucl Phys,* **41**: 192 (1963).

[M7] A. Makishima, T. Ishii, M. Nakajima, M. Ogawa & M. Ishii. *Z Phys A,* **349**: 133 (1994).
[M8] E. C. Mallary & M. L. Pool. *Phys Rev,* **76**: 1454 (1949).
[M9] E. C. Mallary & M. L. Pool. *Phys Rev,* **77**: 75 (1950).
[M10] C. E. Mandeville, E. Shapiro, R. I. Mendenhall, E. R. Zucker & G. L. Conklin. *Phys Rev,* **88**: 554 (1952).
[M11] P. D. Marmol & J. Colard. *Nucl Phys,* **36**: 109 (1962).
[M12] E. A. Martell & W. F. Libby. *Phys Rev,* **80**: 977 (1950).
[M13] C. P. Massolo et al. *Phys Rev C,* **43**: 1687 (1991).
[M14] M. Matoba, K. Tsuji, K. Marubayashi, T. Shintake, K. Ohba & T. Nomiyama. *Phys Rev C,* **27**: 2598 (1983).
[M15] R. H. Mayer et al. *Z Phys A,* **342**: 247 (1992).
[M16] R. H. Mayer et al. *Phys Lett B,* **336**: 308 (1994).
[M17] C. Mazzocchi et al. *Phys Rev Lett,* **98**: 212501 (2007).
[M18] A. L. McCarthy & T. W. Conlon. *Phys Rev,* **147**: 881 (1966).
[M19] C. L. McGinnis. *Phys Rev,* **81**: 734 (1951).
[M20] C. L. McGinnis. *Phys Rev,* **97**: 93 (1955).
[M21] C. L. McGinnis. *Phys Rev,* **109**: 888 (1958).
[M22] D. A. McClure & J. W. Lewis, III. *Phys Rev C,* **5**: 922 (1972).
[M23] K. A. Mezilev, Y. N. Novikov, A. V. Popov, B. Fogelberg & L. Spanier. *Phys Scr,* **T56**: 272 (1995).
[M24] J. W. Mihelich & R. D. Hill. *Phys Rev,* **79**: 781 (1950).
[M25] W. Mittig et al. *Nucl Phys A,* **616**: 329c (1997).
[M26] K. Miura, Y. Hiratate, T. Shoji, T. Suehiro, H. Yamaguchi & Y. Ishizaki. *Nucl Phys A,* **436**: 221 (1985).
[M27] K. Miyano, H. Nakahara & C. Gil. *J Phys Soc Jpn,* 33: 1505 (1972).
[M28] K. Miyano & C. Gil. *J Phys Soc Jap,* **33**: 1509 (1972).
[M29] D. Mo, G. L. Zhang, Z. N. Liang & L. Niesen. *Hyperfine Interact,* **56**: 1621 (1990).
[M30] D. L. Mock, R. C. Waddel, L. W. Fagg & R. A. Tobin. *Phys Rev,* **74**: 1536 (1948).
[M31] P. Mohr. *Eur Phys J A,* **31**: 23 (2007).
[M32] P. Mohr. *Phys Rev C,* **86**: 068803 (2012).
[M33] P. Möller, J. R. Nix & K.-L. Kratz. *At Data Nucl Data Tables,* **66**: 131 (1997).
[M34] T. D. Morris et al. *Phys Rev Lett,* **120**: 152503 (2018).
[M35] B. Mouginot et al. *Phys Rev C,* **83**: 037302 (2011).
[M36] B. J. Mount, M. Redshaw & E. G. Myers. *Phys Rev Lett,* **103**: 122502 (2009).
[M37] I. Mukha et al. *Nucl Phys A,* **746**: 66c (2004).
[M38] E. L. Murri, L. D. McIsaac & R. G. Helmer. *Phys Rev,* **155**: 1263 (1967).
[M39] R. T. Myers. *J Chem Edu,* **67**: 307 (1990).
[N1] R. Naeumann, H. Folger & H. O. Denschlag. *J Inorg Nucl Chem,* **34**: 1785 (1972).
[N2] R. Naidu. *Nature,* **137**: 578 (1936).
[N3] H. Naik et al. *Eur Phys J A,* **49**: 94 (2013).
[N4] H. Naik, G. N. Kim & K. Kim. *Phys Rev C,* **97**: 014614 (2018).
[N5] T. D. Nainan, A. S. Johnston & S. Jha. *Phys Rev,* **135**: B601 (1964).
[N6] M. de Napoli et al. *Bull Russ Aca Sci (Phys),* **78**: 588 (2014).
[N7] D. Navas-Nicolás & P. Sarriguren. *Phys Rev C,* **91**: 024317 (2015).
[N8] C. L. Nealy & R. K. Sheline. *Phys Rev,* **135**: B325 (1964).

[N9] J. L. Need & B. Linder. *Phys Rev,* **129**: 1298 (1963).
[N10] P. van Nes, K. Allaart, W. H. A. Hesselink, J. Konijin & H. Verheul. *Z Phys A,* **301**: 137 (1981).
[N11] I. Netterdon, J. Mayer, P. Scholz & A. Zilges. *Phys Rev C,* **91**: 035801 (2015).
[N12] R. T. Nichols, R. E. McAdams & E. N. Jensen. *Phys Rev,* **122**: 172 (1961).
[N13] T. Nishi et al. *Phys Rev Lett,* **120**: 152505 (2018).
[N14] J. Nishiyama, M. Igashira, T. Ohsaki, G. Kim, W.-C. Chung & T.-I. Ro. *J Nucl Sci Technol,* **45**: 352 (2008).
[N15] L. R. Norris & C. F. Moore. *Phys Rev,* **136**: B40 (1964).
[N16] M. Nozawa. *Nucl Phys,* **37**: 411 (1962).
[N17] L. Nunnelley, B. Boynton & W. D. Loveland. *Nucl Instr Methods,* **105**: 593 (1972).
[N18] L. L. Nunnelley & W. Loveland. *Phys Rev C,* **13**: 2017 (1976).
[O1] F. Oberli, P. Gartenmann, M. Meier, W. Kutschera, M. Suter & G. Winkler. *Intl J Mass Spec*, **184**: 145 (1999).
[O2] M. Ogawa et al. *Phys Scr*, **T56**: 289 (1995).
[O3] T. Ohnishi et al. *J Phys Soc Jap,* **79**: 073201 (2010).
[O4] S. Ohya & T. Tamura. *Nucl Data Sheets,* **70**: 531 (1993).
[O5] S. Ohya. *Nucl Data Sheets,* **102**: 547 (2004).
[O6] S. Ohya. *Nucl Data Sheets,* **111**: 1619 (2010).
[O7] K. Okano & Y. Kawase. *Nucl Instr Methods,* **108**: 503 (1973).
[O8] J. L. Olsen, L. G. Mann & M. Lindner. *Phys Rev,* **106**: 985 (1957).
[O9] L. Oncley. *J Chem Edu,* **15**: 291 (1938).
[O10] C. J. Orth, B. J. Dropesky & N. J. Freeman. *Phy Rev C,* **3**: 2402 (1971).
[O11] K. Oxorn, A. J. Houdayer & S. K. Mark. *Z Phys A,* **279**: 289 (1976).
[O12] N. Özkan et al. *Phys Rev C,* **75**: 025801 (2007).
[P1] S. D. Pain et al. *Nucl Instr Methods Phys Res B*, **261**: 1122 (2007).
[P2] P. J. Pan, D. W. Hetherington, D. B. McConnell & H. W. Taylor. *Can J Phys*, **48**: 1687 (1970).
[P3] A. C. Pappas & D. R. Wiles. *J Inorg Nucl Chem*, **2**: 69 (1956).
[P4] S. Parashari, S. Mukherjee, V. Vansola, R. Makwana, N. L. Singh & B. Pandey. *Appl Radiat Isot*, **133**: 31 (2018).
[P5] R. C. Pardo, E. Kashy, W. Benenson & L. W. Robinson. *Phys Rev C*, **18**: 1249 (1978).
[P6] J. Park et al. *Phys Rev C*, **96**: 044311 (2017).
[P7] J. Park et al. *Phys Rev C*, **97**: 051301(R) (2018).
[P8] V. V. Parkar et al. *Phys Rev C*, **97**: 014607 (2018).
[P9] E. S. Paul et al. *Phys Rev C*, **51**: 78 (1995).
[P10] R. M. Pearce & E. K. Darby. *Phys Rev*, **86**: 1049 (1952).
[P11] R. A. Peck, Jr. & J. Lowe. *Phys Rev*, **114**: 847 (1959).
[P12] E. Pellereau et al. *Phys Rev C*, **95**: 054603 (2017).
[P13] M. L. Perlman, J. P. Welker & M. Wolfsberg. *Phys Rev*, **110**: 381 (1958).
[P14] G. Perrin, G. Duhamel, C. Perrin, E. Gerlic, S. Galès & V. Comparat. *Nucl Phys A*, **356**: 61 (1981).
[P15] L. Pfeiffer, A. P. Mills, Jr., R. S. Raghavan & E. A. Chandross. *Phys Rev Lett,* **41**: 63 (1978).
[P16] B. Pfeiffer, K.-L. Kratz & P. Möller. *Prog Nucl Energy,* **41**: 39 (2002).
[P17] M. Pfützner et al. *Nucl Phys A,* **581**: 205 (1995).
[P18] S. Pietri et al. *Phys Rev C,* **83**: 044328 (2011).

[P19] J. A. Pinston et al. *Phys Rev C,* **61**: 024312 (2000).
[P20] J. A. Pinston & J. Genevey. *J Phys G,* **30**: R57 (2004).
[P21] J. Plch & J. Zderadička. *Czech J Phys B,* **27**: 865 (1977).
[P22] F. Pleiter. *Nucl Phys A,* **184**: 443 (1972).
[P23] A. Plochocki et al. *Nucl Phys A,* **332**: 29 (1979).
[P24] A. van Poelgeest et al. *Nucl Phys A,* **346**: 70 (1980).
[P25] M. de Poli et al. *Phys Scr,* **T56**: 296 (1995).
[P26] M. L. Pool, J. M. Cork & R. L. Thornton. *Phys Rev,* **52**: 239 (1937).
[P27] M. L. Pool. *Phys Rev,* **53**: 611 (1938).
[P28] Y. S. Popov, L. V. Zakharova, V. N. Kupriyanov, O. I. Andreev, V. Z. Vakhetov & Y. G. Toporov. *Radiochem,* **45**: 537 (2003).
[P29] J. L. Pore et al. *Eur Phys J A,* **53**: 27 (2017).
[P30] G. Potel, F. Barranco, F. Marini, A. Idini, E. Vigezzi & R. A. Broglia. *Phys Rev Lett,* **107**: 092501 (2011).
[P31] G. Potel, F. Barranco, F. Marini, A. Idini, E. Vigezzi & R. A. Broglia. *Phys Rev Lett,* **108**: 069904 (2012).
[P32] H. Prade et al. *Nucl Phys A,* **425**: 317 (1984).
[P33] M. H. Prior, A. Dymanus, H. A. Shugart & P. A. V. Bout. *Phys Rev,* **181**: 1665 (1969).
[P34] V. V. Parkar et al. *Phys Rev C,* **82**: 054601 (2010).
[Q1] Y.-Z. Qian, P. Vogel & G. J. Wasserburg. *Astrophys J,* **506**: 868 (1998).
[R1] S. Rab. *Nucl Data Sheets,* **75**: 491 (1995).
[R2] D. Rabenstein. *Z Phys,* **240**: 244 (1970).
[R3] R. S. Raghavan. *Phys Rev Lett,* **37**: 259 (1976).
[R4] P. Raghavan. *At Data Nucl Data Tables,* **42**: 189 (1989).
[R5] S. Rahaman et al. *Phys Lett B,* **703**: 412 (2011).
[R6] O. Rahmouni. *J Phys (Paris),* **29**: 550 (1968).
[R7] S. Raman & H. J. Kim. *Nucl Data Sheets,* **5**: 181 (1971).
[R8] S. Raman & H. J. Kim. *Nucl Data Sheets,* **6**: 39 (1971).
[R9] S. Raman, H. J. Kim, T. A. Walkiewicz & M. J. Martin. *Phys Lett B,* **44**: 255 (1973).
[R10] S. Raman et al. *Nucl Phys A,* **206**: 343 (1973).
[R11] S. Raman, R. L. Auble & F. F. Dyer. *Phys Rev C,* **9**: 426 (1974).
[R12] S. Raman, R. F. Carlton, G. G. Slaughter & M. R. Meder. *Phys Rev C,* **18**: 1158 (1978).
[R13] S. Raman, T. A. Walkiewicz, L. G. Multhauf, K. G. Tirsell, G. Bonsignori & K. Allaart. *Phys Rev C,* **37**: 1203 (1988).
[R14] S. Raman et al. *Phys Rev C,* **43**: 521 (1991).
[R15] M. K. Ramaswamy, W. L. Skeel, D. L. Hutchins & P. S. Jastram. *Phys Rev,* **121**: 553 (1961).
[R16] D. Ramos et al. *Phys Rev C,* **97**: 054612 (2018).
[R17] C. Rangacharyulu, Y. Aoki, K. Yagi, M. Matoba & M. Hyakutake. *Phys Rev C,* **20**: 397 (1979).
[R18] K. B. Rao & V. S. Rao. *Nuovo Cimento A*, **107**: 1625 (1994).
[R19] J. Rapaport et al. *Phys Rev Lett,* **54**: 2325 (1985).
[R20] G.-E. Rathke et al. *Z Phys A,* **321**: 599 (1985).
[R21] A. Ray, P. Das, S. K. Saha, A. Goswami & A. De. *Phys Lett B,* **679**: 106 (2009).
[R22] L. A. Rayburn. *Phys Rev,* **122**: 168 (1961).

[R23] R. A. Rebeles, A. Hermanne, S. Takács, F. Tárkányi, S. F. Kovalev & A. Ignatyuk. *Nucl Instr Methods Phys Res B,* **260**: 672 (2007).
[R24] G. A. Rech, E. Browne, I. D. Goldman, F. J. Schima & E. B. Norman. *Phys Rev C,* **65**: 057302 (2002).
[R25] J. J. Ressler et al. *Phys Rev C,* **65**: 044330 (2002).
[R26] T. W. Richards. *Chem Rev,* **1**: 1 (1924).
[R27] P. Richard, C. F. Moore, J. A. Becker & J. D. Fox. *Phys Rev,* **145**: 971 (1966).
[R28] B. C. Robertson, J. T. Sample, D. R. Goosman, K. Nagatani & K. W. Jones. *Phys Rev C,* **4**: 2176 (1971).
[R29] V. A. Rodin, A. Faessler, F. Šimkovic & P. Vogel. *Nucl Phys A,* **766**: 107 (2006).
[R30] K. J. R. Rosman, R. D. Loss & J. R. de Laeter. *Intl J Mass Spec Ion Proces*, **56**: 281 (1984).
[R31] K. J. R. Rosman & P. D. P. Taylor. *Pure Appl Chem,* **70**: 217 (1998).
[R32] M. Roteta, V. Peyres & E. García-Toraño. *Appl Radiat Isot,* **87**: 162 (2014).
[R33] J.-Z. Ruan, Y. Yoshizawa & Y. Koh. *Nucl Phys,* **36**: 431 (1962).
[R34] G. Rudstam. *Nucl Instr Methods,* **139**: 239 (1976).
[R35] G. Rudstam, K. Aleklett & L. Sihver. *At Data Nucl Data Tables,* **53**: 1 (1993).
[R36] R. A. Rydin. *Anna Nucl Energy,* **38**: 2356 (2011).
[R37] K. Rykaczewski et al. *Phys Rev C,* **52**: R2310 (1995).
[S1] M. Sakai & K.-I. Kubo. *Nucl Phys A,* **185**: 217 (1972).
[S2] M. Sakai, M. Sekiguchi, F. Soga, Y. Hirao, K. Yagi & Y. Aoki. *Phys Lett B,* **51**: 51 (1974).
[S3] C. Samour, J. Julien, J. M. Kuchly, R. N. Alves & J. Morgenstern. *Nucl Phys A,* **122**: 512 (1968).
[S4] M. Sanchez-Vega et al. *Phys Rev C,* **60**: 024303 (1999).
[S5] A. Savelius et al. *Nucl Phys A,* **637**: 491 (1998).
[S6] R. P. Scharenberg, M. G. Stewart & M. L. Wiedenbeck. *Phys Rev,* **101**: 689 (1956).
[S7] D. Schardt et al. *Nucl Phys A,* **326**: 65 (1979).
[S8] D. Schardt et al. *Nucl Phys A,* **368**: 153 (1981).
[S9] H. Schatz et al. *Phys Rev Lett,* **86**: 3471 (2001).
[S10] M. Schimmer et al. *Z Phys A,* **338**: 117 (1991).
[S11] M. Schimmer, S. Albers, A. Dewald, A. Gelberg, R. Wirowski & P. von Brentano. *Nucl Phys A,* **539**: 527 (1992).
[S12] M. Schimmer, R. Wirowski & P. von Brentano. *Nucl Phys A,* **569**: 458 (1994).
[S13] J. M. Schippers, J. M. Schreuder, S. Y. van der Werf, K. Allaart, N. Blasi & M. Waroquier. *Nucl Phys A,* **510**: 70 (1990).
[S14] J. M. Schippers et al. *Nucl Phys A,* **548**: 271 (1992).
[S15] K.-H. Schmidt, B. Jurado, C. Amouroux & C. Schmitt. *Nucl Data Sheets,* **131**: 107 (2016).
[S16] M. Schmorak, G. T. Emery & G. Scharff-Goldhaber. *Phys Rev,* **124**: 1186 (1961).
[S17] E. J. Schneid, A. Prakash & B. L. Cohen. *Phys Rev,* **156**: 1316 (1967).
[S18] Ø. Scheidemann & E. Hagebø. *J Inorg Nucl Chem,* **35**: 3055 (1973).
[S19] R. Schneider et al. *Z Phys A,* **348**: 241 (1994).
[S20] R. Schneider et al. *Nucl Phys A,* **588**: 191c (1995).
[S21] R. Schneider et al. *Phys Scr,* **T56**: 67 (1995).
[S22] R. Schubart et al. *Z Phys A,* **340**: 109 (1991).
[S23] R. Schubart et al. *Z Phys A,* **343**: 123 (1992).

[S24] R. Schubart, H. Grawe, J. Heese, H. Kluge, K. H. Maier & M. Schramm. *Z Phys A,* **352**: 373 (1995).
[S25] F. Schussler, J. Blachot, J. P. Bocquet & E. Monnand. *Z Phys A,* **281**: 229 (1977).
[S26] N. D. Scielzo et al. *Phys Rev C,* **80**: 025501 (2009).
[S27] D. K. Scott et al. *Phys Rev Lett,* **34**: 895 (1975).
[S28] G. T. Seaborg. *Rev Mod Phys,* **16**: 1 (1944).
[S29] G. T. Seaborg & I. Perlman. *Rev Mod Phys,* **20**: 585 (1948).
[S30] J. M. Sears, D. B. Fossan, S. E. Gundel, I. Thorslund, P. Vaska & K. Starosta. *Phys Rev C,* **55**: 1096 (1997).
[S31] J. M. Sears et al. *Phys Rev C,* **58**: 1430 (1998).
[S32] M. L. Sehgal. *Phys Rev,* **125**: 968 (1962).
[S33] M. Sekiguchi, Y. Shida, F. Soga, Y. Hirao & M. Sakai. *Nucl Phys A,* **278**: 231 (1977).
[S44] L. Seren, H. N. Friedlander & S. H. Turkel. *Phys Rev,* **72**: 888 (1947).
[S35] Y. V. Sergeenkov & V. M. Sigalov. *Nucl Data Sheets,* **34**: 475 (1981).
[S36] Y. V. Sergeenkov & V. M. Sigalov. *Nucl Data Sheets,* **49**: 639 (1986).
[S37] Y. V. Sergeenkov. *Nucl Data Sheets,* **58**: 765 (1989).
[S38] Y. V. Sergeenkov. *Nucl Data Sheets,* **65**: 277 (1992).
[S39] D. Seweryniak et al. *Phys Rev C,* **66**: 051307 (2002).
[S40] D. Seweryniak et al. *Phys Rev C,* **73**: 061301 (2006).
[S41] D. Seweryniak et al. *Phys Rev Lett,* **99**: 022504 (2007).
[S42] S. Shastry, H. Bakhru & I. M. Ladenbauer-Bellis. *Phys Rev C,* **1**: 1835 (1970).
[S43] S. Shalev & G. Rudstam. *Nucl Phys A,* **230**: 153 (1974).
[S44] E. S. Shepherd. *J Phys Chem,* **6**: 519 (1902).
[S45] J. Shergur et al. *Nucl Phys A,* **682**: 493c (2001).
[S46] J. Shergur et al. *Phys Rev C*, **65**: 034313 (2002).
[S47] J. Shergur et al. *Phys Rev C*, **71**: 064321 (2005).
[S48] J. Shergur et al. *Phys Rev C*, **72**: 024305 (2005).
[S49] J. Shergur et al. *Eur Phys J A*, **25**: s121 (2005).
[S50] M. Shibata et al. *Phys Rev C*, **55**: 1715 (1997).
[S51] R. Shoup, J. D. Fox & G. Vourvopoulos. *Nucl Phys A*, **135**: 689 (1969).
[S52] G. S. Simpson et al. *Phys Rev Lett,* **113**: 132502 (2014).
[S53] M. Singh, J. W. Sunier, R. M. DeVries & G. E. Thompson. *Nucl Phys A,* **193**: 449 (1972).
[S54] B. Singh. *Nucl Data Sheets,* **81**: 1 (1997).
[S55] B. Singh. *Nucl Data Sheets,* **93**: 33 (2001).
[S56] B. Singh. *Nucl Data Sheets,* **109**: 297 (2008).
[S57] B. Singh, A. A. Rodionov & Y. L. Khazov. *Nucl Data Sheets,* **109**: 517 (2008).
[S58] K. Sistemich et al. *Z Phys A,* **285**: 305 (1978).
[S59] H. A. Smith, Jr., M. E. Bunker, J. W. Starner, C. J. Orth & K. E. G. Löbner. *Phys Rev C,* **13**: 387 (1976).
[S60] R. E. Snyder & G. B. Beard. *Phys Lett,* **15**: 264 (1965).
[S61] R. E. Snyder & G. B. Beard. *Nucl Phys A,* **113**: 581 (1968).
[S62] A. A. Sonzogni. *Nucl Data Sheets,* **95**: 837 (2002).
[S63] A. A. Sonzogni. *Nucl Data Sheets,* **103**: 1 (2004).
[S64] D. P. Sousa et al. *Nucl Phys A,* **836**: 1 (2010).
[S65] L. Spanier, K. Aleklett, B. Ekström & B. Fogelberg. *Nucl Phys A,* **474**: 359 (1987).

[S66] H. Spieler, H. J. Körner, K. E. Rehm, M. Richter & H. P. Rother. *Z Phys A,* **278**: 241 (1976).
[S67] P. Stähelin, D. Maeder & M. Pochon. *Z Phys,* **140**: 498 (1955).
[S68] P. H. Stelson, W. T. Milner, F. K. McGowan, R. L. Robinson & S. Raman. *Nucl Phys A,* **190**: 197 (1972).
[S69] U. Stöhlker, A. Blönnigen, W. Lippert & H. Wollnik. *Z Phys A,* **336**: 369 (1990).
[S70] J. R. Stokeley & F. L. Moore. *Anal Chem,* **36**: 1203 (1964).
[S71] C. A. Stone, S. H. Faller & W. B. Walters. *Phys Rev C,* **39**: 1963 (1989).
[S72] P. O. Strom, D. L. Love, A. E. Greendale, A. A. Delucchi, D. Sam & N. E. Ballou. *Phys Rev,* **144**: 984 (1966).
[S73] A. Strömich, B. Steinmetz, R. Bangert, B. Gonsior, M. Roth & P. von Brentano. *Phys Rev C,* **16**: 2193 (1977).
[S74] K. Sümmerer et al. *Nucl Phys A,* **616**: 341c (1997).
[S75] R. Surman, J. Beun, G. C. McLaughlin & W. R. Hix. *Phys Rev C,* **79**: 045809 (2009).
[S76] K. Suzuki et al. *Nucl Phys A,* **721**: 831c (2003).
[S77] K. Suzuki et al. *Phys Rev Lett,* **92**: 072302 (2004).
[S78] J. Szerypo et al. *Nucl Phys A,* **507**: 357 (1990).
[S79] K. P. Santhosh, S. Krishnan & B. Priyanka. *Phys Rev C,* **91**: 044603 (2015).
[S80] M. Schmorak, A. C. Li & A. Schwarzschild. *Phys Rev,* **130**: 727 (1963).
[S81] N. N. Sergeeva et al. *J Org Chem,* **74**: 7140 (2009).
[T1] K. Takahashi, D. L. Swindle & P. K. Kuroda. *Phys Rev C,* **4**: 517 (1971).
[T2] H. Taketani et al. *Phys Lett B,* **90**: 214 (1980).
[T3] T. Tamura, Z. Matumoto & M. Ohshima. *Nucl Data Sheets,* **32**: 497 (1981).
[T4] T. Tamura, H. Iimura, K. Miyano & S. Ohya. *Nucl Data Sheets,* **64**: 323 (1991).
[T5] T. Tamura. *Nucl Data Sheets,* **90**: 107 (2000).
[T6] M. Tanaka et al. *Phys Lett B,* **78**: 221 (1978).
[T7] M. Thoennessen et al. *Phys Rev C,* **51**: 3148 (1995).
[T8] D. A. Thomas, S. K. Haynes, C. D. Broyles & H. C. Thomas. *Phys Rev,* **82**: 961 (1951).
[T9] J. C. Thompson, K. Talbot & G. Parry. *Nucl Phys,* **89**: 209 (1966).
[T10] P. Tidemand-Petersson, R. Kirchner, O. Klepper, W. Kurcewicz, E. Roeckl & E. F. Zganjar. *Z Phys A,* 302: 343 (1981).
[T11] R. J. Tighe, D. M. Moltz, J. C. Batchelder, T. J. Ognibene, M. W. Rowe & J. Cerny. *Phys Rev C,* **49**: 2871 (1994).
[T12] J. Timar, Z. Elekes & B. Singh. *Nucl Data Sheets,* **121**: 143 (2014).
[T13] L. J. Titus, F. M. Nunes & G. Potel. *Phys Rev C,* **93**: 014604 (2016).
[T14] H. K. Toft et al. *Phys Rev C,* **81**: 064311 (2010).
[T15] H. K. Toft et al. *Phys Rev C,* **83**: 044320 (2011).
[T16] S. Tolansky. *Proc Roy Soc,* **A144**: 574 (1934).
[T17] V. A. Tolstikov, V. P. Koroleva, V. E. Kolesov, A. G. Dovbenko & Y. N. Shubin. *Sov At Energy,* **24**: 709 (1968).
[T18] I. Tomandl et al. *Phys Rev C,* **83**: 044326 (2011).
[T19] C. Travaglio, F. K. Röpke, R. Gallino & W. Hillebrandt. *Astrophy J,* **739**: 93 (2011).
[T20] D. E. Troutner, A. C. Wahl & R. L. Ferguson. *Phys Rev,* **134**: B1027 (1964).
[T21] K. Takahashi, K. Blaum & Y. Novikov. *Astrophys J,* **819**: 118 (2016).
[U1] Y. Umemoto, S. Hirenzaki, K. Kume & H. Toki. *Prog Theor Phys,* **103**: 337 (2000).

[U2] W. Urban et al. *Eur Phys J A,* **5**: 239 (1999).
[U3] W. Urban et al. *Phys Rev C,* **94**: 011302(R) (2016).
[U4] M. P. Unterweger, D. D. Hoppes & F. J. Schima. *Nucl Instr Methods Phys Res A,* **312**: 349 (1992).
[U5] H. Utsunomiya et al. *Phys Rev C,* **80**: 055806 (2009).
[U6] H. Utsunomiya et al. *Phys Rev C,* **84**: 055805 (2011).
[V1] C. Vaman et al. *Phys Rev Lett,* **99**: 162501 (2007).
[V2] V. Vaquero et al. *Phys Rev Lett,* **118**: 202502 (2017).
[V3] V. V. Varlamov, B. S. Ishkhanov, V. N. Orlin & V. A. Chetvertkova. *Bull Russ Aca Sci (Phys),* **74**: 833 (2010).
[V4] B. J. Varley, G. S. Foote & W. Gelletly. *J Phys G,* **3**: 1099 (1977).
[V5] B. J. Varley, G. S. Foote, C. Garrett & W. Gelletly. *J Phys G,* **4**: 1643 (1978).
[V6] L. Vesser & J. Ellis. *Nucl Phys A,* **115**: 185 (1968).
[V7] R. Vianden, K. Krien & H. U. Schmidt. *Nucl Phys A,* **243**: 29 (1975).
[V8] F. Videbaek, O. Hansen, B. S. Nilsson, E. R. Flynn & J. C. Peng. *Nucl Phys A,* **433**: 441 (1985).
[V9] S. E. Vigdor & W. Haeberli. *Nucl Phys A,* **253**: 55 (1975).
[V10] D. A. Viggars, H. W. Taylor, B. Singh & J. C. Waddington. *Phys Rev C,* **36**: 1006 (1987).
[W1] R. Wadsworth et al. *Nucl Phys A,* **559**: 461 (1993).
[W2] R. Wadsworth et al. *Phys Rev C,* **50**: 483 (1994).
[W3] R. Wadsworth et al. *Phys Rev C,* **53**: 2763 (1996).
[W4] R. Wadsworth et al. *Phys Rev Lett,* **80**: 1174 (1998).
[W5] A. C. Wahl & D. R. Nethaway. *Phys Rev,* **131**: 830 (1963).
[W6] N. S. Wall. *Phys Rev,* **92**: 1526 (1953).
[W7] S.-Y. Wang et al. *Chin Phys C,* **33**: 838 (2009).
[W8] S. Y. Wang et al. *Phys Rev C,* **81**: 017301 (2010).
[W9] M. Wang et al. *Chin Phys C,* **36**: 1603 (2012).
[W10] H. Wang et al. *Prog Theor Exp Phys,* **023D02** (2014).
[W11] M. Wang, G. Audi, F. G. Kondev, W. J. Huang, S. Naimi & X. Xu. *Chin Phys C,* **41**: 030003 (2017).
[W12] H.-K. Wang, K. Kaneko, Y. Sun, Y.-Q. He, S.-F. Li & J. Li. *Phys Rev C,* **95**: 011304(R) (2017).
[W13] A. H. Wapstra, G. Audi & C. Thibault. *Nucl Phys A*, **729**: 129 (2003).
[W14] R. C. Weast, M. J. Astle & W. H. Beyer. *CRC Handbook of Chemistry and Physics,* **69th** edn, CRC Press, Inc., Florida (1988).
[W15] S. Y. van der Werf, B. R. Kooistra, W. H. A. Hesselink, F. Iachello, L. W. Put & R. H. Siemssen. *Phys Rev Lett*, **33**: 712 (1974).
[W16] S. Y. van der Werf, M. N. Harakeh, L. W. Put, O. Scholten & R. H. Siemssen. *Nucl Phys A*, **289**: 141 (1977).
[W17] S. Y. van der Werf et al. *Phys Lett B*, **166**: 372 (1986).
[W18] S. Y. van der Werf et al. *Phys Rev C*, **36**: 1796 (1987).
[W19] J. R. White & A. E. Cameron. *Phys Rev,* **74**: 991 (1948).
[W20] J. van de Wiele et al. *Phys Rev C*, **50**: 2935 (1994).
[W21] J. van de Wiele, E. Gerlic, H. Langevin-Joliot & G. Duhamel. *Nucl Phys A*, **297**: 61 (1978).
[W22] J. S. E. Wieslander et al. *Phys Rev Lett*, **103**: 122501 (2009).
[W23] M. E. J. Wigmans, R. J. Heynis, P. M. A. van der Kam & H. Verheul. *Phys Rev C,* **14**: 229 (1976).

[W24] K. Wisshak et al. *Phys Rev C,* **54**: 1451 (1996).
[W25] K. Wisshak, F. Voss & F. Käppeler. *Phys Rev C,* **54**: 2732 (1996).
[W26] R. Wirowski, M. Schimmer, L. Eβer, S. Albers, K. O. Zell & P. von Brentano. *Nucl Phys A,* **586**: 427 (1995).
[W27] M. Wolińska-Cichocka et al. *Acta Phys Pol B*, **34**: 2305 (2003).
[W28] M. Wolińska-Cichocka et al. *Acta Phys Pol B,* **34**: 2309 (2003).
[W29] M. Wolińska-Cichocka et al. *Eur Phys J A,* **24**: 259 (2005).
[X1] Z. Xin et al. *J Radioanal Nucl Chem,* **170**: 99 (1993).
[Y1] K. Yagi et al. *Nucl Phys A,* **111**: 129 (1968).
[Y2] K. Yagi, Y. Aoki, C. Rangacharyulu, K. Matoba, M. Hyakutake & J. Nidome. *Phys Lett B,* **44**: 447 (1973).
[Y3] T. Yamazaki & G. T. Ewan. *Phys Lett B,* **24**: 278 (1967).
[Y4] Y. Yamaguchi, J.-Z. Ruan & T. Nagahara. *J Phys Soc Jap,* **38**: 911 (1975).
[Y5] T. Yamazaki, G. T. Ewan & S. G. Prussin. *Phys Rev Lett,* **20**: 1376 (1968).
[Y6] T. Yamazaki & G. T. Ewan. *Nucl Phys A,* **134**: 81 (1969).
[Y7] S. Yoshida. *Nucl Phys,* **33**: 685 (1962).
[Y8] H. Yuta & H. Morinaga. *Nucl Phys,* **16**: 119 (1960).
[Y9] K. Yagi, S. Kunori, Y. Aoki, K. Nagano, Y. Tagishi & Y. Toba. *Phys Rev C,* **19**: 285 (1979).
[Y10] E. Yamazaki et al. *J Archaeologic Sci,* **52**: 458 (2014).
[Z1] V. A. B. Zagatto et al. *Phys Rev C,* **95**: 064614 (2017).
[Z2] S. Zhang, J. Guo, A. Cui, D. Li & D. Liu. *J Radioanal Nucl Chem Lett,* **212**: 93 (1996).
[Z3] C. T. Zhang et al. *Phys Rev C,* **62**: 057305 (2000).
[Z4] S.-S. Zhang, M. S. Smith, G. Arbanas & R. L. Kozub. *Phys Rev C,* **86**: 032802(R) (2012).
[Z5] V. A. Zheltonozhsky, A. M. Savrasov, N. V. Strilchuk & V. I. Tretyak. *EPL,* **121**: 12001 (2018).
[Z6] C. T. Zhang et al. *Phys Rev Lett,* **77**: 3743 (1996).

-: 0 :-

THE END

University of Ottawa
Canada